QUANTIFIYING THE ABILITY FOR HIGH SPECTRAL RESOLUTION INFRARED SOUNDERS TO DETECT REGIONAL PRECIPITABLE WATER VAPOR TRENDS DETERMINED BY CLIMATE MODELS

by

Jacola A. Roman

A thesis submitted in partial fulfillment of

the requirements for the degree of

Master of Science

(Atmospheric and Oceanic Science)

at the

UNIVERSITY OF WISCONSIN-MADISON

2013

Abstract

The IPCC 4th assessment stated that global warming is occurring and will continue to rise with continuous greenhouse gas emission. Climate change may cause more extreme weather events, which are expected to have severe socio-economical impacts. To help in adaptation policies for climate change, the atmosphere needs to be accurately monitored and trends in variables such as precipitable water vapor, which is a necessity for precipitation, need to be closely observed. Global Climate Models (GCMs) provide an easy way to understand the atmosphere and project into the future, but high uncertainty exists in models. It is essential to detect these predicted trends with observations, such as the Atmospheric Infrared Sounder (AIRS) and the Advanced Microwave Scanning Radiometer-EOS (AMSR-e). Observations, however, also have uncertainties including measurement error, often due to both instrument noise and algorithm assumptions. This study determined the theoretical Time To Detect (TTD) for 100 Year Precipitable Water Vapor (PWV) trends with a certain measurement error. These TTDs ranged from 2-50 years for global averages and 5-50 years for regional averages. In addition, this study performed an analysis on AIRS L3 to determine its measurement error, which was found to range form less than 1% to greater than 5% depending on the location. On average the measurement error was around 3%. This implies that with the current accuracy of Infrared (IR) Sounders it would take at least 20 years to detect a global PWV trends and might exceed 50 years.

Table of Contents

I. INTRODUCTION

The Intergovernmental Panel on Climate Change (IPCC) 4th assessment stated, with high certainty, that the continued release of greenhouse gas emissions will cause a warming of 0.2°C per decade. This rise in greenhouse gasses could also create changes in the overall climate, altering wind and precipitation patterns and leading to more extreme weather events. In the next 100 years, the sea level is expected to rise, droughts may become more frequent, and the intensity of rainfall may lead to more flooding. These extreme weather events have secondary consequences, including severe socio-economical impacts, increases in water-borne diseases, and escalating cleanup costs (Solomon et al. 2007). Understanding the projected changes in the climate is a necessity and attempting to quantify and monitor the current atmospheric state is fundamental to making future policy decisions.

To help in the adaptation policies for climate change, an understanding of the predicted trends and their consequences is needed, especially in the case of flooding. Limitations to Global Climate Models (GCMs) exist, models do not always agree and the climate is a complex system to emulate. Sun et al. (2006) found that some models are able to simulate land precipitation, most, however, were unable to reproduce spatial patterns of precipitation and frequency, a key to understanding regional changes. Furthermore, most models underestimated the intensity of heavy precipitation, making it difficult to characterize flash flooding events (Sun et al. 2006, Stephens et al. 2012). Measurements of precipitation also have large

uncertainties. Rain gauges and radar systems are costly and not readily available around the world. In addition, biases exist in both datasets (Seo et al. 2002, Ciach et al. 1999). Satellites provide the best way to measure precipitation over all terrains, but the measurement uncertainties can be considerably large. One study by Tian et al. (2010) found that the uncertainty for the ensemble of 6 different TRMM-era data was 40-60% over the ocean and 100-140% over high latitudes. Sea surface temperatures (SST) are much easier to measure and predict. Precipitable Water Vapor (PWV) is a function of sea surface temperature and the Clausius-Clapeyron relation characterizes phase changes on a pressure-temperature coordinate system; it can determine the water-holding capacity of the atmosphere. A study by Trenberth et al. (2003) found that the water-holding capacity of the atmosphere increases by 7% per degree Celsius. In addition, another study found that the relative humidity in GCMs remain constant, implying that the PWV will rise (Soden et al. 2005). PWV, although not a direct measurement of precipitation, is a requirement for rain to occur which is largely governed by convergence of water vapor, making PWV an alternative variable to precipitation and one that is currently easier to measure and model.

With high uncertainty in models, it is essential to detect these predicted trends with observations (Ohring et al. 1982, Ohring et al. 2005, Wielicki et al. 2013). Currently, the satellite era has provided several new advanced IR sounders that provide or are expected to provide, high quality measurements of PWV. The NASA Atmospheric Infrared Sounder (AIRS) on board the Aqua satellite is part of

the NASA Earth Observation System and is meant to support climate research and facilitate better weather forecasting. AMSR-e, the Advanced Microwave Scanning Radiometer-EOS, also onboard Aqua, was created to observe the hydrological system on Earth. One of the newest instruments is the Cross-track Infrared Sounder (CrIS), launched on Soumi NPP. CrIS is designed to provide high-resolution information on the atmospheric state, which in turn will provide more knowledge about the climate and help improve forecasting systems. Observations, however, have errors, for example measurement errors created through instrument noise and algorithm assumptions. Theoretically, the Time To Detect (TTD) depends on both natural variability and measurement error. By understanding the uncertainty of these measurements and utilizing the models, the amount of time it takes to detect PWV trends can be calculated, leading to a better understanding of the effectiveness of current instruments in distinguishing between climate change and variability. Furthermore, if PWV trends can be detected by observations in an appropriate amount of time, the secondary consequences of high PWV can be further analyzed (i.e. precipitation and flash floods) and adaptation policies can be created based on observations not models.

This paper will be broken into five main sections. The first section is Observations and Model Output in which the different datasets will be discussed. Next the Methodology section will go into detail how each analysis is performed, including the GCM and observational analyses. The Theoretical Prediction of PWV discusses the predicted GCM PWV trends and possible societal impacts. Next is the

Result section, which is broken into three parts: GCM Predicted Trends and TTD, Case Study Regions TTD, and Estimate AIRS PWV Uncertainty. The first part will discuss the GCM TTD results for different measurement errors examining both annual and seasonal effects. The second part will examine the TTD for four different case study regions. Finally, the last sub-section in the Results will examine the current accuracy of AIRS and what the measurement error is for the instrument in terms of several truth datasets. Lastly, the Conclusions will bring the observations and models together to discuss the TTD based on the current measurement errors.

II. OBSERVATIONS AND MODEL OUTPUT

This paper makes use of ground-based observations, satellite observations, and model output relevant to the assessment of trends in atmospheric water vapor. The ground observations are from a unique network, the SuomiNet, which has a site density in the central U.S. that allows traditional point measurements to be extended to regional scales. A detailed description of the use of SuomiNet data in a regional climatology can be found in Roman et al. (2012). The satellite observations considered are restricted to the microwave and hyperspectral infrared sensors on the NASA EOS Aqua platform, which represent a new generation of atmospheric sounders. The GCM models used here are a subset of those studied in Roman et al. (2012) with the addition of results from the most recent Coupled Model Intercomparison Project model comparison.

A. Ground-based

The ground-based GPS PWV observations come from the SuomiNet network and the NOAA GPS-Met. The SuomiNet data comes from a network of GPS receivers that measure several atmospheric variables, including PWV, in real time. The GPS data was obtained through the ARM Climate Research Facility data archive (http://www.arm.gov/data/vaps/suomigps). Two types of files containing GPS station data were used sgp30suomigpsX1 and 30wpdngps.

The first file, sgp30suomigps, provided 30-minute data from the Continuous Untied States (CONUS) sites starting 7 June 2001 until the present. This file provides data from the SuomiNet network and has been processed with the updated Bernese

GPS software version 5 (B5.0) since 2006, before 2006 the data was processed with the previous version of the software (B4.0) (Rothacher 1992). Each file contains one day of measurements with a temporal sampling of 30 minutes for each station. All files contain the stations names, network ID, station latitude and longitude, and station elevation. For each station, measurements include duration of validity of measurement, precipitable water vapor, precipitable water vapor error, surface atmospheric pressure, surface temperature, and surface relative humidity.

The second file, 30wpdngps, contains data from over 500 sites, primarily in the CONUS area. For this study, all stations that lie within the Oklahoma/Kansas region were used. Data is available starting 1 January 1996 until the present. NOAA's Earth System Research Laboratory, formally the Forecast Systems Laboratory, processed the data using GAMIT software (King and Bock 1996). Every file contains a day's worth of data at every station with a measurement every 30 minutes. Each file is comprised of station names, station numbers, station latitude and longitude, and station elevation. For each station, the measurements provided are PWV, surface pressure, temperature, and relative humidity (available starting 9 December 2001).

The last ground-based instrument used for this study is the Microwave Radiometer (MWR) at the Southern Great Plains (SGP) Central Facility site in Lamont, OK. Unlike the SuomiNet method, the MWR is a single point measurement with one instrument that is periodically calibrated. The files used are called sgpmwrret1liljclouC1.c1 and measurements are retrieved using a statistical

methodology that utilizes site-dependent monthly retrieval coefficients (Turner et al. 2007). Data is available starting on 1 January 2000 until the present and each file contains total column water vapor, liquid water path, surface temperature, surface pressure, etc.

B. Satellite

Two satellite instruments are used in this study for assessment and validation. They are the Atmospheric Infrared Sounder (AIRS) and the Advanced Microwave Scanning Radiometer – EOS (AMSR-e).

AIRS, a cross-track scanning instrument, was launched onboard the AQUA satellite, part of the NASA Earth Observation System, on May 4, 2002. The sounder was the first of a new generation of satellite sensors that provided the capability to retrieve water vapor profiles at high vertical resolution and good absolute accuracy over both ocean and land areas using the same algorithm. AIRS data is distributed by the NASA Goddard Earth sciences Data Information and Services Center (DISC) and was downloaded using the data service MIRADOR (http://mirador.gsfc.nasa.gov/). The files downloaded are products retrieved using AIRS IR and AMSU, the Advanced Microwave Sounding Unit also on AQUA. Three versions are used to assess differences between algorithms; V5.0 (2002-2005), V5.2 (2002-2012), and V6 (2005-2012). For this study, L2 and L3 products were utilized. The NASA AIRS L3 products are monthly averages at a 1^{o} x 1^{o} grid, and for this study V5.0, V5.2 and V6 were used. Each file contains a monthly gridded data for both ascending and descending. The data available includes latitude, longitude, total

column water vapor, and temperature. The NASA AIRS L2 products are granules every 6-minutes, each day has a total of 240 granules for the whole globe. Each file contains the latitude, longitude, time, total column water vapor, along with other atmospheric variables (Susskind et al. 2011).

AMSR-e, a passive microwave radiometer, was launched on the NASA AQUA satellite on May 4, 2002 (Kawanishi et al. 2003). The instrument has produced a long record of PWV over ice-free ocean areas. The L2B and L3 standard products are processed by the Global Hydrology Resource Center SIPS. For this study the AE_MoOCN product was used which is a L3 monthly gridded (0.25^{o} x 0.25^{o}) product over the ocean and was downloaded at the National snow and Ice Data Center (NSIDC) (http://n4eil01u.ecs.nasa.gov:22000/WebAccess/drill?attrib=esdt&esdt=AE_MoOcn.2&group=AMSA). Data is available starting in June of 2002 and ending in September of 2011, when the instrument stopped producing data. Each file contains a month of data for the globe with measurements of wind speed, water vapor, cloud liquid water and sea surface temperature.

C. NWP

The National Centers for Environmental Predication (NCEP) North American Regional Reanalysis (NARR) output used in this study was provided by the NOAA/OAR/ESRL PSD, Boulder, Colorado, USA from their site (http://www.esrl.noaa.gov/psd/). Output is available starting in 1979 till present at 3-hourly, daily, and monthly forecasts. After 2007, GPS PWV observations were

assimilated over North America. The NARR uses assimilated observational data from dropsondes, pibals, rawinsondes, aircraft, surface observations, and geostationary satellites. Other data assimilated includes precipitation datasets from various sources, Television and Infrared Observation Satellite Operational Vertical Sounder (TOVS), hourly and 3-hourly surface stations, ship and buoy data. Variables available include surface temperature, relative humidity, surface pressure, specific humidity, and total column water vapor (Mesinger et al. 2006).

D. GCM

This paper makes use of GCM output retrieved through the World Climate Research Programme (WCRP) Coupled Model Intercomparison Project Phase 3 (CMIP3) and Phase 5 (CMIP5).

The CMIP3 output was accessed through the portal Earth System Grid (ESG). Two models from the CMIP3, which were used in the IPCC 4th Assessment, were used in this study: the NCAR Community Climate System Model Version 3 (CCSM3) and the NASA Goddard Institute for Space Studies Model E20/Russell GISS. The Special report on Emissions Scenarios (SRES) A2 run 1 experiment was selected, which is described as: "a very heterogeneous world with continuously increasing global population and regionally oriented economic growth that is more fragment and slower than in other storylines" (URL: http://www.ipcc.data.org/ar4/scenario-SRA2.html). Each file contains latitudes, longitudes, and time. The global spatial resolutions vary: CCSM3 128^{o} x 25^{o} and GISS 46^{o} x 72^{o}. Each model data type spans the 100-year period, 2000-2100, although models have various initiation dates. This

study used monthly averages of PWV (URL: https://esgcet.llnl.gov:8443/home/publicHomePage.do).

The CMIP5 output was obtained through the new portal, the Earth System Grid-Center for Enabling Technologies (ESG-CET). The model counterparts to the CMIP3 were used in this study: the NCAR Community Climate System Model Version 4 (CCSM4) and the NASA GISS-E2. These models are available starting January 2004 (CCSM4) or January 2006 (GISS) and runs through December 2100, however, each model has different initiation dates. The scenario used was the Representative Concentration Pathways (RCPs) 8.5 which is described as: "Rising radiative forcing pathway leading to 8.5 W/m^2 in 2100" (URL: sedacciesin.columbia.edu/did/ar5_scenario_process/RCPs.html). Each file contains latitudes, longitudes, and time and the global spatial resolutions vary: CCSM4 192^o x 288^o and GISS 90^o x 144^o. This study used monthly averages of PWV (URL: pcmdi9.llnl.gov/esgf-web-fe/).

III. METHODOLOGY

This section describes the details of the methodology used in this thesis for the analysis of GCM model fields and the assessment of satellite measurements of PWV.

A. GCM Case Studies of Regional PWV

To illustrate the potential societal impact of predicted changes in water vapor due to climate change over the next 100 years, Probability Distribution Functions (PDFs) of precipitable water vapor (PWV) were created for four case study regions: United States, India, China, and Europe (bounding box shown in Figure 1). To create these PDFs the monthly PWV is extracted for each region from model output interpolated to a 1^{o} x 1^{o} grid. For each region, the 100-year data is split into two indexes, PWV monthly values for the first 25 years (2000-2025) and PWV monthly values for the last 25 years (2075-2100). Next a histogram of the data for 100 bins was created. Finally the PDF was calculated by dividing the number of elements in each bin by the sum of the number of elements. This creates two PDFs for each region, one for the first 25 years and one for the last 25 years. The PDF shift is calculated by differencing the first PDF (first 25 years) from the last PDF (last 25 years). Statistics on the PDFs were calculated including the maximum, mean, median, mode, minimum, 25^{th} percentile, 50^{th} percentile, 75^{th} percentile, 95^{th} percentile, and 99^{th} percentile. In addition, two values called integrated 95^{th} percentile and integrated 99^{th} percentile value were calculated, labeled $\Sigma P(>95\%)$ and $\Sigma P(>99\%)$. The integrated 95^{th} percentile is calculated by first determining the

cumulative sum for the PDF for the first 25 years. Then the PWV bin that most closely represents the 95th percentile for the PDF is determined. Finally, the likelihood of occurrence of values greater than this PWV is computed by finding the cumulative sum for the PDF of the last 25 years starting at the PWV bin representing the 95th percentile of the PDF of the first 25 years. The actual method used is to integrate the PDF of the last 25 years from zero to the desired bin value and then subtract the integral from one. This value shows how the highest 5% has shifted from the beginning to the end of the century. For example, what represented the extreme 95th percentile in the first 25 years represents the 75th percentile in the last 25 years, a shift of the PWV distribution to higher values. This is calculated for the 99th percentile in the same manner. The method was also used to calculate a global PDF shift for reference. Seasonal PDFs were calculated by extracting the 1^{o} x 1^{o} interpolated monthly PWV data for each season. From the seasonal data the same method above was utilized to determine the PDFs and PDF statistics. Results of application of this method are presented in the next section.

B. Extend GCM Regional Analysis to Global Analysis

To create the global grids, GCM PWV that covered the 100-year period (2000-2100) over the whole globe was extracted. These monthly averaged values were interpolated to a 1^{o} x 1^{o} grid using a linear interpolation. This interpolation was then replicated to an 180^{o} x 1080^{o} grid (3x the longitudes) to account for different origins of the grid (i.e. some models start at 0^{o} and go to 359^{o} while some start at 0.5^{o} or 1^{o}). Next, 15^{o} x 30^{o} (regional), 15^{o} x 360^{o} (zonal), and an 180^{o} x 360^{o}

(global) grids were created from the 1^o x 1^o interpolated grid using a running average. This moving average smooth's the 1^o x 1^o data with a boxcar window of size (2M+1) x (2N+1), averaging each element centered on the box with the elements surrounding it that fit within the box. For the global1^o x 1^o grid an area-weighted average was applied to correctly account for PWV values on a sphere (180^o x 360^o). To do this the PWV is multiplied by the cosine of the latitude and then normalized.

C. Compute GCM Global and Zonal Trends

For each grid (15^o x 30^o [regional], 15^o x 360^o [zonal], 180^o x 360^o [global]), a 100-year trend was calculated using the monthly anomaly time series. The trend was computed at each grid box using a least squares fit with equal weighting for each estimated monthly mean PWV anomaly value. Seasonal trends were calculated by extracting the PWV into four seasons: December/January/February (DJF), March/April/May (MAM), June/July/August (JJA)/ and September/October/November (SON). Once the PWV was extracted for each season, the months were averaged, for each year one value would be created for each season. This created a 100-year seasonal time series from which the trend would be calculated using the same method as above. Case study trends were calculated by extracting the desired areas (U.S., India, China, and Europe) from the regional grids and averaging over them.

D. Time to Detect Trends (TTD) with Measurement Uncertainty

To calculate the number of years of monthly data needed to detect the 100-year trends at a 95% confidence level with a probability of 0.90, the following equation was used:

$$n^{*} = (3.3 \times (\frac{\sigma_N}{\omega_0}) \times \sqrt{\frac{1+\Phi}{1-\Phi}})^{2/3}$$

where the standard deviation, $\sigma_N = (\sigma^2_{NatVar} + \varepsilon^2_m)^{½}$, is the monthly standard variation taking into account the de-trended natural variability and the measurement error of the instrument. ω_0 is the 100-year trend and ϕ is the autocorrelation. This is a modified version of the Weatherhead et al. (1999) equation. Unlike the formalism of Leroy et al. (2008), here the measurement error is assumed to have a random component with the same time scale as the natural variability. The autocorrelation factor was defined as $1+\phi/1-\phi$. The TTD was calculated for each grid using the 100-year trend found at each grid box. For this study three measurement errors, characterizing the error from both measurement noise and algorithm uncertainties, were used for the regional grids. The first was a measurement error of 0%, which represents an ideal sensor. The second was a measurement error of 1% to represent a CLARREO sensor. Finally, a 5% measurement error was used to represent the current accuracy of sounders. For zonal and global grids, six different measurement errors were utilized. This consisted of the previous three mentioned along with 2%, 3%, and 4% measurement error. The seasonal TTD was calculated by using the same method as

above but using the 100-year trend for each season. Case study TTDs were calculated by extracting from the regional grids over the desired areas and averaging.

E. Building a Measured Regional Climatology

NASA AIRS L3 PWV data (already on a 1 degree grid) was extracted out for a bounding box representing the Oklahoma/Kansas region by picking the latitude and longitudes lying within this area (34^{o}N to 39^{o}N and 87^{o}W to 100^{o}W) for every month, creating the regional monthly data for ascending and descending orbits. This method is also used to extract the NARR output. The AIRS L2 PWV data is extracted over the region by collecting all granules in a given day and averaging over the area creating two variables one for ascending PWV and one for descending PWV. These daily averages are then averaged to create monthly regional statistics, again with two separate variables for ascending and descending. The SuomiNet and NPN data are extracted by looping through the 30-minute files and creating daily averages for each station. Three variables are created, one that correlates to the ascending AIRS overpass time (averages only over 8 UTC), the descending AIRS overpass time (averages only over 19 UTC), and all times (averaged for the whole day). Next, the data is averaged over the days to create monthly statistics at each station, again creating three variables for the different overpass times and all times. Finally, the monthly data is extracted for the region by choosing the stations that lie within the bounding box. Prior to computing the regional averages from the GPS station data, an elevation correction was applied to each station time series to adjust the PWV

values for the elevation differences between the individual sites and the regional geographical mean elevation for the bounding box. The MWR data is extracted by looping through daily files and creating daily averages. Similar to the GPS extraction, the MWR is then averaged over the days to create monthly statistics at the site. Finally, the daily data is averaged to create monthly data for the site in Lamont, OK.

F. Calculate Measured Decadal Trend and Trend Error

The trend error is determined by calculating the difference between the monthly regional time series of two observations. The monthly regional data is averaged to create one regional time series for each observation. Next, the difference is calculated by subtracting the SuomiNet GPS, MWR, NARR, and NPN from the AIRS for both ascending and descending times creating an anomaly time series. This anomaly time series is then split into two time zones, months before January 2008 and months after January 2008. For each of these time periods the coefficients of a polynomial of degree 1 are determined that fit the time series using a method of least squares. In addition, trend error estimates are calculated using time series analysis (Weatherhead et al. 1998)

G. Measured Probability Distribution of PWV

The regional monthly data created through the extraction process is used to create Probability Distribution Functions (PDFs). The PDFs are calculated by differencing one observation from another. Four comparisons are created, AIRS – MWR, AIRS – SuomiNet, AIRS – NPN, and AIRS – NARR. For each comparison the difference is calculated for the ascending and descending overpasses separately.

Once the difference is calculated a histogram is created and the Gaussian fit is determined. Statistics are calculated including the mean, standard deviation, and percent error for the histogram. The percent error of the histogram is calculated by taking the average bias (AIRS L3 – Observation) over the whole time span and dividing it by the average PWV value over the region for the observation (NARR, NPN, SuomiNet, and MWR) and then the value is multiplied by 100 to get a percent error.

IV. MOTIVATION

A. Theoretical Prediction of PWV

Case study PDF results are discussed below by first analyzing the "all seasons" results for the four different regions (China, Europe, India, and U.S.). The PDF results will first show figures of the PDF shifts and then tables of PDF statistics will be examined for further analysis. Finally, the seasons will be separated and the same method of showing the results (PDF shift figures and PDF statistics) will be applied.

1. All Season Shifts

Figure 1 shows the projected population density in 2015. The four regions, shown by the bounding boxes, represent areas of high population increases per km^2. Each region of interest also lies in areas with high PWV trend gradients (except for Europe). Therefore, these areas are of particular interest for societal impacts since they will be heavily populated and experience higher amounts of PWV which could lead to more severe floods *with the potential for greater loss of life and property*.

Figure 2 shows China's predicted PWV PDF shift between the period 2000-2025 and 2075-2100. China is expected to increase in the highest PWV amounts, similar to India, these amounts will be greater than 50 mm, sometimes exceeding 75 mm. This distribution is quite broad varying from 0 to 80 mm indicting a large range of water amounts is contained in this region. Table 1a shows the PDF statics for the first 25 years in China and Table 1b shows the PDF statistics for the last 25 years. The maximum is expected to increase by at least 10 mm in all the models ranging

from 70 to 80 mm in the last 25 years; however, the minimums stay roughly the same increasing at most by 1 mm. The median, mode, and mean also shift to higher amounts by around 5-10 mm. For all the models, the standard deviation increases, which is expected since the distributions get broader as seen in Figure 2. All the percentiles shift to higher numbers in the last 25 years, with the CCSM4 having the greatest changes. The lines in Table 1b labeled ΣP(>X%) are the cumulative probability of occurrence in 2075-2100 of PWV values exceeding the Xth percentile in 2000-2025 (integrated 95th and 99th percentile). The PWV value of the 95th percentile in 2000-2025 is expected to become more like the 80th percentile in 2075-2100, while the 99th percentile is expected to drop to about the 90th percentile. *These increases in the PWV extremes in China are substantial and all models expect similar results.*

Figure 3 shows Europe's PWV PDFs shift. Europe is expected to shift to higher PWV amounts, but not as prominently as India, China, or the United States. Similar to India, there are two peaks in the distributions, except for CCSM3, but different to India the drier peak has the highest probability. Table 2a shows Europe's first 25 years PWV PDF statistics and Table 2b shows the last 25 years. The maximum is expected to increase, but not nearly as much as China's did, increasing by only about 5 mm. Again, the minimum does not significantly change, and in fact, in the CCSM3 it decreases by 0.5 mm. The median, mode, and mean all shift to higher values, by about 2-3 mm, or stay the same and the standard deviation does not change by that much, suggesting the distribution is very similar in shape for both

time periods. *Generally, for Europe, it is not the average that will change but the extremes, with the chance of extreme events in 2000-2025 increasing from 1% to 4%-14% in 2075-2100 depending on the model, an increase of a factor of 4 to 14.*

Figure 4 shows the PWV PDF shift for India. India is also expected to shift to higher PWV amounts, but in this case these amounts will well exceed 50 mm sometimes even reaching 80 mm. There are two modes, generally, with the second mode being higher than the first, except in the GISS. Table 3a shows the first 25 years PWV PDF statistics, while Table 3b shows the last 25 years for India. India shows quite an increase in the max, median, mode, and mean of values greater than 10 mm. The minimum, similar to the other regions, does not really change, and the standard deviation increases similar to China due to the broader range of PWV amounts. Each percentile increases by at least 4 mm for all the models and at most 12 mm. The 95^{th} percentile is expected to be the 70^{th} percentile, while the 99^{th} percentile will be the 80^{th} percentile. India, by far, has the most drastic change both in the averages and the extremes. *The likelihood of extreme high PWV events (> 99%) increases by a factor of 18 or more. This has serious implications for flooding potential in the 2075-2100 time period.*

Figure 5 shows the PWV PDF shift of the United States. The U.S. PWV is expected to shift to higher amounts (30 mm and above) in all models. Generally, there is a wide distribution and the distribution becomes even broader in the last 25 years, spanning from 0 to almost 60 mm. Table 4a shows the first 25 years PWV PDF statistics for the U.S. and Table 4b shows the last 25 years. The CCSM3 shows

the lowest maximum for this region, while the other models are about 10 mm higher in both the first 25 years and the last 25 years, however, all models do show an increase of around 10 mm from the first 25 years to the last. The median, mode, and mean do not change by that much, and it appears they change more in the CMIP5 models than the CMIP3 models. The standard deviation increases minimally. For all the models at all the percentiles, an increase is expected ranging form 1 mm to 7mm, not nearly as high as India. The 95th percentile and the 99th percentile, however, are expected to change to the 80th and 90th percentile respectively, similar to Europe. *The likelihood of extreme high PWV events (> 99%) increases by a factor of 10 or more between 2075-2100. This in turn could stress the U.S. infrastructure, which might not be able to handle such an increase in PWV and associated precipitation.*

For comparison, Table 5a gives the whole globes PWV PDF statistics for the first 25 years and Table 5b gives the last 25 years. The maximum is expected to increase by at least 10 mm in all the models, with the GISS-E2 showing the smallest PWV maximum. Similar to the regions chosen, the minimum is not expected to increase substantially. The median is expected to increase by a few mm while the mode stays the same, except for the GISS in which it increases by 1 mm. Generally, the mean increase by 3-4 mm and the standard deviation increases by 2 to 3 mm, suggesting a broader range of PWV values again. The percentiles increase to higher PWV amounts, but the 95th percentile is only expected to become the 89th percentile, while the 99th percentile will become the 91st percentile. This global analysis again

shows that certain regions will be impacted more or less than other regions, and that a global analysis smooth's out the variation and averages out the extremes.

2. Seasonal Shifts

Figure 6 shows the DJF PWV PDF shift for China. In China, the Northern Hemisphere winter PWV is expected to shift to higher amounts and there is a sharp decrease in the probability of amounts from 0-5 mm. The PDF, however, is quite broad and the models differ on how many peaks exist. For example, the GISS and GISS-E2 show two peaks of high probability, one around 5 mm and another around 40 mm, while the CCSM4 shows one around 5 mm. Table 6a shows the Northern Hemisphere winter DJF PDF statistics for China for the first 25 years and Table 6b shows the last 25 years. The maximum is expected to increase by at least 10 mm in all models, while the minimum is expected to remain about the same. The mode, median, and mean are expected to increase but very minimally, about 2-3 mm. All of the percentiles are expected to increase, but it is not until the most extreme values that dramatic increases of around 10 mm are seen. The 95th percentile is expected to become the 75th – 80th percentile, while the 99th percentile will become the 94th percentile, suggesting that the Northern Hemisphere winter extremes will increase in PWV but not by as much as in Northern Hemisphere summer. Figure 7 shows the JJA PDF shift for China, which shows the peak is expected to shift more than 8 mm higher. The models, disagree in the shape of the PDF; the GISS-E2 shows a much broader PDF compared to the other three models. In addition, the GISS and GISS-E2 show an increase in the probability of the peak amount, whereas the peak amount in

the CCSM3 and CCSM4 decreases, usually a sign of broader PDFs. Table 7a shows the first 25 years of PWV PDF statistics for China and Table 7b shows the last 25 years. These changes are much more significant than in Northern Hemisphere winter; the maximum is expected to increase by over 10 mm, along with the median, mean, and mode. Similar to Northern Hemisphere winter, however, the minimum barely changes and the standard deviation increase by 1 to 2 mm, suggesting the PDF does get broader but not by much. The greatest increase is in the percentile numbers, for example, the 25th percentile, which was around 40 for CCSM3, GISS, and CCSM4, is expected to increase to 50, this is 4x larger than the increase in Northern Hemisphere winter. Most striking is the 95th percentile and 99th percentile changes. For CCSM4, what marked 5% of the PWV amounts will encompass 58%, and what was 1% will become 39%. Even, the GISS-E2, which showed the lowest changes and lowest PWV increases, suggests a change of the 95th percentile to the 63rd percentile and the 99th percentile to the 69th percentile. The Northern Hemisphere spring PDF shift for China is shown in Figure 8. In China, the MAM PWV is generally expected to shift to higher amounts, but the PDF is broad. Furthermore, the PDF is bimodal and much harder to determine what will happen in terms of extremes. Table 8a shows the first 25 years for Northern Hemisphere spring PDF statistics in China and Table 8b shows the last 25 years. Similar to the previous season, the maximum is supposed to increase by more than 10 mm, while the minimum remains the same. Unlike the Northern Hemisphere summer results, which showed large increases in the averages and extremes, the median, mode, and the mean will only increase by 5

mm. The standard deviation is expected to increase by 2-3 mm, suggesting wider PDFs and the percentiles increase by 2-12 mm depending on the model, with the greatest increases occurring in the higher percentiles. Although slightly higher than the Northern Hemisphere winter integrated 95th percentile, the Northern Hemisphere spring is expected to increase less than the Northern Hemisphere summer to the 70th - 80th percentile, while the 99th percentile will become the 80th-90th percentile. Figure 9 shows the SON PWV PDF shift for China. Like the previous season, the Northern Hemisphere fall PWV is expected to increase, but the PDFs are extremely broad ranging from 5 to 70 mm, and the peaks are not nearly as sharp as seen in China for the Northern Hemisphere summer. Table 9a shows the Northern Hemisphere fall PWV PDF statistics for the first 25 years and Table 9b shows them for the last 25 years for China. The maximum is expected to increase by about 10 mm again, while the minimum only increases by 1-2 mm. The mean, mode, and median are expected to increase substantially more than shown in Northern Hemisphere winter or Northern Hemisphere spring, roughly 10 mm, suggesting the overall PWV average will increase significantly. In addition, the standard deviation is expected to increase, indicating wider ranges of PWV. The percentile increases are expected to change by at least 3 mm and at most 11 mm. Similar to Northern Hemisphere spring, what consisted of the extreme 5% have a probability of 20-30% and what consisted of the extreme 1% will be at least 15% of the values. Since both the Northern Hemisphere fall and Northern Hemisphere spring are supposed to

become more moist, China might expect a longer wet season with monsoons possibly lasting longer and starting earlier.

The DJF PWV PDF Shift for Europe is shown in Figure 10. For Europe, the Northern Hemisphere winter PWV is expected to shift to higher amounts, but not nearly as much as seen in other regions, in terms of absolute PWV. In all the models, the PDF tends to be narrow, only spanning 0 to 20 mm. In addition, there is only one mode at around 10 mm. Table 10a shows the Northern Hemisphere winter PWV PDF statistics for the first 25 years in Europe and Table 10b shows the last 25 years. Generally, the maximum increases by 3-5 mm, while the minimum, median, mode, and mean increase by at most 2 mm, suggesting little change in the seasonal averages. All models are in good agreement with where the percentiles are at in both time periods, and the standard deviation barely changes, suggesting a narrow PDF. The most substantial changes come in the integrated 95^{th} and 99^{th} percentile, in which the 5% will become 26% to 38% of the PWV values, and what was the extreme 1% will become the 10-15%, *indicating substantial increases greater than those seen in Northern Hemisphere winter for China can be expected for Europe*. Figure 11 shows the JJA PWV PDF shift for Europe, which is expected to shift to higher PWV amounts and become broader. Generally, however, the PDF is narrow compared to the three other regions, especially China and India. The Northern Hemisphere summer PDF statistics for the first 25 years in Europe are shown in Table 11a and for the last 25 years in Table 11b. The increases in the maximum are very similar to the increases in the Northern Hemisphere winter months, increasing

at most by 5-6 mm and the mean, mode, and median only increase by 2-3 mm. The percentiles increase by at least 2 mm and at most 6 mm. Again, the most striking changes occur in the 95th percentile, which becomes the 50-80th percentile, depending on the model, and the 99th percentile becomes the 62nd – 88th percentile. The models in this season have greater variance than seen in Northern Hemisphere winter. Europe's PWV in Northern Hemisphere spring is not expected to change much as seen in Figure 12. The MAM PDF peak, however, is expected to shift to slightly higher amounts and increase in probability. Table 12a shows the PDF statistics for the first 25 years and Table 12b shows the PDF statistics for the last 25 years. In Northern Hemisphere spring, the PWV maximum is expected to increase minimally by at most 3 mm. The minimum is also predicted to increase about 3 mm, larger than what was seen in Northern Hemisphere winter. The median, mode, and mean all increase by about 2 mm for all four models, but the GISS-E2 generally has a lower minimum than the other three models. Each percentile is expected to increase by at least 2 mm and at most 3mm, indicating that this season will change minimally in terms of PWV. The integrated 95th percentile however, ranges from 17% to 36%, while the integrated 99th percentile is 5% to 20%, showing that the very extreme amounts of PWV will increase resulting in more moisture in Northern Hemisphere spring. The Northern Hemisphere fall PDF PWV shift for Europe is shown in Figure 13. For Europe, the SON PWV is expected to increase, but similar to the MAM PWV, this increase is relatively small. Furthermore, the PDF is again narrow and has one mode. Northern Hemisphere fall PDF statistics for the first 25 years in Europe are

shown in Table 13a and the last 25 years are shown in Table 13b. These results are very similar to the Northern Hemisphere spring results for Europe. Generally, the maximum is expected to increase by 3 to 7mm, and the minimum only by 2-3 mm. The mode, mean, and median, also increase by 2-3 mm. Again, the standard deviation increases slightly, by maximum 1 mm. The percentiles provide the most noteworthy changes, increasing by 2-5mm, and the 95th percentile will become the 60th-85th percentile and the 99th percentile will become the 70th-95th percentile. There are more discrepancies between the models and the GISS and GISS-E2 tend to expect smaller changes, almost 4x smaller than the CCSM3 and CCSM4.

Figure 14 shows the Northern Hemisphere winter PWV PDF shift for India, which is expected to shift to higher amounts. The PDF is much broader, especially compared to Europe, but it is clear that PWV amounts greater than 35 mm are expected to increase in probability substantially. Table 14a shows the Northern Hemisphere winter PWV PDF statistics for India in the first 25 years while Table 14b shows the last 25 years. The maximum increases by at least 10mm, while the minimum only increases by 1-2 mm. Similar to the other regions, the mean, median, and mode increase by smaller amounts, 4-5 mm, and the standard deviation increases by 1-3 mm. Each percentile increases by at least 4 mm and at most 13 mm, which might suggest a large integrated 95th and 99th percentile, however, the integrated 95th percentile is around 17% while the 99th is around 10%, relatively small for other seasons and regions. *The Northern Hemisphere summer PWV PDF shift for India is shown in Figure 15 and shows the most distinct increase in extremes*

than any other region or season. For India, the JJA PDF peak is expected to shift to higher amounts, originally around 50 mm it is expected to increase by almost 15 mm to around 65-70 mm depending on the model. Generally, there is one peak and the PDF is not nearly as broad as seen in the previous Northern Hemisphere winter PDF for India. Table 15a shows the Northern Hemisphere summer PWV PDF statistics for the first 25 years and Table 15b shows the last 25 years. This region and season has by far the most salient changes. The maximum is expected to increase by at least 11 mm and the minimum by 4 mm. The median, mean, and mode increase by about 10mm, suggesting the seasonal averages will be significantly different. Each percentile increases by a minimum 7 mm, the largest minimal change seen, and at most 14 mm. Most notable are the integrated 95th percentile and 99th percentile. The 95th percentile will become the 27th – 44th percentile that is a 51% to 69% increase, while the integrated 99th percentile will become the 37th -62nd percentile. **By far, these are the biggest increases in the extremes seen in any region or season, which could have substantial consequences in terms of the monsoon season and regional flooding**. Figure 16 shows the MAM PWV PDF shift for India, which again is expected to shift to higher amounts. The PDF, however, is broad and the models disagree on the relative shape and number of modes. Northern Hemisphere spring PWV PDF statistics for the first 25 years is shown in Table 16a and the last 25 years is shown in Table 16b. Generally, the maximum increases by 10 mm and the minimum by 2 mm. The median, minimum, and mode increase by 6-10 mm and the standard deviation

increases by 2 mm. Each percentile shifts to higher PWV amounts by 4 mm to 10 mm depending on the model. What contained the extreme 5% will now be around 20% of the PWV values and what contained the top 1% highest values will be around 10% of the PWV values. The shift is towards higher values, but not nearly as high as Northern Hemisphere summer. Northern Hemisphere fall PWV in India is expected to increase by about 10 mm in the CCSM3 and CCSM4 as shown in Figure 17. The PDFs generally have one peak, although the GISS model PDF is much broader than the others. Table 17a shows the Northern Hemisphere fall India first 25 years PWV PDF statistics while Table 17b shows the last 25 years. All the other regions have shown similar results between Northern Hemisphere spring and Northern Hemisphere fall (i.e. Europe's SON results were identical to the MAM results). India is starkly different. First, the maximum is expected to increase by at least 10 mm. In addition, the mean, mode, and median are all expected to increases by 10-15 mm, significantly larger than in Northern Hemisphere spring. The 25th percentile is expected to increase by at least 7 mm, while the 95th percentile is expected to increase by at least 9 mm; overall there is a huge shift to higher amounts. Most staggering in the integrated 95th percentile, which ranges between 36% and 60%. Even more astonishing the top 1% is expected to become at least the top 27%. *These high values along with the similarly high values in Northern Hemisphere summer for India, suggest that a longer season of high moisture content, running from June through November, should be expected, which could lead to a notably longer wet season.*

Figure 18 shows the DJF PWV PDF shift for the Eastern United States. The Northern Hemisphere winter PWV is expected to shift to higher amounts. Generally, the PDF is bimodal with the first peak having the greatest probability. Table 18a shows the DJF PWV PDF statistics for the U.S. for the first 25 years while Table 18b shows for the last 25 years. These differences are quite small in the maximum, only increasing by 2 to 6 mm, and even smaller in the minimum increasing at most by 2 mm. The median, mode, and mean only increase by 2-3 mm. Each percentile increases by at least 2 mm, with the largest increases occurring at the higher percentiles. Similar to China, the Northern Hemisphere winter integrated 95th percentile is around 18% and the 99th percentile range from 6% to 11%. Generally, the models agree well with each other. The Northern Hemisphere summer PWV in the U.S. is expected to increase substantially, values greater than 30-40 mm depending on the model, instead of 20-30 mm, as shown in Figure 19. Typically, the PDF has one peak, except in the GISS-E2, and this peak tends to shift 5-10 mm higher. Table 19a shows the Northern Hemisphere summer first 25 years PWV PDF statistics and Table 19b shows the last 25 years. For Northern Hemisphere summer, similar to the other regions, both the averages and the extremes are expected to increase. The maximum is expected to increase by 7-10 mm, while the median, mode, and mean are expected to increase by 6 mm. Each percentile will increase by at least 5 mm and at most 7 mm, suggesting a broad shift to higher amounts. Most notable are the integrated 95th and 99th percentiles. The integrated 95th percentile is 28% to 53%, instead of 5%, while the integrated 99th percentile is 16% to 40%. The

GISS-E2 has dramatically smaller integrated percentiles and shifts compared to the other three models, almost half the magnitude. Figure 20 shows the Northern Hemisphere spring PWV PDF shift for the U.S., which is expected, as in all the other cases, to shift to higher amounts, but not nearly as much as in the previous season, Northern Hemisphere summer. The PDF has one peak around 20 mm that increases about 5 mm. Northern Hemisphere spring PWV PDF statistics for the first 25 years are shown in Table 20a and for the last 25 years in Table 20b. Generally, only the extremes will increase, with the maximum becoming 7-10 mm and the mean mode and median shifting 4-5 mm higher. The percentiles range from an increase of 3 mm to an increase of 7 mm. What contained the 5% of extreme PWV values will be 14% - 30% and what contained the top 1% will be 6% to 18%. Generally, the GISS and GISS-E2 show smaller shifts than the CCMS3 and CCSM4. Northern Hemisphere fall PWV in the U.S. is expected to shift towards higher PWV amounts, as shown in Figure 21. The shape of the PDF varies between models, the GISS and GISS-E2 tend to have broader shapes while the CCSM3 and CCSM4 tend to have definitive peaks around 30 -40 mm. Table 21a shows the PWV PDF shift for the first 25 years, while Table 21b shows the statistics for the last 25 years. In Northern Hemisphere fall, the maximum is expected to increase by at least 5 mm and the median, mode, and mean are expected to increase by 1 to 8 mm. Each percentile shifts between 4 mm and 8 mm. Divergent from Europe and China, the integrated 95th percentile and 99th percentile are substantially changed, although not as remarkably high as India did. The 95th percentile will become the 66th to 80th percentile while the 99th percentile

will become the 75th – 85th percentile. An increase in moisture in Northern Hemisphere fall for the Eastern part of the U.S. could mean more moisture available for hurricanes or in general more precipitation which could lead to greater probability of flooding.

Similar to the all season analysis, the global PWV PDF statistics will be analyzed for comparison. Table 22a shows the DJF PWV PDF statistics for the first 25 years for the whole globe, while Table 22b shows the last 25 years. Generally, the maximum is expected to increase by more than 10 mm, and the minimum is only increased by 0.1 mm. The median, mode, and mean increased slightly by 2-4 mm, suggesting little change in the Northern Hemisphere winter averages. Each percentile increases by a minimum of 1 mm and a maximum of 12 mm. The integrated 95th percentile and 99th percentile are much smaller than most of the regions previously discussed, only 11% and 8% respectively. All the models agree very well with each other except the GISS-E2 which has significantly lower PWV amounts, however, the integrated 95th and 99th percentile are similar to the other models, suggesting that the shifts are similar even though the exact PWV numbers are not. Table 23a shows the JJA PWV PDF statistics for the first 25 years and Table 23b shows them for the last 25 years. These results are very similar to the DJF results, most likely due to the fact that this is for the whole globe; the seasons effect the results very little (i.e. during JJA the Northern Hemisphere experiences more moisture effecting the result for all the regions [since they all were located in the Northern Hemisphere] and the opposite was seen in DJF). Table 24a shows the MAM

PWV PDF statistics for the first 25 years and Table 24b shows them for the last 25 years. Generally the maximum is expected to increase by at least 10 mm and the minimum barely changes. The mean and median increased by 2 to 3 mm, along with the standard deviation. The percentiles shift to higher amounts by at least 1 mm and at most 12 mm. These results are similar to the previous seasons due to the spatial averaging over the globe, hence the integrated 95th percentile is around 12% and the integrated 99th percentile is around 9%, similar to Northern Hemisphere summer and Northern Hemisphere winter. Table 25a shows the Northern Hemisphere fall global PWV PD statistics for the first 25 year while Table 25b shows them for the last 25 years. Again, the results are almost identical to the previous seasons due to the spatial averaging.

V. RESULTS

A. GCM Predicted Trends and TTD

1. All Seasons TTD PWV Trends

Monthly, all season TTD results are presented below by first discussing regional (15^{o}x30^{o} grid), then zonal (15^{o}x360^{o} grid), and lastly global (180^{o}x360^{o} grid) results. Within each grid size the 100-year trend will be discussed followed by the standard deviation for each measurement error, and lastly the TTD for each corresponding measurement error. The TTD contour intervals are every 10 years for regional analysis.

i. Regional

Figure 22 shows the mean climatological PWV (mm) for all models from 2000-2100. The greatest PWV occurs in the Tropics from 15^{o}S to 15^{o}N, around the ITCZ. The amounts decrease towards the poles. Figure 23 shows the 100-year trend for all models, which is positive in all cases for the whole globe. The largest trends occur in the ITCZ, with the greatest in magnitude occurring off the east coast of China and Indonesia (Western Pacific Ocean). CCSM4 and CCSM3 show the largest magnitudes of trends higher than 0.2 mm/year in some areas; however, all models are consistent in the location of the greatest trend. Figure 24 shows the autocorrelation factor for each model. The autocorrelation factor is smallest in southern hemisphere. The CCSM3 also has large autocorrelation factors in the Northern Hemisphere. Figure 25 shows the standard deviation with 0% measurement error. The natural variability is greatest in the CCSM4 with the largest

amounts occurring in Indonesia, the Middle East, and the Pacific Ocean. In the CCSM3, these locations also experience the greatest variability but at a smaller magnitude, less than 1 mm. Both GISS model versions generally show smaller variability with an emphasis over sub Sahara Africa, India, and Indonesia. The TTD with 0% measurement error is shown in Figure 26. Generally, the longest TTD occurs in the South Pole, possibly due to the area experiencing the smallest predicted trend value. Overall, the GISS models have larger TTDs than the CCSM models. In all models, there is a band near the ITCZ that runs from South America to Indonesia that has the lowest TTDs, less than 15 years, suggesting that high trends (greater than 0.1 mm/year) can be detected much faster than small trends. These areas are also characterized by small natural variability, which may assist in detecting the trends faster. Figure 27 shows the natural variability plus a 1% measurement error. This measurement error does not affect the overall standard deviation greatly, especially when compared to the effect of the 5% measurement error in Figure 29 where the measurement error overwhelms the natural variability. Figure 28 shows the TTD for the 1% measurement error and although the TTD is still relatively low over most areas, there are more localized areas of long TTD, in particular around North America, the Middle East, and near the Poles, where TTDs exceed 50 years, however, the TTD is generally less than 30 years. Figure 30 shows the TTD with a measurement error of 5%. Generally, the TTD is 30 years or more with a few areas of around 20 years, indicating the measurement error has

overwhelmed the natural variability to the point where trend detection is not realistically achievable.

ii. Zonal

Figure 31 shows how the zones, each 15^{o} in width, are laid out for the zonal analysis. Each number represents a latitude zone and each zone number corresponds to the following latitudes (numbers 1-11): 75^{o}S, 60^{o}S, 45^{o}S, 30^{o}S, 15^{o}S, 0^{o}, 15^{o}N, 30^{o}N, 45^{o}N, 60^{o}N, 75^{0}N. These latitudes represent where the data is extracted from each zone. In the smoothing process, the zonal smoother has created 15^{o} x 360^{o} grids, that is starting at 90^{o}N the latitudes are smoothed every 15^{o}. For example, zone 11 represents a smoothed averaged from 90^{o}N to 75^{o}N; therefore by extracting out at 75^{o}N the data is for that zones average (90^{o}N to 75^{o}N). Figure 32 shows the 100-year trend for each latitude zone. The average of all zones is labeled 'ZA'. From this figure, the greatest trend occurs at the equator in all the models and the trends decrease towards the poles. The North Pole has a larger PWV trend than the South Pole and the zonal average trend (average over all 11 zones) is numerically similar to 30^{o}N and 30^{o}S. Figure 33 shows the autocorrelation factor that is lowest at the equator and highest in the mid latitudes, except for the GISS-E2. The South Pole has smaller autocorrelation factors than the North Pole, the asymmetry in the autocorrelation leads to generally longer TTDs in the Northern Hemisphere. Figure 34 shows the standard deviation for each measurement error (0% through 5%). As the measurement error increases the total variability increases by the root sum square (RSS). In areas of already high natural variability

(0% measurement error), for example zone 6, the differences between measurement error of 0% and measurement error of 5% is much greater, more than 1.5 mm, implying the effect of the measurement error is greatest in these areas due to the fact that these regions experience higher PWV amounts than, for example, the North Pole (zone 11). The South Pole has smaller natural variability than the North Pole and the zonal average is similar to the 30^{o} latitude zone. Figure 35 shows the TTD for all models and measurement errors. All the models, except the GISS, show the longest TTDs occurring in the Northern Hemisphere mid-latitudes, suggesting that the high autocorrelation factors and standard deviation in this zone cause longer TTDs. The measurement error has the strongest effect in the tropics, where the gradient between the TTD of different errors is largest. For example, the GISS model at zone 6, the equator, has a large difference between each measurement error (> 10 years difference) whereas zone 11, the North Pole, the measurement error barely effects the TTD (< 5 years difference). This would be expected since measurement error is a percent of the water vapor and the greatest amounts of PWV occur in the tropics. With zero measurement error the Northern Hemisphere TTDs are generally smaller than the Southern Hemisphere TTDs, however, this hemisphere difference is reduced when the measurement error reaches 4% or higher. The effect of measurement error is to increase zonally averaged TTDs by about 10 years for a 5% error.

iii. Global

Global trends are shown in Table 26a. All models show similar trends around 0.025 mm/year. The global autocorrelation timescale is shown in Table 26b and all the models have similar autocorrelation factors around 1 except for the GISS which is greater than 3. Table 26c shows the global standard deviation. All the models have standard deviation with 0% measurement error of less than 0.05 mm; the GISS has the smallest while the GISS-E2 has the largest. Each standard deviation value increases with each accession of measurement error, maxing out at around 1.3 mm for the 5% measurement error. Table 26d shows the global TTD. The smallest TTD occurs in the CCSM3 with 2.6 years. Each increment of measurement error increases the TTD by at least 4x and the TTD exceeds 47 years in the GISS for a measurement error of 5%.

2. Seasonal TTD PWV Trends

Seasonal TTD results are presented below by first discussing regional (15^{o}x30^{o} grid), then zonal (15^{o}x360^{o} grid), and lastly global (180^{o}x360^{o} grid) results for each season. The four seasons are Northern Hemisphere Northern Hemisphere winter (DJF), Northern Hemisphere summer (JJA), Northern Hemisphere spring (MAM), and Northern Hemisphere fall (SON). Within each grid size the 100-year trend will be discussed followed by the standard deviation for each measurement error, and lastly the TTD for each corresponding measurement error. The TTD contour intervals are every 10 years for regional analysis.

i. Regional

Figure 36 shows an example of the DJF PWV. The PWV maximums shift southward which would be expected since DJF is Northern Hemisphere winter for the Northern Hemisphere and Northern Hemisphere summer for the Southern Hemisphere. Figure 37 shows the 100-year Northern Hemisphere winter PWV trend in mm/years. The Northern Hemisphere winter PWV trend is greatest nearest the tropics, more specifically south of the equator around 0^{o}S to 30^{o}S, which is most likely to do the shifts in moisture from the Northern Hemisphere to the Southern Hemisphere during the different seasons. The greatest trends occur in the Pacific Ocean, but the magnitude of this trend varies by model. Figure 38 shows the Northern Hemisphere winter autocorrelation factor, which is generally less than 1 in all models. The CCSM3 and GISS-E2 have autocorrelation factors that exceed 3. Figure 39 shows the Northern Hemisphere winter standard deviation with a 0% measurement error. Generally, the standard deviation is low in the poles and higher near the tropics. In all models, the maximum standard deviation occurs in the eastern part of the Pacific Ocean and over the Indian Ocean, but the magnitude of this value is almost twice the size in the CCSM3 and CCSM4 than in the GISS and GISS-E2. . The Northern Hemisphere winter TTD is shown in Figure 40. The smallest TTDs (less than 10 years) occur near the equator in all the models, possibly due to the high trends in this region. CCSM3 showed the smallest TTDs for this season. The GISS models (GISS and GISS-E2), however, tend to be much higher everywhere else then in the CCSM models, especially in the poles and sub-Sahara Africa where TTDs are larger than 50 years. Figure 41 shows the standard deviation with a 1%

measurement error in Northern Hemisphere winter, which does not change significantly from the natural variability (Figure 39). The Northern Hemisphere winter TTDs with a 1% measurement error are shown in Figure 42. The 1% measurement error does not change the magnitude of the TTD significantly; the TTDs are generally less than 20 years, suggesting this error does not have much influence on detecting trends. Figure 43 shows the Northern Hemisphere winter standard deviation with a 5% measurement error. The 5% measurement error has drastically altered the total variability. There is a wide band from about 40°S to 40°N with high standard deviation ranging from 3 to 5 mm, indicating that the measurement error has overwhelmed the natural variability. Figure 44 shows the Northern Hemisphere winter TTDs with the 5% measurement error. Generally the TTDs are at least 20-30 years and greater in the GISS and GISS-E2 models than the CCSM3 and CCSM4. The 5% measurement error has caused the TTD to increase by a factor of 2 in some regions.

An example of Northern Hemisphere summer PWV is shown in Figure 45. The Northern Hemisphere summer PWV shifts northward compared to the Northern Hemisphere winter PWV, with the greatest amounts occurring between the equator and 30°N. Figure 46 shows the Northern Hemisphere summer 100-year PWV trend. The greatest PWV trends occur north of the equator; emulating the high PWV values are in Figure 45, which would be expected. The CCSM3, CCSM4, and GISS show the highest PWV trends occurring over Japan, China, India, and Indonesia, while the GISS-E2 has lower PWV trends overall. In addition, the eastern half of

North America is also a region of relatively high PWV trends, greater than 0.1 mm/year. Figure 47 shows the Northern Hemisphere summer autocorrelation factor, which is generally 0-1, similar to the Northern Hemisphere winter autocorrelation factor. The Northern Hemisphere summer standard deviation with 0% measurement error is shown in Figure 48. Generally, the natural variability is low, less than 1 mm, in most places except for localized areas over Indonesia, the Middle East, and India. The GISS has the lowest values of all the models, not exceeding 2 mm. Figure 49 shows the Northern Hemisphere summertime TTD, which is low in most places, generally ranging from 5-15 years. The longest TTD, greater than 50 years, occurs in the Southern Hemisphere, especially near the South Pole. This area has relatively low PWV and small trends, which might explain the long TTD. Figure 50 shows the Northern Hemisphere summer standard deviation with a 1% measurement error, which does not affect the Northern Hemisphere summer standard deviation greatly, except near areas of already high natural variability. The Northern Hemisphere summer TTD with 1% measurement error is shown in Figure 51, which has only slightly increased from the 0% measurement errors. Generally, the TTDs are between 5 and 15 years. Figure 52 shows the standard deviation with a 5% measurement error for Northern Hemisphere summer. The 5% measurement error increases the standard deviation by almost 3X that of the natural variability in the Northern Hemisphere, specifically between 0^{o} and 30^{o}N. Figure 53 shows the Northern Hemisphere summer TTD with 5% measurement error, which is longer, ranging from 15 to 50 years. The longest time

occurs in the Southern Hemisphere, coinciding with the area of generally smaller PWV amounts.

Figure 54 shows an example of Northern Hemisphere springtime PWV. The PWV is highest near the equator and there is no shift towards the south or north as seen in the Northern Hemisphere summer and Northern Hemisphere winter PWVs. Figure 55 shows the Northern Hemisphere spring 100-year trend, which is highest in the Pacific Ocean. Generally the GISS-E2 has the smallest PWV trends, with nothing larger than 0.15 mm/years overall. The Northern Hemisphere spring autocorrelation factor is shown in Figure 56. The highest autocorrelation factors generally occur in the CCSM3 especially near the equator around South America, Africa, and Indonesia, with values exceeding 3. Figure 57 shows the Northern Hemisphere spring standard deviation with 0% measurement error. The CCSM4 has the highest standard deviation compared to all the models. Generally, however, the standard deviation is low, 0-1 mm, with higher values near the tropics, reaching 2-4 mm. The Northern Hemisphere spring TTDs are shown in Figure 58, which tend to be small (5-10 years), especially in the CCSM3 and CCSM4. The GISS and GISS-E2 have more localized areas of extremely long TTDs, greater than 40 years, particularly in the Polar Regions. Figure 59 shows the Northern Hemisphere spring standard deviation with 1% measurement error. This is almost identical to the 0% measurement error in Figure 57. The Northern Hemisphere spring TTDs with 1% measurement error do not change much from the 0% error, as shown in Figure 60. Figure 61 shows the Northern Hemisphere spring standard deviation with a 5%

measurement error, which is drastically different from the 0% measurement error. The greatest standard deviation occurs in the tropics and there is a broad area from 35°S to 35°N with values between 2-5 mm or higher. The 5% measurement error has overwhelmed the natural variability and has created long Northern Hemisphere spring TTDs, shown in Figure 62. Generally, the Northern Hemisphere spring TTDs with 5% measurement error are between 15-30 years.

Figure 63 shows the Northern Hemisphere fall PWV that is greatest near the tropics. There is a slight shift to the north of the equator compared to the Northern Hemisphere spring PWV, but it is not as enhanced as the Northern Hemisphere summer and Northern Hemisphere winter PWV shifts. The 100-year trend for Northern Hemisphere fall is greatest near the equator, especially over India, Indonesia and the Pacific Ocean as seen in Figure 64. The GISS-E2 generally has the smallest trends with nothing greater than 0.1 mm/years. Figure 65 shows the autocorrelation factor for the Northern Hemisphere fall, which is generally less than 1. The natural variability is largest in the CCSM3 and the CCSM4 as seen in Figure 66, with the largest values, greater than 5 mm, in the Pacific Ocean and Indonesia. Figure 67 shows the TTDs for Northern Hemisphere fall with a 0% measurement error. The TTDs are low in the CCSM3 and CCSM4 ranging from 5-15 years, while the GISS and GISS-E2 are larger with more localized areas of long TTDs (greater than 50 years), however, the TTDs are generally less than 15 years in these two models. The 1% measurement error does not affect the Northern Hemisphere fall standard deviation (Figure 68) or the TTDs (Figure 69) substantially. Figure 70

shows the Northern Hemisphere fall standard deviation with a 5% measurement error. In Northern Hemisphere fall, this measurement error severely affects the standard deviation similarly to the Northern Hemisphere spring standard deviation with a 5% measurement error; values exceed 5 mm in some areas. A wide band with high standard deviations (> 2 mm) is created between 35°S to 35°N. These high standard deviations in turn affect the Northern Hemisphere fall TTDs, which are substantially larger (Figure 71). The CCSM3 and CCMS4 have TTDs larger than 15 years, while the GISS and GISS-E2 generally have values higher than 20 years.

ii. Zonal

Figure 72 shows the Northern Hemisphere winter 100-year PWV trend. In all models, the trend is largest in the tropics, where more water vapor exists, and decreases toward the poles. The lowest trends occur in the South Pole. Figure 73 shows the Northern Hemisphere winter autocorrelation factor. The autocorrelation factor is smallest in the tropics but generally does not exceed 2. Figure 74 shows the Northern Hemisphere winter standard deviation, which is highest in the tropics, where the natural variability is the greatest. The standard deviation never exceeds 3.5 mm in any of the models. The Northern Hemisphere winter TTDs are shown in Figure 75. The TTDs tend not to vary by zone as much as the all season TTDs do, except for the GISS, which shows significantly higher TTDs (greater than 30 years) in the Southern Hemisphere. Overall, the TTDs are mostly less than 20 years.

Figure 76 shows the Northern Hemisphere summer 100-year PWV trends, which are greater in the tropics and the Northern Hemisphere. The autocorrelation

factor generally has no pattern as shown in Figure 77. Overall, the autocorrelation factors are smaller than 2. Figure 78 shows the Northern Hemisphere summer standard deviation, which is highest in the tropics and generally larger in the Northern Hemisphere than in the Southern Hemisphere, by at most 1 mm. The measurement error affects the standard deviation more in the tropics than in the South Pole (zone 1). Figure 79 shows the Northern Hemisphere summer TTDs. The TTDs are greatest in the Southern Hemisphere, where it is Northern Hemisphere winter and generally lower PWV amounts would be expected. The TTD does not change by much from one zone to the next except for zone 1, the South Pole, where the TTD is highest, about 20-25 years. The zonal average in Northern Hemisphere summer is higher than most zones in the Northern Hemisphere.

Figure 80 shows the 100-year Northern Hemisphere spring PWV trend. The trend is greatest near the equator and decreases poleward. The smallest amounts occur in the South Pole. The Northern Hemisphere spring autocorrelation is shown in Figure 81 and is generally less than 1. The GISS-E2 has the largest autocorrelation factor, almost reaching 2 in zone 3 and zone 8. Figure 82 shows the Northern Hemisphere spring standard deviation. The standard deviation is smallest near South Pole and greatest near the equator. The difference between the South Pole and North Pole is not as big as seen in the Northern Hemisphere winter and Northern Hemisphere summer standard deviation, with a difference of less than 0.25 mm. The Northern Hemisphere spring TTDs are shown in Figure 83. The highest TTDs occur in the Poles, but tend not to change that much across the zones,

except in the GISS-E2. The zonal average is sometimes larger than certain zones, for example near the equator, but small in others, like in the South Pole. Generally the TTDs are less than 20 years for 5% measurement error.

Figure 84 shows the Northern Hemisphere fall PWV trend. The PWV trend is greatest in the tropics and smallest in the South Pole. Generally, the Northern Hemisphere has higher trend than the Southern Hemisphere. The CCSM3, CCSM4, and GISS-E2 have the smallest autocorrelation factor near the equator as seen in Figure 85, whereas the GISS-E2 has the largest autocorrelation factor near the equator, almost 2.5. Figure 86 shows the Northern Hemisphere fall standard deviation, which is greatest in the tropics and smallest at the poles but never exceeds 3 mm. The zonal average tends to be in between the standard deviation of all the individual zones. The smallest standard deviation occurs in the South Pole. Figure 87 shows the Northern Hemisphere fall TTD that is greatest at the South Pole, most likely to the small trends that are predicted in this area. All the other zones show similar TTDs, there is not much difference between each individual zone or the zonal average. TTDs are usually less than 15 years is all zones.

iii. Global

Table 27 shows the global TTD statistics for Northern Hemisphere winter. The Northern Hemisphere winter trend ranges from 0.024 to 0.031 (Table 27a). Table 27b shows the Northern Hemisphere winter autocorrelation. The models all have autocorrelation factors less than 2 except for the CCSM4 which has an autocorrelation factor greater than 7. The Northern Hemisphere winter standard

deviation (Table 27c) is largest in the GISS for 0% measurement error. The TTDs, Table 27d, are within 4 years of each model. The measurement error increases the TTD differently for each model. For example, the difference between the TTD for a measurement error of 5% compared to 0% is greatest in the CCSM4 model (53.3 to 4.8 years), a difference of almost 50 years, while the difference in the CCSM3 is only 24 years.

Table 28 shows the global TTD statistics for Northern Hemisphere summer. The trends are similar (Table 28a) to those seen in the Northern Hemisphere winter ranging from 0.02 to 0.03 mm/year. The autocorrelation is largest in the CCSM4 and smallest in the GISS. CCSM3 has the smallest natural variability, 0.01 mm and CCSM4 has the largest, 0.04 mm. CCSM3 has the smallest TTD, Table 28d, of 1.6 years with a 0% measurement error, which would be expected due to low natural variability and autocorrelation factor. The CCSM4 has the largest TTD for 0% measurement error at around 5.5 years. Generally, all models agree within 4 year and no model exceeds 51 years.

Table 29 shows the MAM Global TTD statistics. The 100-year trend is between 0.02 and 0.03 mm/years, similar to the previous trends. The autocorrelation factor is smallest in the CCSM4, but no models exceed 2. The Northern Hemisphere spring standard deviation is largest in the CCSM4, 0.09 mm, and is almost double that seen in the GISS at 0.05 mm (Table 29c). The GISS has the lowest standard deviation, but does not have the smallest TTD (Table 29d), possibly due to the large autocorrelation factor and small trend. The largest Northern

Hemisphere spring TTD, 39.4 years, occurs in the GISS with a 5% measurement error.

Table 30 shows the Northern Hemisphere fall TTD statistics. The range of PWV trends is again between 0.02 to 0.03 mm/year. The lowest autocorrelation factor is in the CCSM3 and more than triples in size in the CCSM4. Northern Hemisphere fall global standard deviation is around 0.02 mm for CCSM3, the smallest, while the CCSM4 has the largest at 0% measurement error 0.078 mm. The CCSM3 had the lowest TTD of 1.3 years (Table 30d), most likely due to the low standard deviation and autocorrelation factor. The largest TTD occurs in the CCSM4 model at 43.1 years, which might be due to the relatively high autocorrelation factor and standard deviation.

B. Case-Study Regions TTD PWV Trends

Case study TTD results are discussed below by first analyzing the all seasons results for the four different regions (China, Europe, India, and U.S.). Figure 1 shows the bounding box for each of these regions. The TTD results will include the trend, autocorrelation timescale, standard deviation, and TTD. Then the TTD results will be broken into the four seasons.

1. All Seasons TTD PWV Trends

Table 31a shows the all seasons trend results for China. The models are within 0.2 mm/year of each other, with the largest trend in the CCSM4 and the smallest in the GISS-E2. The CMIP3 models agree with each other within 0.0003 mm/year and the CMIP5 models agree with each within 0.2 mm/year. Table 31b

shows the autocorrelation timescale for china. These values due not change by much from one model version to another (CMIP3 to CMIP5), however, the CCSM3 and CCSM4 show values over 2 while the GISS and GISS-E2 show values less than 2. The standard deviation is shown in Table 31c for China. The numbers remain relatively similar between the version change. The CCMS3 and CCMS4 have the highest values (almost greater than 2 mm), while the GISS and GISS-E2 remain slightly under 2 mm. Table 31d shows the TTD for China. The TTD is around 25 years for 0% measurement error and increases to at most 32 years with a 5% measurement error.

Table 32a shows the all season trend results for Europe. The trends range from 0.03 mm/year to 0.04 mm/year, significantly smaller than the trends in the other three regions. The autocorrelation timescale is largest the GISS at 1.9 as seen in Table 32b. Table 32c shows the standard deviation for Europe, in which the models agree relatively well (within 0.3 mm). The measurement error affects the standard deviation minimally, increasing it by 0.4 at the most. Table 32d shows the TTD for Europe. The smallest TTD occurs in the CCSM4 at 19.1 years and the largest occurs in the GISS-E2 at 27.3 years for 0% measurement error. These TTDs never exceed 34 years.

Table 33a shows the all season trend for India, which is around 0.11 mm/year for all models. This trend is the largest out of all the case-study regions, indicating the greatest increase in PWV, which in turn could affect the amount of rain in the region. The autocorrelation timescale is shown in Table 33b for India.

The timescale are greatest in the GISS models, close to 2. Table 33c shows the India standard deviation. All the models agree within 0.7 mm. The largest natural variability (0% measurement error) occurs in the CCSM4 (2.7 mm) and the largest standard deviation occurs in the CCSM4 with a 5% measurement error (3.5 mm). India TTDs are shown in Table 33d. The range of TTDs is 16 years to 30 years; this is the largest range of TTDs out of all the regions. India, also, has the smallest 0% measurement error TTD, suggesting that the large predicted trend might help significantly in detecting the trend, but the large standard deviations with increasing measurement error hampers this effect.

The U.S. all season trends are shown in Table 34a. These trends increase from the CMIP3 models (0.0552 mm/year and 0.0555 mm/year for the CCSM3 and GISS respectively) to the CMIP5 models (0.0681 mm/year and 0.0576 mm/year for the CCSM4 and GISS-E2 respectively). Table 34b shows the autocorrelation timescale for the United States. The largest timescale is with the CCSM3, 2.2, while the other models are less than 2. In addition, the autocorrelation timescale has dropped from the older models (CMIP3) to the newer models (CMIP5), suggesting differences in the scenario used or model changes. Table 34c shows the U.S. standard deviation, in which the models agree to 0.1 mm. The largest standard deviation is 2.2 mm in the CCSM4 at 5% measurement error, while the largest natural variability actually occurs in the CCSM3. Table 34d shows the TTD for the United States. The range is 20 years to 32 years.

2. Seasonal TTD PWV Trends

The DJF trend is expected to be the smallest out of all the seasons for China, at around 0.045 mm/year, as shown in Table 35a. China's DJF autocorrelation timescale is shown in Table 35b. All the models agree within .6 and the GISS, CCSM4, and GISS-E2 are all less than 1. The Northern Hemisphere winter standard deviation for china is smallest in the CCSM3 and increased by almost double in the CCSM4, while the GISS-E2 decreased only slightly from the GISS (Table 35c). The DJF TTD for china is smallest in the GISS and GISS-E2 models, probably due to the smaller autocorrelation factor, as seen in Table 35d. The maximum TTD that occurs in the GISS-E2, which has the smallest overall TTDs, is 18 years, suggesting that looking at regional and seasonal trends could lead to faster TTDs. The JJA trend for China is shown in Table 36a and ranges from 0.098 mm/year to 0.14 mm/year. The trends are larger in the CCSM models. The autocorrelation timescale for JJA is shown in Table 36b. The values range from 0.05 to 1 and are larger in the CCSM models. The Northern Hemisphere summer standard deviation for china is shown in Table 36c and is similar to the Northern Hemisphere winter standard deviation. Northern Hemisphere summer china TTDs are the smallest for any season, as low as 7.8 years, which might be due to the high trends. The longest TTD value is 17.3 years. Table 37a shows the Northern Hemisphere spring China trend that is around 0.065 mm/year. The autocorrelation timescale for all the models, shown in Table 37b, agrees within 0.3, while the standard deviation had a significant increase from the CCSM3 to the CCSM4 of more than .5 mm as shown in Table 37c. This increase is similar to the increase seen in the Northern Hemisphere winter standard deviation.

The Northern Hemisphere spring TTDs range from 11.3 years to 20.7 years. Table 38a shows the SON trend for China, which ranges from 0.06 mm/year to 0.11 mm/year. The autocorrelation timescale is greatest in the CCSM3, 1.1, and smallest in the GISS-E2, 0.6, as shown in Table 38b. The standard deviation for Northern Hemisphere fall increases in the newer models by at most .7 mm (Table 38c). Lastly, the Northern Hemisphere fall TTDs, shown in Table 38d, are relatively small ranging from 11.7 years to 19.7 years. An interesting note is the CCSM4 has the smallest TTD with a 5% measurement error but has the second highest TTD with a 0% measurement error, implying that since the CCSM4 has relatively smaller absolute PWV values; the increase in the measurement error does not affect the TTD as much. Seasonal TTDs are smaller than the all season TTDs by 10-15 years.

The DJF trend for Europe is shown in Table 39a. These values are the smallest out of all the regions, ranging between 0.025 mm/year and 0.033 mm/year. The autocorrelation timescale for Northern Hemisphere winter is shown in Table 39b and the models agree within 0.2. Table 39c shows the Northern Hemisphere winter standard deviation for Europe. The values never exceed 1 mm and generally the models agree within .2 mm. The Northern Hemisphere winter TTDs are shown in Table 39d and never exceed 25 years. The TTDs range from 15 years to 25 years and the smallest occurs in the CCSM3, which had both the smallest standard deviation and smallest autocorrelation timescale. Table 40a shows the JJA trend for Europe, which is around 0.05 mm/year. The JJA autocorrelation timescale is shown in Table 40b and ranges from 0.6 to 1.4. The autocorrelation decreases from the

older versions to the newer versions by .1 to 1. Table 40c shows the Northern Hemisphere summer standard deviation, which agree within 0.1 mm and never exceeds 2 mm. The TTDs are 14 to 26 years, as shown in Table 40d. All the TTDs, no matter the measurement error are substantially smaller than the all season TTDs, demonstrating the need to break down seasons. Table 41a as shows the Northern Hemisphere spring trend for Europe, which is relatively small, nothing greater than 0.03 mm/year. The autocorrelation timescale for Northern Hemisphere spring is shown in Table 41b and the values range from 0.6 to 1.1. Table 41c shows the MAM standard deviation for Europe, which is generally around 0.5 mm. The Northern Hemisphere spring TTDs are shown in Table 41d. These values increase from the older models to the newer models by 1-2 years. The TTDs, however, are still lower than the all season TTDs, not exceeding 26 years. Table 42a shows the SON Europe trend, which ranges form 0.03 mm/year to 0.05 mm/year. The autocorrelation timescale, shown in Table 42b, is smallest in the CCSM3 and GISS. SON standard deviation is shown in Table 42c, and ranges from 0.6 mm to 1.3 mm. Table 42d shows the Northern Hemisphere fall TTD, with the highest TTD in the GISS-E2 of 23.1 years, the other models never even exceed 20 years. The smallest TTD is 12.5 years, again illustrating the benefits of regional seasonal trend detection.

Table 43a shows the DJF trend for India, which is greater than 0.07 mm/year for all models, much larger than what was found in Europe or China. The Northern Hemisphere winter autocorrelation timescale for India is shown in Table 43b and ranges from as low as 0.55 to 0.98. The Northern Hemisphere winter standard

deviation is greatest in this region than in any other region in Northern Hemisphere winter, as seen in Table 43c; never less than 1.7 mm and never greater than 3 mm. India's TTDs range from 14 years to 23 years as shown in Table 43d. Table 44a shows the Northern Hemisphere summer trend for India, which is the greatest out of all seasons, around 0.1 mm/year. The Northern Hemisphere summer autocorrelation timescale decreases from the older models to the newer models, similar to the previous regions. The Northern Hemisphere summer standard deviation, shown in Table 44c, ranges are 1.1 mm to 3.3 mm. Table 44d shows the Northern Hemisphere summer TTD for India, which range from 8.5 years to 17.2 years. Generally, the TTD difference between the 0% and 5% measurement error is 7 years. The CCSM4 has the second smallest TTD at 0% measurement error, even though it has a large natural variability, suggesting that higher trends are easier detect even with high natural variability. Table 45a shows the MAM trend for India, which ranges from 0.07 mm/year to 0.1 mm/year. The autocorrelation timescale for Northern Hemisphere spring, Table 45b, decreases from the CMIP3 models to the CMIP5 models, and the standard deviation is within .6 mm of all the models, as seen in Table 45c. Correspondingly, the Northern Hemisphere spring TTD is smallest, around 12 years, with models that have the lowest natural variability and autocorrelation timescales, as shown in Table 45d. The TTDs, however, do not exceed 24 years, implying again that the seasonal TTDs are better than the all season. Table 46a shows the Northern Hemisphere fall trends for India, which is around 0.12 mm/year. The autocorrelation timescale, Table 46b, for Northern

Hemisphere fall ranges from 0.8 to 1.3. The Northern Hemisphere fall standard deviation is greatest in the CCSM4 and smallest in the CCSM3, but the models again agree within .5 mm. Northern Hemisphere fall TTDs are comparatively small to the all season TTDs, ranging from 10 years to 19.3 years, Table 46d. Models with higher natural variability and autocorrelation factors had higher TTDs, and the GISS-E2, which had the smallest trend, had the largest TTD.

Table 47a shows the Northern Hemisphere winter U.S. trend, which increases from the CMIP3 models to the CMIP5 models, ranging from 0.03 mm/year to 0.05 mm/year. The Northern Hemisphere winter autocorrelation timescale for the U.S. is shown in Table 47b, and is around 0.9 for all models except the GISS-E2, which is 0.685. Table 47c shows the Northern Hemisphere winter U.S. standard deviation, which, similar to the other regions, increases from the CCSM3 to the CCSM4 and decreases from the GISS to GISS-E2. The smallest natural variability occurs in the CCSM3 at 0.84 mm while the largest occurs in the CCSM4 at 1.1 mm for 0% measurement error. Consequently, the CMIP3 models have higher TTDs than the CMIP5 models as shown in Table 47d. The CMIP3 models range from 17 to 24.4 years, while the CMIP5 models do not exceed 24 years. Table 48a shows the Northern Hemisphere summer U.S. trend, which is around 0.07 mm/year for all models. The Northern Hemisphere summer U.S. autocorrelation timescale is shown in Table 48b and is around 1 for all the models, except CCSM4. Table 48c shows the Northern Hemisphere summer U.S. standard deviation that increases from the CCSM3 to the CCSM4 and decreases from GISS to GISS-E2. The natural variability

ranges from 0.68 to 0.88 mm. Table 48d shows the Northern Hemisphere summer TTDs that range from 10.3 to 21.2 years, notably smaller than the all season TTDs for this region. The models all show a TTD of around 11 years for 0% measurement error. Table 49a shows the Northern Hemisphere spring U.S. trend, which ranges from 0.066 mm/year to 0.0556 mm/year and again these trends increase or stay roughly the same in the newer models. The Northern Hemisphere spring autocorrelation timescale for the U.S. is shown in Table 49b and ranges from 0.65 to 1.02. Table 49c shows the Northern Hemisphere spring standard deviation, which is greatest in the CCSM4 at 1.04 mm for 0% measurement error. Consequentially, the Northern Hemisphere spring TTD is largest in the CCSM4 for 0% measurement error at 15.8 years, as seen in Table 49d, however, none of the models exceed 22 years. Northern Hemisphere fall U.S. trends are shown in Table 50a and range from 0.062 mm/year to 0.082 mm/year, increasing in the CMIP5 models. The autocorrelation timescale for Northern Hemisphere fall ranges from 0.65 to 0.83, almost a .4 difference. Table 50c shows the Northern Hemisphere fall U.S. standard deviation, which increases in the new models, CMIP5. The standard deviation ranges from 0.8 to 2 mm. Accordingly, the U.S. Northern Hemisphere fall TTDs are largest in the CCSM3, which had the lowest trend. The TTDs never exceed 19 years and are at least 11 years, as seen in Table 50d.

C. Estimate AIRS PWV Uncertainty

1. Satellite Comparison over Ocean

To evaluate the models and the NASA AIRS product over the ocean, AMSR-e was used to represent truth data in the absence of SuomiNet GPS. For this evaluation, two months were analyzed, February 2006 and August 2006 to explore seasonal effects. In addition, two transects were examined that allowed for the assessment of latitude and longitude dependence. Figure 88 shows the constant latitude transect, which was an average from 34°N to 39°N which includes the DOE ARM site and the surrounding Oklahoma/Kansas region used for SuomiNet validation. This latitude swath crosses over both ocean and land, as well as very dry areas, deserts, and more moist mid-latitude areas. Figure 89 shows the models and observations of PWV over this region by longitude for August 2006. The PWV ranges from 8 mm to 52 mm. In areas of higher amounts of PWV, the GISS-E2 and the CCSM3 model tend to have substantially lower amounts of PWV compared to the observations. For example, around 75°W the CCSM4 and GISS-E2 are more than 10 mm less than the other models and observations or 25% error. Although there are differences between AIRS L3 ascending and descending over the ocean, AIRS L3 V5.0 agrees well with AMSR-e as seen in Figure 91 which shows the percent error for AIRS L3 as compared to AMSR-e; the red lines represent the 5% error. The percent error ranges from -30% to 30%, with the extremes predominantly occurring near 0°. On average (average of the percent errors), however, AIRS agrees with the AMSR-e in August within 2.5% for 08 UTC and 6% for 19 UTC. Figure 90, which shows the same observations and models over this region but for February 2006, indicates greater differences among models, especially in the Western

Hemisphere but still good agreement among the observations. CCSM4 tends to over estimate the PWV in the Atlantic Ocean (70E-40E) while the GISS-ER underestimates it. Figure 92 shows the percent error for AIRS in February, where the red lines show the 5% error. Generally, AIRS L3 is within 6% of the AMSR-e at 08UTC and 3% at 19UTC. Table 51a and 51b shows the 95th percentile for this region. The lower bound is -14% for all months and times, while the upper bound is either 8% or 10%. AIRS L3 descending (night) appears to agree better with AMSR-e over the oceans than the ascending (day). Figure 93 shows the second transect, which was an average from 87^{o}W to 100^{o}W for all latitudes. This swath is primarily over ocean in the Southern Hemisphere and land in the northern, including the SuomiNet validation region from Texas to Minnesota (Roman et al. 2012). Figure 94 shows the models and observations for August 2006 over this region. CCSM3 and GISS-E2 are almost 10 mm too low between 20^{o}N and 40^{o}N. This region is the U.S. Great Plains, which in Northern Hemisphere summer experiences intense moisture flow from the Gulf of Mexico up to the Great Plains and northern states that is not well represented in these models. AIRS L3 A and D agree well with the SuomiNet observations that are available over land, deviating at most by 10%. From 0^{o}S to 20^{o} S AIRS L3 A tends to agree well with AMSR-e, which can be better observed in Figure 96 which shows the percent error for august, but then becomes too low around 50^{o}S, where the percent error is almost 20%. The AIRS L3 is generally within 2% of the AMSR-e for 08UTC and 4% for 19 UTC. In contrast, Figure 95 shows the February 2006 PWV, in which the models and observations agree well in

the Northern Hemisphere but experience large differences near the equator and southward. Figure 97 shows the percent error for AIRS L3 in February for this region, which shows the larger percent error in the Southern Hemisphere, exceeding 20% in some cases. On average though, AIRS L3 is within 6% of the AMSR-e measurements in the region. Table 52a and 52b shows the 95th percentile for this region, which has higher upper bounds than the previous region. The variation between month and overpass time is greater for the upper bound, ranging from 10-16%. Again, the lower bound is -14%.

2. Satellite Comparison over Land

i. AIRS L3 PWV Climatology Trend Validation

The AIRS L3 product is intended to be a climate product, to assess climatological trends. A previous study by the author found an anomalous trend in the AIRS L3 product detected after 2007 when compared to ground-based SuomiNet stations (Roman et al. 2013). Figure 98 shows this analysis performed over the Oklahoma/Kansas region. At the beginning of 2008 there is a steep upward trend in the difference between AIRS L3 and SuomiNet of around 1 mm/year. Note that AIRS L3 v5.0 is used through 2006 while AIRS L3 v5.2 is used from 2007-2012. The following results will further investigate this difference. Many things could potentially be the cause of this difference: the different versions of AIRS L3, elevation correction problems, and sampling issues. Figure 103 shows an updated version (through December 2012) of the SuomiNet comparison to AIRS L3 v5.2. Adding one year of data has decreased the trend error by almost half at the 08 UTC

time, however, this could possibly be do to the positioning of the trend error (i.e. choosing the cut off point to start the trend and to end the trend). When compared to v6 in Figure 104, the trend error decreases even more, especially at the 19UTC time, indicting this difference might have been resolved over version changes, however, the peak-to-peak difference between the two measurements still ranges from plus or minus 2 mm. The MWR at Lamont, OK, provides a third truth dataset that has been well tested and assessed to compare the AIRS L3 difference. Figure 99 shows the AIRS L3 v5.2 differenced to the MWR. From this figure there is a slight trend, 0.281 mm/year at 08 UTC and 0.422 mm/year at the 19 UTC, but not nearly as large as seen in the SuomiNet analysis. When compared to AIRS L3 v6 in Figure 100, the trend error drops significantly to about 0.1 mm/year in both times, again suggesting there was a correction change from v5.2 to v6. Since the difference between the MWR and AIRS is relatively small compared to the difference between SuomiNet and AIRS, there might be a problem with the SuomiNet data. To further investigate this the NPN dataset was used, which uses the same stations but processes the GPS data differently (King and Bock 1996). Figure 101 shows the AIRS L3 v5.2 compared to the NPN data. The trend error is significantly lower, 0.02 mm/year at 08 UTC and 0.211 mm/year at 19 UTC. This remains small and further decreases in the v6 comparison, shown in Figure 102, with a trend error around 0.05 mm/year at both times, suggesting that there may be an issues with the SuomiNet GPS dataset. Figure 105 shows the NARR compared to the AIRS L3 v5.2 and Figure 106 shows v6. In Figure 106, similar trend errors are seen when AIRS L3

v6 is compared to SuomiNet, which might be due to the assimilation of SuomiNet into the NARR starting in 2007. To better quantify these results, Table 53 shows the AIRS L3 v5.2 trend error values and Table 54 shows the AIRS L3 v6 trend error values. From Table 53, it is clear that the 19 UTC overpass has a greater trend error, at least double, than the 08 UTC for all datasets. Table 54 shows the opposite; for v6 the 19 UTC has a smaller trend error than the 08 UTC, but the difference is only .02 to .03. From the version change (v5.2 to v6), all the trend errors have decreased except for the NARR in which the trend error has more than doubled in v6.

From this analysis, it appears this trend error is reduced through versions changes (5.2 to 6). One of the main differences in version 6 is the number of points used to calculate the $1^{o}x1^{o}$ grid value. Figure 107 shows the number of points used to calculate the Oklahoma/Kansas regional average for the AIRS L3 v5.2. The number stays around 160 for both ascending and descending, with drops around November 2003 and January of 2010. Figure 108 shows the same thing but for the new version, v6, of AIRS. The number fluctuates around 700 points, with a drop to 300 occurring in January 2010. This implies that the number of sounding points available to calculate the grid box averages has dramatically increased from v5.2 to v6, suggesting the change might have created a product that is more similar to the ground-based data.

Although the version change of AIRS explains some of the error trend, there is still a substantial difference between SuomiNet and AIRS not seen in the MWR or NPN datasets. When creating the regional averages, an elevation correction is

applied to account for topographic differences (Roman et al. 2012). A quadratic equation was used to calculate the PWV correction based on the height of each individual station, and originally the coefficients for this equation were based off all stations available in the CONUS area, i.e. one set of coefficients for the whole continental United States, not limited to each individual region. Figure 111 shows the elevation correction for the Oklahoma/Kansas region done using this method but also by creating a correction using only the stations that lie within the region (i.e. one set of coefficients for each region). From the figure, there is little difference between the two methods, except for stations that lie around 300-500 meters above sea level and generally this difference is greater in the Northern Hemisphere summer. This difference, however, is only 2-3 mm, suggesting that this is not affecting the SuomiNet data enough to create the large trend errors.

From this investigation, it has become clear that something is causing the SuomiNet data to be different from the MWR and the NPN, creating the large error trends after 2007 when compared to AIRS. Figure 109 shows the number of SuomiNet stations used to calculate the monthly regional average. The number of stations used increases from 2002, with around 15 being used, to a maximum of 25 at the beginning of 2008. From there the number of stations continuously drops. This suggests that the decrease in the number of stations might be affecting the monthly regional PWV values. Figure 110, however, shows the number of NPN stations used to calculate the same monthly regional averages. The number stays around 26 for many years, but then begins to drop after 2007. Since these two

datasets generally use the same GPS sites, it is not surprising that the number of stations used is similar. The NPN dataset, however, did not have the error trend that the SuomiNet dataset had, implying that this reduction in the number of stations should not be affecting the SuomiNet dataset.

The NPN GPS data sites are essentially the same as the SuomiNet dataset sites, the raw GPS data should be the same and the sites used should be the same. The main difference is the processing; NPN is processed through the NOAA's Earth System Research Laboratory using the GAMIT software. The SuomiNet dataset, obtained through the ARM program, is processed using the Bernese 5.0 software from January 2006 onward. Prior to 2006, the data was processed using an earlier version of the software, v4.2. Although there could still be many possible reasons for the discrepancy between AIRS and SuomiNet, this study has suggested that the SuomiNet processing might be a potential problem.

ii. AIRS PWV Diurnal Sampling Validation

AIRS PWV products have two types of errors, sampling and measurement. Bedka et al. (2010) characterized this measurement error at the U.S. ARM SGP site and concluded that the AIRS L2 v5.0 product had an accuracy of about 5% for all skies. A dry bias, however, was observed at night during the Northern Hemisphere summer of about 10% when compared to the MWR sensor in Lamont, OK (Bedka 2010). A further study was completed that compared the AIRS L2 v5.0 product to the SuomiNet dataset. Figure 112 shows the difference between AIRS L2 v5.0 in the Oklahoma/Kansas region to the SuomiNet GPS. The SuomiNet GPS data is for all

times, meaning an average over the day. A previous study by this author has shown that no diurnal variation occurs in the GPS product, eliminating the need to perform the analysis at the same time stamp as AIRS. There is a seasonal dry bias in the AIRS nighttime (08 UTC) PWV product during Northern Hemisphere summer of up to 10 mm. The daytime AIRS overpasses show errors that range from +5 to -15 mm, but without a distinctive pattern. Figure 113 shows a nine-year histogram of the difference with a nine-year nighttime (08 UTC) mean bias between -3.5 mm +- 5 mm, or less than 10% (Roman et al. 2013). The AIRS L3 product was also examined, but due to the discrepancy in the trend error, further analysis will be performed and new results are discussed below using AIRS v5.2 and v6, both updates to the previous v5.0.

Figure 114 shows the 10-year (December 2002 – December 2012) AIRS L3 v5.2 histogram difference to SuomiNet. The mean difference is largest at 08 UTC (nighttime overpass), about -0.758 mm with a standard deviation of 2.31 mm. When the same comparison is done for v6, Figure 115, but from January 2006-November 2012, the mean is now smallest over the nighttime overpass with a mean of -0.072 mm and a standard deviation of 1.65 mm. A substantial change has been made from v5.2 to v6, possibly to do with the large increase in the number of samples utilized that was previously discussed. When compared to the MWR in Figure 116, AIRS L3 v 5.2 shows the largest 10-year mean bias at night but this drops in the version change to v6 (6 year difference) as seen in Figure 117. Figure 118 shows the 10-year AIRS L3 v5.2 difference to the NPN network, the bias is smaller then the SuomiNet (-

0.564 mm with a standard deviation of 2.36 mm). Like the other datasets, this dry bias at night decreases with the version change to v6 (Figure 119), however, the dry bias increases during the daytime overpass (19 UTC) going from -0.07 mm to -0.399 mm. The difference to the NARR has the largest range of biases -15 mm to 15 mm. Figure 120 shows the 10-year AIRS L3 v5.2 compared to the NARR and Figure 121 shows 6-year AIRS L3 v6 difference to the NARR. Again, the nighttime bias decreases in the newest version but the daytime increases. Even though the standard deviation is quite large, the mean bias is similar to that in the NPN.

To better understand these results Table 55 shows the calculated percent error for AIRS L3 v5.2 and Table 56 shows the calculated percent error for AIRS L3 v6. The greatest percent error occurs with the MWR with an 8% dry bias for AIRS L3 v5.2 08 UTC. In all cases, the nighttime bias decreases from v5.2 to v6, and the daytime biases increase, becoming drier in the new version. Averaging over a region improves the statistical uncertainty relative to the single point measurement of the MWR, as seen in the larger bias in the MWR compared to the regional datasets (NPN, Suomi, and NARR).

VI. CONCLUSIONS

The all season PDF shifts in model derived PWV for the case study regions showed interesting results, suggesting that the high end extremes are what really will be effected, more so than the average of the distributions. India experienced the greatest change with the 99th percentile becoming the 75th to 80th percentile, a change from 1% to 20%-25%. When compared to the global results, the regional analysis provided more information and showed drastic increases in PWV extremes that were averaged out in the global averages. This demonstrated the need for regional analysis; different regions will experience different trends and furthermore the societal impact in different regions will be affected by population density increases.

Seasonal PDF shifts for the regions provided more detail on what will happen in terms of extremes. Generally, all seasons in all regions are expected to increase in PWV amounts; however, this was most substantial in the Northern Hemisphere summer months (JJA) for all regions. All regions showed an increase in the maximum of around 10 mm and a slight increase in the minimum of 1-2 mm. For every season, except Northern Hemisphere summer, the regions showed little increases in the mean, medians, or modes while the higher percentiles increase dramatically, emphasizing the value of this 'extreme analysis'. In all of the regions, the Northern Hemisphere springtime PDF shift was the most difficult to analyze due to generally broad PDFs with varying shapes, suggesting further analysis, maybe monthly, needs to be pursued. The CCSM4 generally showed higher PWV amounts

compared to its previous version, the CCSM3 while the GISS-E2 showed smaller PWV amounts compared to its previous version the GISS, implying different changes were made during the development of the CMIP5 models.

China's most extreme 1% in PWV is expected to become the highest 10% in Northern Hemisphere fall and Northern Hemisphere spring and the roughly 30% for Northern Hemisphere summer, indicating longer periods of extremely high PWV amounts, perhaps leading to a longer wet season and the potential for more torrential downpours throughout the year. Europe's greatest change is expected in Northern Hemisphere summer, and although it is difficult to interpret the change in the PDF shift figure, the extreme 1% is expected to become the extreme 12%, while the extreme 5% is expected to consist of 21% to 50% of the PWV amounts in the last 25 years. Again, this shows that the PWV extremes will change drastically, which could in turn effect flooding, and that only analyzing seasonal averages would not reveal such dramatic results. For India, the Northern Hemisphere fall PWV PDF shift showed to be quite substantial, this coupled with the shift in Northern Hemisphere summer suggest that perhaps a longer monsoon season will occur, which usually runs form June to September. The United States showed a large increase in the probability of PWV amounts in Northern Hemisphere summer and Northern Hemisphere fall, suggesting a longer period of high water vapor amounts. In turn, this could potentially lead to more flash floods during Northern Hemisphere spring and Northern Hemisphere fall. The region did not cover the whole United States; further analysis would be needed to determine what each region in the U.S. would

experience. The global results demonstrated the need for regional seasonal analysis. For the globe, little difference was seen between each season, due to the spatial averaging. The regions, however, proved to be significantly different between each region and for each season, establishing the power of regional seasonal analysis for climate studies.

This thesis has shown that measurement error can severely affect the ability for a satellite sensor to detect a trend in PWV. In addition, the spatial sampling can help or deter the TTD. Although global TTDs are fairly low with 0% and 1% measurement error the number is too large for current measurement errors, greater than 1%. Regional TTDs offer a chance to narrow down the trend in particular regions, which may be important in the future when considering societal impact of climate change. The global TTDs ranged from 2 to 50 years depending on the model and measurement error, but certain regions were able to detect these trends generally within 10-30 years for measurement errors of up to 5%. Zonal TTDs varied from 5 to 50 years, suggesting regional studies may prove to be an advantage over zonal analysis in some areas.

Seasonal dependence can also change the TTD trends in PWV. In Northern Hemisphere winter, the regional trends tend to be smaller in the Northern Hemisphere, probably due to the shift of moisture to the Southern Hemisphere during these months, which in turn creates longer regional TTDs in the Northern Hemisphere. Whereas in Northern Hemisphere summer the PWV is greatest in the Northern Hemisphere and larger regional trends are seen, making the TTDs shorter.

Overall, the measurement error affects the TTD similarly to the results in the all seasons (i.e. a 1% measurement error does not alter the standard deviation or the TTD that much but the 5% measurement error causes much longer TTDs). Northern Hemisphere spring and Northern Hemisphere fall regional TTDs are very similar to each other and the regional all season results. The zonal seasonal results showed that the standard deviation and trends change drastically by each zone, highest in the equator and lowest in the poles, but the TTDs generally are similar among each zone, suggesting zonal averages may not provide the best option for detecting trends. Generally, the South Pole had the highest TTDs in every season even though the trends and standard deviation shifted hemispheres during each season. Overall, the global seasonal statistics do not change much from season to season. Averaging over the globe may reduce the TTD at 0% measurement error, but differentiating by season has little affect over large spatial averages and the TTDs are still too large exceeding 20 years at measurement errors greater than 2% in some cases .

The four case study regions provide a wide range of expected trends for all seasons (0.05 to 0.1 mm/years). India had the greatest trends and the smallest TTDs for 0% measurement error, indicating that large trends are easier to detect. The TTDs for all the regions were about the same, generally starting around 25 years and maxing out around 30 years. This could mean that these regions, which appear to be distinctive with individual characteristics (i.e. India and China experience monsoons, while the U.S. and Europe do not), might not be differentiable in the models or there is no need to differentiate them (i.e. the TTD analysis ends up

averaging out or balancing the extremes). For example, India had a high trend, so the TTD would be small, but the standard deviation is higher, compared to, for example, the U.S., increasing the TTD and 'balancing' out the regions.

Overall, the seasonal TTDs are almost 10 years smaller than the all season TTDs for China, suggesting the need for regional seasonal trend studies. Europe, India, and the U.S.'s seasonal TTDs were notably smaller than the all season TTDs, except in the Northern Hemisphere winter. For all regions, the smallest TTDs tended to occur in Northern Hemisphere summer when the trends were high and the natural variability was not exceedingly large. Furthermore, the natural variability generally increased in the CMIP5 models for all regions. In addition, the trends always increased in the newer models for all regions and all seasons, suggesting that significant model changes have occurred or differences exist between scenarios. This analysis has clearly demonstrated the need for seasonal regional trend detection instead of the typical global or zonal detection. Although global TTDs are smaller, the trends are significantly different for each region and each season, which will affect these regions differently leading to various societal impacts.

Over oceans, AIRS L3 v5.0 agrees well with AMSR-e both in February of 2006 and August 2006. Model discrepancy is greatest over land, reaching 30% error, and areas of high PWV amounts, especially in August over the U.S. Great Plains, suggesting a lack of moisture transport from the Gulf of Mexico that is captured in both the ground-based data and the satellites. In drier areas, models and observations tend to agree better with each other, within 5%.

A previous study by the author found that over land an anomaly occurred in the difference between AIRS L3 v5.0 and v5.2 and the SuomiNet dataset. Further investigation suggested that the trend error, which was not seen in the MWR and NPN, could potentially be due to problems with SuomiNet. Both the MWR and NPN data showed little trend errors in the AIRS L3 v6 product, while the SuomiNet, even with the addition of a year, still showed an error trend of around 0.4-0.45 mm/year. Furthermore, both data sets saw a decrease in the trend error when switching to the newer version of AIRS (v6), implying there was a change that has created a product more similar to the ground-based data, potentially due to the 6x increase in the number of data points used to calculate each region. Although the number of stations used in calculating the monthly regional SuomiNet values has decreased since 2008, the number of stations has also decreased in the NPN dataset. The primary difference then between these two ground-based datasets is the processing software, indicating there could be a problem with the Bernese 5.0 software. A new software version will soon be available; version 5.2, and further analysis will need to be conducted to better understand this complex problem.

The diurnal sampling has been shown to be a problem with the AIRS L2 product in previous studies. AIRS L3 products, however, have less statistical uncertainty due to the number of profiles averaged. The AIRS version change (v5.2 to v6), which increased the number of profiles being used in the averaging, has decreased the difference between sounder and the ground-based instruments at night, less than 2%, but has actually increased the difference, creating a larger dry

bias, during the day, greater than 2%. These differences, however, are relatively small, meaning the AIRS L3 product, both versions, is generally unbiased for both daytime and nighttime overpasses.

Over the ocean, AIRS had a larger measurement error with respect to AMSR-e, ranging between +/-30%. On average, the measurement error was around 6% and for the 95% confidence level this measurement ranged between -14% and 12%. Over land, AIRS L3 v5.2 had a measurement error at 19 UTC of less than 1% while at 08 UTC the measurement error was around 3%. In AIRS L3 v6, the measurement error becomes about 1% for 08 UTC and 3% at 19 UTC. This analysis suggests the measurement error ranges from 1% to greater than 10%. Combining this with the TTD analysis, it would take at least 10 years and possibly more than 50 years to detect a global averaged trend in AIRS. At 3% measurement error, what was determined in the AIRS analysis over land, the TTD for the global average would exceed two decades, ranging from 22 to 34 years. The zonal TTDs would range from 10 to more than 50 years, while the regional TTDs could be as low as 5 years, or, depending on the region, more than 50 years. In most of these cases, the TTD is longer than the operational time span of a satellite platform, which implies that a record from multiple satellite sensors will be used in the trend detection. For this reason, absolute accuracies of 1 to 3% in each sensor record will be required so that measured trends can be determined in a reasonable time period. Additional calibration and validation of current and future satellite climatologies of water vapor are needed to demonstrate that the desired level of absolute accuracy has

been achieved before these data can be used to detect the significant regional climate trends in PWV predicted by global climate models.

VII. REFERENCES

Bedka, S., R. Knuteson, H. Revercomb, D. Tobin, and D. Turner, 2010: An assessment of the absolute accuracy of the Atmospheric Infrared Sounder v5 precipitable water vapor product at tropical, midlatitude, and arctic ground-truth sites: September 2002 through August 2008. *J. Geophys. Res.*,**115**, D17310, doi:10.1029/2009JD013139.

Ciach GJ, Krajewski WF (1999b) Radar-rain gauge comparisons under observational uncertainties. J Appl Meteorol 38:1519–1525

Fetzer, E.J., B. H. Lambrigtsen, A. Eldering, H.H. Aumann, and M.T. Chahine, 2006: Biases in total precipitable water vapor climatologies from Atmospheric Infrared Sounder and Advanced Microwave Scanning Radiometer. *Journal of Geophysical Research – Atmospheres*, 111(D9), D09816.

Kawanishi, T.; Sezai, T.; Ito, Y.; Imaoka, K.; Takeshima, T.; Ishido, Y.; Shibata, A.; Miura, M.; Inahata, H.; Spencer, R.W., "The Advanced Microwave Scanning Radiometer for the Earth Observing System (AMSR-E), NASDA's contribution to the EOS for global energy and water cycle studies," *Geoscience and Remote Sensing, IEEE Transactions on* , vol.41, no.2, pp.184,194, Feb. 2003 doi: 10.1109/TGRS.2002.808331

King, R. W., and Y. Bock, 1996: Documentation of the GAMIT GPS analysis software, version 9.4. Massachusetts Institute of Technology and Scripps Institution of Oceanography Rep.,192 pp.

Leroy, Stephen, James Anderson, John Dykema, Richard Goody, 2008: Testing Climate Models Using Thermal Infrared Spectra. *J. Climate*, **21**, 1863–1875. doi: http://dx.doi.org/10.1175/2007JCLI2061.1

Mesinger, Fedor, and et al, 2006: North American Regional Reanalysis. *Bull. Amer. Meteor. Soc.*, **87**, 343–360. doi: http://dx.doi.org/10.1175/BAMS-87-3-343

Ohring, G., and A. Gruber, 1982: Satellite radiation observations and climate theory. Advances in Geophysics, Vol. 25, Academic Press, 237–304

Ohring, George, Bruce Wielicki, Roy Spencer, Bill Emery, Raju Datla, 2005: Satellite Instrument Calibration for Measuring Global Climate Change: Report of a Workshop. Bull. Amer. Meteor. Soc., 86, 1303–1313. doi: http://dx.doi.org/10.1175/BAMS-86-9-1303

Roman, Jacola A., Robert O. Knuteson, Steven A. Ackerman, David C. Tobin, Henry E. Revercomb, 2012: Assessment of Regional Global Climate Model Water Vapor Bias

and Trends Using Precipitable Water Vapor (PWV) Observations from a Network of Global Positioning Satellite (GPS) Receivers in the U.S. Great Plains and Midwest. *J. Climate*, **25**, 5471–5493. doi: http://dx.doi.org/10.1175/JCLI-D-11-00570.1

Roman, Jacola A., Robert Knuteson, Steve Ackerman, David Tobin, William Smith, Henry Revercomb, 2013L Using AIRS to assess the precipitbale water vapor in global climate models (GCMs) with regional validation from SuomiNet. *AIP Conference Proceedings*, **1531**, pp. 480-483; doi:http://dx.doi.org/10.1063/1.4804811

Rothacher, M., 1992: Orbits of satellite systems in space geodesy. Ph.D. dissertation, University of Bern, 243 pp.

Seo, Dong-Jun, J. P. Breidenbach, 2002: Real-Time Correction of Spatially Nonuniform Bias in Radar Rainfall Data Using Rain Gauge Measurements.*J. Hydrometeor*, **3**, 93–111. doi: http://dx.doi.org/10.1175/1525-7541(2002)003<0093:RTCOSN>2.0.CO;2

Soden, B. J.,, D. L. Jackson, V. Ramaswamy, D. Schwarzkopf, and X. Huang, 2005: The radiative signature of upper tropospheric moistening. Science, 310, 841–844.

Solomon, S., D. Qin, M. Manning, M. Marquis, K. Averyt, M. M. B. Tignor, H. L. Miller Jr., and Z. Chen, Eds., 2007: Climate Change 2007: The Physical Science Basis. Cambridge University Press, 996 pp.

Stephens, G. L., et al. (2012), An update on Earth's energy balance in light of the latest global observations, *Nat. Geosci.*, **5**, 691–696, doi:10.1038/ngeo1580.

Sun, Ying, Susan Solomon, Aiguo Dai, Robert W. Portmann, 2006: How Often Does It Rain?. *J. Climate*, **19**, 916–934.=doi: http://dx.doi.org/10.1175/JCLI3672.1

Susskind, J., Blaisdell, J.M., Iredell, L., Keita, F.,Improved Temperature Sounding and Quality Control Methodology using AIRS/AMSU Data: The AIRS Science Team Version 5 Retrieval Algorithm, Geoscience and Remote Sensing, IEEE Transactions, March 2011, Volume 49, Issue 3, pages 883-907

Tian Y, Peters-Lidard DC. 2010. A global map of uncertainties in satellite-based precipitation measurements. *Geophysical Research Letters* 37. DOI: 10.1029/2010GL046008

Trenberth, Kevin E., Aiguo Dai, Roy M. Rasmussen, David B. Parsons, 2003: The Changing Character of Precipitation. *Bull. Amer. Meteor. Soc.*, 84, 1205–1217. doi: http://dx.doi.org/10.1175/BAMS-84-9-1205

Turner, D.D., S.A. Clough, J.C. Liljegren, E.E. Clothiaux, K. Cady-Pereira, and K.L. Gaustad, 2007: Retrieving liquid water path and precipitable water vapor from Atmospheric Radiation Measurement (ARM) microwave radiometers. IEEE Trans. Geosci. Remote Sens., 45, 3680-3690, doi:10.1109/TGRS.2007.903703.

Weatherhead, E., G.C.,Reinsel, C., Tiao, X-L. Meng., D. Choi, W-K., Cheang, T. Keller, J. DeLuisi, D.J. Wuebbles, J.B Kerr, A.J. Mille, S.J. Oltmans, and J.E. Frederick, 1998: Factors affecting the detection of trends: Statistical considerations and applications to environmental data. J. Geophys. Res., 103, 17149–17161.

Wielicki, et al. 2013. Achieving Climate Change Absolute Accuracy in Orbit Bulletin of the American Meteorological Society 2013 (In Press) ; e-View doi: http://dx.doi.org/10.1175/BAMS-D-12-00149.1

VIII. TABLES

Table 1a: China First 25 Years PWV PDF Statistics

Variable/GCM	CCSM3	GISS	CCSM4	GISS-E2
Max	65.0055	64.6395	70.8516	60.852
Min	2.5207	1.8486	2.1255	2.5835
Median	31.8312	34.7271	33.783	29.4663
Mode	46	35	52	32
Mean	30.6561	33.1423	32.9786	29.3429
Std	15.3093	15.8007	16.9285	14.5265
25th Percentile	15	20	16	15
50th Percentile	30	34	32	27
75th Percentile	42	45	46	39
95th Percentile	52	56	56	51
99th Percentile	57	59	60	54

Table 1b: China Last 25 Years PWV PDF Statistics

Variable/GCM	CCSM3	GISS	CCSM4	GISS-E2
Max	78.9029	77.5392	80.8958	70.815
Min	3.45	2.7677	2.8897	3.1618
Median	38.1731	41.0817	40.0573	34.4932
Mode	52	42	63	39
Mean	36.88	39.3306	39.4486	34.3265
Std	18.2946	18.4379	20.3048	16.5368
25th Percentile	17	22	19	17
50th Percentile	35	39	38	31
75th Percentile	50	52	56	45
95th Percentile	61	64	67	58
99th Percentile	67	68	72	62
ΣP(>95%)	0.2103	0.2038	0.2535	0.1555
ΣP(>99%)	0.1198	0.152	0.1856	0.1158

Table 2a: Europe First 25 Years PWV PDF Statistics

Variable/GCM	CCSM3	GISS	CCSM4	GISS-E2
Max	27.6005	40.1268	34.3162	34.4958
Min	6.6942	3.8191	5.2255	3.5759
Median	15.3185	14.9437	17.5499	15.0473
Mode	9	9	10	12
Mean	15.4986	16.2364	18.211	15.885
Std	3.3867	6.2262	5.4675	5.3864
25th Percentile	7	8	9	9
50th Percentile	9	12	13	12
75th Percentile	12	18	18	17
95th Percentile	15	25	22	22
99th Percentile	17	28	24	26

Table 2b: Europe Last 25 Years PWV PDF Statistics

Variable/GCM	CCSM3	GISS	CCSM4	GISS-E2
Max	31.5228	46.626	40.7447	40.788
Min	6.3912	4.6725	7.6115	4.821
Median	17.7416	16.9029	20.0688	17.0262
Mode	11	10	10	12
Mean	18.0472	18.8592	21.0779	18.0727
Std	3.7853	7.2078	6.249	5.8309
25th Percentile	9	9	9	9
50th Percentile	12	13	13	13
75th Percentile	15	20	19	18
95th Percentile	18	28	25	25
99th Percentile	21	33	27	29
ΣP(>95%)	0.2714	0.1279	0.1539	0.1215
ΣP(>99%)	0.1353	0.064	0.0798	0.0378

Table 3a: India First 25 Years PWV PDF Statistics

Variable/GCM	CCSM3	GISS	CCSM4	GISS-E2
Max	70.3763	69.5453	74.1551	65.2707
Min	5.1167	4.4092	4.0714	4.7839
Median	41.0046	39.8532	44.3055	36.7446
Mode	50	53	52	47
Mean	39.6644	38.5682	42.304	35.6881
Std	14.4311	13.5672	14.5804	12.5698
25th Percentile	23	25	26	22
50th Percentile	36	36	40	33
75th Percentile	48	46	51	43
95th Percentile	54	54	58	49
99th Percentile	58	57	62	52

Table 3b: India Last 25 Years PWV PDF Statistics

Variable/GCM	CCSM3	GISS	CCSM4	GISS-E2
Max	83.769	78.8388	86.7711	74.403
Min	7.3243	5.4249	6.167	5.3642
Median	50.6137	46.8002	52.1822	43.9193
Mode	60	42	62	54
Mean	48.9507	46.1236	50.2055	42.3135
Std	17.1478	16.0621	17.2508	14.0596
25th Percentile	28	30	30	27
50th Percentile	44	42	46	39
75th Percentile	57	54	59	50
95th Percentile	65	65	68	56
99th Percentile	70	68	73	60
ΣP(>95%)	0.3434	0.2634	0.3039	0.2793
ΣP(>99%)	0.2424	0.2124	0.1802	0.1959

Table 4a: U.S. First 25 Years PWV PDF Statistics

Variable/GCM	CCSM3	GISS	CCSM4	GISS-E2
Max	42.7939	53.8696	53.7778	54.0926
Min	4.8088	3.2679	4.198	3.264
Median	25.0973	27.8213	30.3247	25.3081
Mode	28	28	28	24
Mean	24.1764	27.1659	29.4976	25.5629
Std	7.6848	10.9905	10.5205	10.6736
25th Percentile	15	15	18	15
50th Percentile	21	25	26	22
75th Percentile	26	33	34	30
95th Percentile	31	41	41	41
99th Percentile	33	44	44	45

Table 4b: U.S. Last 25 Years PWV PDF Statistics

Variable/GCM	CCSM3	GISS	CCSM4	GISS-E2
Max	50.0942	62.5547	61.5144	59.6274
Min	6.3383	3.9447	5.1593	2.9834
Median	29.7122	31.7214	35.3653	29.7219
Mode	27	28	31	30
Mean	28.5095	31.3687	34.5044	29.8096
Std	8.6869	12.5885	11.9266	12.1271
25th Percentile	16	19	21	19
50th Percentile	24	29	30	28
75th Percentile	29	39	40	37
95th Percentile	35	48	47	48
99th Percentile	38	51	50	52
ΣP(>95%)	0.1977	0.2057	0.2238	0.173
ΣP(>99%)	0.1216	0.1371	0.1331	0.1072

Table 5a: Global First 25 Years PWV PDF Statistics

Variable/GCM	CCSM3	GISS	CCSM4	GISS-E2
Max	70.3763	69.5453	74.1551	65.2707
Min	0.0609	0.0572	0.0769	0.0574
Median	14.6189	13.9038	15.673	13.2841
Mode	2	2	2	2
Mean	18.8095	19.1251	20.1683	18.4456
Std	15.2492	16.8439	16.7235	16.1794
25th Percentile	7	5	6	6
50th Percentile	15	14	16	13
75th Percentile	28	29	31	28
95th Percentile	50	54	54	52
99th Percentile	56	60	59	56

Table 5b: Global Last 25 Years PWV PDF Statistics

Variable/GCM	CCSM3	GISS	CCSM4	GISS-E2
Max	83.769	81.0565	86.7711	74.403
Min	0.1084	0.0624	0.1104	0.0813
Median	17.5676	15.8979	18.9602	15.2003
Mode	2	3	2	2
Mean	22.7462	22.3794	24.1822	21.3743
Std	18.2343	19.8994	19.5429	18.7283
25th Percentile	8	6	8	7
50th Percentile	18	16	19	15
75th Percentile	33	34	37	32
95th Percentile	61	64	64	60
99th Percentile	68	71	70	65
ΣP(>95%)	0.1229	0.1161	0.1202	0.1205
ΣP(>99%)	0.0841	0.0796	0.0874	0.0901

Table 6a: DJF China First 25 Years PWV PDF Statistics

Variable/GCM	CCSM3	GISS	CCSM4	GISS-E2
Max	56.4865	54.1537	57.2844	54.3217
Min	2.5207	1.8486	2.1255	2.5835
Median	15.0879	18.1202	14.5442	16.5486
Mode	5	4	4	4
Mean	18.9447	20.3284	19.0351	19.6814
Std	12.6243	13.2725	13.4683	12.1536
25th Percentile	6	7	6	7
50th Percentile	13	17	13	15
75th Percentile	27	31	26	27
95th Percentile	40	42	44	40
99th Percentile	47	47	51	46

Table 6b: DJF China Last 25 Years PWV PDF Statistics

Variable/GCM	CCSM3	GISS	CCSM4	GISS-E2
Max	66.969	61.2273	71.5199	62.0967
Min	2.2129	2.7677	2.8897	3.1618
Median	17.624	22.7749	16.7944	19.9379
Mode	7	5	7	8
Mean	22.2129	24.7249	22.1785	23.5604
Std	14.5111	15.1253	15.6314	13.9978
25th Percentile	8	9	7	9
50th Percentile	16	22	15	18
75th Percentile	31	37	30	33
95th Percentile	48	48	53	47
99th Percentile	57	55	61	52
ΣP(>95%)	0.1243	0.1492	0.1126	0.148
ΣP(>99%)	0.0605	0.0676	0.0648	0.066

Table 7a: JJA China First 25 Years PWV PDF Statistics

Variable/GCM	CCSM3	GISS	CCSM4	GISS-E2
Max	65.0055	64.6395	70.8516	60.1101
Min	12.3065	14.5072	14.3007	10.6751
Median	45.7588	48.6032	51.9116	41.5194
Mode	46	49	52	52
Mean	44.0767	46.8091	49.5379	40.079
Std	9.0309	9.3372	9.3936	11.096
25th Percentile	38	40	43	29
50th Percentile	44	48	50	40
75th Percentile	48	53	54	48
95th Percentile	54	58	59	53
99th Percentile	58	60	63	55

Table 7b: JJA China Last 25 Years PWV PDF Statistics

Variable/GCM	CCSM3	GISS	CCSM4	GISS-E2
Max	78.9029	76.9503	80.8958	70.815
Min	13.7334	15.9607	19.6119	12.4526
Median	54.8805	58.1116	62.4114	49.2346
Mode	56	64	64	60
Mean	53.1658	55.4274	59.7967	47.4314
Std	10.6852	10.4818	11.1302	12.6448
25th Percentile	47	49	53	36
50th Percentile	53	57	60	47
75th Percentile	58	62	66	57
95th Percentile	66	67	72	62
99th Percentile	70	70	75	64
ΣP(>95%)	0.4702	0.4815	0.584	0.3769
ΣP(>99%)	0.2845	0.3902	0.3934	0.3191

Table 8a: MAM China First 25 Years PWV PDF Statistics

Variable/GCM	CCSM3	GISS	CCSM4	GISS-E2
Max	48.8172	51.9516	54.6861	55.2945
Min	4.2745	4.4001	3.7496	3.7159
Median	28.6364	32.2534	29.919	26.3552
Mode	37	36	33	33
Mean	26.9398	29.6166	28.4191	25.8661
Std	10.7443	11.0884	11.9647	11.8116
25th Percentile	16	20	17	13
50th Percentile	27	31	28	24
75th Percentile	34	37	36	34
95th Percentile	40	44	44	42
99th Percentile	44	46	48	46

Table 8b: MAM China Last 25 Years PWV PDF Statistics

Variable/GCM	CCSM3	GISS	CCSM4	GISS-E2
Max	61.0492	62.7937	69.3475	61.2204
Min	5.5301	4.9859	4.684	4.2724
Median	33.5988	37.2833	34.0733	31.5117
Mode	40	43	39	40
Mean	32.1391	34.6202	33.7021	30.9219
Std	13.0089	13.06	14.3606	13.3223
25th Percentile	19	23	20	17
50th Percentile	32	36	32	30
75th Percentile	41	44	43	40
95th Percentile	49	52	54	49
99th Percentile	53	56	60	54
ΣP(>95%)	0.2931	0.2601	0.2409	0.2116
ΣP(>99%)	0.1833	0.1961	0.162	0.1177

Table 9a: SON China First 25 Years PWV PDF Statistics

Variable/GCM	CCSM3	GISS	CCSM4	GISS-E2
Max	63.8496	64.3181	64.6862	59.2963
Min	4.187	3.7144	4.4143	4.6932
Median	32.3172	37.3894	35.1265	30.9849
Mode	51	54	50	15
Mean	32.663	35.7851	34.647	31.4754
Std	15.6853	6.2262	15.4796	14.2773
25th Percentile	17	22	19	17
50th Percentile	30	36	33	29
75th Percentile	45	48	47	42
95th Percentile	54	57	55	52
99th Percentile	58	59	58	54

Table 9b: SON China Last 25 Years PWV PDF Statistics

Variable/GCM	CCSM3	GISS	CCSM4	GISS-E2
Max	76.7036	77.5392	76.4714	67.2175
Min	5.4136	4.765	5.7729	5.8322
Median	41.1891	45.4739	43.425	33.8352
Mode	61	63	57	19
Mean	40.0021	42.7859	42.205	35.4457
Std	18.227	18.6088	17.8764	16.0646
25th Percentile	21	26	25	20
50th Percentile	39	44	41	32
75th Percentile	54	58	56	48
95th Percentile	64	67	66	60
99th Percentile	69	70	69	63
ΣP(>95%)	0.2634	0.2839	0.2849	0.1838
ΣP(>99%)	0.186	0.2439	0.2188	0.1506

Table 10a: DJF Europe First 25 Years PWV PDF Statistics

Variable/GCM	CCSM3	GISS	CCSM4	GISS-E2
Max	19.9927	18.8672	20.3023	19.9822
Min	6.7511	3.8191	5.2255	3.5759
Median	12.4965	10.6128	12.8473	11.0662
Mode	8	8	8	8
Mean	12.5687	10.6964	12.9666	11.1461
Std	2.1732	2.621	2.5745	2.4777
25th Percentile	6	6	6	6
50th Percentile	7	8	8	8
75th Percentile	9	10	10	10
95th Percentile	11	12	12	12
99th Percentile	13	13	14	14

Table 10b: DJF Europe Last 25 Years PWV PDF Statistics

Variable/GCM	CCSM3	GISS	CCSM4	GISS-E2
Max	23.1949	21.0231	24.4418	22.0305
Min	6.3912	4.6725	7.7548	4.821
Median	14.7019	12.6222	15.1843	12.8441
Mode	10	11	11	10
Mean	14.8186	12.64222	15.3215	12.9629
Std	2.4115	2.7343	2.8489	2.6029
25th Percentile	8	8	8	8
50th Percentile	10	10	10	10
75th Percentile	12	12	12	12
95th Percentile	14	14	15	14
99th Percentile	15	16	17	16
ΣP(>95%)	0.3873	0.2631	0.3358	0.2861
ΣP(>99%)	0.147	0.1579	0.1477	0.0941

Table 11a: JJA Europe First 25 Years PWV PDF Statistics

Variable/GCM	CCSM3	GISS	CCSM4	GISS-E2
Max	27.6005	40.1268	34.3162	34.1758
Min	12.9567	13.965	15.0917	11.062
Median	18.9639	23.7397	24.862	21.6165
Mode	15	21	21	19
Mean	19.0945	24.1672	24.7164	21.7974
Std	2.1263	3.4419	2.623	3.4973
25th Percentile	13	19	18	16
50th Percentile	14	21	20	19
75th Percentile	15	23	22	21
95th Percentile	18	27	24	25
99th Percentile	20	30	25	27

Table 11b: JJA Europe Last 25 Years PWV PDF Statistics

Variable/GCM	CCSM3	GISS	CCSM4	GISS-E2
Max	31.5228	46.626	40.7447	40.788
Min	13.6858	16.688	18.0095	10.4262
Median	21.6495	27.6963	28.496	24.1285
Mode	17	24	24	21
Mean	21.8499	28.1179	28.5477	24.5381
Std	2.7627	4.3603	3.2447	3.9894
25th Percentile	15	22	21	19
50th Percentile	17	25	23	21
75th Percentile	19	28	26	24
95th Percentile	22	33	29	29
99th Percentile	24	36	31	32
ΣP(>95%)	0.3894	0.3533	0.4994	0.2118
ΣP(>99%)	0.1729	0.1627	0.3882	0.1188

Table 12a: MAM Europe First 25 Years PWV PDF Statistics

Variable/GCM	CCSM3	GISS	CCSM4	GISS-E2
Max	19.0494	23.9203	24.1462	25.6703
Min	6.6942	4.2899	6.1755	4.4867
Median	13.6804	13.7504	15.107	13.0447
Mode	10	12	11	12
Mean	13.616	13.8088	15.1956	12.8992
Std	1.9531	3.5298	3.054	3.0279
25th Percentile	7	8	8	8
50th Percentile	9	11	10	10
75th Percentile	10	13	12	12
95th Percentile	12	17	15	15
99th Percentile	13	18	17	17

Table 12b: MAM Europe Last 25 Years PWV PDF Statistics

Variable/GCM	CCSM3	GISS	CCSM4	GISS-E2
Max	22.6755	26.778	28.179	27.2002
Min	9.503	7.0439	7.6115	5.3777
Median	15.8368	15.3168	17.1191	14.7657
Mode	12	13	12	13
Mean	15.8355	15.6033	17.2405	14.7404
Std	2.0855	3.599	3.2013	3.0212
25th Percentile	9	10	10	10
50th Percentile	11	12	12	12
75th Percentile	12	15	14	14
95th Percentile	14	19	18	17
99th Percentile	16	21	20	19
ΣP(>95%)	0.3627	0.1688	0.2447	0.1803
ΣP(>99%)	0.2072	0.1025	0.1069	0.0548

Table 13a: SON Europe First 25 Years PWV PDF Statistics

Variable/GCM	CCSM3	GISS	CCSM4	GISS-E2
Max	24.9701	35.7668	31.7255	34.4958
Min	8.506	5.7943	6.7383	5.9604
Median	16.8382	18.2681	19.9458	17.5338
Mode	14	14	16	16
Mean	16.7154	16.2756	19.8359	17.6593
Std	2.5062	4.9617	3.9197	4.2987
25th Percentile	10	10	12	11
50th Percentile	12	13	15	15
75th Percentile	14	16	18	18
95th Percentile	16	23	21	22
99th Percentile	17	28	23	25

Table 13b: SON Europe Last 25 Years PWV PDF Statistics

Variable/GCM	CCSM3	GISS	CCSM4	GISS-E2
Max	31.0356	43.4709	38.755	37.6055
Min	10.7939	6.7582	10.73	7.7016
Median	19.7968	18.2681	23.48	19.8053
Mode	17	13	19	18
Mean	19.6849	19.171	23.2937	20.029
Std	2.6576	5.8342	4.4114	4.655
25th Percentile	13	12	15	14
50th Percentile	15	15	18	17
75th Percentile	17	19	22	20
95th Percentile	19	28	25	26
99th Percentile	20	33	28	29
ΣP(>95%)	0.4047	0.1403	0.3332	0.1614
ΣP(>99%)	0.2705	0.0586	0.1809	0.067

Table 14a: DJF India First 25 Years PWV PDF Statistics

Variable/GCM	CCSM3	GISS	CCSM4	GISS-E2
Max	60.3529	61.2489	61.1352	56.0766
Min	5.1167	4.4092	4.0714	4.7839
Median	26.9752	29.204	29.7128	24.8373
Mode	20	33&34	22 & 23	18
Mean	27.7023	29.1458	30.8577	26.4868
Std	10.1744	12.7869	11.6705	11.6484
25th Percentile	15	15	18	13
50th Percentile	22	26	26	21
75th Percentile	30	36	35	31
95th Percentile	41	47	48	44
99th Percentile	47	52	53	49

Table 14b: DJF India Last 25 Years PWV PDF Statistics

Variable/GCM	CCSM3	GISS	CCSM4	GISS-E2
Max	70.7637	74.2043	73.8061	66.5827
Min	7.3243	5.4249	6.167	5.3642
Median	32.972	34.7867	34.9758	30.0371
Mode	24	36	27	22
Mean	34.1109	35.1908	36.6388	32.186
Std	11.708	15.0172	13.1792	13.6099
25th Percentile	21	20	22	17
50th Percentile	28	32	31	26
75th Percentile	37	43	42	38
95th Percentile	50	58	57	53
99th Percentile	57	65	62	58
ΣP(>95%)	0.1757	0.1948	0.1557	0.1691
ΣP(>99%)	0.0831	0.1222	0.0915	0.1033

Table 15a: JJA India First 25 Years PWV PDF Statistics

Variable/GCM	CCSM3	GISS	CCSM4	GISS-E2
Max	70.3763	69.5453	74.1551	62.5859
Min	18.8583	24.3332	23.987	13.6264
Median	55.0096	53.6169	57.0534	47.4163
Mode	51	55	52	48
Mean	54.4219	51.8379	56.562	44.7435
Std	6.219	6.7629	6.2685	8.4274
25th Percentile	47	45	50	35
50th Percentile	50	51	53	43
75th Percentile	53	54	57	47
95th Percentile	58	57	61	51
99th Percentile	60	60	64	54

Table 15b: JJA India Last 25 Years PWV PDF Statistics

Variable/GCM	CCSM3	GISS	CCSM4	GISS-E2
Max	83.769	78.8388	86.7711	74.403
Min	24.9035	29.3079	27.8522	20.0898
Median	66.7336	63.6934	68.5322	55.7847
Mode	62	66	65	55
Mean	65.7694	61.268	67.508	52.8958
Std	7.6181	8.9036	8.0691	9.0556
25th Percentile	57	52	60	43
50th Percentile	62	61	65	52
75th Percentile	66	65	69	55
95th Percentile	71	69	74	60
99th Percentile	74	71	78	64
ΣP(>95%)	0.7353	0.6433	0.7315	0.5612
ΣP(>99%)	0.6331	0.5482	0.5666	0.385

Table 16a: MAM India First 25 Years PWV PDF Statistics

Variable/GCM	CCSM3	GISS	CCSM4	GISS-E2
Max	57.9257	59.4103	56.6705	58.7412
Min	5.9557	5.1216	6.3513	5.1467
Median	32.0496	35.7279	32.6337	33.5386
Mode	29 & 31	35	29	36
Mean	31.7005	34.6143	32.7926	32.5814
Std	11.6605	10.1465	10.7546	10.3629
25th Percentile	18	25	21	21
50th Percentile	27	33	29	30
75th Percentile	36	39	37	36
95th Percentile	45	47	47	45
99th Percentile	49	51	50	49

Table 16b: MAM India Last 25 Years PWV PDF Statistics

Variable/GCM	CCSM3	GISS	CCSM4	GISS-E2
Max	68.8339	72.9324	68.6359	64.7277
Min	8.1555	6.7159	8.3711	8.2899
Median	39.7513	41.6206	38.1471	40.1789
Mode	28 & 31	44	33	44
Mean	39.5644	40.0996	38.3036	39.114
Std	13.5566	11.2159	12.3611	11.4737
25th Percentile	25	30	25	27
50th Percentile	35	39	34	36
75th Percentile	46	45	43	44
95th Percentile	55	54	56	52
99th Percentile	59	59	60	56
ΣP(>95%)	0.2708	0.1941	0.1719	0.2313
ΣP(>99%)	0.1896	0.0975	0.1247	0.1218

Table 17a: SON India First 25 Years PWV PDF Statistics

Variable/GCM	CCSM3	GISS	CCSM4	GISS-E2
Max	65.3816	62.8625	67.1524	58.5758
Min	11.5588	5.5636	14.5362	6.5443
Median	47.8515	39.9162	51.7656	40.3992
Mode	48	43	51	47
Mean	44.8328	38.6928	48.6369	38.5391
Std	10.1912	11.9933	9.7417	11.4852
25th Percentile	33	27	39	26
50th Percentile	43	37	48	36
75th Percentile	48	45	52	45
95th Percentile	52	53	56	49
99th Percentile	54	56	59	52

Table 17b: SON India Last 25 Years PWV PDF Statistics

Variable/GCM	CCSM3	GISS	CCSM4	GISS-E2
Max	78.4415	76.4962	82.2179	68.0097
Min	10.8458	8.5892	15.4795	10.2816
Median	60.3962	49.461	61.6854	47.9384
Mode	61	60	63	55
Mean	56.358	48.272	58.2344	45.4109
Std	12.2982	14.6193	10.9628	12.5121
25th Percentile	43	35	49	32
50th Percentile	55	46	58	44
75th Percentile	61	57	62	52
95th Percentile	66	67	67	58
99th Percentile	69	70	70	60
ΣP(>95%)	0.6005	0.3581	0.5792	0.3692
ΣP(>99%)	0.556	0.2888	0.4644	0.2714

Table 18a: DJF U.S. First 25 Years PWV PDF Statistics

Variable/GCM	CCSM3	GISS	CCSM4	GISS-E2
Max	41.2277	42.0558	43.7445	42.5519
Min	4.8088	3.2679	4.198	3.264
Median	19.7847	18.0774	22.2301	17.7267
Mode	7	6	8	7
Mean	19.6305	18.4352	21.7693	18.345
Std	8.0026	8.6054	9.1726	8.806
25th Percentile	8	7	10	8
50th Percentile	16	15	19	16
75th Percentile	23	23	27	24
95th Percentile	28	29	33	31
99th Percentile	30	33	36	35

Table 18b: DJF U.S. Last 25 Years PWV PDF Statistics

Variable/GCM	CCSM3	GISS	CCSM4	GISS-E2
Max	43.6829	48.4605	51.8975	52.0712
Min	6.3383	3.9447	5.1593	2.9834
Median	22.515	20.6091	26.0432	20.435
Mode	9	7	33	9
Mean	22.42	20.9567	25.4388	21.4652
Std	8.7056	9.737	10.1956	10.4705
25th Percentile	10	9	13	10
50th Percentile	19	18	23	18
75th Percentile	26	26	31	28
95th Percentile	32	33	38	37
99th Percentile	35	38	42	42
ΣP(>95%)	0.1894	0.1735	0.1985	0.1855
ΣP(>99%)	0.1106	0.0644	0.1001	0.0926

Table 19a: JJA U.S. First 25 Years PWV PDF Statistics

Variable/GCM	CCSM3	GISS	CCSM4	GISS-E2
Max	40.4004	53.8696	50.788	51.8196
Min	15.2828	17.1795	14.807	16.0584
Median	29.9565	38.3783	39.171	33.6317
Mode	29	40	39	30
Mean	29.036	37.6388	38.2357	34.236
Std	4.5514	5.9685	5.5089	7.4317
25th Percentile	22	31	32	26
50th Percentile	26	35	36	32
75th Percentile	29	39	39	38
95th Percentile	31	43	43	44
99th Percentile	33	45	45	47

Table 19b: JJA U.S. Last 25 Years PWV PDF Statistics

Variable/GCM	CCSM3	GISS	CCSM4	GISS-E2
Max	50.0942	60.3611	59.7674	58.6131
Min	18.1081	22.6747	19.6438	17.2027
Median	35.0797	44.4418	45.7526	39.4235
Mode	34	47	45	36
Mean	34.4812	43.6228	44.6999	39.4982
Std	5.0115	6.5579	5.9498	8.0783
25th Percentile	27	36	38	31
50th Percentile	31	41	43	37
75th Percentile	34	46	46	44
95th Percentile	38	50	50	50
99th Percentile	40	52	52	53
ΣP(>95%)	0.5384	0.4388	0.5188	0.2783
ΣP(>99%)	0.3928	0.3209	0.3601	0.1617

Table 20a: MAM U.S. First 25 Years PWV PDF Statistics

Variable/GCM	CCSM3	GISS	CCSM4	GISS-E2
Max	36.7174	44.5165	46.8656	44.5298
Min	6.6158	5.085	6.0486	4.3214
Median	22.6707	24.3134	25.7717	21.1633
Mode	22	24	28	21
Mean	21.9636	24.0435	25.0799	21.223
Std	5.8713	8.1054	7.2722	7.4815
25th Percentile	14	15	17	14
50th Percentile	19	21	23	19
75th Percentile	22	27	28	24
95th Percentile	27	34	33	32
99th Percentile	29	38	36	36

Table 20b: MAM U.S. Last 25 Years PWV PDF Statistics

Variable/GCM	CCSM3	GISS	CCSM4	GISS-E2
Max	44.9149	52.3217	49.783	50.5584
Min	8.637	6.3244	7.2935	4.9317
Median	26.9175	27.9425	30.5331	24.8298
Mode	27	28	33	25
Mean	26.0943	27.7145	29.6031	24.7038
Std	6.5261	8.7903	7.9438	8.1299
25th Percentile	17	18	21	17
50th Percentile	23	25	28	23
75th Percentile	27	31	33	28
95th Percentile	31	39	38	36
99th Percentile	34	43	41	41
ΣP(>95%)	0.2962	0.1723	0.2602	0.1481
ΣP(>99%)	0.1814	0.0782	0.1294	0.0614

Table 21a: SON U.S. First 25 Years PWV PDF Statistics

Variable/GCM	CCSM3	GISS	CCSM4	GISS-E2
Max	42.7939	50.5418	53.7778	54.0926
Min	6.6193	5.2378	7.7548	6.2925
Median	27.2717	29.2685	34.1449	27.1359
Mode	31	33	41	20
Mean	26.0756	28.4868	32.568	28.1637
Std	8.0132	10.4643	10.4235	10.6389
25th Percentile	16	17	21	18
50th Percentile	23	26	31	25
75th Percentile	29	34	39	35
95th Percentile	33	41	44	44
99th Percentile	35	44	46	47

Table 21b: SON U.S. Last 25 Years PWV PDF Statistics

Variable/GCM	CCSM3	GISS	CCSM4	GISS-E2
Max	49.5053	62.5547	61.5144	59.6274
Min	8.4733	7.1555	10.4203	6.5703
Median	32.3381	33.7516	41.0987	33.1468
Mode	35	34	49	27
Mean	31.0424	33.1957	38.5363	33.7065
Std	8.5656	12.0272	11.9534	11.9253
25th Percentile	20	21	26	22
50th Percentile	28	31	38	31
75th Percentile	34	40	46	42
95th Percentile	39	49	51	51
99th Percentile	41	52	54	54
ΣP(>95%)	0.3369	0.2374	0.3414	0.2095
ΣP(>99%)	0.2368	0.1595	0.2575	0.1441

Table 22a: DJF Globe First 25 Years PWV PDF Statistics

Variable/GCM	CCSM3	GISS	CCSM4	GISS-E2
Max	67.3536	66.1698	68.3258	63.3733
Min	0.2595	0.1513	0.2705	0.163
Median	12.6797	12.3852	12.8873	11.6126
Mode	4	2	4	2
Mean	18.0704	18.2344	18.9777	17.4825
Std	15.7623	17.1592	17.0932	16.4508
25th Percentile	5	3	4	3
50th Percentile	13	12	13	12
75th Percentile	28	29	30	28
95th Percentile	51	54	54	51
99th Percentile	57	60	59	56

Table 22b: DJF Globe Last 25 Years PWV PDF Statistics

Variable/GCM	CCSM3	GISS	CCSM4	GISS-E2
Max	78.7885	79.9451	81.372	73.2866
Min	0.3542	0.1997	0.3998	0.2351
Median	15.178	13.9294	15.6517	13.0926
Mode	7	3	5	3
Mean	21.8047	21.3065	22.7812	20.2872
Std	18.6821	20.322	20.0219	19.0998
25th Percentile	7	4	6	4
50th Percentile	15	14	16	13
75th Percentile	32	34	36	32
95th Percentile	61	64	64	60
99th Percentile	69	71	71	65
ΣP(>95%)	0.1163	0.1137	0.1167	0.1224
ΣP(>99%)	0.0801	0.0793	0.0847	0.0867

Table 23a: JJA Globe First 25 Years PWV PDF Statistics

Variable/GCM	CCSM3	GISS	CCSM4	GISS-E2
Max	70.3763	69.5453	74.1551	62.5859
Min	0.0609	0.0572	0.0769	0.0643
Median	16.7674	15.8715	18.5403	15.1707
Mode	1	1	1	1
Mean	20.264	20.8107	22.2986	19.7171
Std	14.6566	16.326	16.3586	15.5283
25th Percentile	10	9	11	9
50th Percentile	17	16	19	15
75th Percentile	29	31	33	28
95th Percentile	50	54	55	51
99th Percentile	56	59	59	55

Table 23b: JJA Globe Last 25 Years PWV PDF Statistics

Variable/GCM	CCSM3	GISS	CCSM4	GISS-E2
Max	83.769	78.8388	86.7711	74.403
Min	0.1084	0.0624	0.1104	0.0813
Median	20.3393	18.4361	22.6351	17.6954
Mode	1	1	1	1
Mean	24.5889	24.4185	26.843	22.9513
Std	17.7001	19.2683	19.2865	18.0304
25th Percentile	13	11	14	10
50th Percentile	20	18	23	18
75th Percentile	35	36	39	33
95th Percentile	61	64	65	60
99th Percentile	68	70	71	64
ΣP(>95%)	0.1269	0.1236	0.1244	0.1309
ΣP(>99%)	0.0849	0.0899	0.0984	0.0997

Table 24a: MAM Globe First 25 Years PWV PDF Statistics

Variable/GCM	CCSM3	GISS	CCSM4	GISS-E2
Max	64.1611	66.267	67.4659	63.0782
Min	0.1081	0.0617	0.117	0.0853
Median	13.6267	13.4571	14.5249	12.7154
Mode	8	1	4	3
Mean	18.3939	18.7837	19.5339	18.2668
Std	15.3602	16.9282	16.661	16.5967
25th Percentile	6	5	6	5
50th Percentile	14	13	15	13
75th Percentile	27	29	30	28
95th Percentile	50	54	54	53
99th Percentile	56	60	58	57

Table 24b: MAM Globe Last 25 Years PWV PDF Statistics

Variable/GCM	CCSM3	GISS	CCSM4	GISS-E2
Max	78.4396	81.0565	77.7776	74.1508
Min	0.1489	0.0703	0.1447	0.112
Median	16.1841	15.2936	17.3986	14.5692
Mode	2	`	2	4
Mean	22.1513	21.9915	23.4144	21.1574
Std	18.4367	20.0854	19.5301	19.2674
25th Percentile	8	6	8	6
50th Percentile	16	15	17	15
75th Percentile	32	34	35	32
95th Percentile	61	65	64	61
99th Percentile	68	72	69	67
ΣP(>95%)	0.1233	0.1144	0.1191	0.1193
ΣP(>99%)	0.0861	0.0815	0.0945	0.0929

Table 25a: SON Globe First 25 Years PWV PDF Statistics

Variable/GCM	CCSM3	GISS	CCSM4	GISS-E2
Max	65.3816	65.1558	67.1524	60.0668
Min	0.0901	0.0603	0.0815	0.0765
Median	13.9507	13.0378	14.8343	12.8199
Mode	6	1	1	1
Mean	18.5099	18.6256	19.7321	18.2114
Std	15.1004	16.7948	16.4509	15.951
25th Percentile	7	5	6	6
50th Percentile	14	13	15	13
75th Percentile	28	29	31	28
95th Percentile	50	54	53	51
99th Percentile	55	59	57	55

Table 25b: SON Globe Last 25 Years PWV PDF Statistics

Variable/GCM	CCSM3	GISS	CCSM4	GISS-E2
Max	79.1521	78.4207	82.2179	70.5822
Min	0.1125	0.0678	0.1152	0.0916
Median	16.6887	14.8082	18.043	14.6549
Mode	1	1	2	1
Mean	22.4399	21.8767	23.8414	21.2009
Std	17.9723	19.8391	19.1871	18.4648
25th Percentile	9	6	9	7
50th Percentile	17	15	18	15
75th Percentile	33	34	37	32
95th Percentile	60	64	63	59
99th Percentile	67	70	68	64
ΣP(>95%)	0.119	0.1139	0.1232	0.1272
ΣP(>99%)	0.0861	0.0826	0.0954	0.0942

Table 26a: Global Trend (mm/year)

M.E./GCM	CCSM3	GISS	CCSM4	GISS-E2
0%	0.0273	0.0241	0.0306	0.0248
1%	0.0273	0.0241	0.0306	0.0248
2%	0.0273	0.0241	0.0306	0.0248
3%	0.0273	0.0241	0.0306	0.0248
4%	0.0273	0.0241	0.0306	0.0248
5%	0.0273	0.0241	0.0306	0.0248

Table 26b: Global Autocorrelation Timescale (1+phi)/(1-phi)

M.E./GCM	CCSM3	GISS	CCSM4	GISS-E2
0%	1.6433	3.3437	1.9850	0.9293
1%	1.6433	3.3437	1.9850	0.9293
2%	1.6433	3.3437	1.9850	0.9293
3%	1.6433	3.3437	1.9850	0.9293
4%	1.6433	3.3437	1.9850	0.9293
5%	1.6433	3.3437	1.9850	0.9293

Table 26c: Global Standard Deviation (mm)

M.E./GCM	CCSM3	GISS	CCSM4	GISS-E2
0%	0.0275	0.0176	0.0427	0.0522
1%	0.2521	0.2615	0.2763	0.2568
2%	0.5020	0.5221	0.5477	0.5056
3%	0.7524	0.7829	0.8202	0.7561
4%	1.0029	1.0438	1.0929	1.0071
5%	1.2534	1.3047	1.3658	1.2583

Table 26d: Global TTD (years)

M.E./GCM	CCSM3	GISS	CCSM4	GISS-E2
0%	2.6252	2.6894	3.4794	3.5525
1%	11.5037	16.2676	12.0811	10.2807
2%	18.2065	25.7940	19.0623	16.1495
3%	23.8441	33.7926	24.9505	21.1201
4%	28.8794	40.9338	30.2134	25.5674
5%	33.5086	47.4978	35.0531	29.6588

Table 27a: DJF Global Trend (mm/year)

M.E./GCM	CCSM3	GISS	CCSM4	GISS-E2
0%	0.0275	0.0244	0.0310	0.0254
1%	0.0275	0.0244	0.0310	0.0254
2%	0.0275	0.0244	0.0310	0.0254
3%	0.0275	0.0244	0.0310	0.0254
4%	0.0275	0.0244	0.0310	0.0254
5%	0.0275	0.0244	0.0310	0.0254

Table 27b: DJF Global Autocorrelation Timescale (1+phi)/(1-phi)

M.E./GCM	CCSM3	GISS	CCSM4	GISS-E2
0%	0.9140	1.0407	7.1770	1.7991
1%	0.9140	1.0407	7.1770	1.7991
2%	0.9140	1.0407	7.1770	1.7991
3%	0.9140	1.0407	7.1770	1.7991
4%	0.9140	1.0407	7.1770	1.7991
5%	0.9140	1.0407	7.1770	1.7991

Table 27c: DJF Global Standard Deviation (mm)

M.E./GCM	CCSM3	GISS	CCSM4	GISS-E2
0%	0.0796	0.1072	0.0371	0.0222
1%	0.2628	0.2819	0.2753	0.2522
2%	0.5072	0.5323	0.5469	0.5029
3%	0.7556	0.7895	0.8192	0.7540
4%	1.0050	1.0484	1.0918	1.0051
5%	1.2548	1.3080	1.3645	1.2562

Table 27d: DJF Global TTD (years)

M.E./GCM	CCSM3	GISS	CCSM4	GISS-E2
0%	4.3700	6.0260	4.8166	2.4710
1%	9.6897	11.4804	18.3367	12.4687
2%	15.0203	17.5398	28.9752	19.7542
3%	19.5921	22.8098	37.9359	25.8759
4%	23.6956	27.5576	45.9424	31.3425
5%	27.4756	31.9376	53.3040	36.3676

Table 28a: JJA Global Trend (mm/year)

M.E./GCM	CCSM3	GISS	CCSM4	GISS-E2
0%	0.0272	0.0238	0.0304	0.0245
1%	0.0272	0.0238	0.0304	0.0245
2%	0.0272	0.0238	0.0304	0.0245
3%	0.0272	0.0238	0.0304	0.0245
4%	0.0272	0.0238	0.0304	0.0245
5%	0.0272	0.0238	0.0304	0.0245

Table 28b: JJA Global Autocorrelation Timescale (1+phi)/(1-phi)

M.E./GCM	CCSM3	GISS	CCSM4	GISS-E2
0%	1.7512	1.2146	5.9890	2.8481
1%	1.7512	1.2146	5.9890	2.8481
2%	1.7512	1.2146	5.9890	2.8481
3%	1.7512	1.2146	5.9890	2.8481
4%	1.7512	1.2146	5.9890	2.8481
5%	1.7512	1.2146	5.9890	2.8481

Table 28c: JJA Global Standard Deviation (mm)

M.E./GCM	CCSM3	GISS	CCSM4	GISS-E2
0%	0.0133	0.0340	0.0491	0.0304
1%	0.2510	0.2632	0.2775	0.2533
2%	0.5015	0.5231	0.5484	0.5039
3%	0.7521	0.7837	0.8207	0.7551
4%	1.0027	1.0445	1.0935	1.0065
5%	1.2534	1.3054	1.3663	1.2579

Table 28d: JJA Global TTD (years)

M.E./GCM	CCSM3	GISS	CCSM4	GISS-E2
0%	1.6566	3.0006	5.5467	3.6260
1%	11.7498	11.7454	17.5991	14.9015
2%	18.6385	18.5665	27.7164	23.5692
3%	24.4202	24.3100	36.2648	30.8635
4%	29.5816	29.4414	43.9087	37.3796
5%	34.3257	34.1594	50.9393	43.3705

Table 29a: MAM Global Trend (mm/year)

M.E./GCM	CCSM3	GISS	CCSM4	GISS-E2
0%	0.0276	0.0244	0.0311	0.0251
1%	0.0276	0.0244	0.0311	0.0251
2%	0.0276	0.0244	0.0311	0.0251
3%	0.0276	0.0244	0.0311	0.0251
4%	0.0276	0.0244	0.0311	0.0251
5%	0.0276	0.0244	0.0311	0.0251

Table 29b: MAM Global Autocorrelation Timescale (1+phi)/(1-phi)

M.E./GCM	CCSM3	GISS	CCSM4	GISS-E2
0%	1.2933	1.9652	1.0458	1.0562
1%	1.2933	1.9652	1.0458	1.0562
2%	1.2933	1.9652	1.0458	1.0562
3%	1.2933	1.9652	1.0458	1.0562
4%	1.2933	1.9652	1.0458	1.0562
5%	1.2933	1.9652	1.0458	1.0562

Table 29c: MAM Global Standard Deviation (mm)

M.E./GCM	CCSM3	GISS	CCSM4	GISS-E2
0%	0.0605	0.0558	0.0928	0.0865
1%	0.2577	0.2667	0.2882	0.2658
2%	0.5046	0.5245	0.5535	0.5100
3%	0.7539	0.7843	0.8237	0.7589
4%	1.0038	1.0445	1.0952	1.0090
5%	1.2539	1.3050	1.3673	1.2595

Table 29d: MAM Global TTD (years)

M.E./GCM	CCSM3	GISS	CCSM4	GISS-E2
0%	4.0771	4.8155	4.6630	5.1552
1%	10.7109	13.6684	9.9227	10.8944
2%	16.7648	21.4574	15.3315	16.8230
3%	21.9094	28.0582	19.9848	21.9263
4%	26.5164	33.9650	24.1649	26.5114
5%	30.7561	39.3994	28.0167	30.7366

Table 30a: SON Global Trend (mm/year)

M.E./GCM	CCSM3	GISS	CCSM4	GISS-E2
0%	0.0271	0.0237	0.0300	0.0244
1%	0.0271	0.0237	0.0300	0.0244
2%	0.0271	0.0237	0.0300	0.0244
3%	0.0271	0.0237	0.0300	0.0244
4%	0.0271	0.0237	0.0300	0.0244
5%	0.0271	0.0237	0.0300	0.0244

Table 30b: SON Global Autocorrelation Timescale (1+phi)/(1-phi)

M.E./GCM	CCSM3	GISS	CCSM4	GISS-E2
0%	0.4897	1.1782	3.5521	6.4214
1%	0.4897	1.1782	3.5521	6.4214
2%	0.4897	1.1782	3.5521	6.4214
3%	0.4897	1.1782	3.5521	6.4214
4%	0.4897	1.1782	3.5521	6.4214
5%	0.4897	1.1782	3.5521	6.4214

Table 30c: SON Global Standard Deviation (mm)

M.E./GCM	CCSM3	GISS	CCSM4	GISS-E2
0%	0.0181	0.0380	0.0778	0.0396
1%	0.2514	0.2638	0.2841	0.2547
2%	0.5019	0.5236	0.5520	0.5048
3%	0.7525	0.7842	0.8235	0.7559
4%	1.0033	1.0450	1.0958	1.0072
5%	1.2540	1.3060	1.3685	1.2587

Table 30d: SON Global TTD (years)

M.E./GCM	CCSM3	GISS	CCSM4	GISS-E2
0%	1.3357	3.2071	6.3796	5.6968
1%	7.7135	11.6756	15.1234	19.7034
2%	12.2285	18.4374	23.5476	31.0870
3%	16.0201	24.1362	30.7421	40.6890
4%	19.4053	29.2290	37.1928	49.2715
5%	22.5170	33.9118	43.1322	57.1639

Table 31a: China Trend (mm/year)

M.E./GCM	CCSM3	GISS	CCSM4	GISS-E2
0%	0.081	0.0807	0.0923	0.0695
1%	0.081	0.0807	0.0923	0.0695
2%	0.081	0.0807	0.0923	0.0695
3%	0.081	0.0807	0.0923	0.0695
4%	0.081	0.0807	0.0923	0.0695
5%	0.081	0.0807	0.0923	0.0695

Table 31b: China Autocorrelation Timescale (1+phi)/(1-phi)

M.E./GCM	CCSM3	GISS	CCSM4	GISS-E2
0%	2.3517	1.8021	2.6053	1.8077
1%	2.3517	1.8021	2.6053	1.8077
2%	2.3517	1.8021	2.6053	1.8077
3%	2.3517	1.8021	2.6053	1.8077
4%	2.3517	1.8021	2.6053	1.8077
5%	2.3517	1.8021	2.6053	1.8077

Table 31c: China Standard Deviation (mm)

M.E./GCM	CCSM3	GISS	CCSM4	GISS-E2
0%	1.9988	1.958	2.2638	1.7497
1%	2.0289	1.9891	2.2932	1.7791
2%	2.1153	2.0791	2.3782	1.8635
3%	2.2488	2.2201	2.5112	1.994
4%	2.4195	2.4022	2.6838	2.1608
5%	2.6186	2.6164	2.8879	2.3554

Table 31d: China TTD (years)

M.E./GCM	CCSM3	GISS	CCSM4	GISS-E2
0%	26.8295	23.5313	27.5599	23.979
1%	27.056	23.7614	27.7613	24.2315
2%	27.7007	24.4219	28.3413	24.9475
3%	28.6822	25.4386	29.2412	26.031
4%	29.9128	26.7238	30.3936	27.3797
5%	31.3196	28.1985	31.7368	28.9101

Table 32a: Europe Trend (mm/year)

M.E./GCM	CCSM3	GISS	CCSM4	GISS-E2
0%	0.0338	0.0346	0.0407	0.029
1%	0.0338	0.0346	0.0407	0.029
2%	0.0338	0.0346	0.0407	0.029
3%	0.0338	0.0346	0.0407	0.029
4%	0.0338	0.0346	0.0407	0.029
5%	0.0338	0.0346	0.0407	0.029

Table 32b: Europe Autocorrelation Timescale (1+phi)/(1-phi)

M.E./GCM	CCSM3	GISS	CCSM4	GISS-E2
0%	1.793	1.8655	1.3094	1.3888
1%	1.793	1.8655	1.3094	1.3888
2%	1.793	1.8655	1.3094	1.3888
3%	1.793	1.8655	1.3094	1.3888
4%	1.793	1.8655	1.3094	1.3888
5%	1.793	1.8655	1.3094	1.3888

Table 32c: Europe Standard Deviation (mm)

M.E./GCM	CCSM3	GISS	CCSM4	GISS-E2
0%	0.9797	1.2242	0.8924	1.039
1%	0.9939	1.2359	0.9128	1.0526
2%	1.0349	1.2704	0.9715	1.0923
3%	1.0995	1.3257	1.062	1.1552
4%	1.1833	1.3991	1.1769	1.2376
5%	1.2824	1.4879	1.3097	1.336

Table 32d: Europe TTD (years)

M.E./GCM	CCSM3	GISS	CCSM4	GISS-E2
0%	25.4304	29.5759	19.1098	27.3036
1%	25.6825	29.7658	19.4001	27.5426
2%	26.4057	30.3202	20.2215	28.2343
3%	27.5183	31.1978	21.4557	29.3134
4%	28.9248	32.3438	22.9727	30.6975
5%	30.5394	33.7008	24.6662	32.3065

Table 33a: India Trend (mm/year)

M.E./GCM	CCSM3	GISS	CCSM4	GISS-E2
0%	0.1209	0.1011	0.1089	0.0908
1%	0.1209	0.1011	0.1089	0.0908
2%	0.1209	0.1011	0.1089	0.0908
3%	0.1209	0.1011	0.1089	0.0908
4%	0.1209	0.1011	0.1089	0.0908
5%	0.1209	0.1011	0.1089	0.0908

Table 33b: India Autocorrelation Timescale (1+phi)/(1-phi)

M.E./GCM	CCSM3	GISS	CCSM4	GISS-E2
0%	1.2365	1.7607	1.383	1.9735
1%	1.2365	1.7607	1.383	1.9735
2%	1.2365	1.7607	1.383	1.9735
3%	1.2365	1.7607	1.383	1.9735
4%	1.2365	1.7607	1.383	1.9735
5%	1.2365	1.7607	1.383	1.9735

Table 33c: India Standard Deviation (mm)

M.E./GCM	CCSM3	GISS	CCSM4	GISS-E2
0%	2.0294	2.3351	2.7407	2.315
1%	2.0779	2.3727	2.7777	2.3473
2%	2.2144	2.4816	2.8854	2.4411
3%	2.4199	2.6521	3.0553	2.5888
4%	2.6758	2.8722	3.277	2.7813
5%	2.9684	3.1311	3.54	3.0095

Table 33d: India TTD (years)

M.E./GCM	CCSM3	GISS	CCSM4	GISS-E2
0%	16.1596	22.4684	21.6605	24.6041
1%	16.4024	22.7055	21.8563	24.8205
2%	17.0729	23.3846	22.4202	25.4445
3%	18.0521	24.4265	23.2937	26.4126
4%	19.2324	25.7384	24.4058	27.6488
5%	20.5372	27.2379	25.6912	29.0817

Table 34a: U.S. Trend (mm/year)

M.E./GCM	CCSM3	GISS	CCSM4	GISS-E2
0%	0.0552	0.0555	0.0681	0.0576
1%	0.0552	0.0555	0.0681	0.0576
2%	0.0552	0.0555	0.0681	0.0576
3%	0.0552	0.0555	0.0681	0.0576
4%	0.0552	0.0555	0.0681	0.0576
5%	0.0552	0.0555	0.0681	0.0576

Table 34b: U.S. Autocorrelation Timescale (1+phi)/(1-phi)

M.E./GCM	CCSM3	GISS	CCSM4	GISS-E2
0%	2.2193	1.9196	1.4925	1.5428
1%	2.2193	1.9196	1.4925	1.5428
2%	2.2193	1.9196	1.4925	1.5428
3%	2.2193	1.9196	1.4925	1.5428
4%	2.2193	1.9196	1.4925	1.5428
5%	2.2193	1.9196	1.4925	1.5428

Table 34c: U.S. Standard Deviation (mm)

M.E./GCM	CCSM3	GISS	CCSM4	GISS-E2
0%	1.4893	1.4184	1.4524	1.4194
1%	1.5122	1.4474	1.4898	1.4467
2%	1.5784	1.5304	1.5939	1.5247
3%	1.6818	1.6581	1.7482	1.6446
4%	1.8152	1.8201	1.9382	1.7965
5%	1.9719	2.0077	2.1536	1.9724

Table 34d: U.S. TTD (years)

M.E./GCM	CCSM3	GISS	CCSM4	GISS-E2
0%	26.137	24.2146	19.9136	22.1562
1%	26.409	24.5329	20.2498	22.4296
2%	27.185	25.4315	21.1618	23.1995
3%	28.3689	26.7808	22.4644	24.3517
4%	29.853	28.4438	24.0057	25.7688
5%	31.5452	30.3103	25.6876	27.3588

Table 35a: DJF China Trend (mm/year)

M.E./GCM	CCSM3	GISS	CCSM4	GISS-E2
0%	0.047	0.0555	0.0498	0.0544
1%	0.047	0.0555	0.0498	0.0544
2%	0.047	0.0555	0.0498	0.0544
3%	0.047	0.0555	0.0498	0.0544
4%	0.047	0.0555	0.0498	0.0544
5%	0.047	0.0555	0.0498	0.0544

Table 35b: DJF China Autocorrelation Timescale (1+phi)/(1-phi)

M.E./GCM	CCSM3	GISS	CCSM4	GISS-E2
0%	1.3712	0.8448	0.7949	0.7197
1%	1.3712	0.8448	0.7949	0.7197
2%	1.3712	0.8448	0.7949	0.7197
3%	1.3712	0.8448	0.7949	0.7197
4%	1.3712	0.8448	0.7949	0.7197
5%	1.3712	0.8448	0.7949	0.7197

Table 35c: DJF China Standard Deviation (mm)

M.E./GCM	CCSM3	GISS	CCSM4	GISS-E2
0%	0.9923	1.0263	1.8461	0.9668
1%	1.0158	1.0547	1.8586	0.9916
2%	1.0822	1.132	1.8956	1.0616
3%	1.1819	1.2446	1.9553	1.1669
4%	1.3062	1.3813	2.0354	1.2979
5%	1.4484	1.5351	2.1332	1.4474

Table 35d: DJF China TTD (years)

M.E./GCM	CCSM3	GISS	CCSM4	GISS-E2
0%	20.2655	15.5461	22.726	14.0441
1%	20.5114	15.7798	22.829	14.2401
2%	21.1983	16.4043	23.1311	14.7878
3%	22.2198	17.2862	23.6137	15.6006
4%	23.4745	18.3274	24.2516	16.5937
5%	24.8851	19.4675	25.0181	17.7028

Table 36a: JJA China Trend (mm/year)

M.E./GCM	CCSM3	GISS	CCSM4	GISS-E2
0%	0.1181	0.111	0.1403	0.098
1%	0.1181	0.111	0.1403	0.098
2%	0.1181	0.111	0.1403	0.098
3%	0.1181	0.111	0.1403	0.098
4%	0.1181	0.111	0.1403	0.098
5%	0.1181	0.111	0.1403	0.098

Table 36b: JJA China Autocorrelation Timescale (1+phi)/(1-phi)

M.E./GCM	CCSM3	GISS	CCSM4	GISS-E2
0%	0.9886	0.5178	0.6868	0.5343
1%	0.9886	0.5178	0.6868	0.5343
2%	0.9886	0.5178	0.6868	0.5343
3%	0.9886	0.5178	0.6868	0.5343
4%	0.9886	0.5178	0.6868	0.5343
5%	0.9886	0.5178	0.6868	0.5343

Table 36c: JJA China Standard Deviation (mm)

M.E./GCM	CCSM3	GISS	CCSM4	GISS-E2
0%	1.1765	0.9667	1.0544	1.1891
1%	1.2668	1.0903	1.1786	1.2661
2%	1.502	1.3863	1.4858	1.4686
3%	1.8234	1.7636	1.8857	1.749
4%	2.1924	2.1804	2.3309	2.075
5%	2.589	2.6183	2.8001	2.4284

Table 36d: JJA China TTD (years)

M.E./GCM	CCSM3	GISS	CCSM4	GISS-E2
0%	10.388	7.7519	7.6346	9.6268
1%	10.8973	8.3707	8.2074	10.028
2%	12.1656	9.7546	9.5419	11.04
3%	13.7934	11.3816	11.1485	12.3629
4%	15.5509	13.0535	12.8116	13.8147
5%	17.336	14.7052	14.4567	15.3074

Table 37a: MAM China Trend (mm/year)

M.E./GCM	CCSM3	GISS	CCSM4	GISS-E2
0%	0.0675	0.0648	0.0737	0.0652
1%	0.0675	0.0648	0.0737	0.0652
2%	0.0675	0.0648	0.0737	0.0652
3%	0.0675	0.0648	0.0737	0.0652
4%	0.0675	0.0648	0.0737	0.0652
5%	0.0675	0.0648	0.0737	0.0652

Table 37b: MAM China Autocorrelation Timescale (1+phi)/(1-phi)

M.E./GCM	CCSM3	GISS	CCSM4	GISS-E2
0%	0.9271	0.7164	0.9634	0.6067
1%	0.9271	0.7164	0.9634	0.6067
2%	0.9271	0.7164	0.9634	0.6067
3%	0.9271	0.7164	0.9634	0.6067
4%	0.9271	0.7164	0.9634	0.6067
5%	0.9271	0.7164	0.9634	0.6067

Table 37c: MAM China Standard Deviation (mm)

M.E./GCM	CCSM3	GISS	CCSM4	GISS-E2
0%	0.92	0.9343	1.4046	0.9757
1%	0.9637	0.9842	1.4376	1.0137
2%	1.083	1.1189	1.5316	1.1197
3%	1.2553	1.31	1.6748	1.2765
4%	1.4615	1.536	1.8549	1.4679
5%	1.6892	1.7837	2.062	1.6821

Table 37d: MAM China TTD (years)

M.E./GCM	CCSM3	GISS	CCSM4	GISS-E2
0%	12.8058	12.2622	16.2242	11.2714
1%	13.1713	12.6582	16.4661	11.5505
2%	14.149	13.6926	17.1426	12.3138
3%	15.5107	15.0974	18.1452	13.4046
4%	17.0743	16.6824	19.3656	14.6816
5%	18.7298	18.3427	20.7218	16.0506

Table 38a: SON China Trend (mm/year)

M.E./GCM	CCSM3	GISS	CCSM4	GISS-E2
0%	0.0921	0.0926	0.1078	0.0626
1%	0.0921	0.0926	0.1078	0.0626
2%	0.0921	0.0926	0.1078	0.0626
3%	0.0921	0.0926	0.1078	0.0626
4%	0.0921	0.0926	0.1078	0.0626
5%	0.0921	0.0926	0.1078	0.0626

Table 38b: SON China Autocorrelation Timescale (1+phi)/(1-phi)

M.E./GCM	CCSM3	GISS	CCSM4	GISS-E2
0%	1.0596	0.7969	0.7424	0.6216
1%	1.0596	0.7969	0.7424	0.6216
2%	1.0596	0.7969	0.7424	0.6216
3%	1.0596	0.7969	0.7424	0.6216
4%	1.0596	0.7969	0.7424	0.6216
5%	1.0596	0.7969	0.7424	0.6216

Table 38c: SON China Standard Deviation (mm)

M.E./GCM	CCSM3	GISS	CCSM4	GISS-E2
0%	1.1891	1.1118	1.8108	1.2204
1%	1.251	1.1811	1.851	1.2674
2%	1.4099	1.3601	1.9655	1.3952
3%	1.6276	1.6046	2.1402	1.5802
4%	1.8816	1.8869	2.3605	1.8034
5%	2.159	2.1925	2.6147	2.0521

Table 38d: SON China TTD (years)

M.E./GCM	CCSM3	GISS	CCSM4	GISS-E2
0%	13.1552	11.7308	13.217	14.2095
1%	13.5458	12.138	13.403	14.5489
2%	14.5134	13.1571	13.9241	15.4464
3%	15.784	14.4882	14.7002	16.6928
4%	17.206	15.9587	15.6517	18.1342
5%	18.7012	17.4855	16.7163	19.6777

Table 39a: DJF Europe Trend (mm/year)

M.E./GCM	CCSM3	GISS	CCSM4	GISS-E2
0%	0.028	0.0262	0.0334	0.0252
1%	0.028	0.0262	0.0334	0.0252
2%	0.028	0.0262	0.0334	0.0252
3%	0.028	0.0262	0.0334	0.0252
4%	0.028	0.0262	0.0334	0.0252
5%	0.028	0.0262	0.0334	0.0252

Table 39b: DJF Europe Autocorrelation Timescale (1+phi)/(1-phi)

M.E./GCM	CCSM3	GISS	CCSM4	GISS-E2
0%	0.8731	1.0023	1.0381	0.952
1%	0.8731	1.0023	1.0381	0.952
2%	0.8731	1.0023	1.0381	0.952
3%	0.8731	1.0023	1.0381	0.952
4%	0.8731	1.0023	1.0381	0.952
5%	0.8731	1.0023	1.0381	0.952

Table 39c: DJF Europe Standard Deviation (mm)

M.E./GCM	CCSM3	GISS	CCSM4	GISS-E2
0%	0.5768	0.765	0.6339	0.5789
1%	0.5924	0.7741	0.6492	0.5916
2%	0.6364	0.8005	0.693	0.6278
3%	0.7031	0.842	0.7599	0.6833
4%	0.7865	0.896	0.8442	0.7533
5%	0.8818	0.9603	0.941	0.8342

Table 39d: DJF Europe TTD (years)

M.E./GCM	CCSM3	GISS	CCSM4	GISS-E2
0%	15.8625	20.8361	16.0237	17.8515
1%	16.159	21.017	16.2824	18.1096
2%	16.9819	21.5339	17.0084	18.8338
3%	18.1857	22.3256	18.0868	19.9124
4%	19.6294	23.325	19.3987	21.2318
5%	21.2104	24.4748	20.8519	22.7036

Table 40a: JJA Europe Trend (mm/year)

M.E./GCM	CCSM3	GISS	CCSM4	GISS-E2
0%	0.0413	0.0521	0.0529	0.0368
1%	0.0413	0.0521	0.0529	0.0368
2%	0.0413	0.0521	0.0529	0.0368
3%	0.0413	0.0521	0.0529	0.0368
4%	0.0413	0.0521	0.0529	0.0368
5%	0.0413	0.0521	0.0529	0.0368

Table 40b: JJA Europe Autocorrelation Timescale (1+phi)/(1-phi)

M.E./GCM	CCSM3	GISS	CCSM4	GISS-E2
0%	1.429	1.0097	1.1697	0.5705
1%	1.429	1.0097	1.1697	0.5705
2%	1.429	1.0097	1.1697	0.5705
3%	1.429	1.0097	1.1697	0.5705
4%	1.429	1.0097	1.1697	0.5705
5%	1.429	1.0097	1.1697	0.5705

Table 40c: JJA Europe Standard Deviation (mm)

M.E./GCM	CCSM3	GISS	CCSM4	GISS-E2
0%	0.8211	0.8463	0.8819	0.78
1%	0.8462	0.8818	0.9197	0.8136
2%	0.9167	0.9802	1.0245	0.9063
3%	1.0225	1.1248	1.1777	1.0418
4%	1.1534	1.3	1.3629	1.2055
5%	1.3018	1.4952	1.5688	1.3875

Table 40d: JJA Europe TTD (years)

M.E./GCM	CCSM3	GISS	CCSM4	GISS-E2
0%	18.3376	14.5642	15.3187	14.1805
1%	18.7194	14.9635	15.7549	14.5826
2%	19.77	16.0443	16.9295	15.664
3%	21.2887	17.5688	18.5753	17.1786
4%	23.0896	19.3328	20.4702	18.923
5%	25.0441	21.2079	22.4776	20.7721

Table 41a: MAM Europe Trend (mm/year)

M.E./GCM	CCSM3	GISS	CCSM4	GISS-E2
0%	0.0275	0.0229	0.0281	0.0238
1%	0.0275	0.0229	0.0281	0.0238
2%	0.0275	0.0229	0.0281	0.0238
3%	0.0275	0.0229	0.0281	0.0238
4%	0.0275	0.0229	0.0281	0.0238
5%	0.0275	0.0229	0.0281	0.0238

Table 41b: MAM Europe Autocorrelation Timescale (1+phi)/(1-phi)

M.E./GCM	CCSM3	GISS	CCSM4	GISS-E2
0%	0.9669	0.6151	0.6549	1.0815
1%	0.9669	0.6151	0.6549	1.0815
2%	0.9669	0.6151	0.6549	1.0815
3%	0.9669	0.6151	0.6549	1.0815
4%	0.9669	0.6151	0.6549	1.0815
5%	0.9669	0.6151	0.6549	1.0815

Table 41c: MAM Europe Standard Deviation (mm)

M.E./GCM	CCSM3	GISS	CCSM4	GISS-E2
0%	0.4244	0.6324	0.6138	0.5759
1%	0.4483	0.6485	0.6351	0.5923
2%	0.513	0.6943	0.6946	0.6387
3%	0.6053	0.764	0.783	0.7089
4%	0.7144	0.8514	0.8916	0.7965
5%	0.8337	0.9515	1.0139	0.8962

Table 41d: MAM Europe TTD (years)

M.E./GCM	CCSM3	GISS	CCSM4	GISS-E2
0%	13.5759	17.3693	14.9718	19.1665
1%	14.0942	17.6844	15.3275	19.5359
2%	15.448	18.562	16.2967	20.5614
3%	17.2741	19.8505	17.6795	22.0608
4%	19.3109	21.3997	19.3	23.8566
5%	21.4195	23.0991	21.042	25.8199

Table 42a: SON Europe Trend (mm/year)

M.E./GCM	CCSM3	GISS	CCSM4	GISS-E2
0%	0.0381	0.0373	0.05	0.032
1%	0.0381	0.0373	0.05	0.032
2%	0.0381	0.0373	0.05	0.032
3%	0.0381	0.0373	0.05	0.032
4%	0.0381	0.0373	0.05	0.032
5%	0.0381	0.0373	0.05	0.032

Table 42b: SON Europe Autocorrelation Timescale (1+phi)/(1-phi)

M.E./GCM	CCSM3	GISS	CCSM4	GISS-E2
0%	0.7859	0.7178	1.1028	0.8564
1%	0.7859	0.7178	1.1028	0.8564
2%	0.7859	0.7178	1.1028	0.8564
3%	0.7859	0.7178	1.1028	0.8564
4%	0.7859	0.7178	1.1028	0.8564
5%	0.7859	0.7178	1.1028	0.8564

Table 42c: SON Europe Standard Deviation (mm)

M.E./GCM	CCSM3	GISS	CCSM4	GISS-E2
0%	0.5783	0.6809	0.7213	0.6678
1%	0.6052	0.7022	0.7513	0.6945
2%	0.6794	0.7624	0.8346	0.7677
3%	0.787	0.8528	0.9568	0.8746
4%	0.916	0.9649	1.105	1.004
5%	1.0588	1.0919	1.2701	1.1482

Table 42d: SON Europe TTD (years)

M.E./GCM	CCSM3	GISS	CCSM4	GISS-E2
0%	12.5372	14.0017	13.5835	16.0952
1%	12.9284	14.2902	13.9725	16.5275
2%	13.972	15.0887	15.0207	17.6803
3%	15.4168	16.2509	16.4905	19.2866
4%	17.063	17.6354	18.1828	21.1379
5%	18.7938	19.1416	19.975	23.1071

Table 43a: DJF India Trend (mm/year)

M.E./GCM	CCSM3	GISS	CCSM4	GISS-E2
0%	0.0908	0.08	0.0906	0.0777
1%	0.0908	0.08	0.0906	0.0777
2%	0.0908	0.08	0.0906	0.0777
3%	0.0908	0.08	0.0906	0.0777
4%	0.0908	0.08	0.0906	0.0777
5%	0.0908	0.08	0.0906	0.0777

Table 43b: DJF India Autocorrelation Timescale (1+phi)/(1-phi)

M.E./GCM	CCSM3	GISS	CCSM4	GISS-E2
0%	0.9814	0.7619	0.9648	0.5484
1%	0.9814	0.7619	0.9648	0.5484
2%	0.9814	0.7619	0.9648	0.5484
3%	0.9814	0.7619	0.9648	0.5484
4%	0.9814	0.7619	0.9648	0.5484
5%	0.9814	0.7619	0.9648	0.5484

Table 43c: DJF India Standard Deviation (mm)

M.E./GCM	CCSM3	GISS	CCSM4	GISS-E2
0%	1.791	1.85	2.4489	1.8054
1%	1.8172	1.8812	2.4718	1.8301
2%	1.8937	1.9707	2.5392	1.902
3%	2.0145	2.1084	2.6472	2.0158
4%	2.1722	2.2837	2.7906	2.1646
5%	2.3592	2.488	2.9641	2.3417

Table 43d: DJF India TTD (years)

M.E./GCM	CCSM3	GISS	CCSM4	GISS-E2
0%	16.0424	17.4143	19.6593	14.8355
1%	16.1951	17.582	19.7786	14.966
2%	16.6363	18.0568	20.1268	15.3434
3%	17.322	18.7758	20.6787	15.9317
4%	18.1974	19.6741	21.4009	16.6859
5%	19.21	20.6987	22.2585	17.5624

Table 44a: JJA India Trend (mm/year)

M.E./GCM	CCSM3	GISS	CCSM4	GISS-E2
0%	0.1447	0.123	0.1441	0.108
1%	0.1447	0.123	0.1441	0.108
2%	0.1447	0.123	0.1441	0.108
3%	0.1447	0.123	0.1441	0.108
4%	0.1447	0.123	0.1441	0.108
5%	0.1447	0.123	0.1441	0.108

Table 44b: JJA India Autocorrelation Timescale (1+phi)/(1-phi)

M.E./GCM	CCSM3	GISS	CCSM4	GISS-E2
0%	0.8844	0.7047	0.8105	0.6264
1%	0.8844	0.7047	0.8105	0.6264
2%	0.8844	0.7047	0.8105	0.6264
3%	0.8844	0.7047	0.8105	0.6264
4%	0.8844	0.7047	0.8105	0.6264
5%	0.8844	0.7047	0.8105	0.6264

Table 44c: JJA India Standard Deviation (mm)

M.E./GCM	CCSM3	GISS	CCSM4	GISS-E2
0%	1.1408	1.3486	1.3048	1.2251
1%	1.2907	1.4622	1.4434	1.3156
2%	1.6386	1.7489	1.7847	1.5511
3%	2.076	2.1315	2.2293	1.8742
4%	2.5572	2.5665	2.726	2.2469
5%	3.0629	3.0319	3.2516	2.6486

Table 44d: JJA India TTD (years)

M.E./GCM	CCSM3	GISS	CCSM4	GISS-E2
0%	8.46	10.3005	9.0144	9.7218
1%	9.2144	10.8287	9.6598	10.1767
2%	10.8246	12.1023	11.144	11.3144
3%	12.6699	13.7034	12.9225	12.7884
4%	14.5467	15.4204	14.766	14.3927
5%	16.3927	17.1623	16.5949	16.0305

Table 45a: MAM India Trend (mm/year)

M.E./GCM	CCSM3	GISS	CCSM4	GISS-E2
0%	0.1021	0.0738	0.0749	0.0893
1%	0.1021	0.0738	0.0749	0.0893
2%	0.1021	0.0738	0.0749	0.0893
3%	0.1021	0.0738	0.0749	0.0893
4%	0.1021	0.0738	0.0749	0.0893
5%	0.1021	0.0738	0.0749	0.0893

Table 45b: MAM India Autocorrelation Timescale (1+phi)/(1-phi)

M.E./GCM	CCSM3	GISS	CCSM4	GISS-E2
0%	0.9894	1.2069	0.8201	0.8905
1%	0.9894	1.2069	0.8201	0.8905
2%	0.9894	1.2069	0.8201	0.8905
3%	0.9894	1.2069	0.8201	0.8905
4%	0.9894	1.2069	0.8201	0.8905
5%	0.9894	1.2069	0.8201	0.8905

Table 45c: MAM India Standard Deviation (mm)

M.E./GCM	CCSM3	GISS	CCSM4	GISS-E2
0%	1.4208	1.3582	1.9312	1.2451
1%	1.4617	1.4093	1.9629	1.2952
2%	1.5781	1.5513	2.0548	1.4349
3%	1.7545	1.7605	2.1987	1.641
4%	1.9749	2.0154	2.3849	1.8918
5%	2.2261	2.3006	2.6041	2.1719

Table 45d: MAM India TTD (years)

M.E./GCM	CCSM3	GISS	CCSM4	GISS-E2
0%	12.7713	16.7463	17.954	12.3226
1%	13.0107	17.1483	18.1585	12.652
2%	13.6792	18.2393	18.7436	13.5471
3%	14.6637	19.7885	19.6391	14.8152
4%	15.8496	21.5979	20.7636	16.2877
5%	17.1508	23.539	22.045	17.8562

Table 46a: SON India Trend (mm/year)

M.E./GCM	CCSM3	GISS	CCSM4	GISS-E2
0%	0.1489	0.1291	0.1332	0.0926
1%	0.1489	0.1291	0.1332	0.0926
2%	0.1489	0.1291	0.1332	0.0926
3%	0.1489	0.1291	0.1332	0.0926
4%	0.1489	0.1291	0.1332	0.0926
5%	0.1489	0.1291	0.1332	0.0926

Table 46b: SON India Autocorrelation Timescale (1+phi)/(1-phi)

M.E./GCM	CCSM3	GISS	CCSM4	GISS-E2
0%	1.2799	0.9063	0.8389	0.9792
1%	1.2799	0.9063	0.8389	0.9792
2%	1.2799	0.9063	0.8389	0.9792
3%	1.2799	0.9063	0.8389	0.9792
4%	1.2799	0.9063	0.8389	0.9792
5%	1.2799	0.9063	0.8389	0.9792

Table 46c: SON India Standard Deviation (mm)

M.E./GCM	CCSM3	GISS	CCSM4	GISS-E2
0%	1.2584	1.543	1.7029	1.2918
1%	1.356	1.6058	1.7837	1.3558
2%	1.6036	1.7767	2.0004	1.5298
3%	1.9372	2.0233	2.3082	1.7798
4%	2.3191	2.3194	2.6742	2.0782
5%	2.7297	2.6479	3.0777	2.4071

Table 46d: SON India TTD (years)

M.E./GCM	CCSM3	GISS	CCSM4	GISS-E2
0%	10.0545	11.5774	11.4859	12.7386
1%	10.5824	11.8706	11.8522	13.1612
2%	11.845	12.6476	12.7965	14.2726
3%	13.4274	13.7237	14.0683	15.7914
4%	15.123	14.9601	15.5017	17.5093
5%	16.8428	16.2752	17.0061	19.3083

Table 47a: DJF U.S. Trend (mm/year)

M.E./GCM	CCSM3	GISS	CCSM4	GISS-E2
0%	0.0387	0.0341	0.0517	0.0422
1%	0.0387	0.0341	0.0517	0.0422
2%	0.0387	0.0341	0.0517	0.0422
3%	0.0387	0.0341	0.0517	0.0422
4%	0.0387	0.0341	0.0517	0.0422
5%	0.0387	0.0341	0.0517	0.0422

Table 47b: DJF U.S. Autocorrelation Timescale (1+phi)/(1-phi)

M.E./GCM	CCSM3	GISS	CCSM4	GISS-E2
0%	0.9615	0.8395	1.116	0.685
1%	0.9615	0.8395	1.116	0.685
2%	0.9615	0.8395	1.116	0.685
3%	0.9615	0.8395	1.116	0.685
4%	0.9615	0.8395	1.116	0.685
5%	0.9615	0.8395	1.116	0.685

Table 47c: DJF U.S. Standard Deviation (mm)

M.E./GCM	CCSM3	GISS	CCSM4	GISS-E2
0%	0.8401	0.843	1.0999	0.8416
1%	0.8702	0.8672	1.129	0.8651
2%	0.9498	0.9345	1.2087	0.9313
3%	1.0628	1.0338	1.3249	1.0305
4%	1.1983	1.1556	1.4666	1.1535
5%	1.3495	1.2933	1.6264	1.2932

Table 47d: DJF U.S. TTD (years)

M.E./GCM	CCSM3	GISS	CCSM4	GISS-E2
0%	17.016	18.9976	18.4631	15.496
1%	17.4288	19.3049	18.7559	15.7346
2%	18.4693	20.1444	19.5375	16.3981
3%	19.8665	21.3557	20.639	17.374
4%	21.4621	22.803	21.9351	18.5547
5%	23.1674	24.3935	23.3487	19.8612

Table 48a: JJA U.S. Trend (mm/year)

M.E./GCM	CCSM3	GISS	CCSM4	GISS-E2
0%	0.0713	0.0797	0.0857	0.0701
1%	0.0713	0.0797	0.0857	0.0701
2%	0.0713	0.0797	0.0857	0.0701
3%	0.0713	0.0797	0.0857	0.0701
4%	0.0713	0.0797	0.0857	0.0701
5%	0.0713	0.0797	0.0857	0.0701

Table 48b: JJA U.S. Autocorrelation Timescale (1+phi)/(1-phi)

M.E./GCM	CCSM3	GISS	CCSM4	GISS-E2
0%	1.0229	1.0183	0.8867	1.1687
1%	1.0229	1.0183	0.8867	1.1687
2%	1.0229	1.0183	0.8867	1.1687
3%	1.0229	1.0183	0.8867	1.1687
4%	1.0229	1.0183	0.8867	1.1687
5%	1.0229	1.0183	0.8867	1.1687

Table 48c: JJA U.S. Standard Deviation (mm)

M.E./GCM	CCSM3	GISS	CCSM4	GISS-E2
0%	0.786	0.8284	0.8805	0.6814
1%	0.8438	0.9178	0.971	0.7728
2%	0.9972	1.1407	1.196	0.992
3%	1.21	1.4339	1.4927	1.272
4%	1.4563	1.7625	1.8268	1.5813
5%	1.7219	2.1103	2.1815	1.9059

Table 48d: JJA U.S. TTD (years)

M.E./GCM	CCSM3	GISS	CCSM4	GISS-E2
0%	11.1012	10.7435	10.3051	10.8354
1%	11.6472	11.5133	10.9923	11.7514
2%	13.0332	13.3184	12.6031	13.8076
3%	14.839	15.5105	14.5785	16.233
4%	16.7989	17.7929	16.6545	18.7215
5%	18.7896	20.058	18.7276	21.1713

Table 49a: MAM U.S. Trend (mm/year)

M.E./GCM	CCSM3	GISS	CCSM4	GISS-E2
0%	0.0494	0.0463	0.0556	0.046
1%	0.0494	0.0463	0.0556	0.046
2%	0.0494	0.0463	0.0556	0.046
3%	0.0494	0.0463	0.0556	0.046
4%	0.0494	0.0463	0.0556	0.046
5%	0.0494	0.0463	0.0556	0.046

Table 49b: MAM U.S. Autocorrelation Timescale (1+phi)/(1-phi)

M.E./GCM	CCSM3	GISS	CCSM4	GISS-E2
0%	1.0224	0.6498	0.9986	0.7615
1%	1.0224	0.6498	0.9986	0.7615
2%	1.0224	0.6498	0.9986	0.7615
3%	1.0224	0.6498	0.9986	0.7615
4%	1.0224	0.6498	0.9986	0.7615
5%	1.0224	0.6498	0.9986	0.7615

Table 49c: MAM U.S. Standard Deviation (mm)

M.E./GCM	CCSM3	GISS	CCSM4	GISS-E2
0%	0.8471	0.9009	1.0396	0.8734
1%	0.8795	0.935	1.0734	0.9021
2%	0.9689	1.0297	1.1676	0.9827
3%	1.0997	1.1692	1.3075	1.1028
4%	1.2582	1.3389	1.4794	1.2504
5%	1.4353	1.5287	1.6733	1.4169

Table 49d: MAM U.S. TTD (years)

M.E./GCM	CCSM3	GISS	CCSM4	GISS-E2
0%	14.9103	13.9046	15.7764	14.4066
1%	15.2829	14.2566	16.1339	14.7187
2%	16.283	15.2083	17.1046	15.5729
3%	17.6877	16.5522	18.4873	16.7987
4%	19.3174	18.1132	20.1095	18.243
5%	21.06	19.7806	21.858	19.8032

Table 50a: SON U.S. Trend (mm/year)

M.E./GCM	CCSM3	GISS	CCSM4	GISS-E2
0%	0.0624	0.0631	0.082	0.0728
1%	0.0624	0.0631	0.082	0.0728
2%	0.0624	0.0631	0.082	0.0728
3%	0.0624	0.0631	0.082	0.0728
4%	0.0624	0.0631	0.082	0.0728
5%	0.0624	0.0631	0.082	0.0728

Table 50b: SON U.S. Autocorrelation Timescale (1+phi)/(1-phi)

M.E./GCM	CCSM3	GISS	CCSM4	GISS-E2
0%	0.8282	0.7939	0.9108	0.6534
1%	0.8282	0.7939	0.9108	0.6534
2%	0.8282	0.7939	0.9108	0.6534
3%	0.8282	0.7939	0.9108	0.6534
4%	0.8282	0.7939	0.9108	0.6534
5%	0.8282	0.7939	0.9108	0.6534

Table 50c: SON U.S. Standard Deviation (mm)

M.E./GCM	CCSM3	GISS	CCSM4	GISS-E2
0%	0.8855	0.8175	1.0754	1.02
1%	0.931	0.8734	1.1353	1.0672
2%	1.053	1.0195	1.2924	1.1941
3%	1.2258	1.2208	1.5107	1.375
4%	1.4301	1.454	1.7663	1.5907
5%	1.6543	1.7063	2.0454	1.829

Table 50d: SON U.S. TTD (years)

M.E./GCM	CCSM3	GISS	CCSM4	GISS-E2
0%	12.2744	11.7651	12.1755	11.1475
1%	12.6876	12.2605	12.6215	11.5095
2%	13.7567	13.5089	13.7405	12.4427
3%	15.1941	15.1414	15.2075	13.6995
4%	16.8053	16.9339	16.8307	15.1149
5%	18.4874	18.7774	18.5151	16.5987

Table 51a: Region 1 95th Percentile Upper Bound

Month/Overpass	08 UTC	19 UTC
August	10	8
February	8	8

Table 51b: Region 1 95th Percentile Lower Bound

Month/Overpass	08 UTC	19 UTC
August	-14	-14
February	-14	-14

Table 52a: Region 2 95th Percentile Upper Bound

Month/Overpass	08 UTC	19 UTC
August	12	10
February	16	12

Table 52b: Region 2 95th Percentile Lower Bound

Month/Overpass	08 UTC	19 UTC
August	-14	-14
February	-14	-14

Table 53: AIRS L3 V5.2 Trend Error

AIRS L3 V5.2 - Dataset Trend Error	08 UTC	19 UTC
MWR	0.281	0.422
SuomiNet	0.485	0.71
NPN	-0.0286	0.211
NARR	0.0937	0.277

Table 54: AIRS L3 V6 Trend Error

AIRS L3 V6 - Dataset Trend Error	08 UTC	19 UTC
MWR	0.139	0.107
SuomiNet	0.445	0.413
NPN	0.067	0.0462
NARR	0.469	0.437

Table 55: AIRS L3 v5.2 Bias Error (%)

AIRS L3 v5.2 - Dataset	08 UTC	19 UTC
MWR	-7.8794	-4.7834
SuomiNet	-3.716	-0.364
NPN	-2.8182	0.3534
NARR	-2.9208	0.3867

Table 56: AIRS L3 v6 Bias Percent Error (%)

AIRS L3 v6 - Dataset	08 UTC	19 UTC
MWR	-4.5647	-6.2115
SuomiNet	-0.3535	-1.9561
NPN	-1.4590	-2.9499
NARR	-0.3059	-1.9636

IX. FIGURES

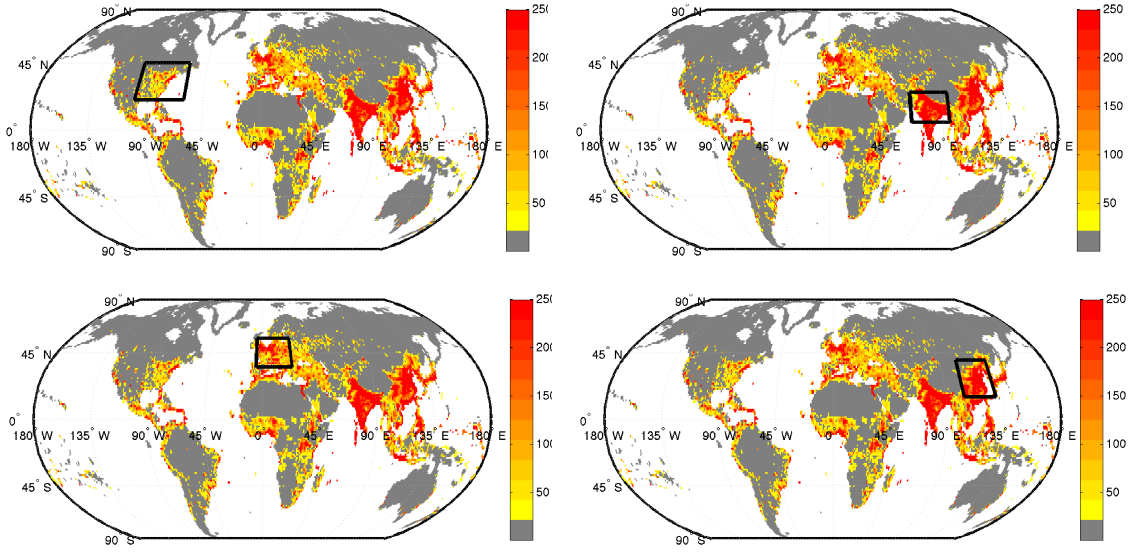

Figure 1: Population Density (population/km2) for Each Region: United States (top left panel), India (top right panel), Europe (bottom left panel), and China (bottom right panel)

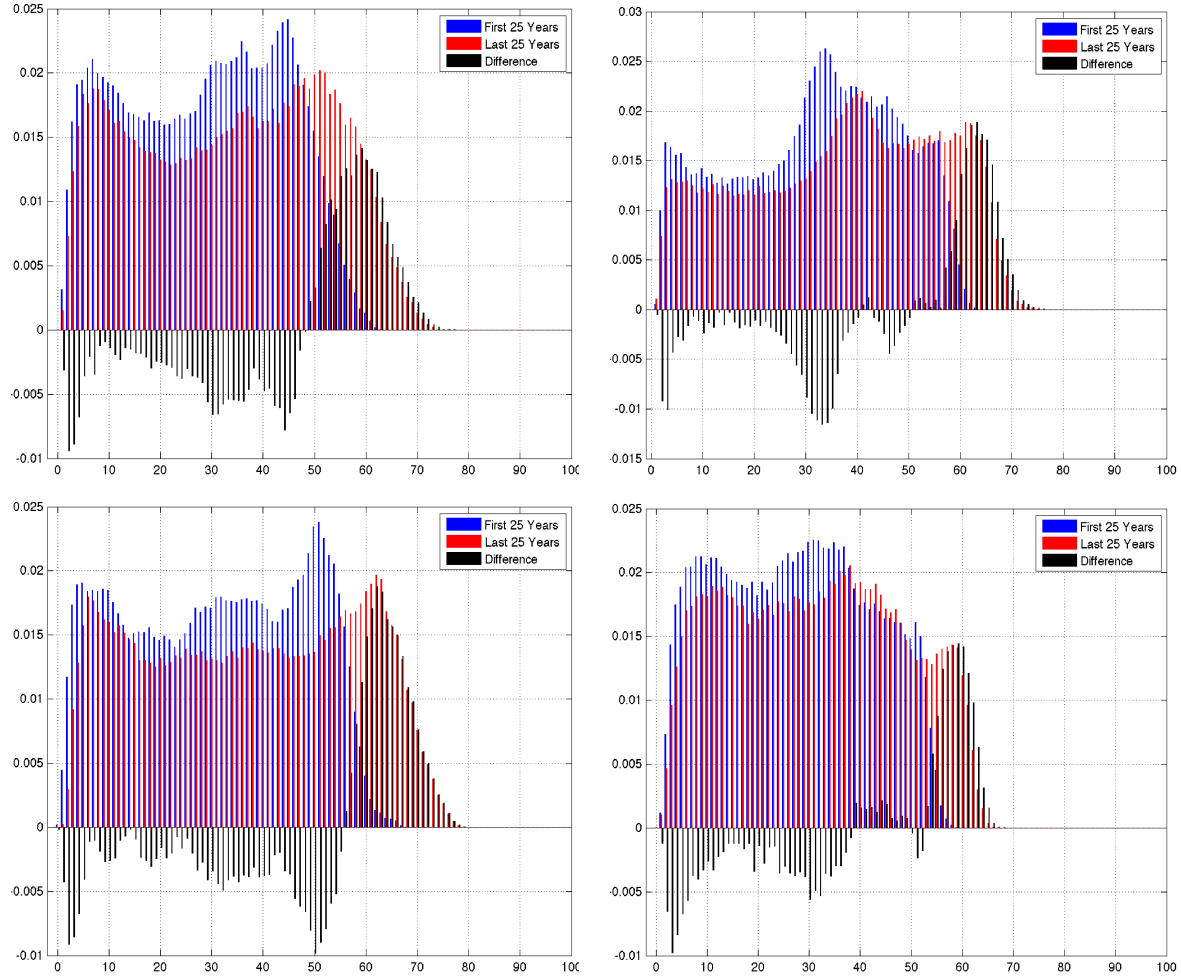

Figure 2: China PWV PDF Shift (Last 25 Years - First 25 Years) (mm) for CMIP3 Models, CCSM3 (top left panel) and GISS (top right panel), and CMIP5 Models, CCSM4 (bottom left panel) and GISS-E2 (bottom right panel)

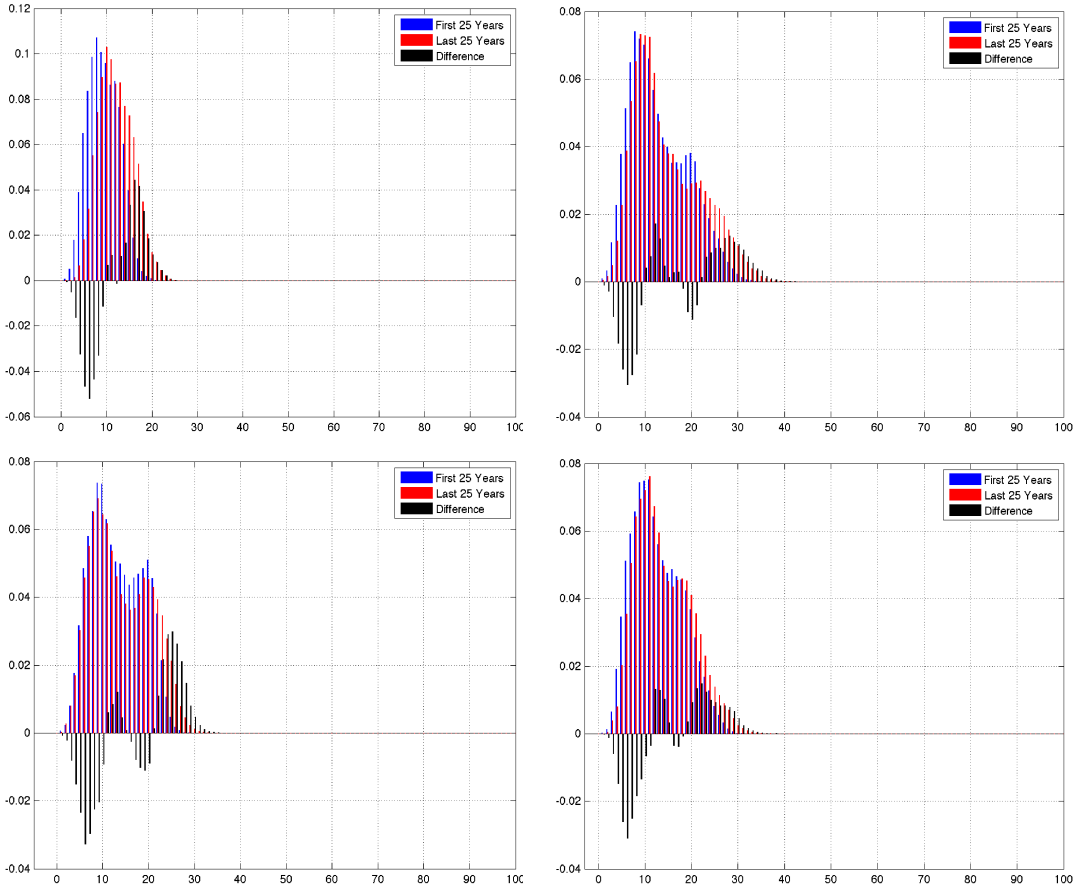

Figure 3: Europe PWV PDF Shift (Last 25 Years - First 25 Years) (mm) for CMIP3 Models, CCSM3 (top left panel) and GISS (top right panel), and CMIP5 Models, CCSM4 (bottom left panel) and GISS-E2 (bottom right panel)

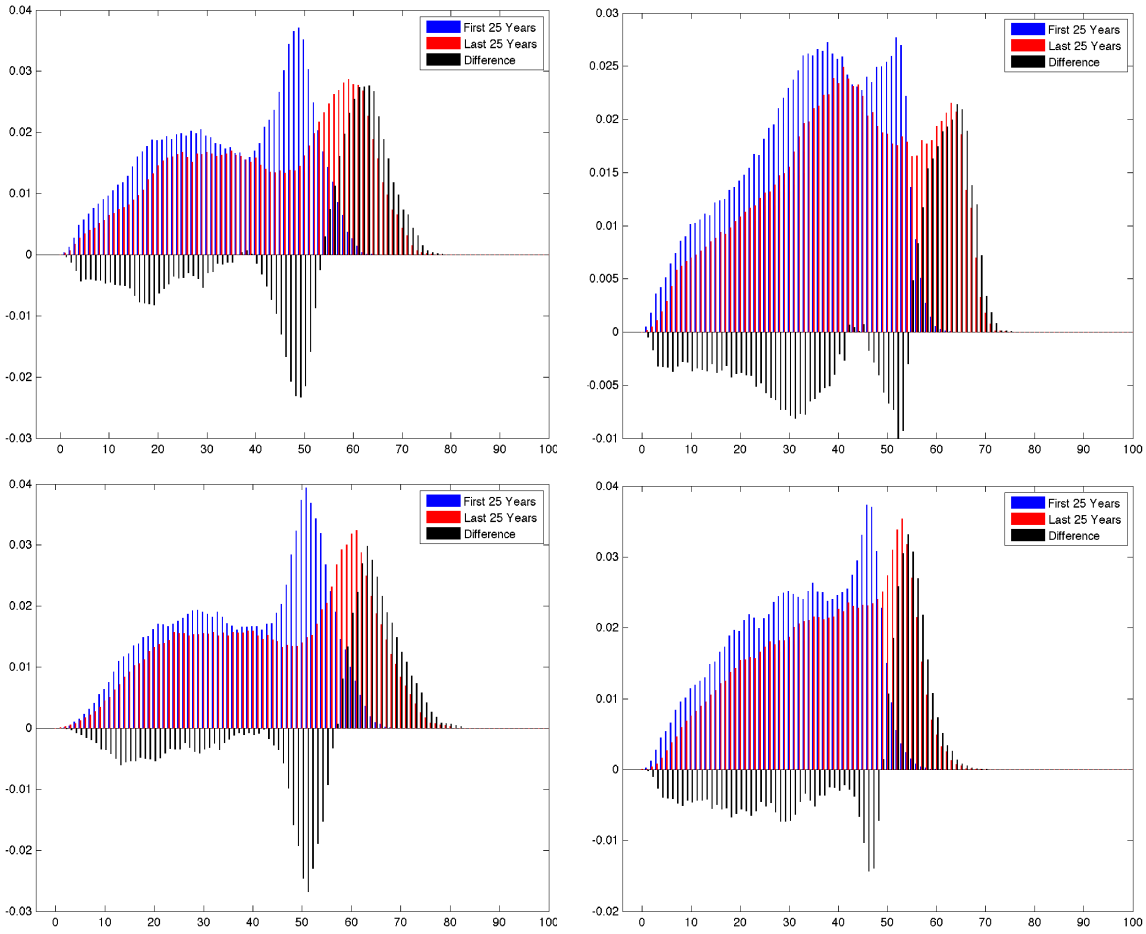

Figure 4: India PWV PDF Shift (Last 25 Years - First 25 Years) (mm) for CMIP3 Models, CCSM3 (top left panel) and GISS (top right panel), and CMIP5 Models, CCSM4 (bottom left panel) and GISS-E2 (bottom right panel)

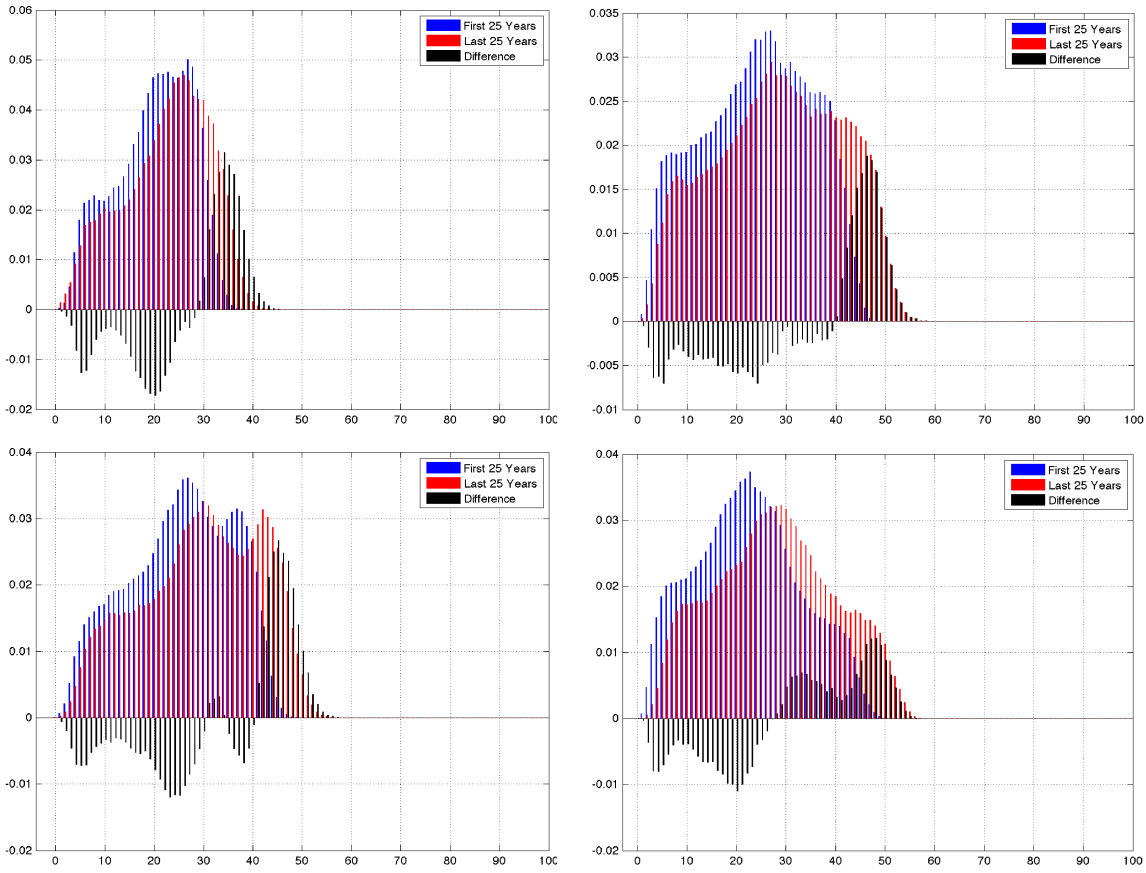

Figure 5: U.S. PWV PDF Shift (Last 25 Years - First 25 Years) (mm) for CMIP3 Models, CCSM3 (top left panel) and GISS (top right panel), and CMIP5 Models, CCSM4 (bottom left panel) and GISS-E2 (bottom right panel)

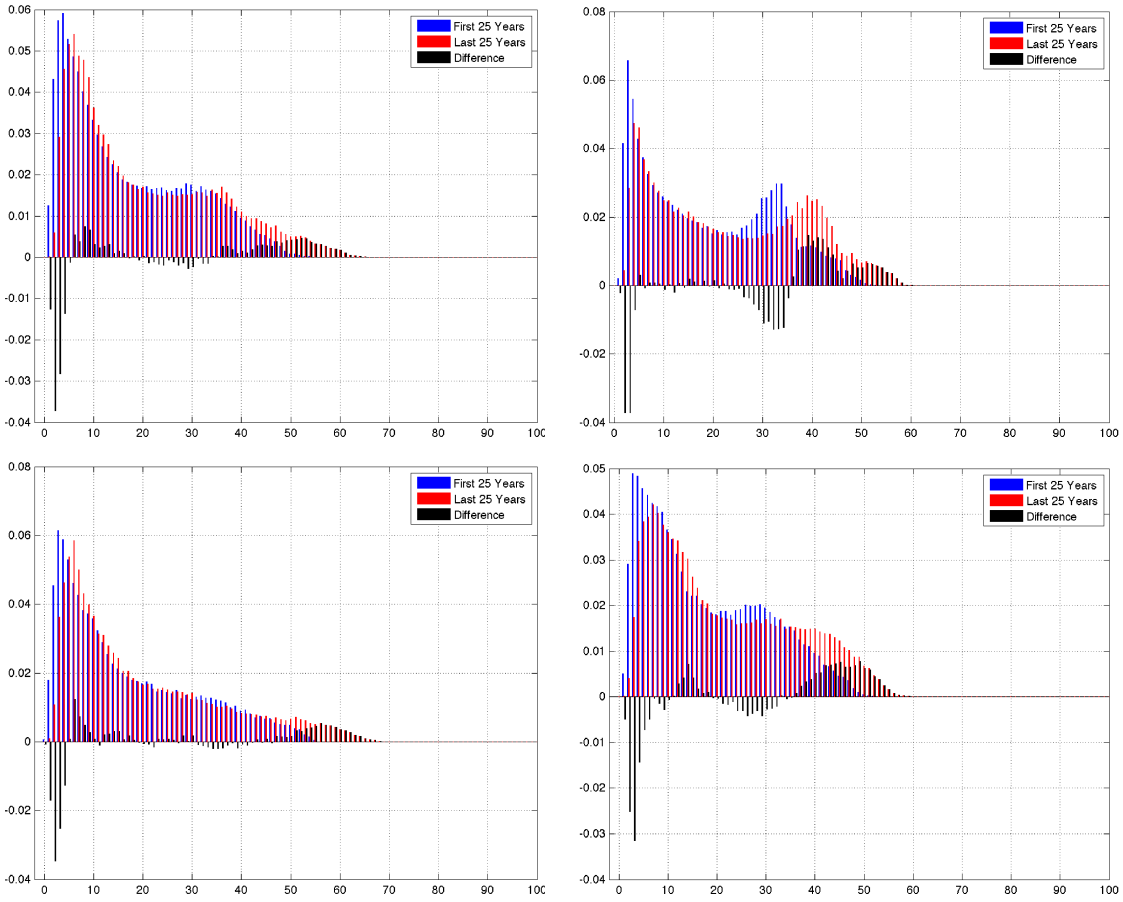

Figure 6: DJF China PWV PDF Shift (Last 25 Years - First 25 Years) (mm) for CMIP3 Models, CCSM3 (top left panel) and GISS (top right panel), and CMIP5 Models, CCSM4 (bottom left panel) and GISS-E2 (bottom right panel)

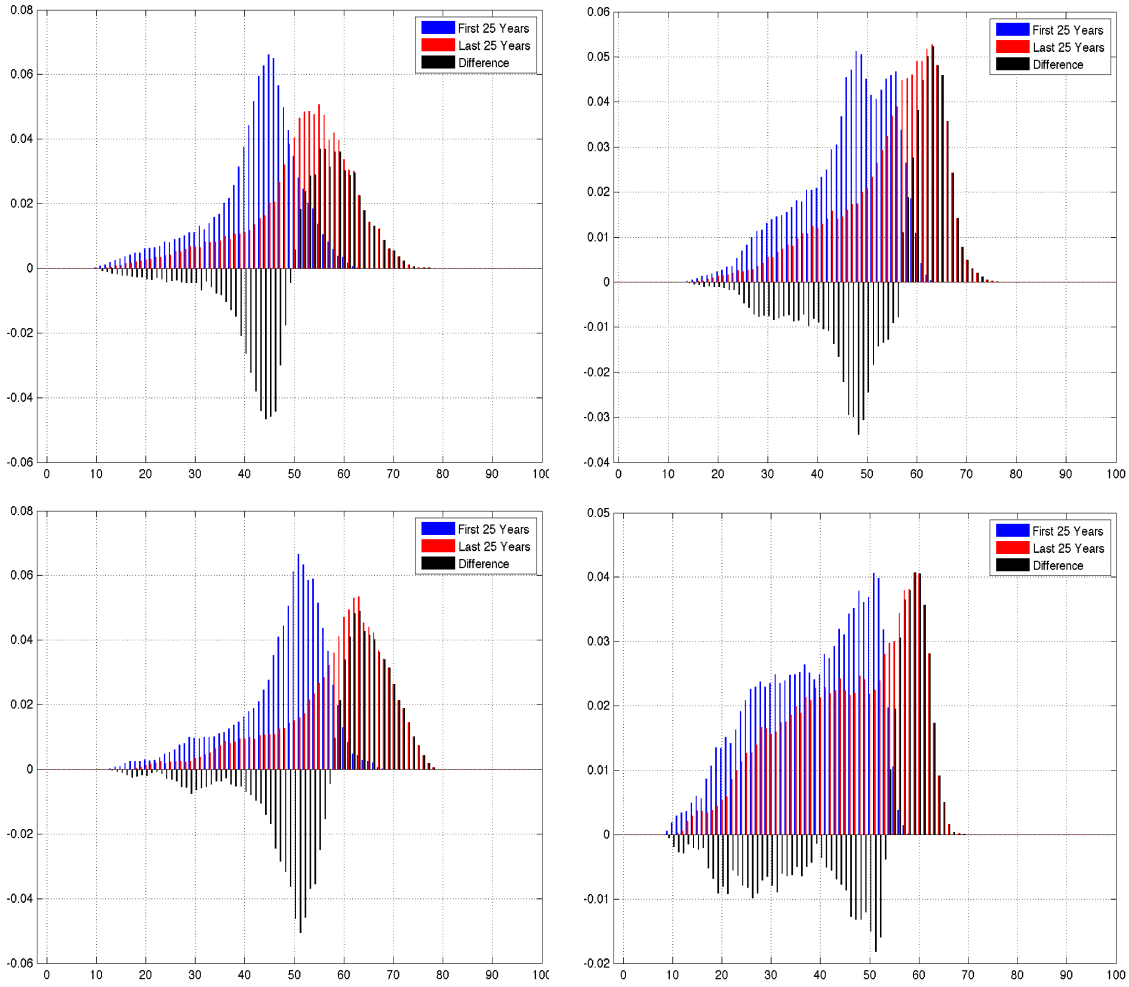

Figure 7: JJA China PWV PDF Shift (Last 25 Years - First 25 Years) (mm) for CMIP3 Models, CCSM3 (top left panel) and GISS (top right panel), and CMIP5 Models, CCSM4 (bottom left panel) and GISS-E2 (bottom right panel)

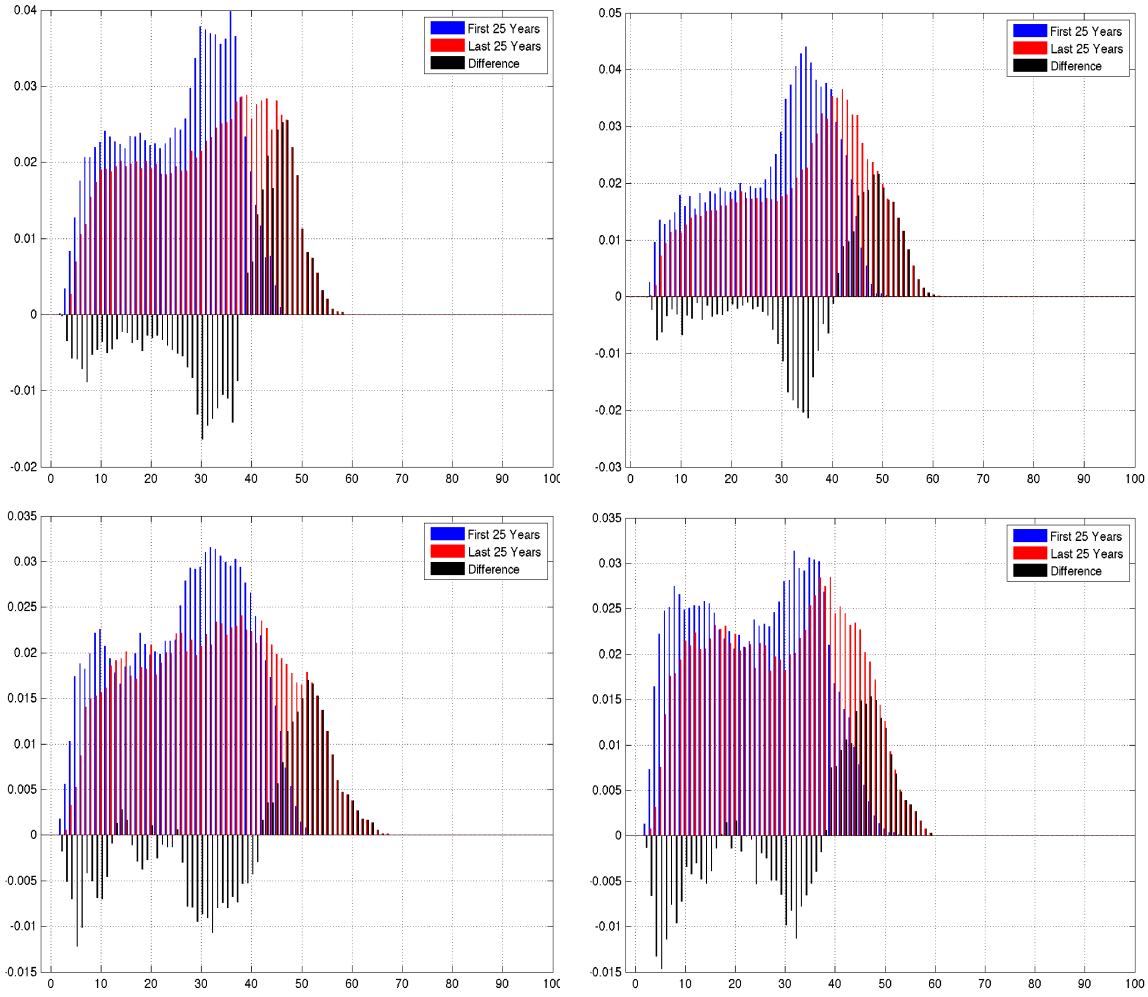

Figure 8: MAM China PWV PDF Shift (Last 25 Years - First 25 Years) (mm) for CMIP3 Models, CCSM3 (top left panel) and GISS (top right panel), and CMIP5 Models, CCSM4 (bottom left panel) and GISS-E2 (bottom right panel)

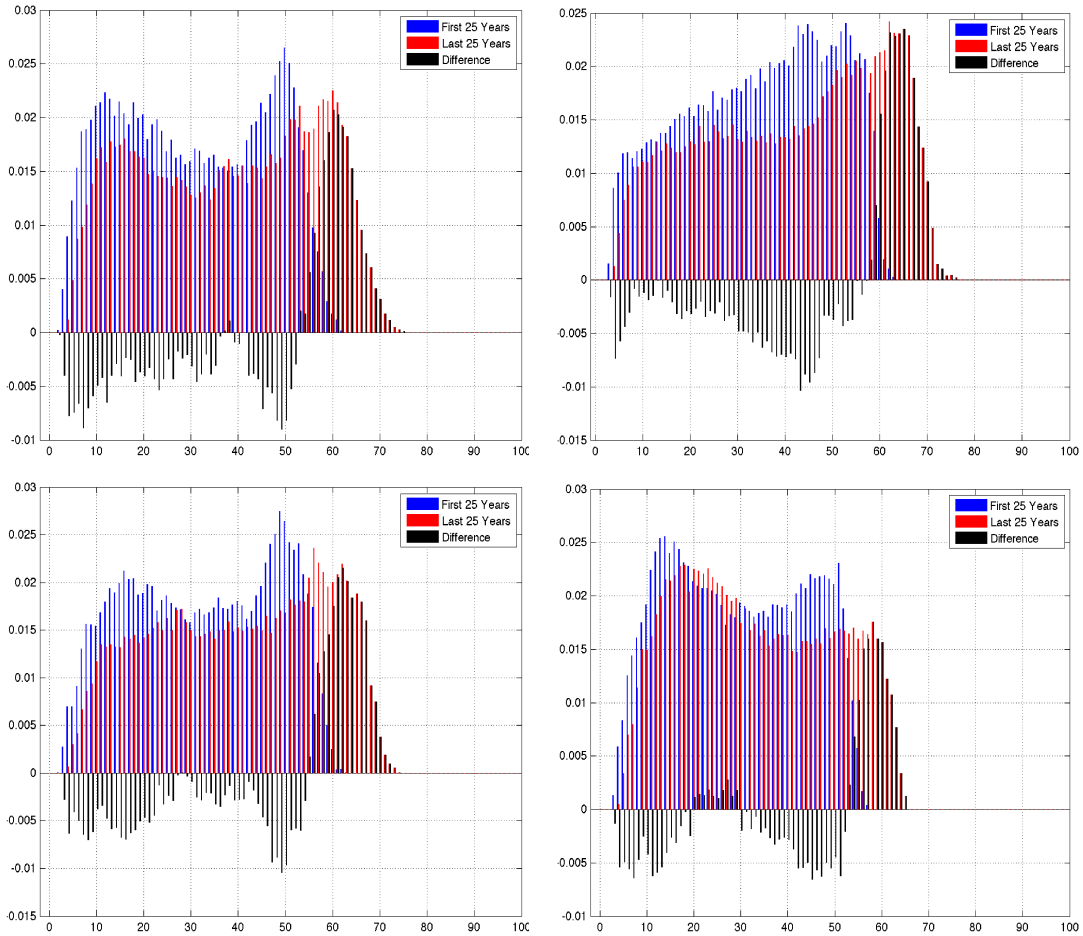

Figure 9: SON China PWV PDF Shift (Last 25 Years - First 25 Years) (mm) for CMIP3 Models, CCSM3 (top left panel) and GISS (top right panel), and CMIP5 Models, CCSM4 (bottom left panel) and GISS-E2 (bottom right panel)

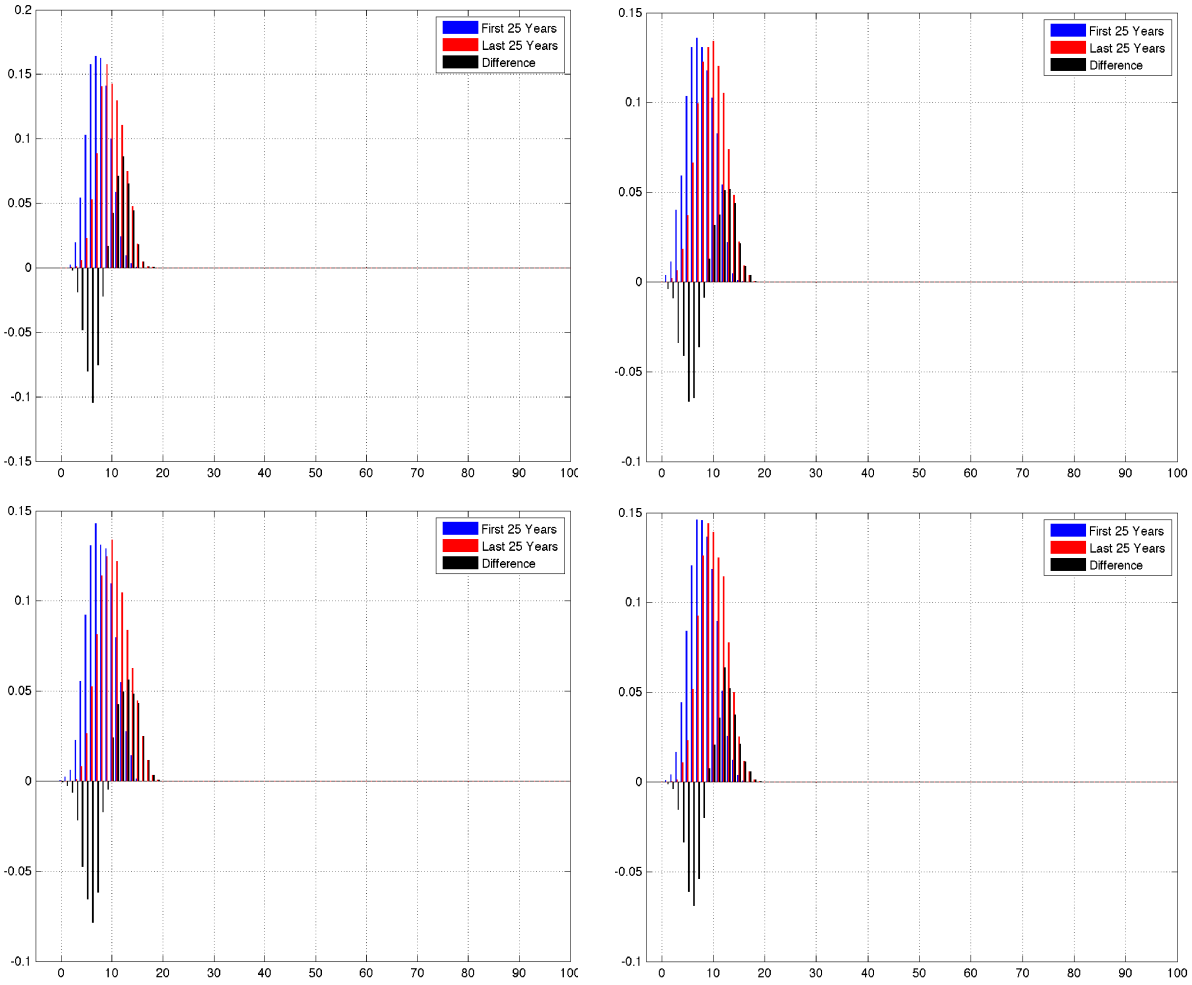

Figure 10: DJF Europe PWV PDF Shift (Last 25 Years - First 25 Years) (mm) for CMIP3 Models, CCSM3 (top left panel) and GISS (top right panel), and CMIP5 Models, CCSM4 (bottom left panel) and GISS-E2 (bottom right panel)

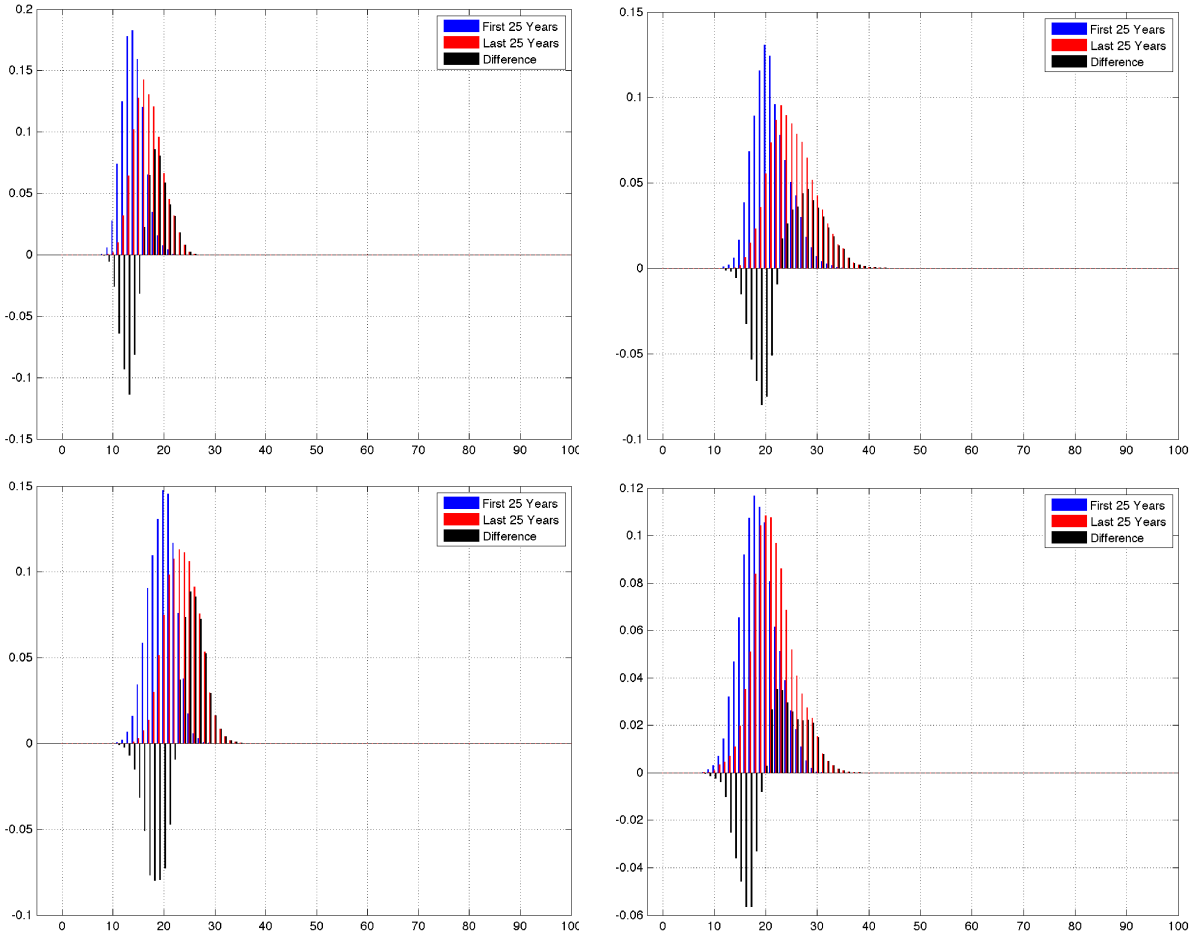

Figure 11: JJA Europe PWV PDF Shift (Last 25 Years - First 25 Years) (mm) for CMIP3 Models, CCSM3 (top left panel) and GISS (top right panel), and CMIP5 Models, CCSM4 (bottom left panel) and GISS-E2 (bottom right panel)

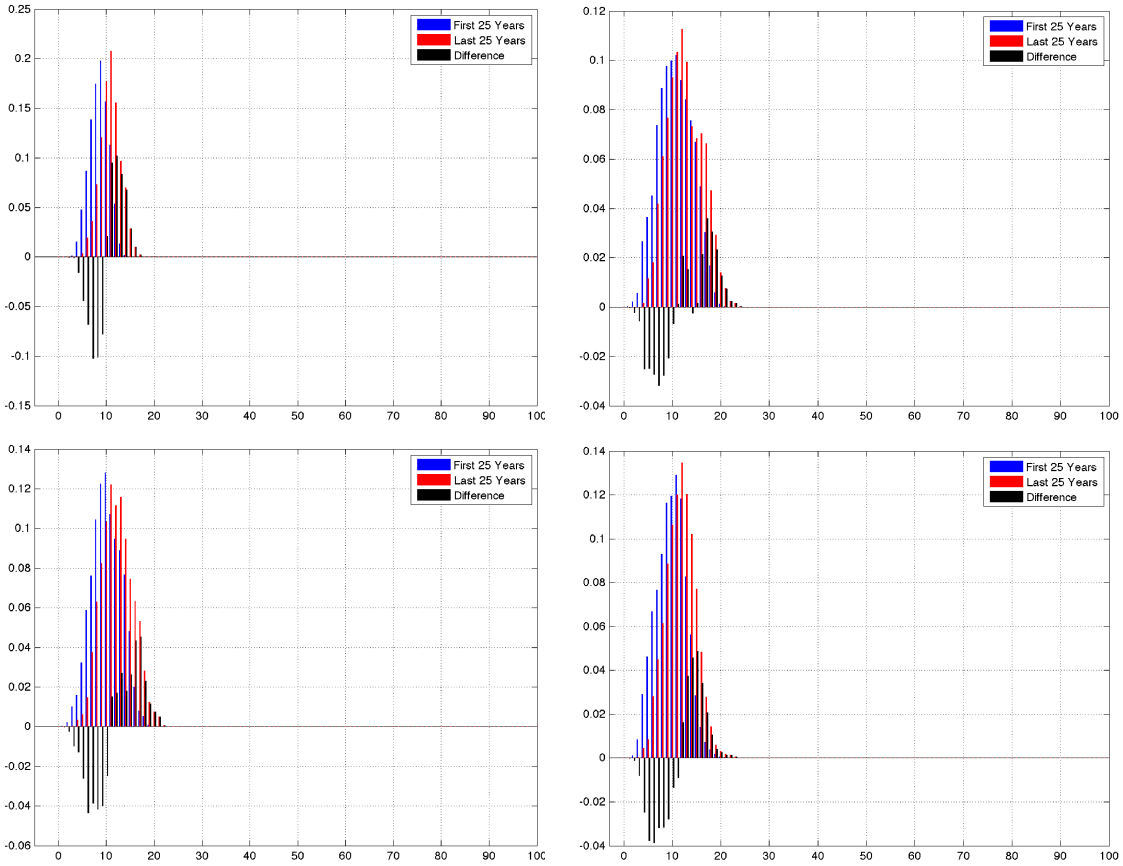

Figure 12: MAM Europe PWV PDF Shift (Last 25 Years - First 25 Years) (mm) for CMIP3 Models, CCSM3 (top left panel) and GISS (top right panel), and CMIP5 Models, CCSM4 (bottom left panel) and GISS-E2 (bottom right panel)

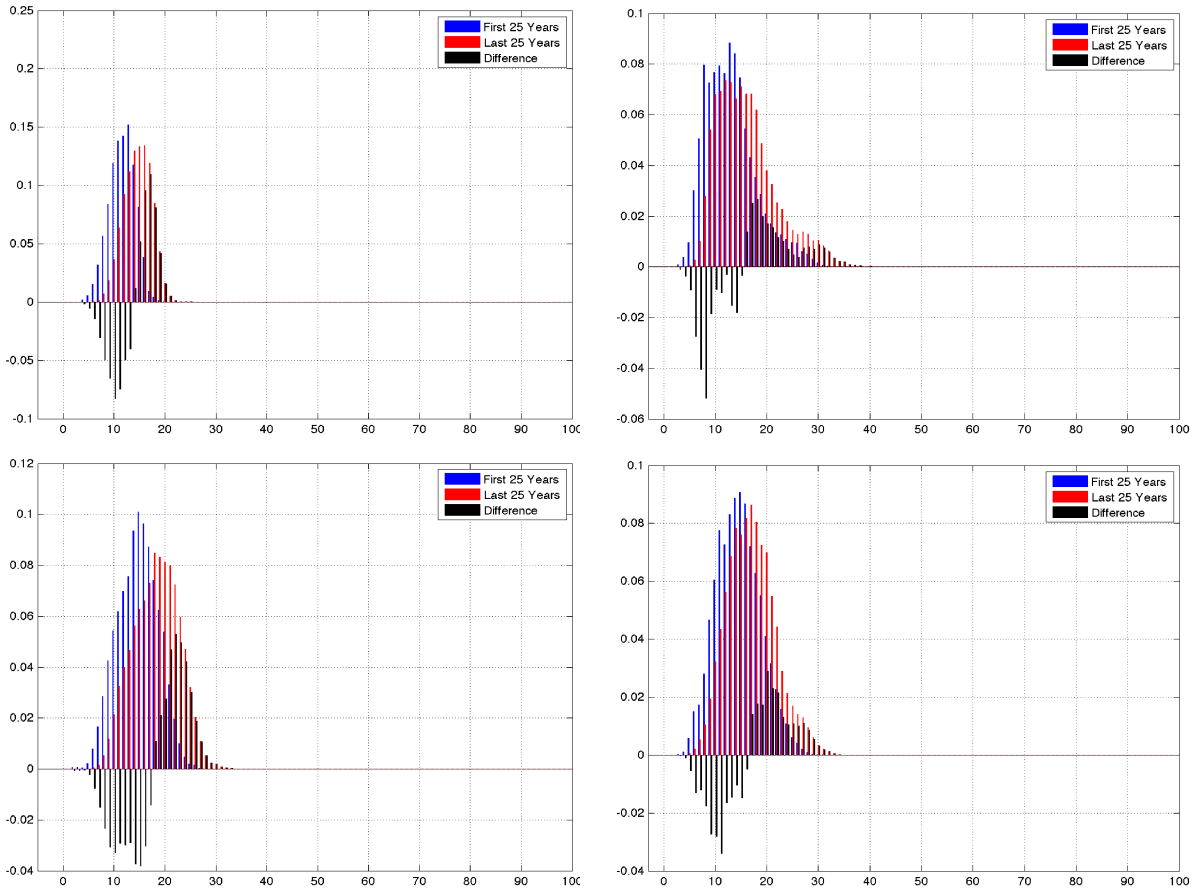

Figure 13: SON Europe PWV PDF Shift (Last 25 Years - First 25 Years) (mm) for CMIP3 Models, CCSM3 (top left panel) and GISS (top right panel), and CMIP5 Models, CCSM4 (bottom left panel) and GISS-E2 (bottom right panel)

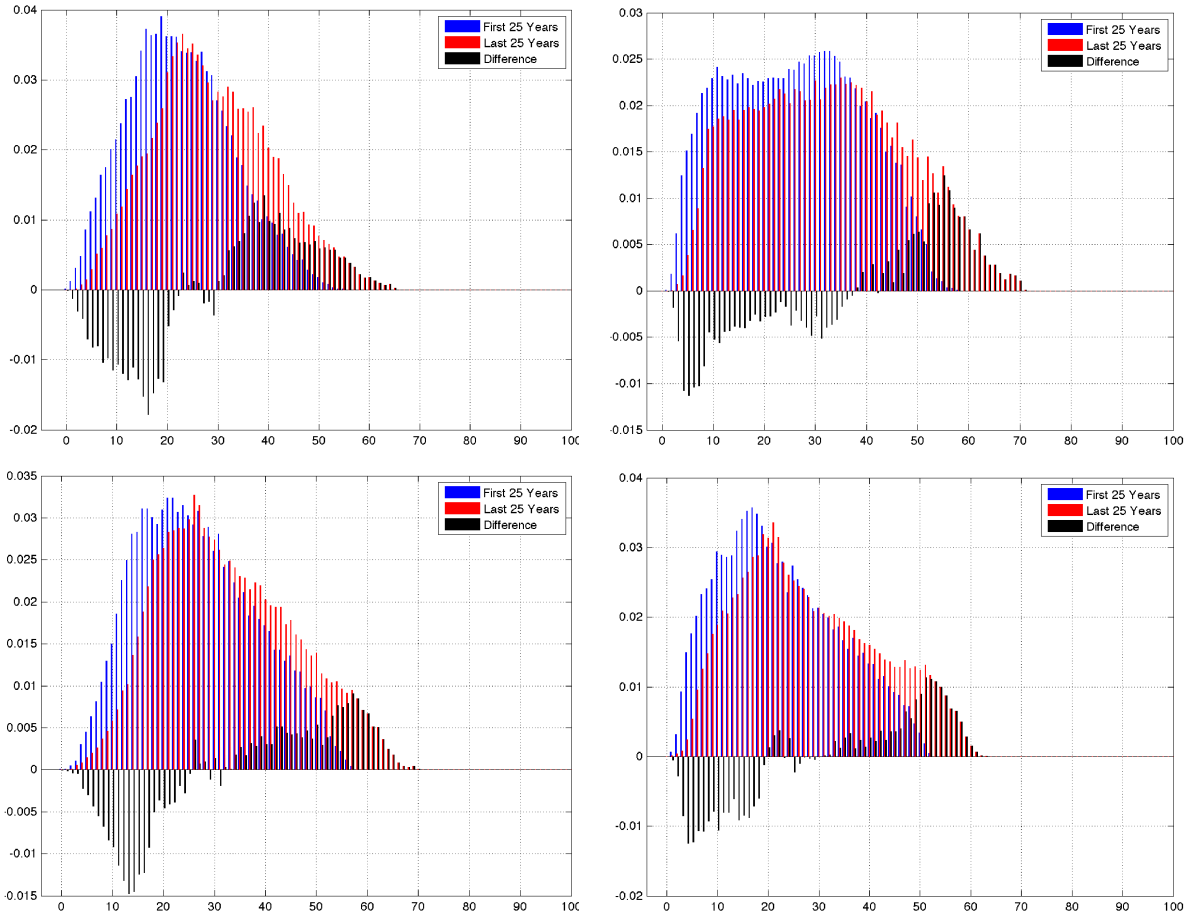

Figure 14: DJF India PWV PDF Shift (Last 25 Years - First 25 Years) (mm) for CMIP3 Models, CCSM3 (top left panel) and GISS (top right panel), and CMIP5 Models, CCSM4 (bottom left panel) and GISS-E2 (bottom right panel)

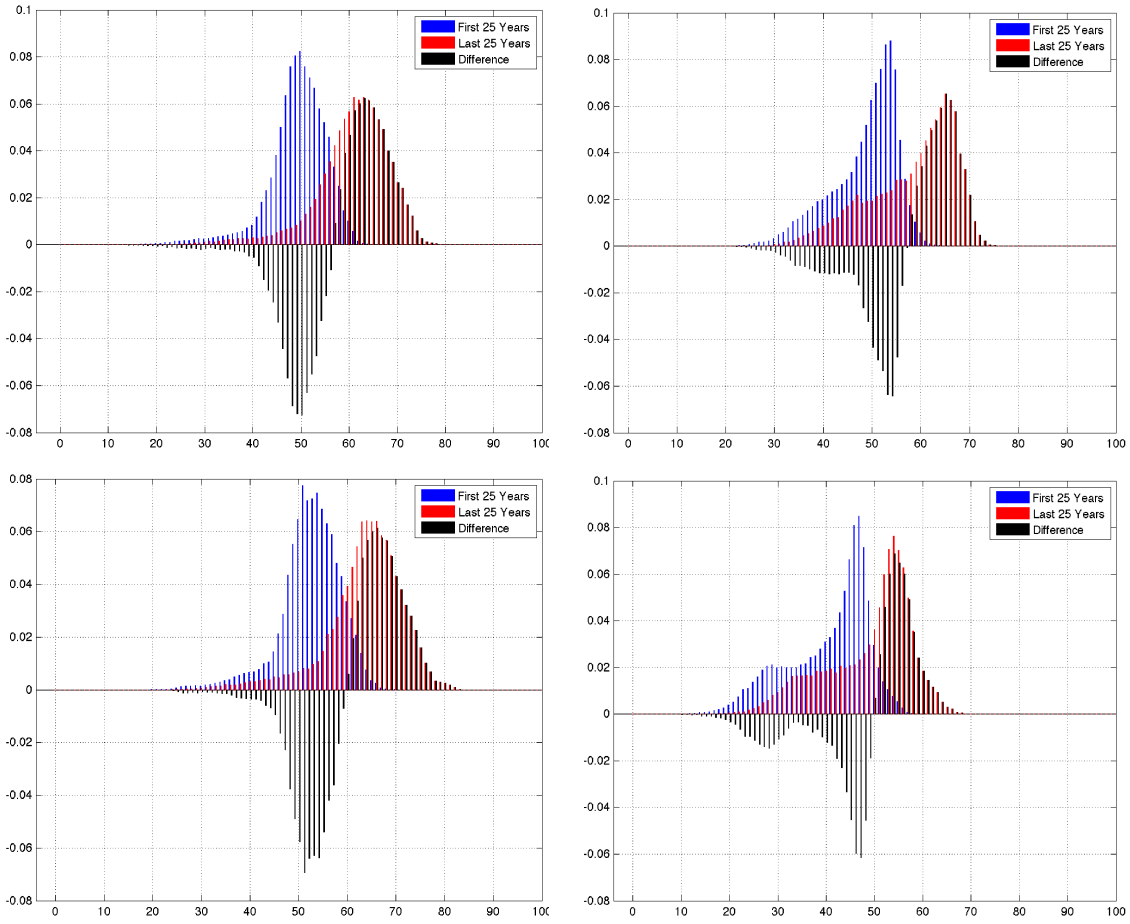

Figure 15: JJA India PWV PDF Shift (Last 25 Years - First 25 Years) (mm) for CMIP3 Models, CCSM3 (top left panel) and GISS (top right panel), and CMIP5 Models, CCSM4 (bottom left panel) and GISS-E2 (bottom right panel)

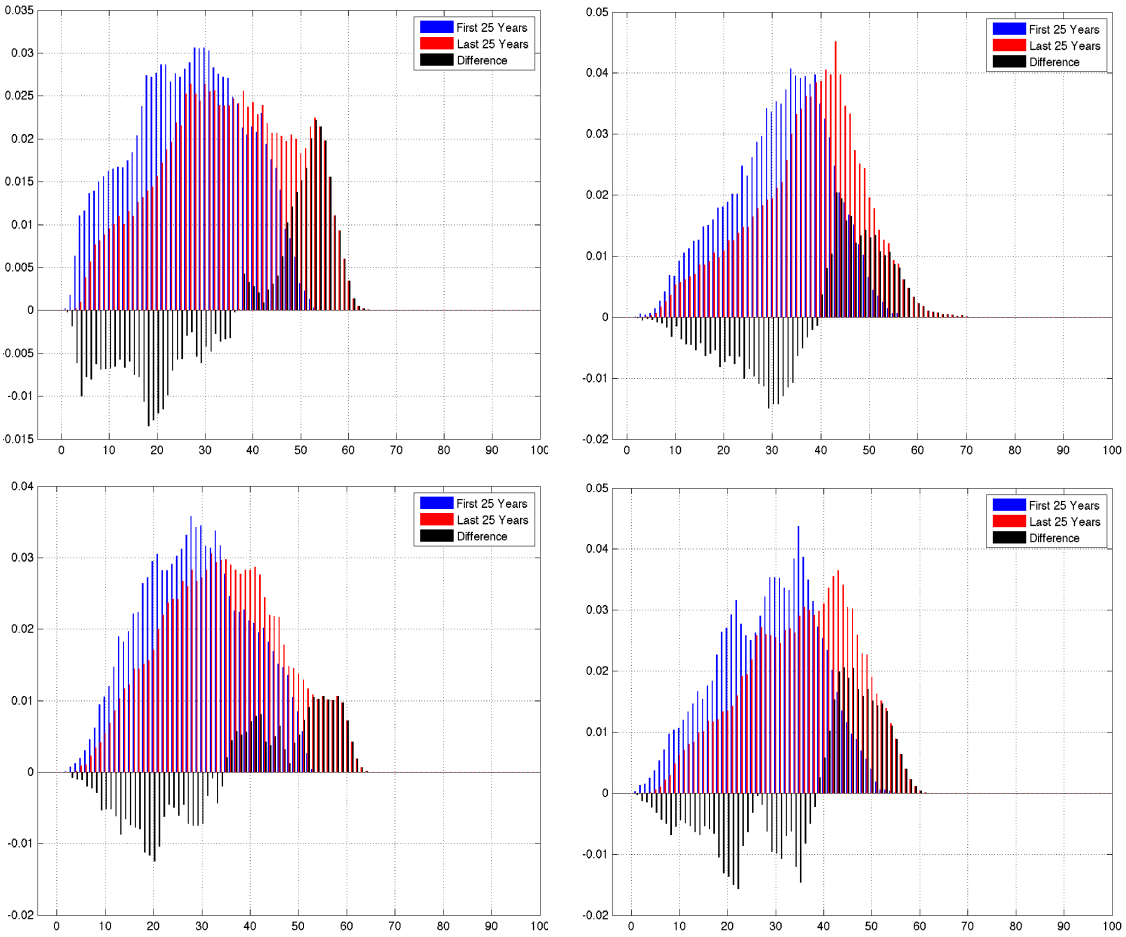

Figure 16: MAM India PWV PDF Shift (Last 25 Years - First 25 Years) (mm) for CMIP3 Models, CCSM3 (top left panel) and GISS (top right panel), and CMIP5 Models, CCSM4 (bottom left panel) and GISS-E2 (bottom right panel)

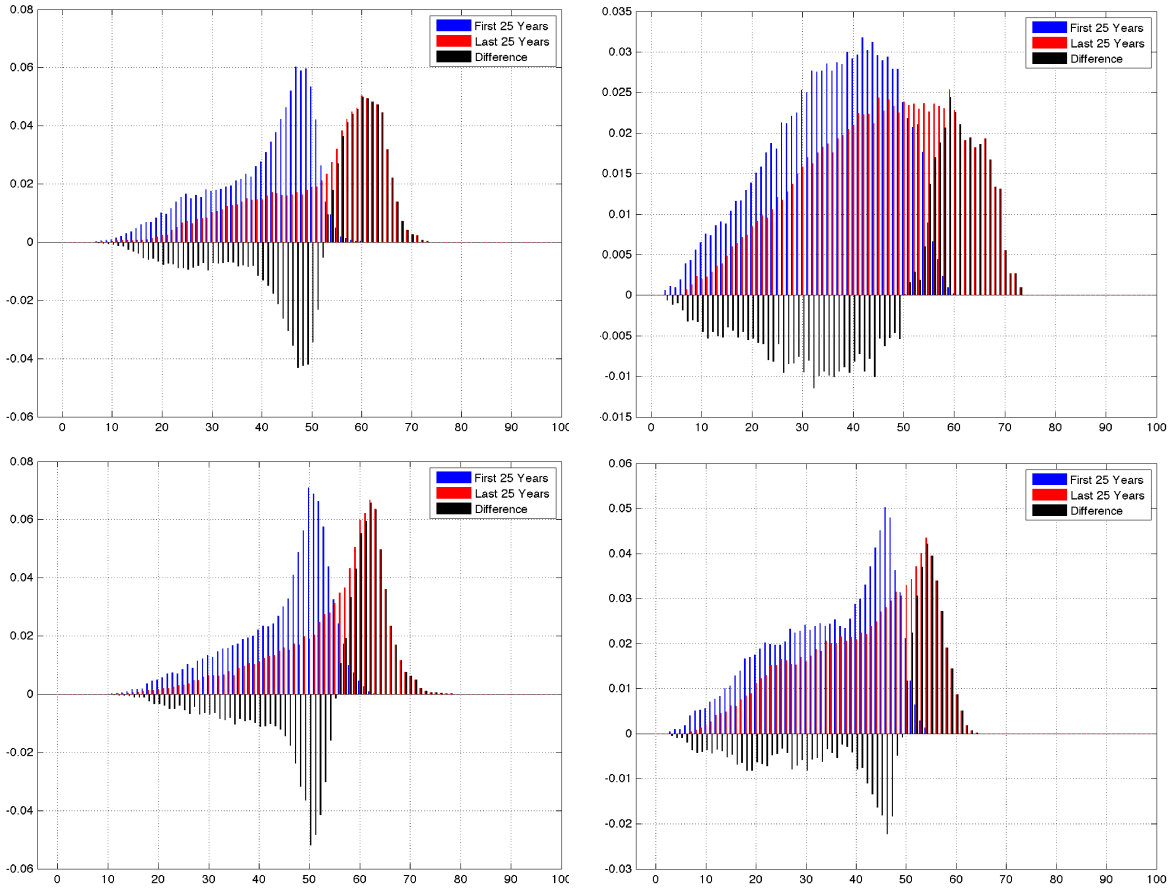

Figure 17: SON India PWV PDF Shift (Last 25 Years - First 25 Years) (mm) for CMIP3 Models, CCSM3 (top left panel) and GISS (top right panel), and CMIP5 Models, CCSM4 (bottom left panel) and GISS-E2 (bottom right panel)

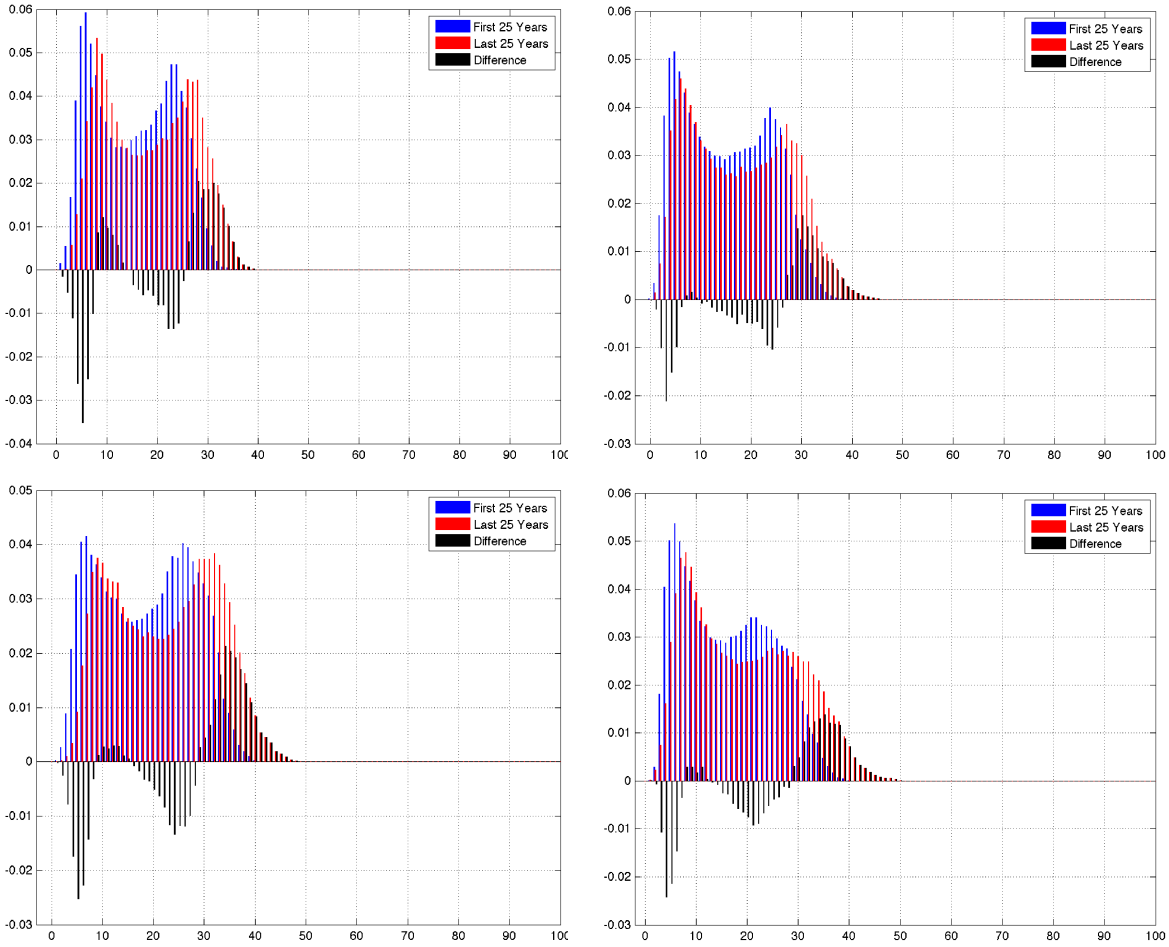

Figure 18: DJF U.S. PWV PDF Shift (Last 25 Years - First 25 Years) (mm) for CMIP3 Models, CCSM3 (top left panel) and GISS (top right panel), and CMIP5 Models, CCSM4 (bottom left panel) and GISS-E2 (bottom right panel)

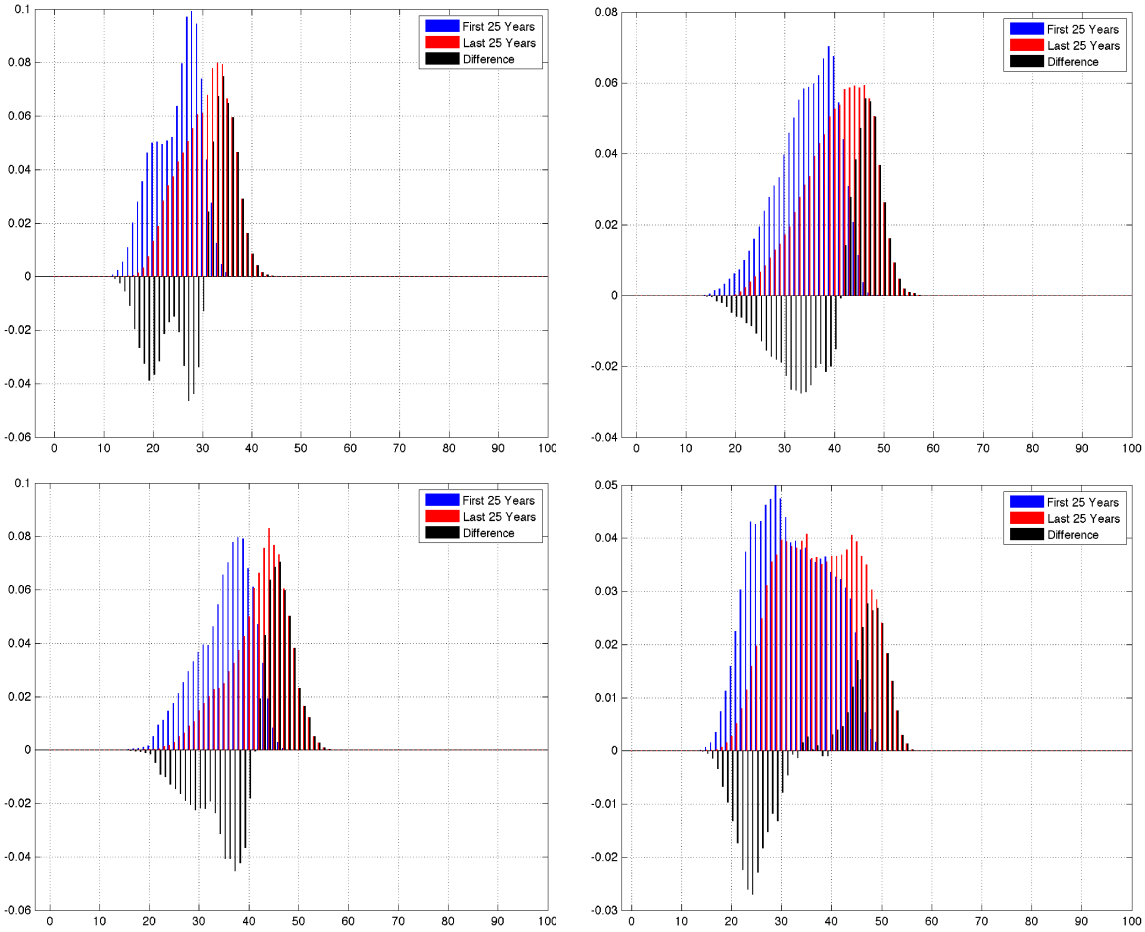

Figure 19: JJA U.S. PWV PDF Shift (Last 25 Years - First 25 Years) (mm) for CMIP3 Models, CCSM3 (top left panel) and GISS (top right panel), and CMIP5 Models, CCSM4 (bottom left panel) and GISS-E2 (bottom right panel)

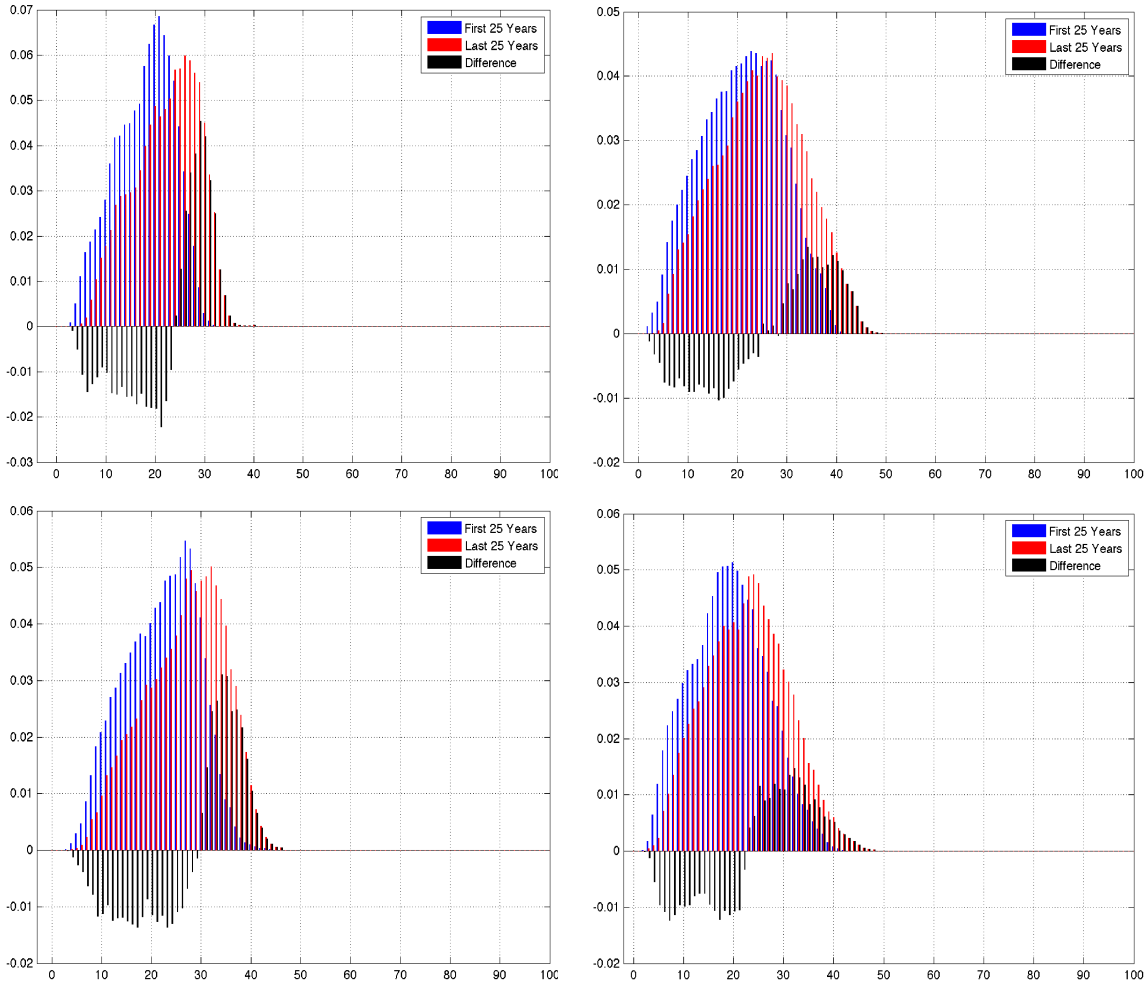

Figure 20: MAM U.S. PWV PDF Shift (Last 25 Years - First 25 Years) (mm) for CMIP3 Models, CCSM3 (top left panel) and GISS (top right panel), and CMIP5 Models, CCSM4 (bottom left panel) and GISS-E2 (bottom right panel)

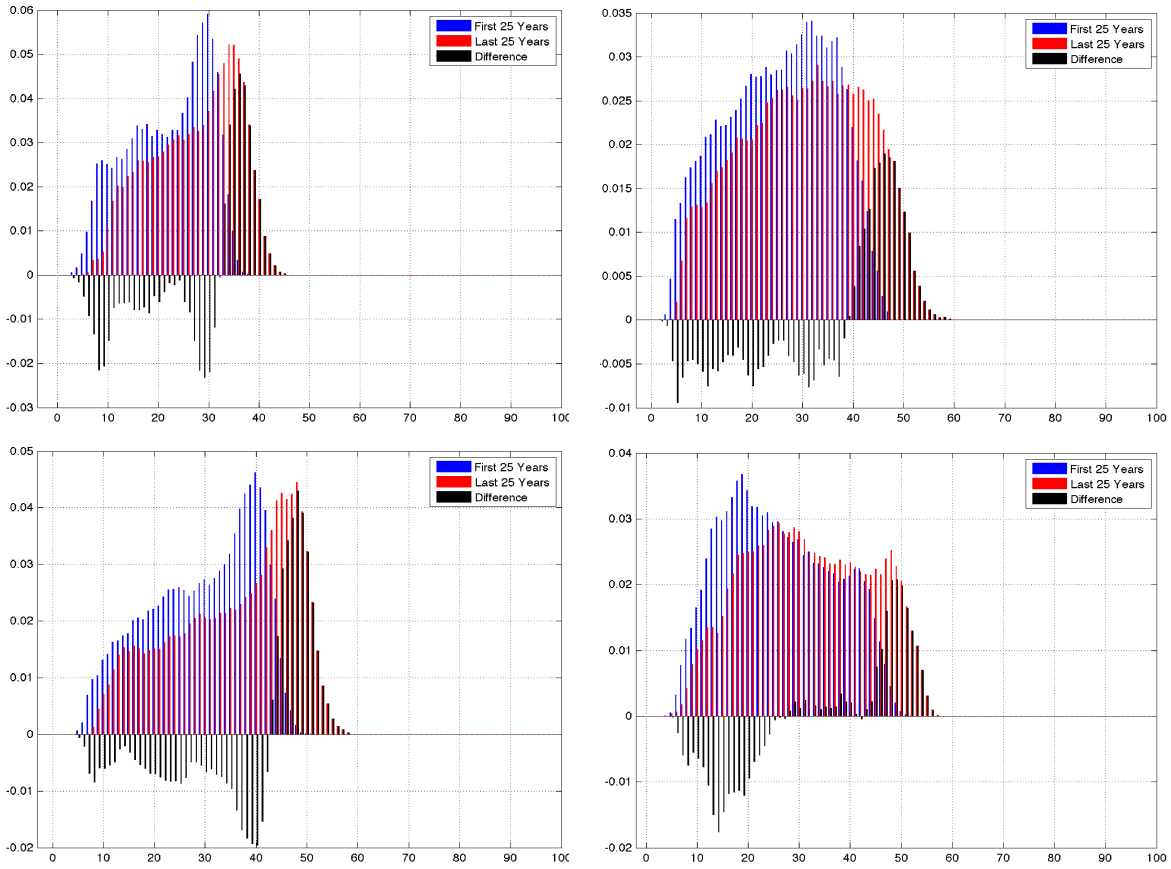

Figure 21: SON U.S. PWV PDF Shift (Last 25 Years - First 25 Years) (mm) for CMIP3 Models, CCSM3 (top left panel) and GISS (top right panel), and CMIP5 Models, CCSM4 (bottom left panel) and GISS-E2 (bottom right panel)

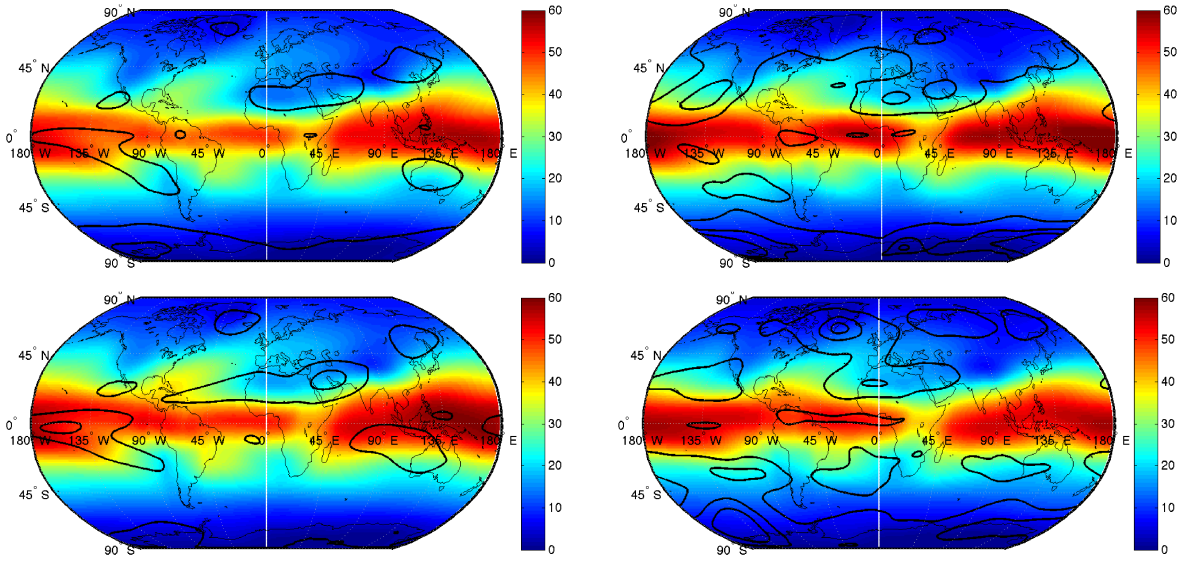

Figure 22: Example of all season PWV (mm) for the CMIP3 Models, CCSM3 (top left panel) and GISS (top right panel), and CMIP5 models, CCSM4 (bottom left panel) and GISS-E2 (bottom right panel)

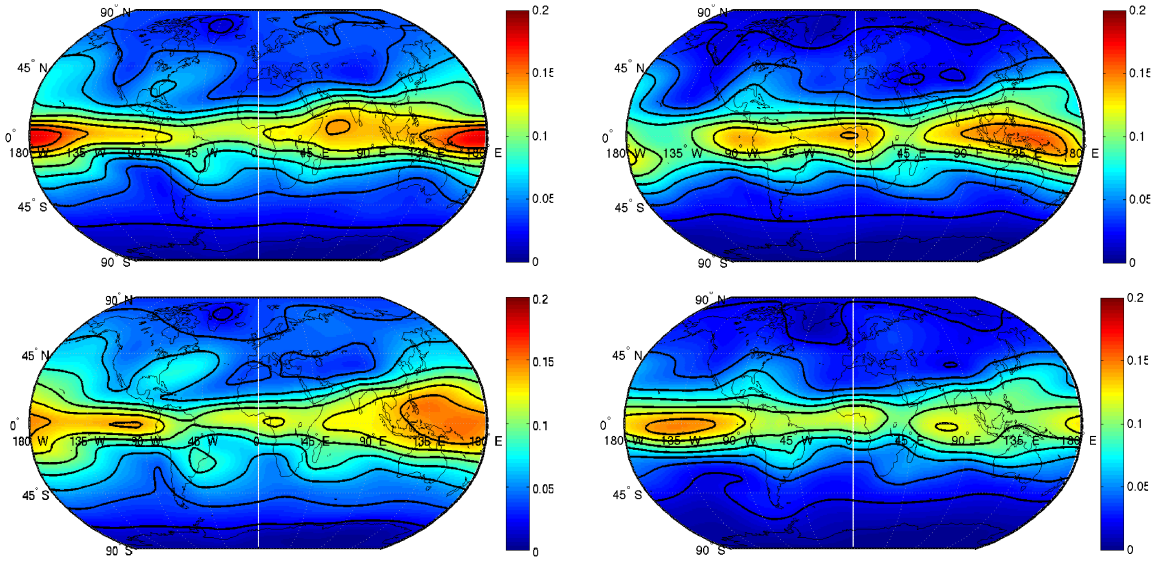

Figure 23: 100 Year Trend (mm/year) for the CMIP3 Models, CCSM3 (top left panel) and GISS (top right panel), and CMIP5 models, CCSM4 (bottom left panel) and GISS-E2 (bottom right panel)

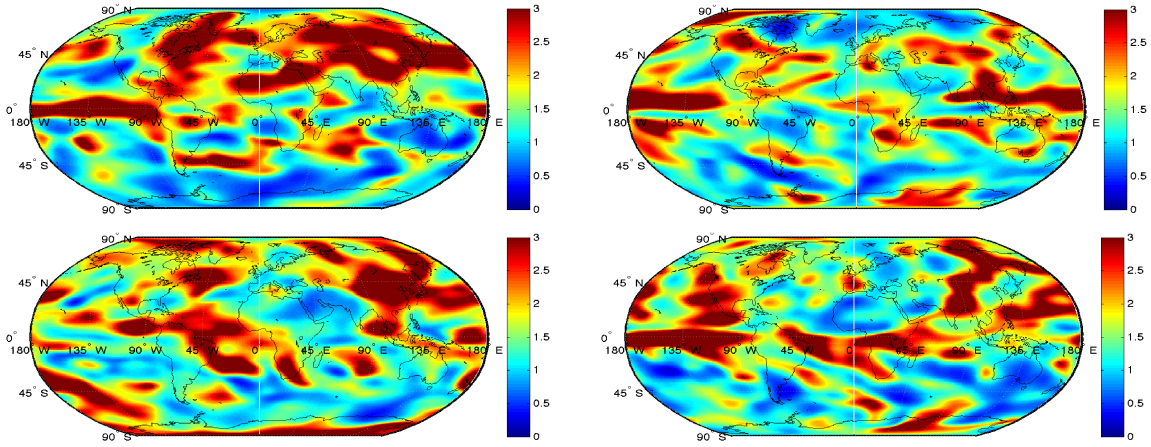

Figure 24: Autocorrelation Factor (1+phi/1-phi) for the CMIP3 Models, CCSM3 (top left panel) and GISS (top right panel), and CMIP5 Models, CCSM4 (bottom left panel) and GISS-E2 (bottom right panel)

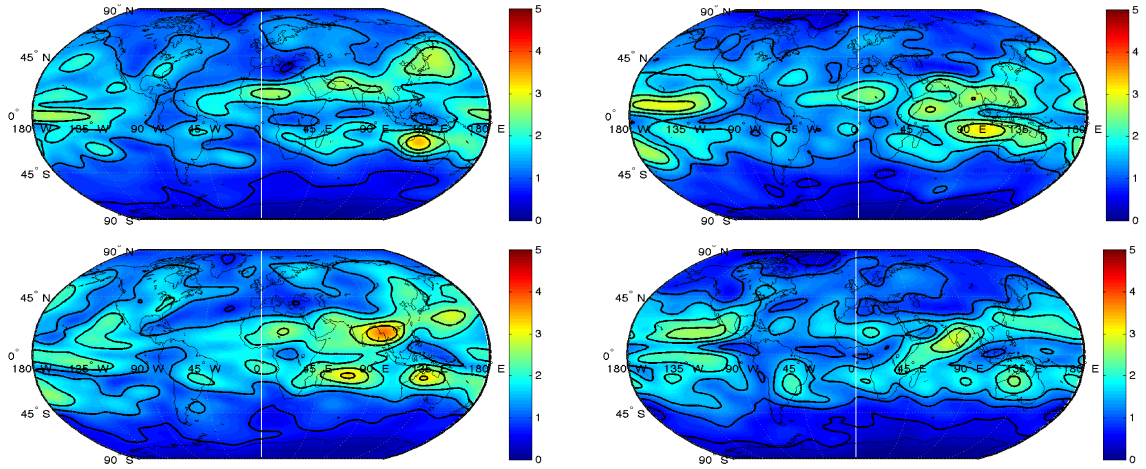

Figure 25: Standard Deviation + 0% Measurement Error (mm) for the CMIP3 Models, CCSM3 (top left panel) and GISS (top right panel), and CMIP5 Models, CCSM4 (bottom left panel) and GISS-E2 (bottom right panel)

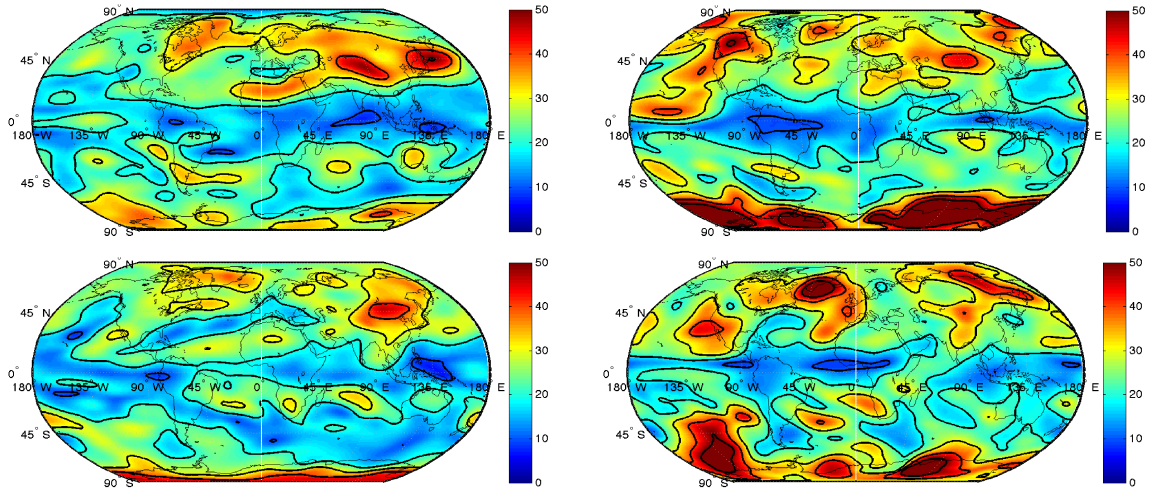

Figure 26: TTD (years) for the CMIP3 Models, CCSM3 (top left panel) and GISS (top right panel), and CMIP5 Models, CCSM4 (bottom left panel) and GISS-E2 (bottom right panel)

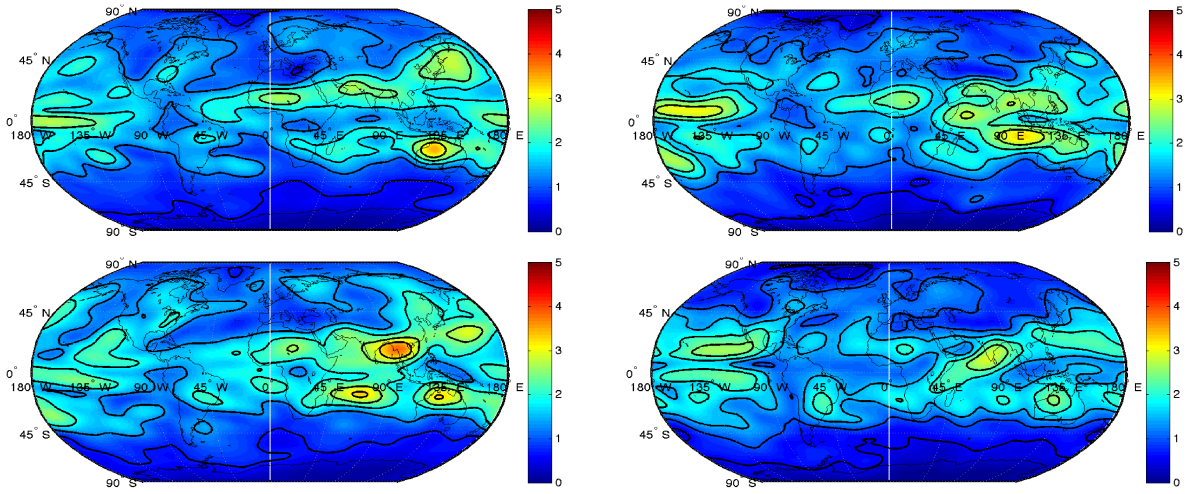

Figure 27: Standard Deviation + 1% Measurement Error (mm) for the CMIP3 Models, CCSM3 (top left panel) and GISS (top right panel), and CMIP5 Models, CCSM4 (bottom left panel) and GISS-E2 (bottom right panel)

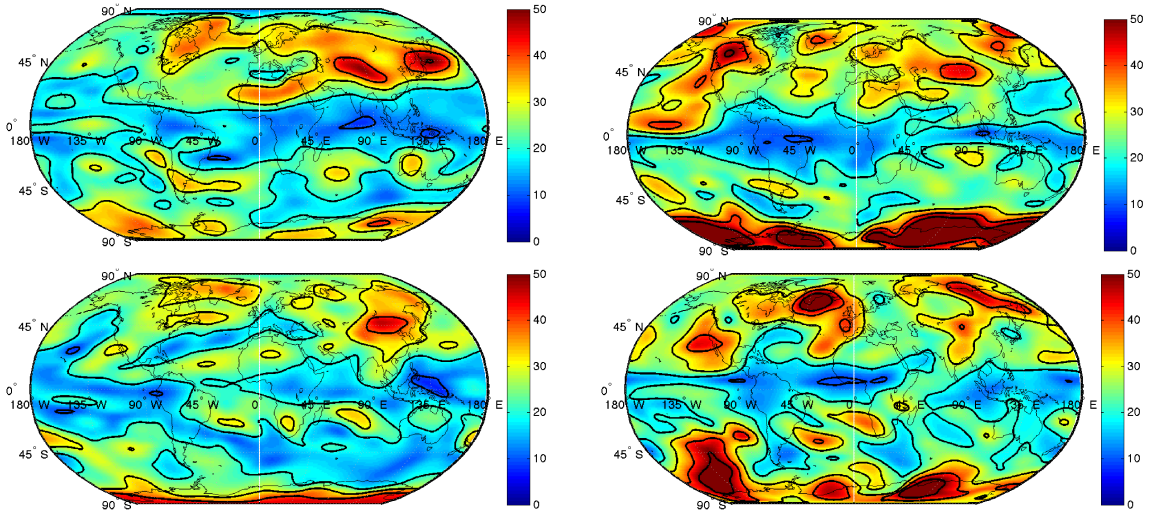

Figure 28: TTD (years) with 1% Measurement Error for the CMIP3 Models, CCSM3 (top left panel) and GISS (top right panel), and CMIP5 Models (CCSM4 (bottom left panel) and GISS-E2 (bottom right panel)

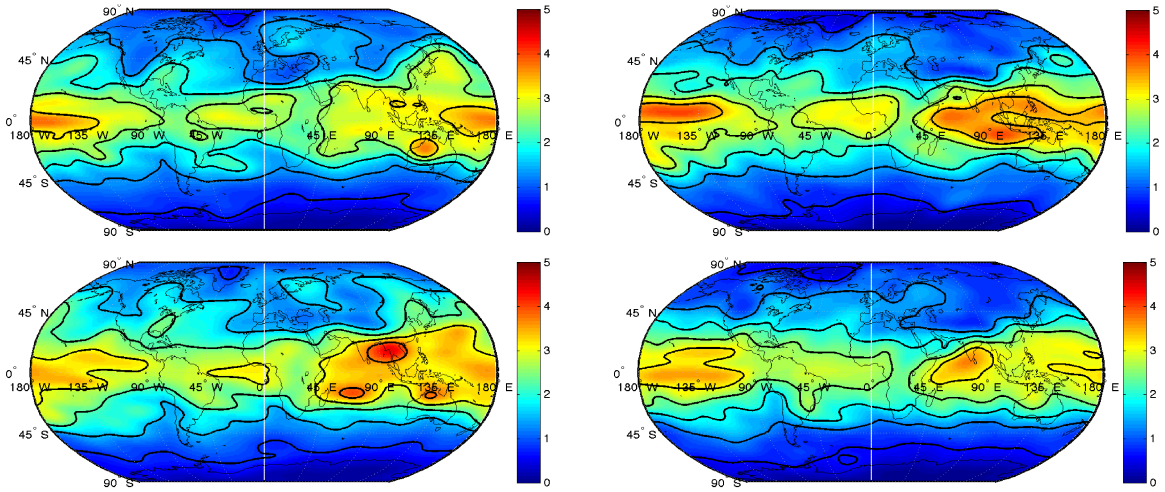

Figure 29: Standard Deviation + 5% Measurement Error (mm) for the CMIP3 Models, CCSM3 (top left panel) and GISS (top right panel), and CMIP5 Models, CCSM4 (bottom left panel) and GISS-E2 (bottom right panel)

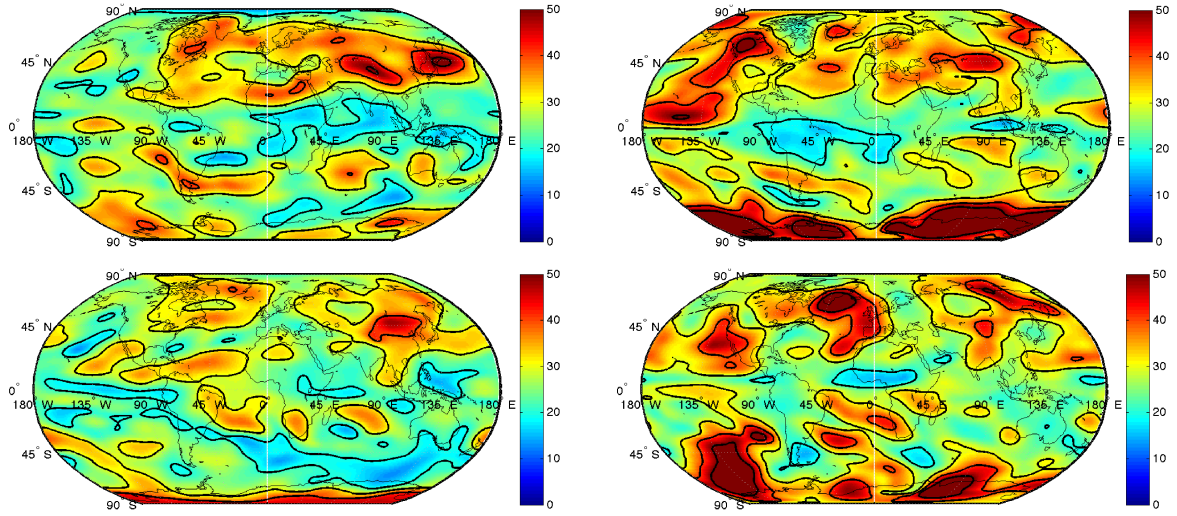

Figure 30: TTD (years) with 5% Measurement Error for the CMIP3 Models, CCSM3 (top left panel) and GISS (top right panel), and CMIP5 Models, CCSM4 (bottom left panel) and GISS-E2 (bottom right panel)

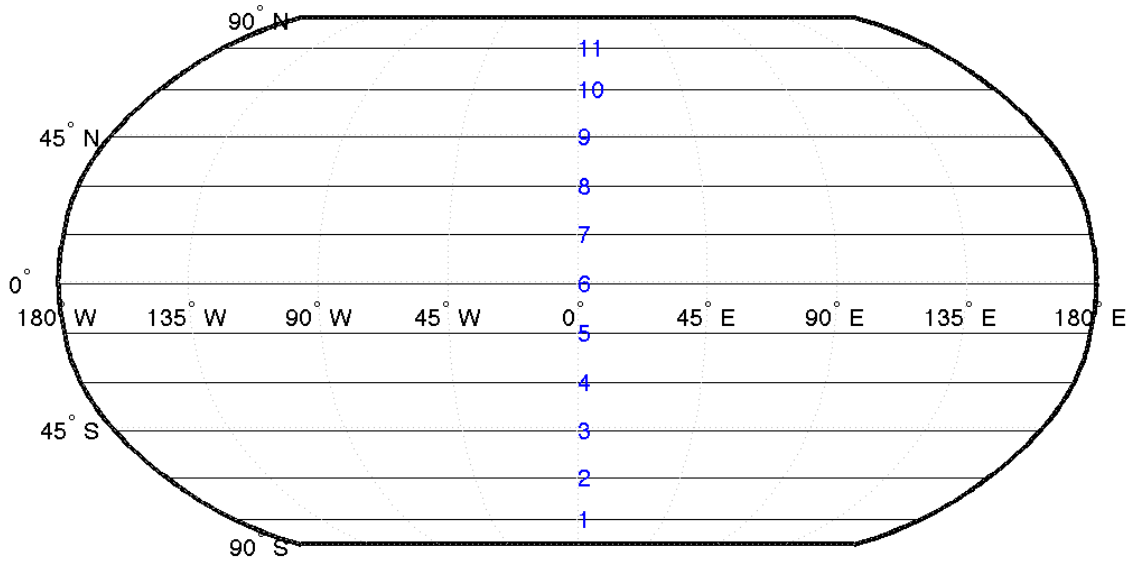

Figure 31: Zone Numbers

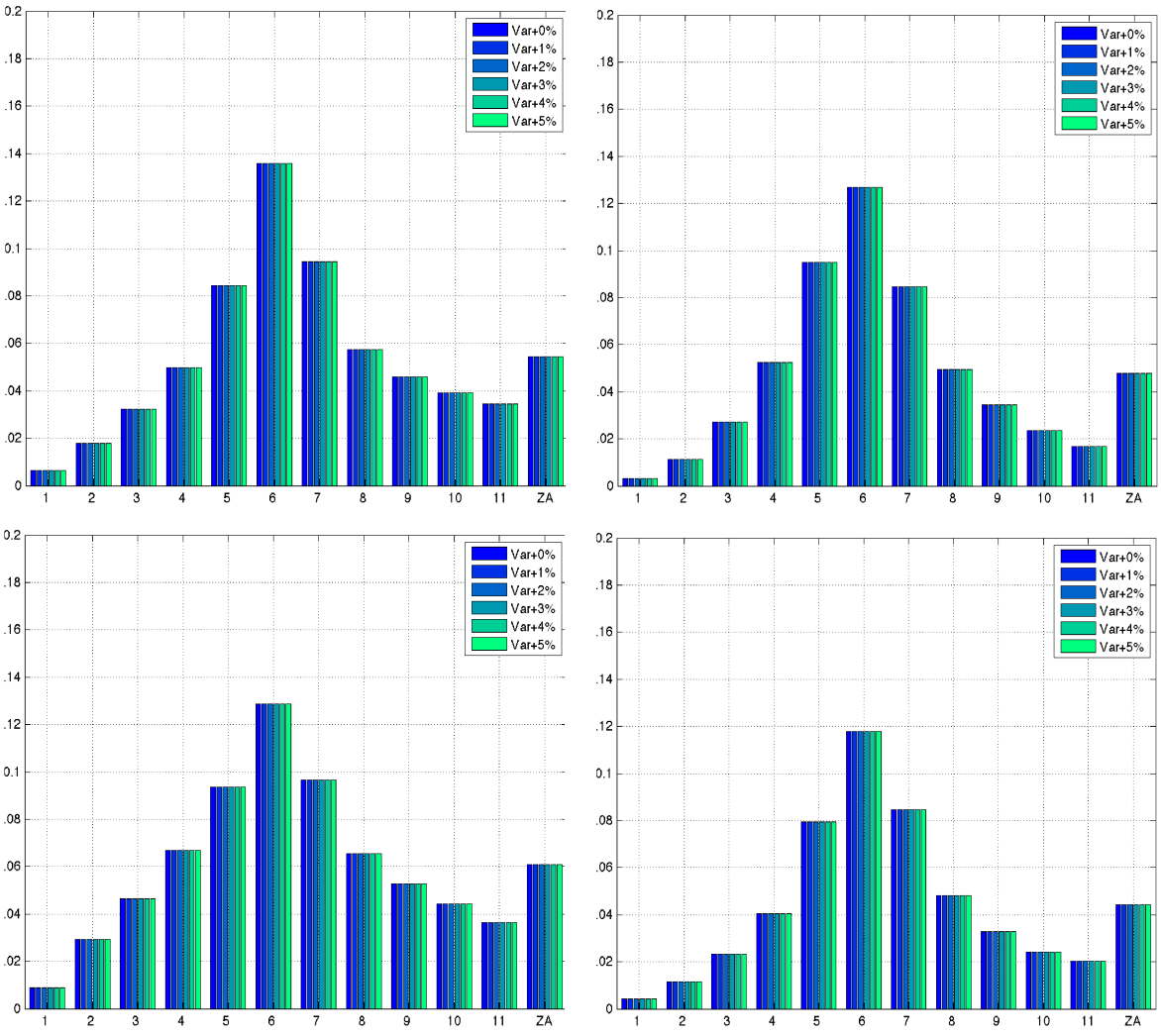

Figure 32: 100 Year Trend (mm/year) for CMIP3 Models, CCSM3 (top left panel) and GISS (top right panel), and CMIP5 Models, CCSM4 (bottom left panel) and GISS-E2 (bottom right panel

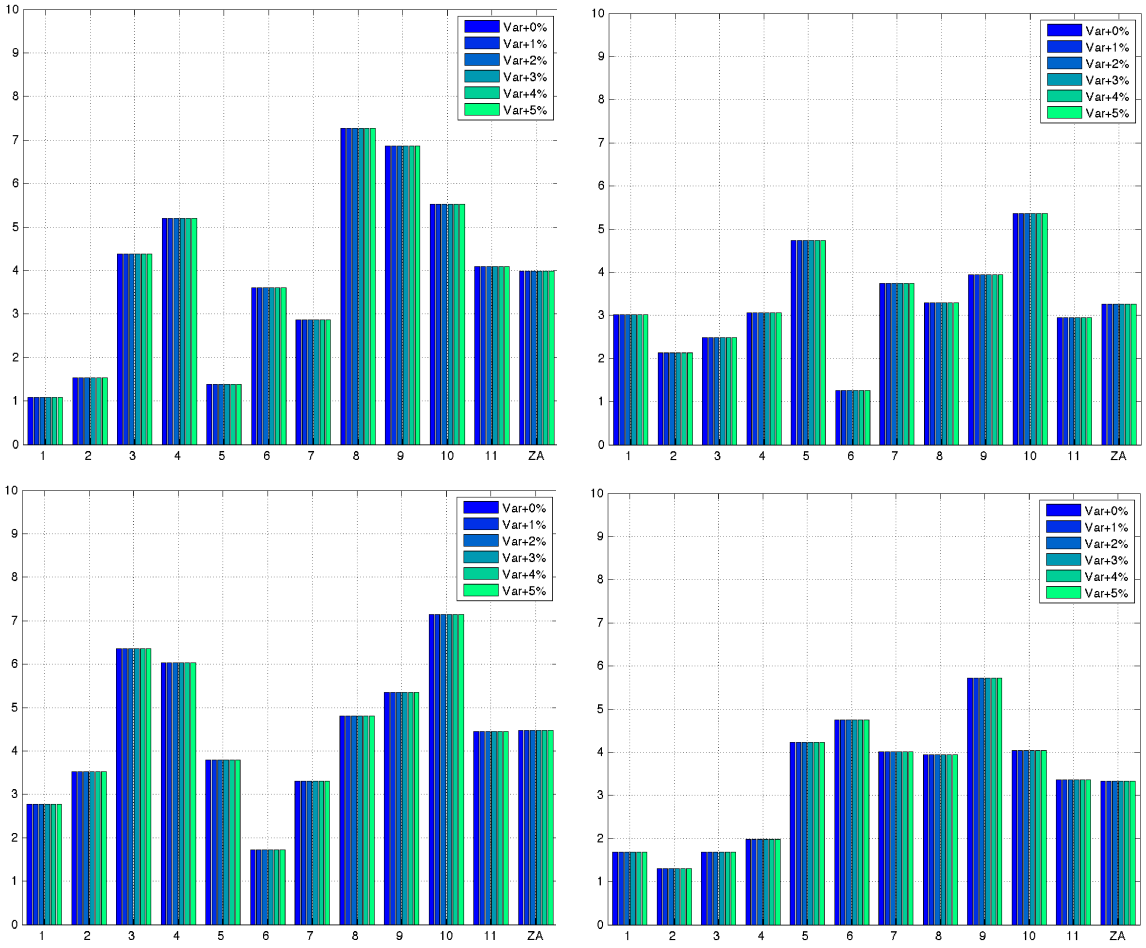

Figure 33: Autocorrelation Factor (1+phi/1-phi) for CMIP3 Models, CCSM3 (top left panel) and GISS (top right panel), and CMIP5 Models, CCSM4 (bottom let panel) and GISS-E2 (bottom right panel)

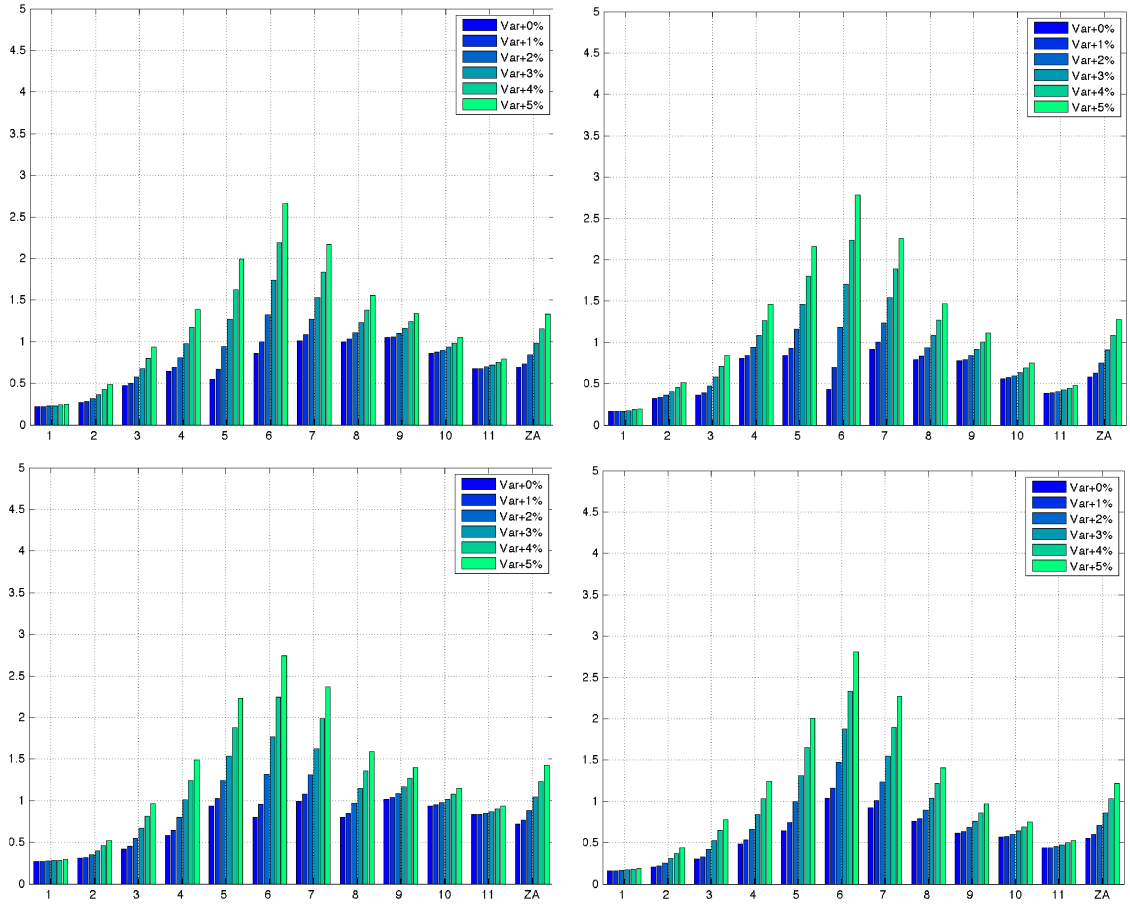

Figure 34: Standard Deviation + Measurement Error (mm) for CMIP3 Models, CCSM3 (top left panel) and GISS (top right panel), and CMIP5 Models, CCSM4 (bottom left panel) and GISS-E2 (bottom right panel)

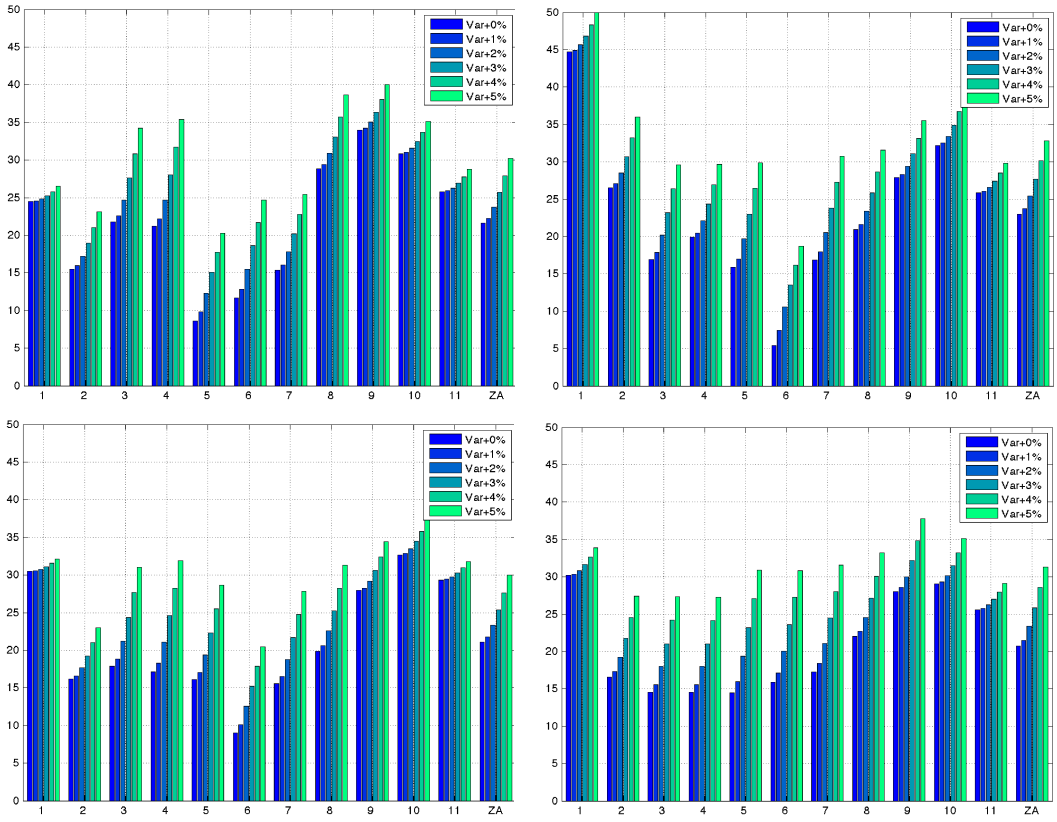

Figure 35: TTD (years) for Measurement Errors for CMIP3 Models, CCSM3 (top left panel) and GISS (top right panel), and CMIP5 Models, CCSM4 (bottom left panel) and GISS-E2 (bottom right panel)

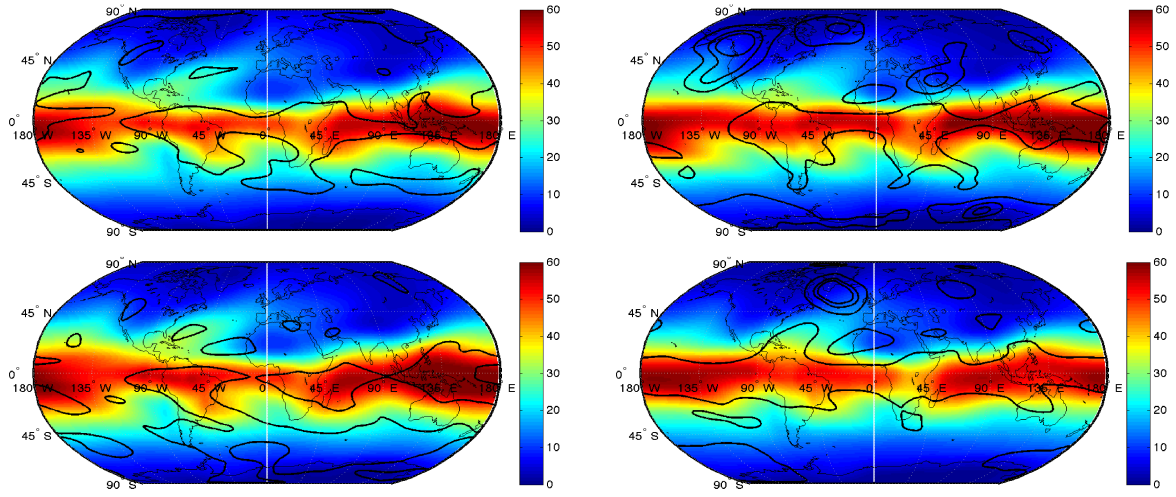

Figure 36: Example DJF PWV (mm) for the CMIP3 Models, CCSM3 (top left panel) and GISS (top right panel), and CMIP5 models, CCSM4 (bottom left panel) and GISS-E2 (bottom right panel)

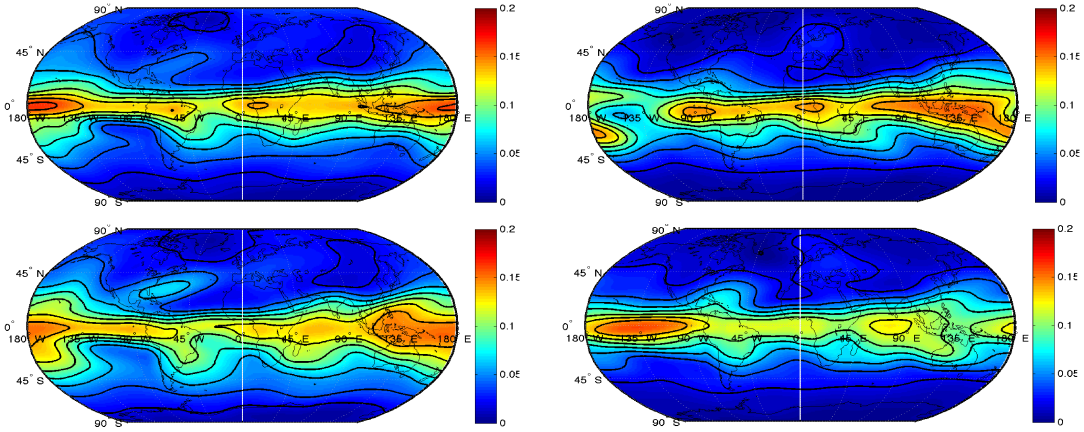

Figure 37: DJF 100 Year Trend (mm/year) for the CMIP3 Models, CCSM3 (top left panel) and GISS (top right panel), and CMIP5 models, CCSM4 (bottom left panel) and GISS-E2 (bottom right panel)

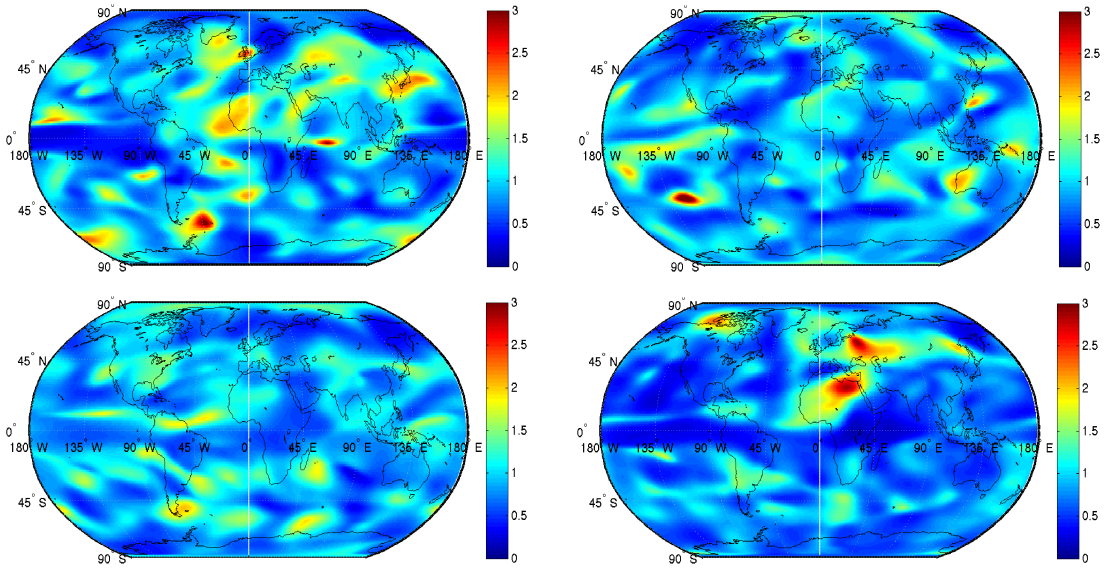

Figure 38: DJF Autocorrelation Factor (1+phi/1-phi) for the CMIP3 Models, CCSM3 (top left panel) and GISS (top right panel), and CMIP5 Models, CCSM4 (bottom left panel) and GISS-E2 (bottom right panel)

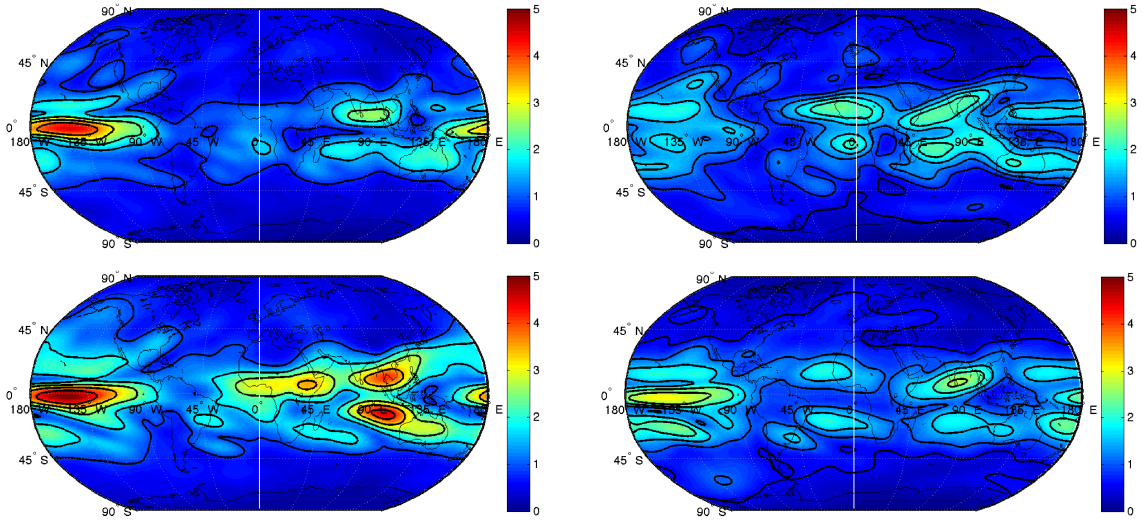

Figure 39: DJF Standard Deviation + 0% Measurement Error (mm) for the CMIP3 Models, CCSM3 (top left panel) and GISS (top right panel), and CMIP5 Models, CCSM4 (bottom left panel) and GISS-E2 (bottom right panel)

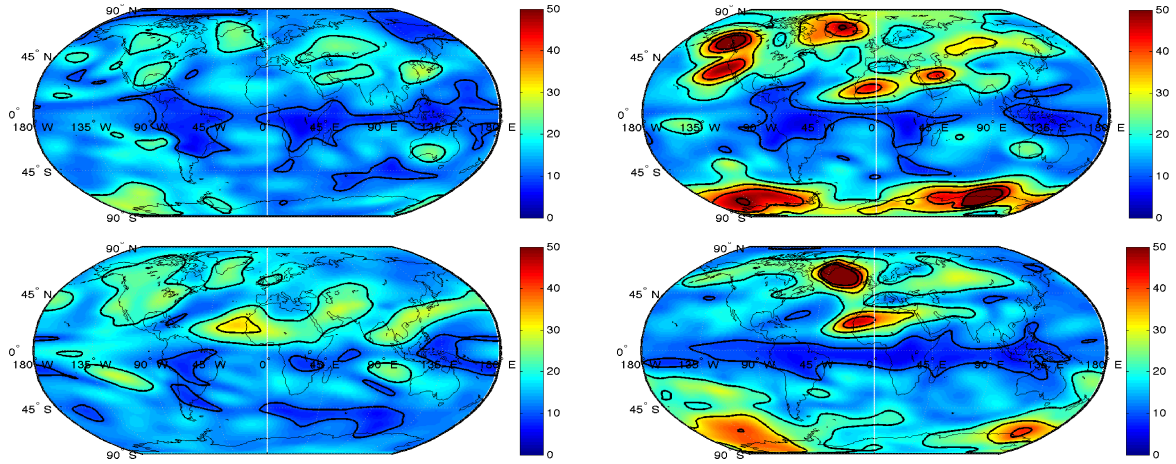

Figure 40: DJF TTD (years) for the CMIP3 Models, CCSM3 (top left panel) and GISS (top right panel), and CMIP5 Models, CCSM4 (bottom left panel) and GISS-E2 (bottom right panel)

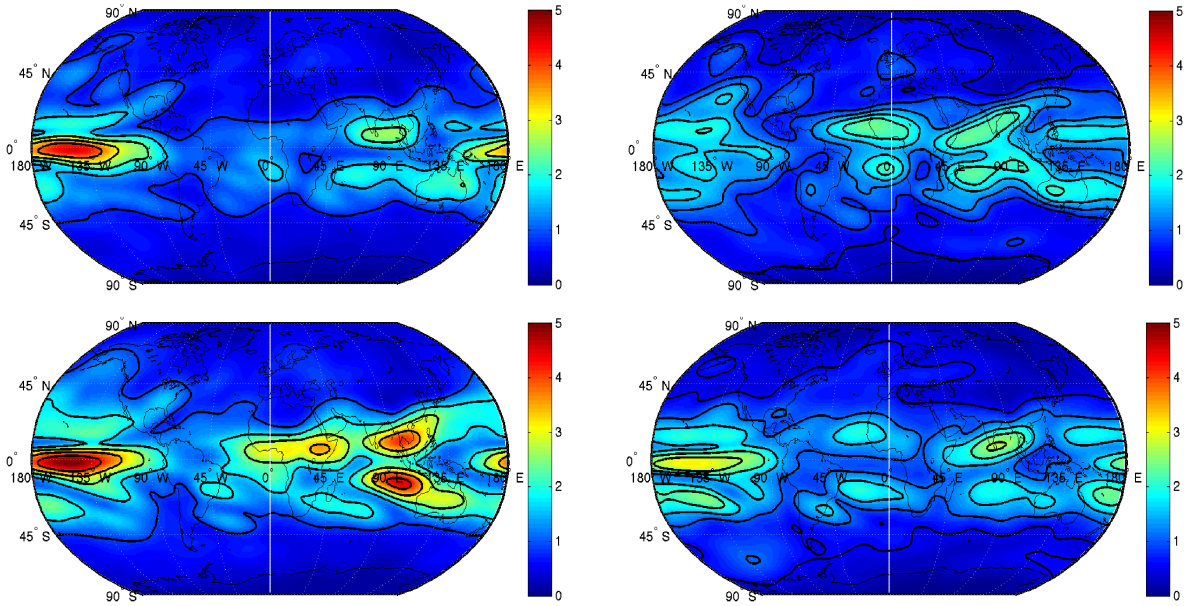

Figure 41: DJF Standard Deviation + 1% Measurement Error (mm) for the CMIP3 Models, CCSM3 (top left panel) and GISS (top right panel), and CMIP5 Models, CCSM4 (bottom left panel) and GISS-E2 (bottom right panel)

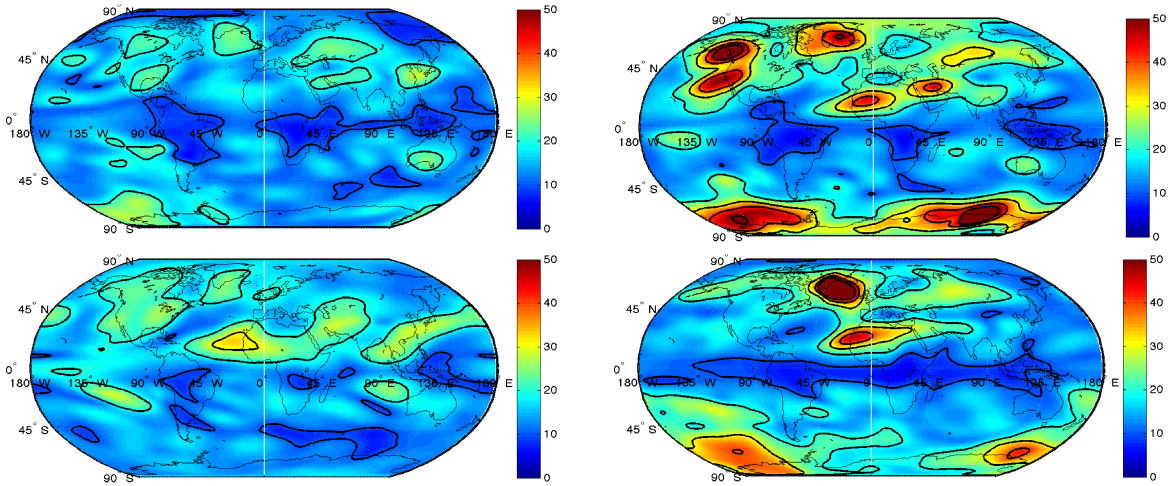

Figure 42: DJF TTD (years) with 1% Measurement Error for the CMIP3 Models, CCSM3 (top left panel) and GISS (top right panel), and CMIP5 Models (CCSM4 (bottom left panel) and GISS-E2 (bottom right panel)

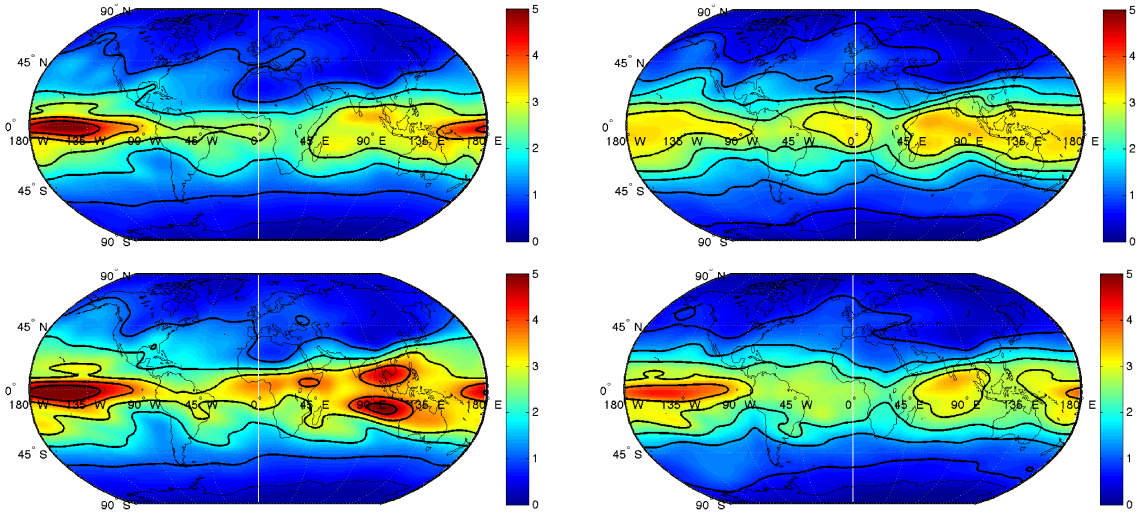

Figure 43: DJF Standard Deviation + 5% Measurement Error (mm) for the CMIP3 Models, CCSM3 (top left panel) and GISS (top right panel), and CMIP5 Models, CCSM4 (bottom left panel) and GISS-E2 (bottom right panel)

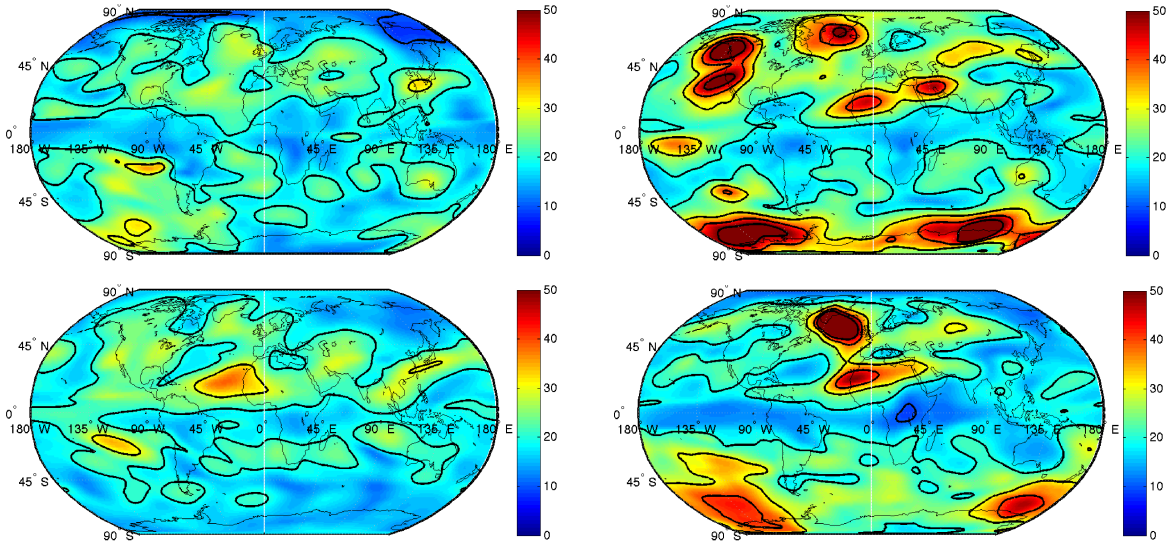

Figure 44: DJF TTD (years) with 5% Measurement Error for the CMIP3 Models, CCSM3 (top left panel) and GISS (top right panel), and CMIP5 Models, CCSM4 (bottom left panel) and GISS-E2 (bottom right panel)

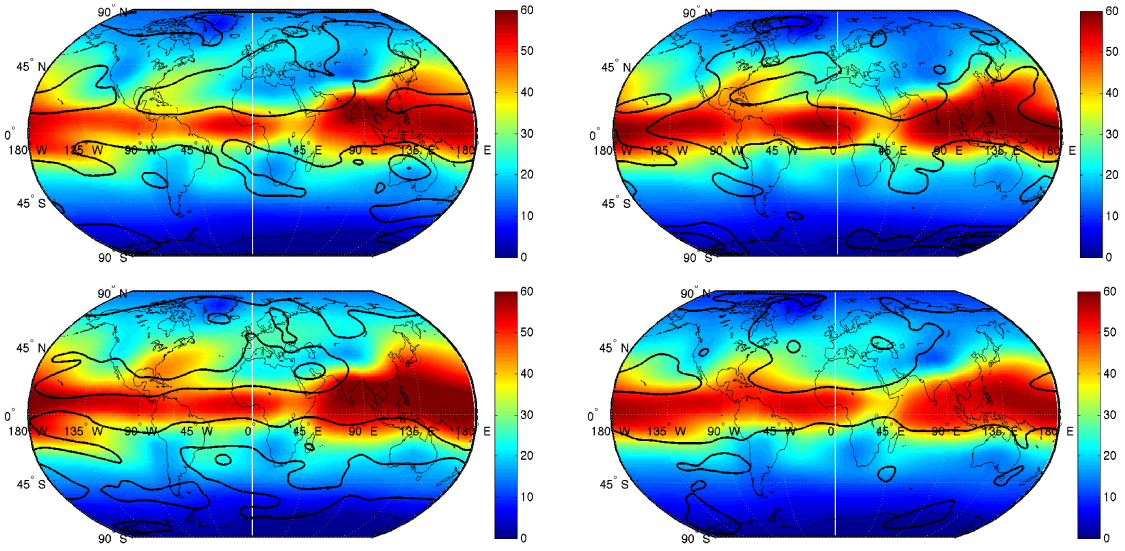

Figure 45: Example of JJA PWV (mm) for the CMIP3 Models, CCSM3 (top left panel) and GISS (top right panel), and CMIP5 models, CCSM4 (bottom left panel) and GISS-E2 (bottom right panel)

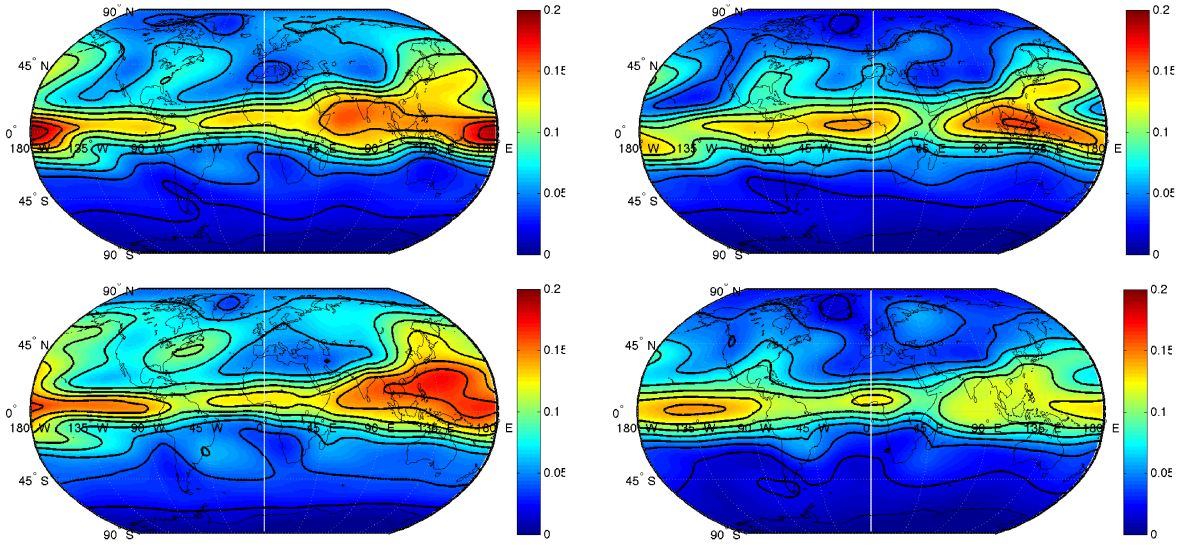

Figure 46: JJA 100 Year Trend (mm/year) for the CMIP3 Models, CCSM3 (top left panel) and GISS (top right panel), and CMIP5 models, CCSM4 (bottom left panel) and GISS-E2 (bottom right panel)

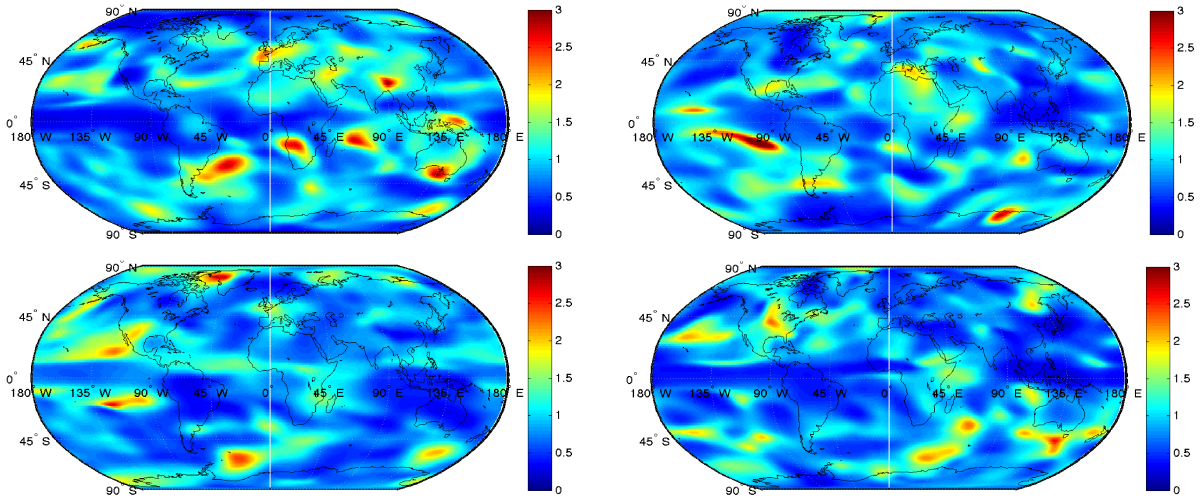

Figure 47: JJA Autocorrelation Factor (1+phi/1-phi) for the CMIP3 Models, CCSM3 (top left panel) and GISS (top right panel), and CMIP5 Models, CCSM4 (bottom left panel) and GISS-E2 (bottom right panel)

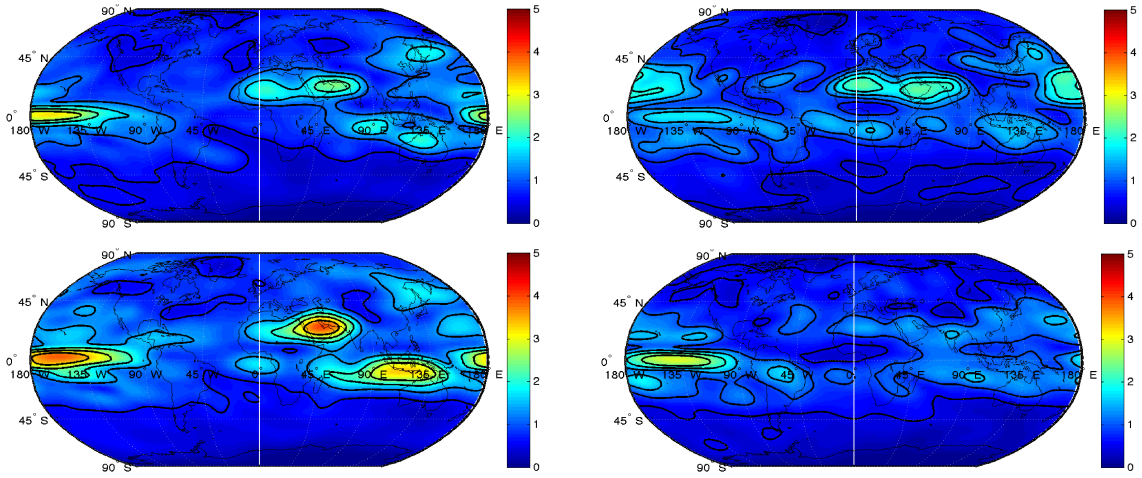

Figure 48: JJA Standard Deviation + 0% Measurement Error (mm) for the CMIP3 Models, CCSM3 (top left panel) and GISS (top right panel), and CMIP5 Models, CCSM4 (bottom left panel) and GISS-E2 (bottom right panel)

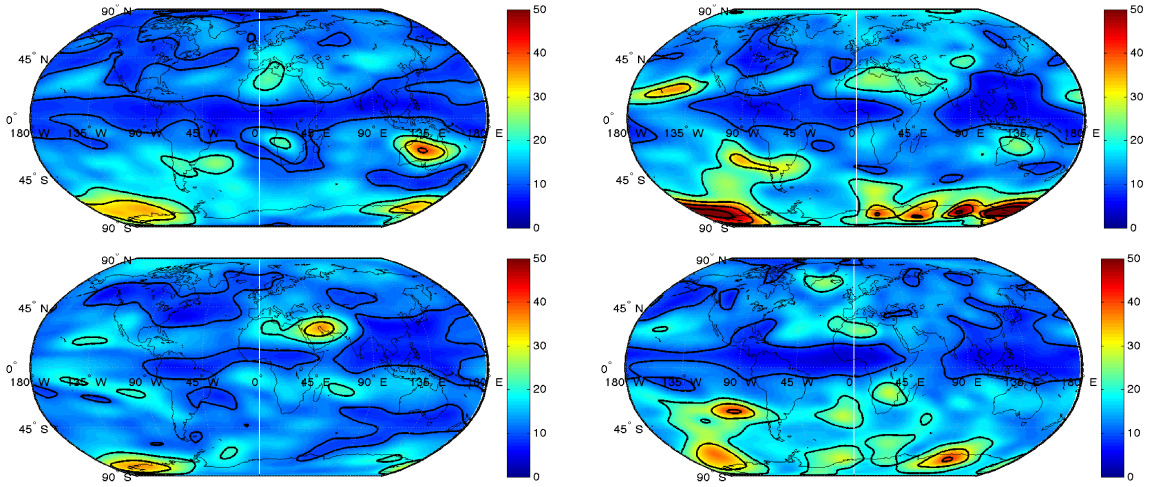

Figure 49: JJA TTD (years) for the CMIP3 Models, CCSM3 (top left panel) and GISS (top right panel), and CMIP5 Models, CCSM4 (bottom left panel) and GISS-E2 (bottom right panel)

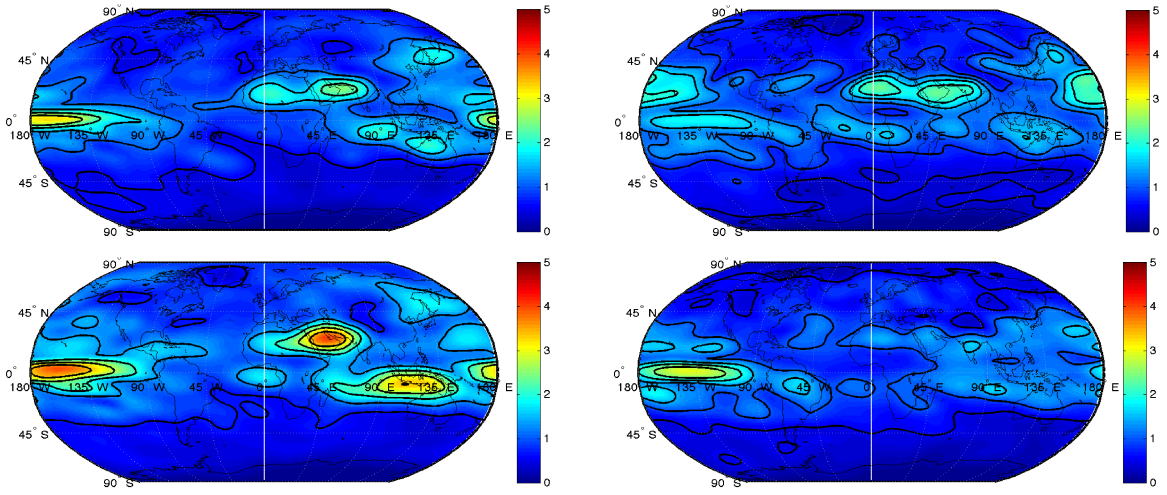

Figure 50: JJA Standard Deviation + 1% Measurement Error (mm) for the CMIP3 Models, CCSM3 (top left panel) and GISS (top right panel), and CMIP5 Models, CCSM4 (bottom left panel) and GISS-E2 (bottom right panel)

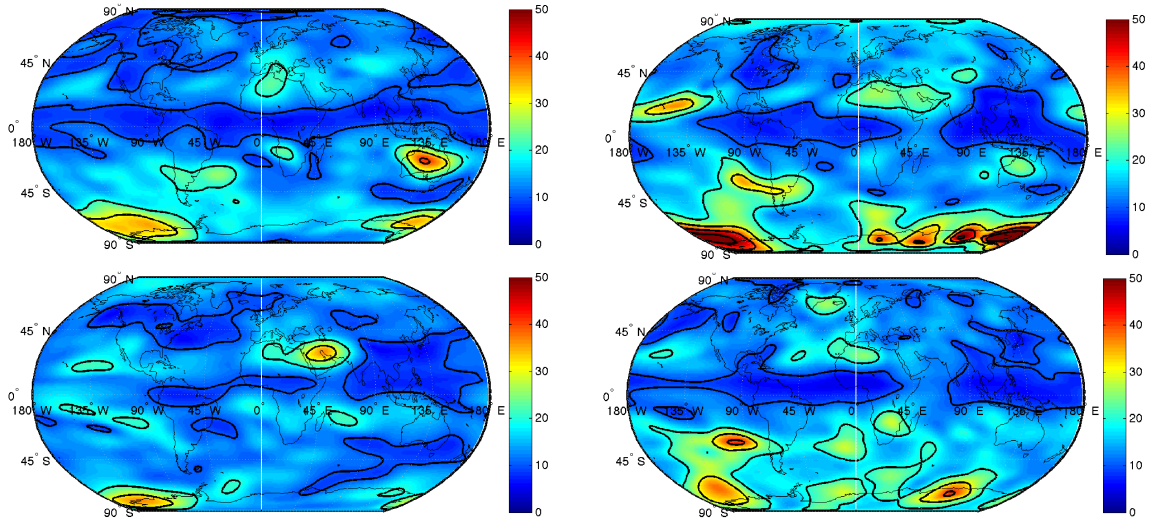

Figure 51: JJA TTD (years) with 1% Measurement Error for the CMIP3 Models, CCSM3 (top left panel) and GISS (top right panel), and CMIP5 Models, CCSM4 (bottom left panel) and GISS-E2 (bottom right panel)

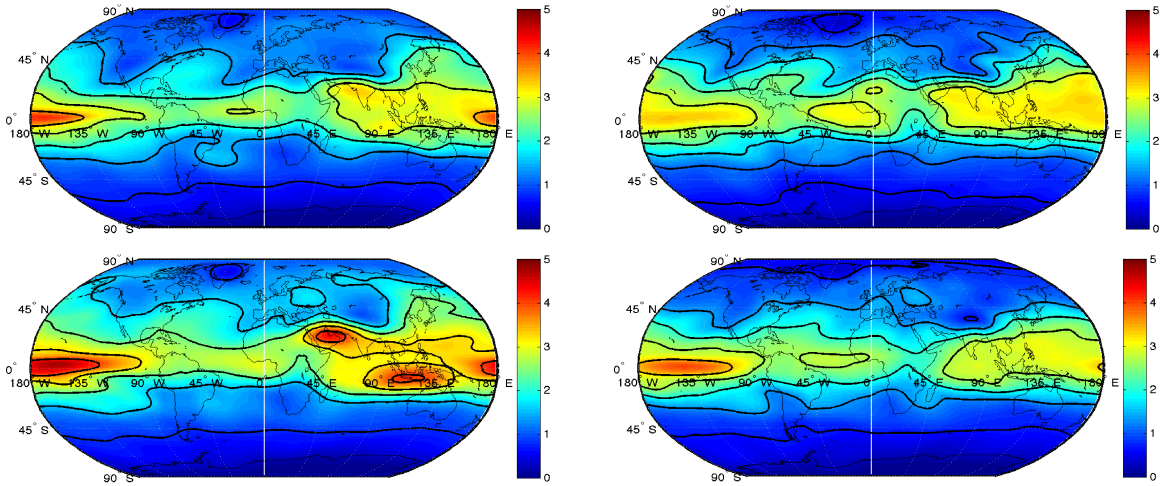

Figure 52: JJA Standard Deviation + 5% Measurement Error (mm) for the CMIP3 Models, CCSM3 (top left panel) and GISS (top right panel), and CMIP5 Models, CCSM4 (bottom left panel) and GISS-E2 (bottom right panel)

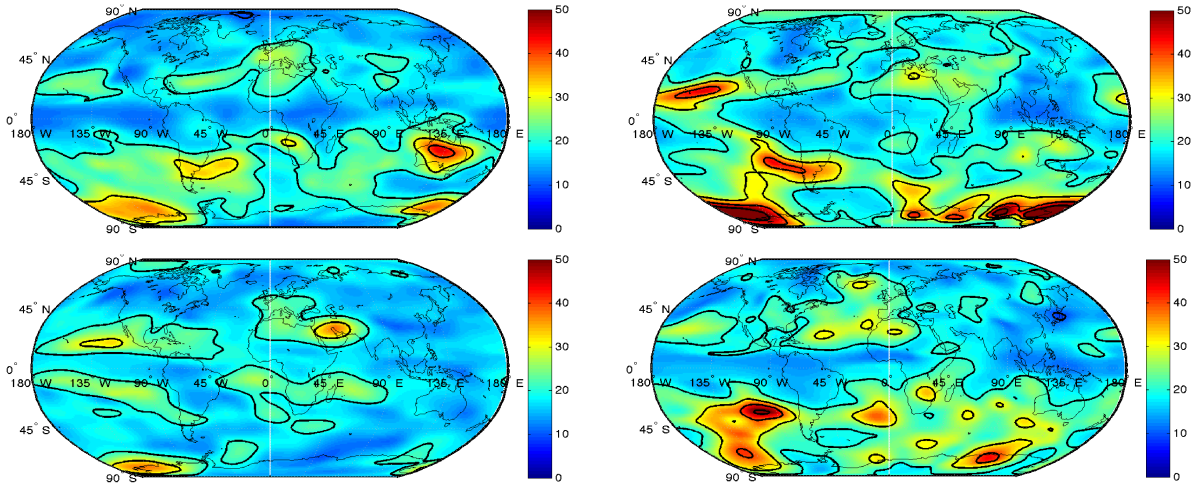

Figure 53: JJA TTD (years) with 5% Measurement Error for the CMIP3 Models, CCSM3 (top left panel) and GISS (top right panel), and CMIP5 Models, CCSM4 (bottom left panel) and GISS-E2 (bottom right panel)

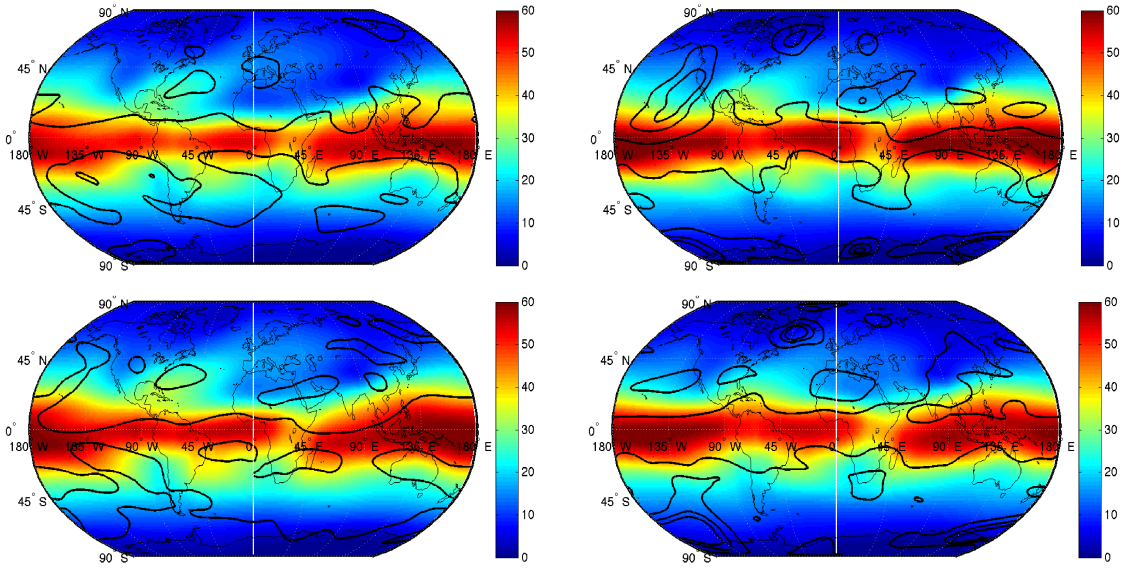

Figure 54: Example of MAM PWV (mm) for the CMIP3 Models, CCSM3 (top left panel) and GISS (top right panel), and CMIP5 models, CCSM4 (bottom left panel) and GISS-E2 (bottom right panel)

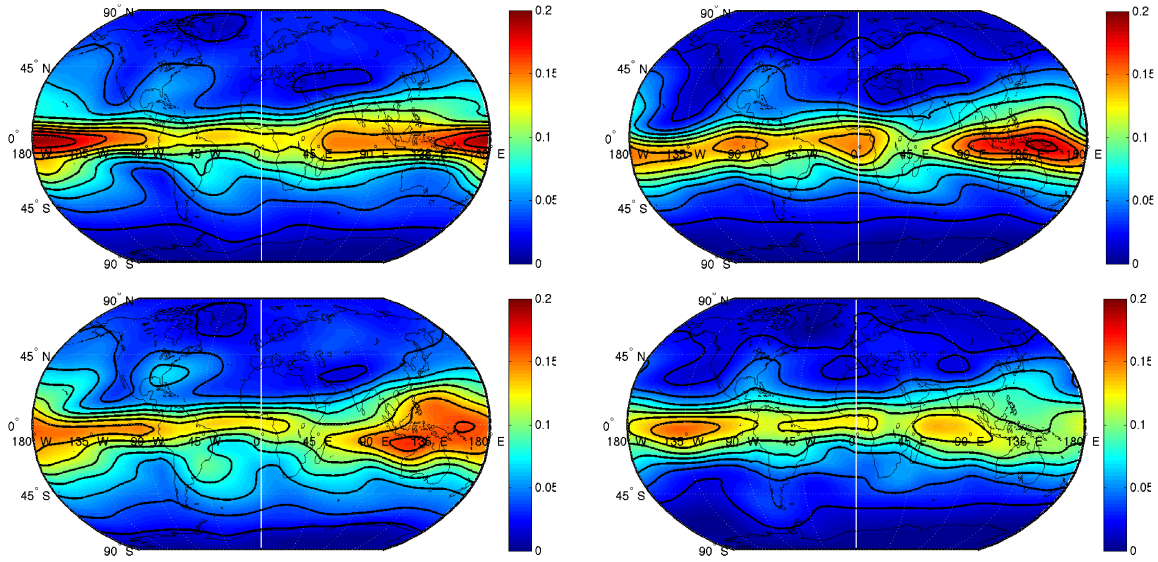

Figure 55: MAM 100 Year Trend (mm/year) for the CMIP3 Models, CCSM3 (top left panel) and GISS (top right panel), and CMIP5 models, CCSM4 (bottom left panel) and GISS-E2 (bottom right panel)

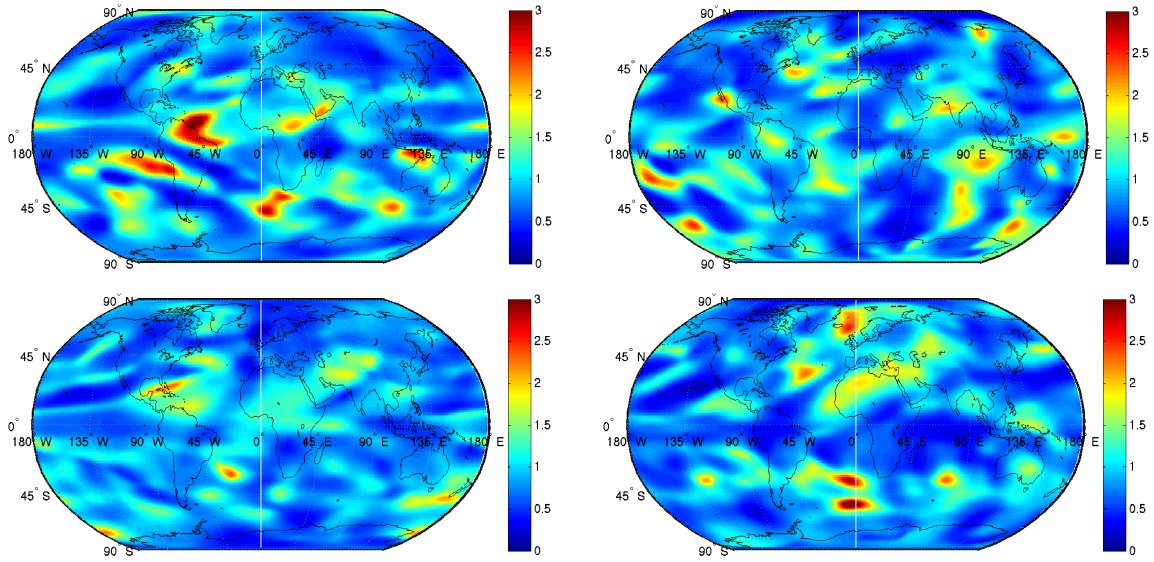

Figure 56: MAM Autocorrelation Factor (1+phi/1-phi) for the CMIP3 Models, CCSM3 (top left panel) and GISS (top right panel), and CMIP5 Models, CCSM4 (bottom left panel) and GISS-E2 (bottom right panel)

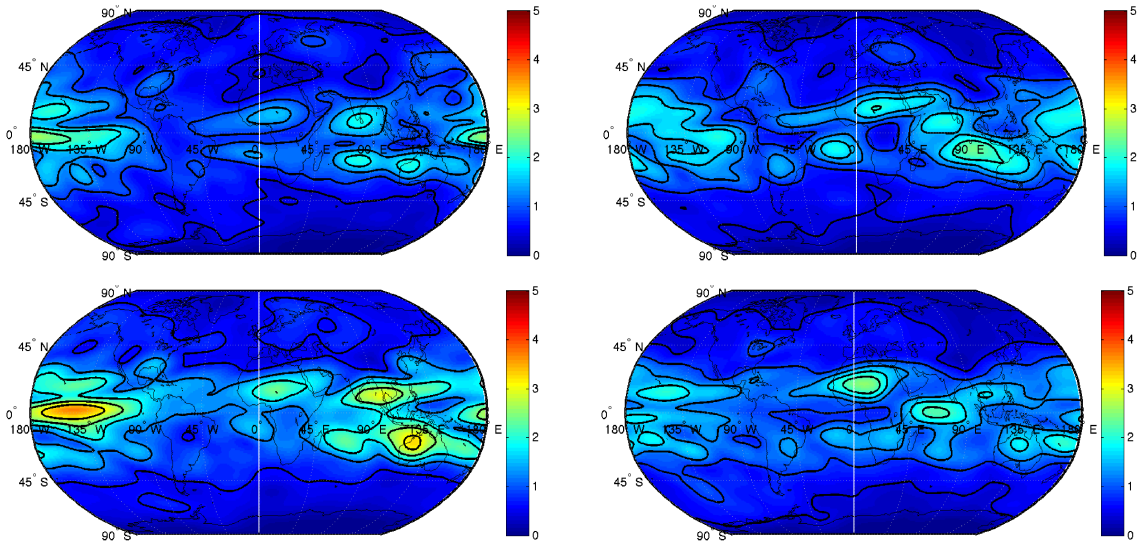

Figure 57: MAM Standard Deviation + 0% Measurement Error (mm) for the CMIP3 Models, CCSM3 (top left panel) and GISS (top right panel), and CMIP5 Models, CCSM4 (bottom left panel) and GISS-E2 (bottom right panel)

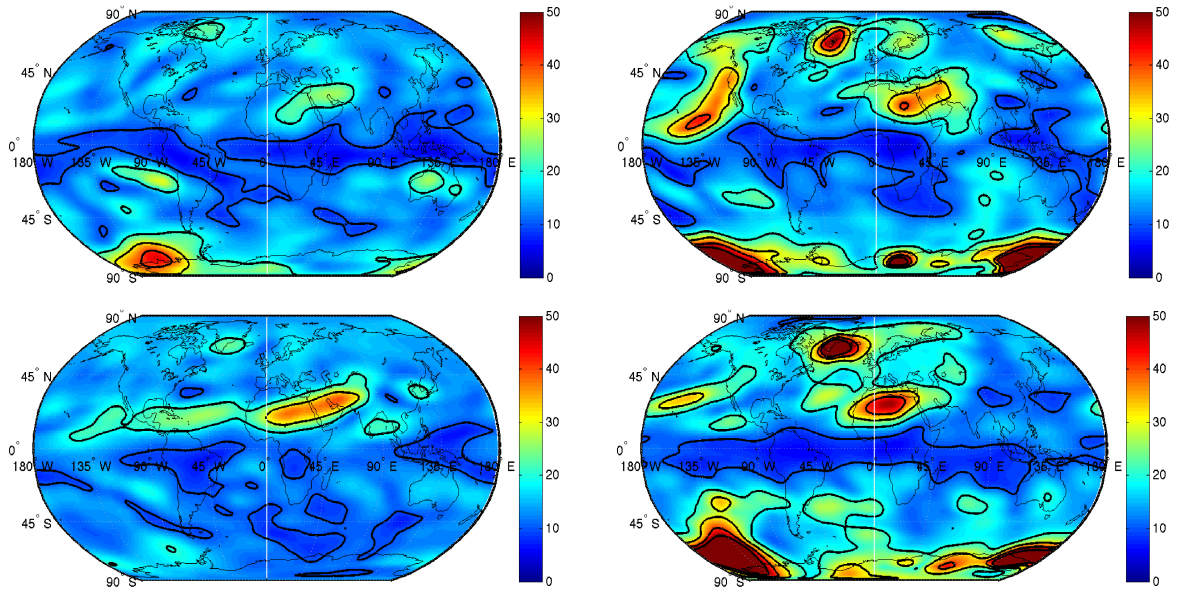

Figure 58: MAM TTD (years) for the CMIP3 Models, CCSM3 (top left panel) and GISS (top right panel), and CMIP5 Models, CCSM4 (bottom left panel) and GISS-E2 (bottom right panel)

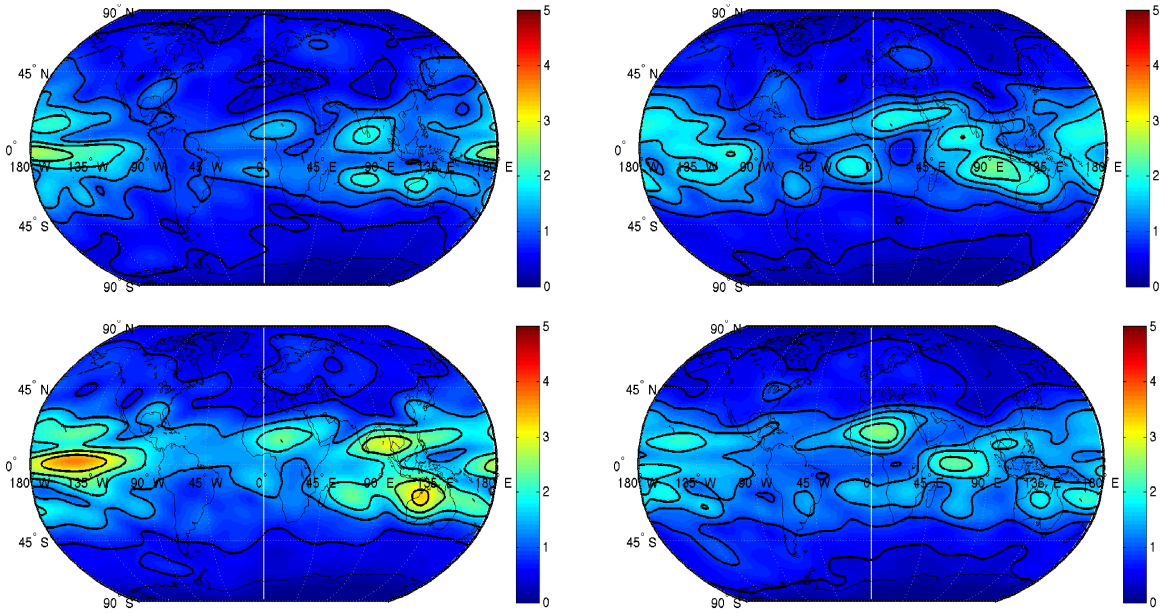

Figure 59: MAM Standard Deviation + 1% Measurement Error (mm) for the CMIP3 Models, CCSM3 (top left panel) and GISS (top right panel), and CMIP5 Models, CCSM4 (bottom left panel) and GISS-E2 (bottom right panel)

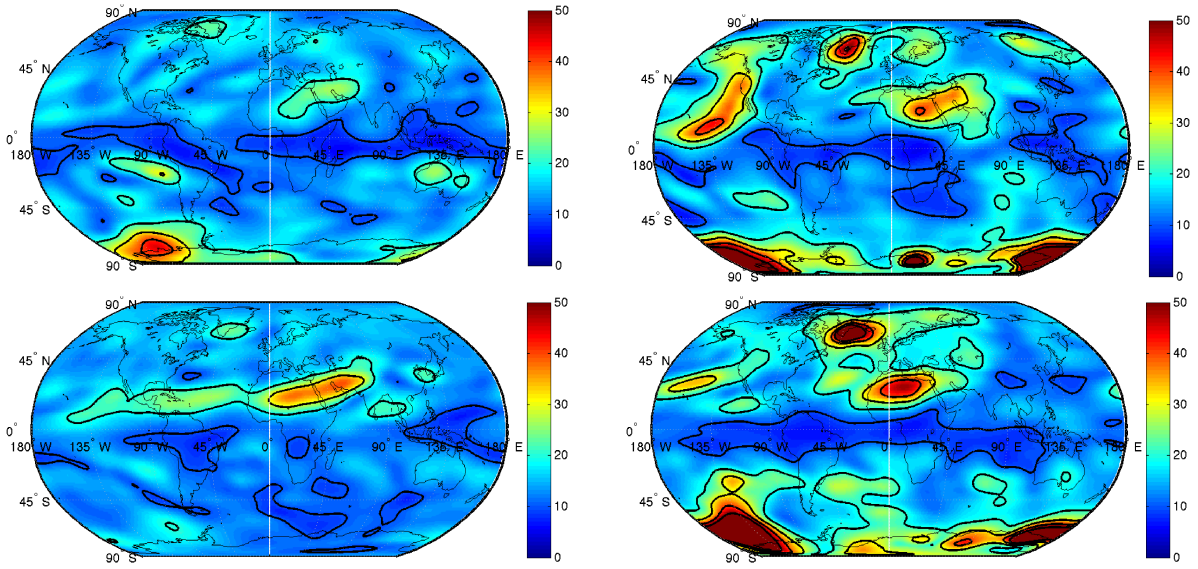

Figure 60: MAM TTD (years) with 1% Measurement Error for the CMIP3 Models, CCSM3 (top left panel) and GISS (top right panel), and CMIP5 Models (CCSM4 (bottom left panel) and GISS-E2 (bottom right panel)

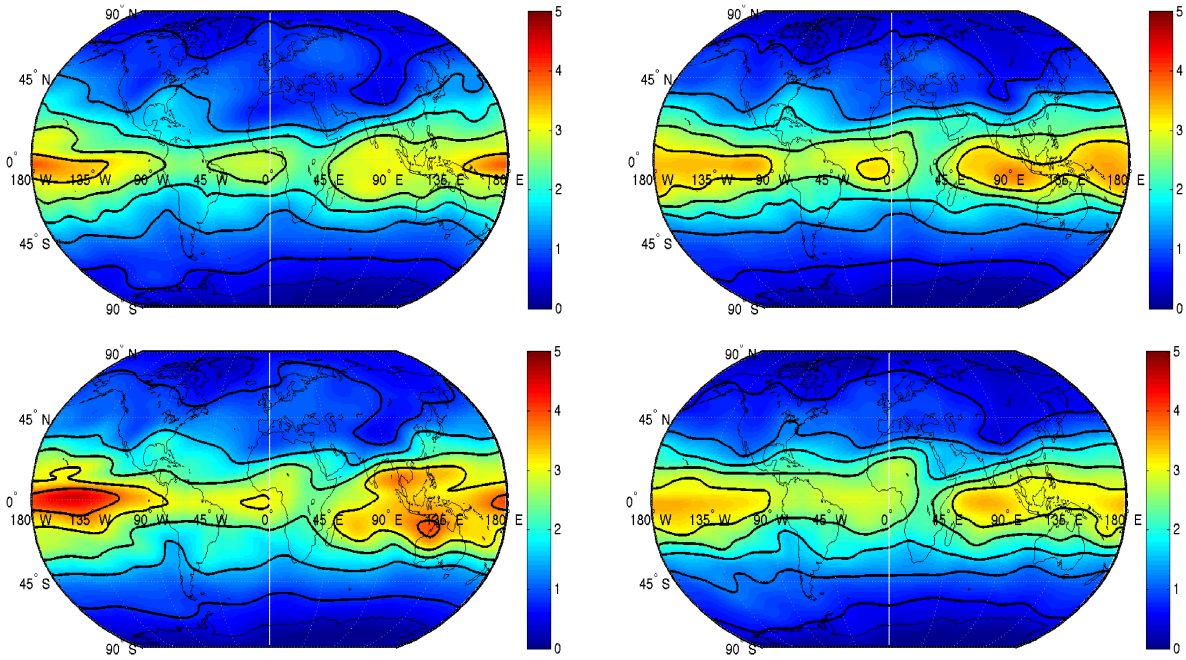

Figure 61: MAM Standard Deviation + 5% Measurement Error (mm) for the CMIP3 Models, CCSM3 (top left panel) and GISS (top right panel), and CMIP5 Models, CCSM4 (bottom left panel) and GISS-E2 (bottom right panel)

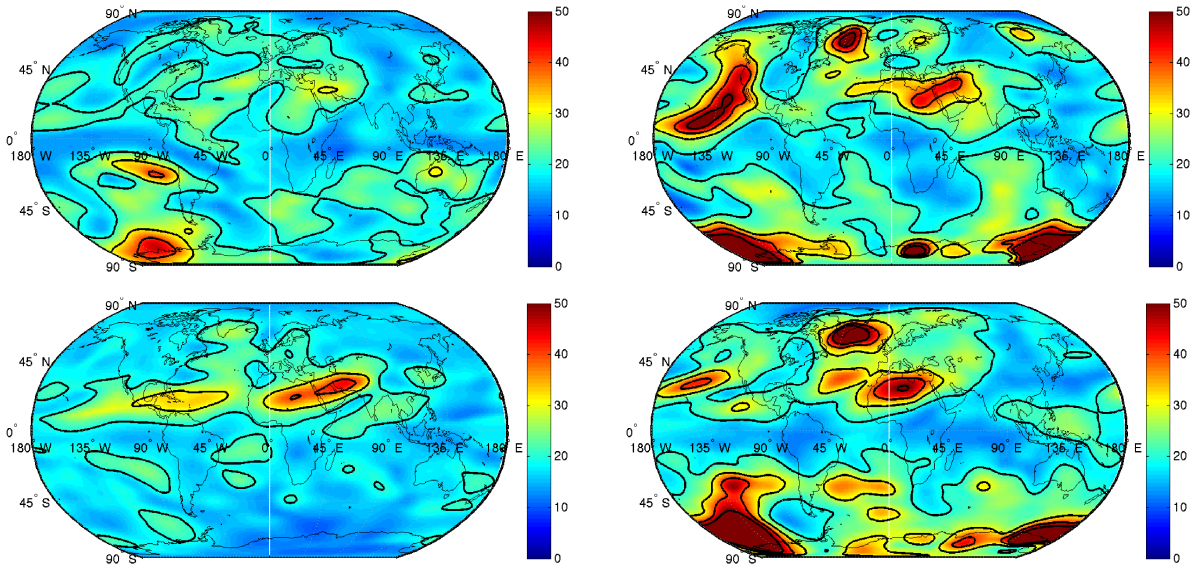

Figure 62: MAM TTD (years) with 5% Measurement Error for the CMIP3 Models, CCSM3 (top left panel) and GISS (top right panel), and CMIP5 Models, CCSM4 (bottom left panel) and GISS-E2 (bottom right panel)

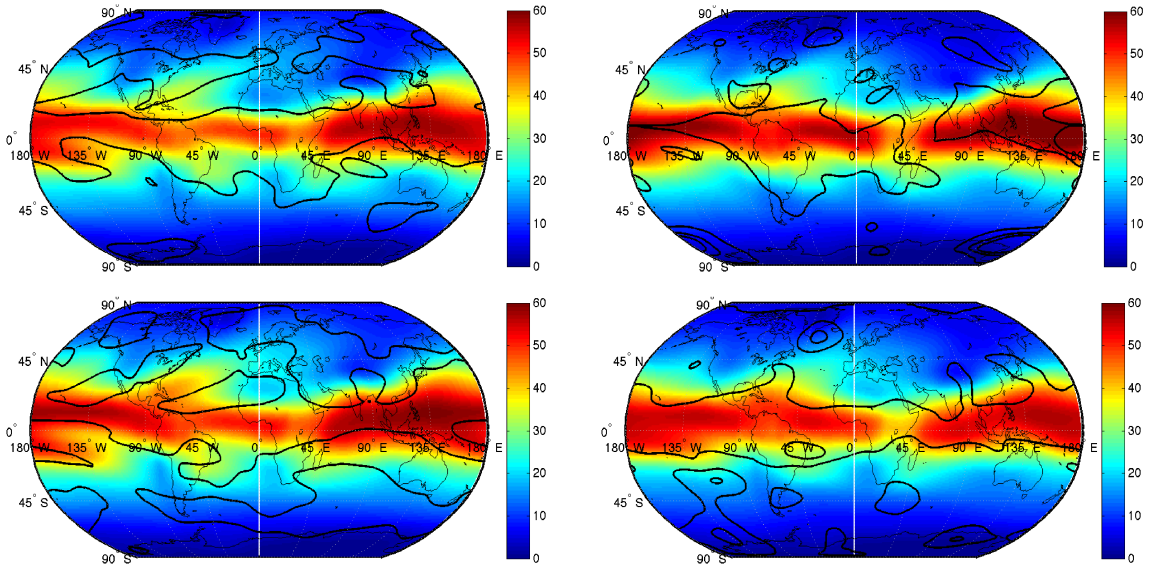

Figure 63: Example of SON PWV (mm) for the CMIP3 Models, CCSM3 (top left panel) and GISS (top right panel), and CMIP5 models, CCSM4 (bottom left panel) and GISS-E2 (bottom right panel)

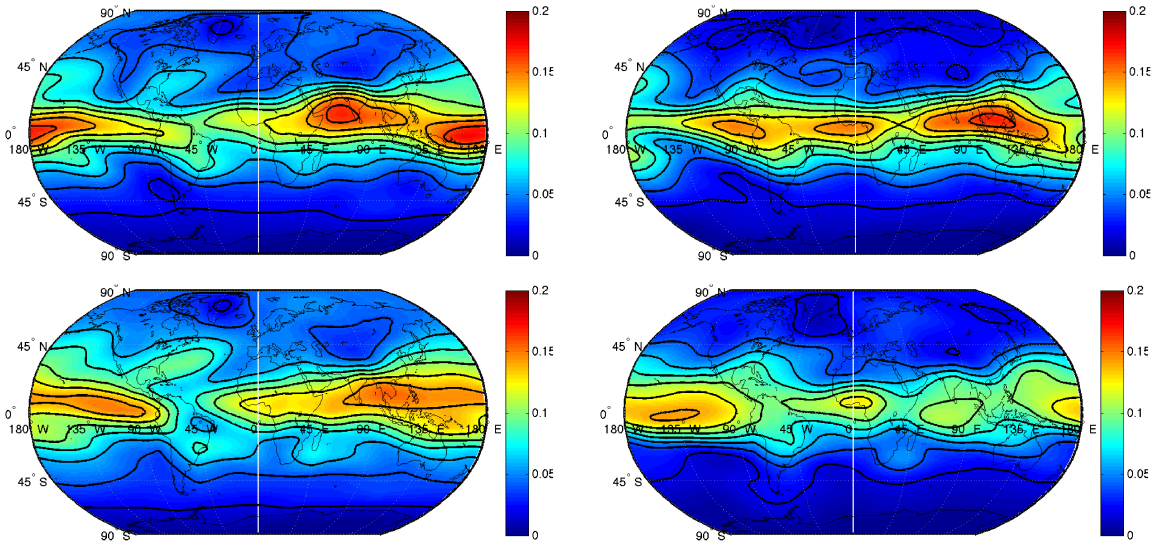

Figure 64: SON 100 Year Trend (mm/year) for the CMIP3 Models, CCSM3 (top left panel) and GISS (top right panel), and CMIP5 models, CCSM4 (bottom left panel) and GISS-E2 (bottom right panel)

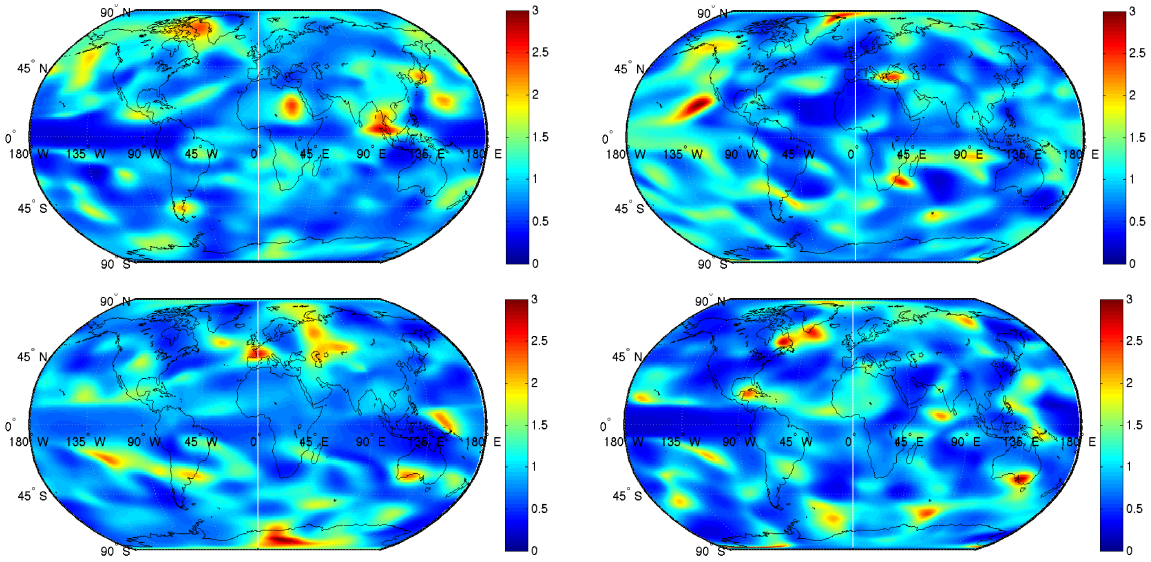

Figure 65: SON Autocorrelation Factor (1+phi/1-phi) for the CMIP3 Models, CCSM3 (top left panel) and GISS (top right panel), and CMIP5 Models, CCSM4 (bottom left panel) and GISS-E2 (bottom right panel)

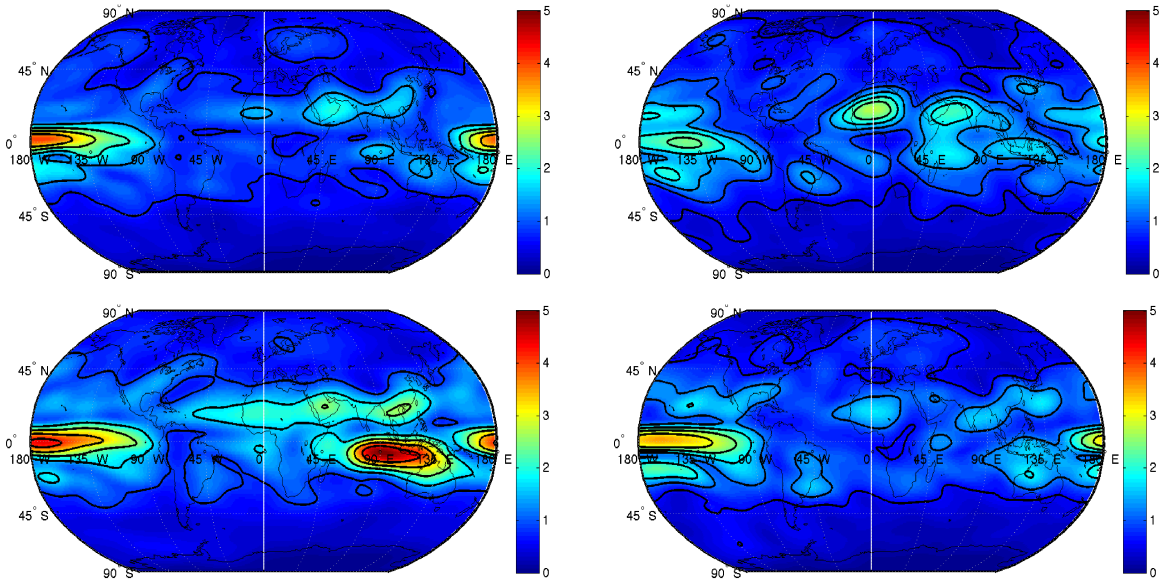

Figure 66: SON Standard Deviation + 0% Measurement Error (mm) for the CMIP3 Models, CCSM3 (top left panel) and GISS (top right panel), and CMIP5 Models, CCSM4 (bottom left panel) and GISS-E2 (bottom right panel)

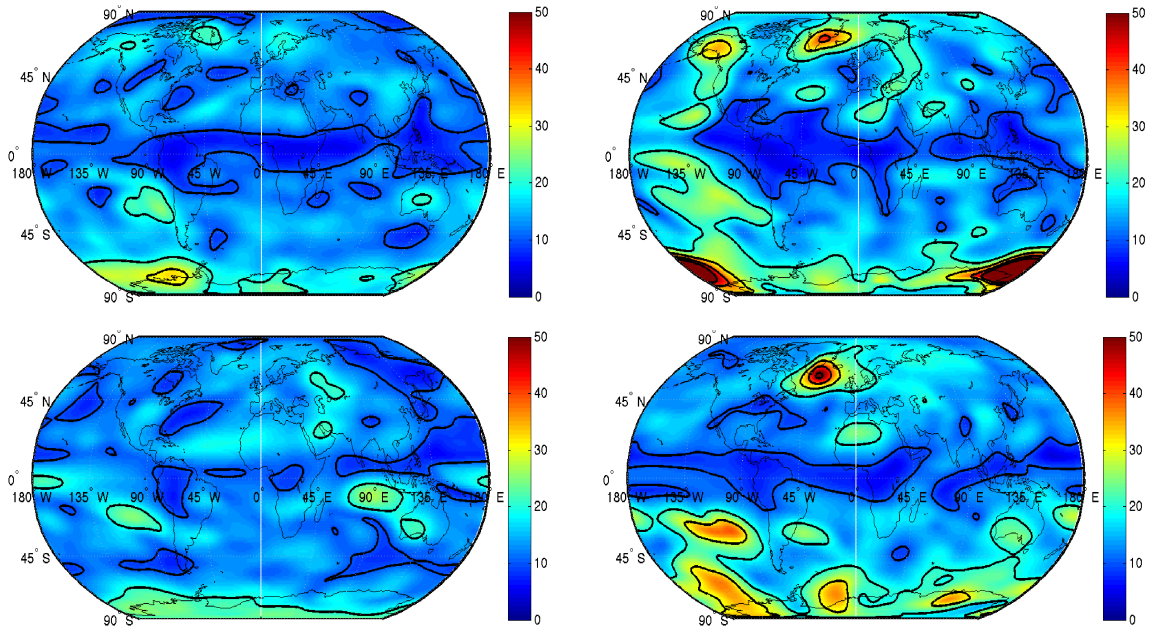

Figure 67: SON TTD (years) for 0% Measurement Error for the CMIP3 Models, CCSM3 (top left panel) and GISS (top right panel), and CMIP5 Models, CCSM4 (bottom left panel) and GISS-E2 (bottom right panel)

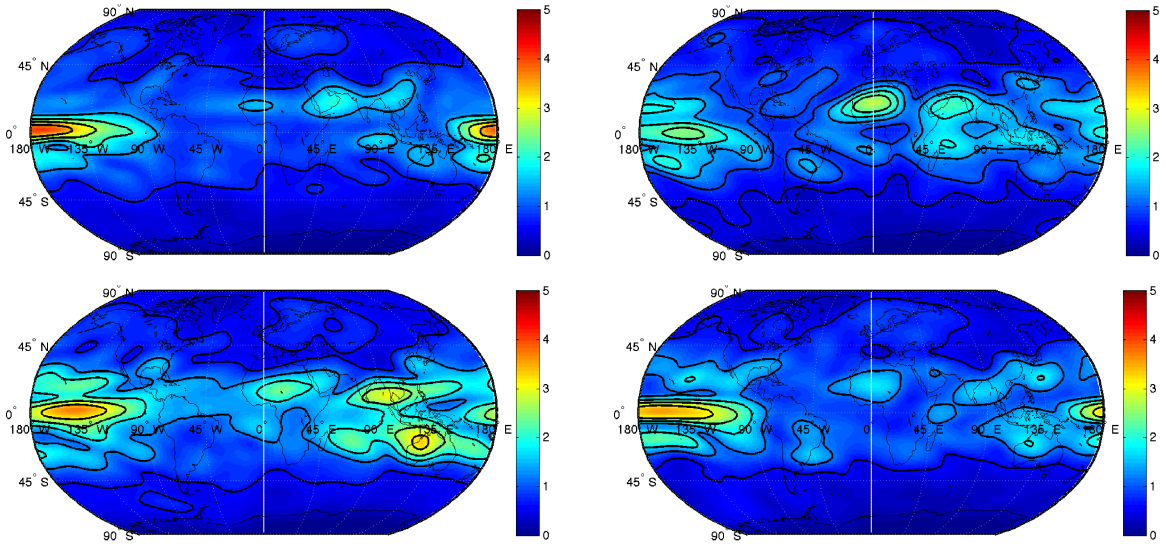

Figure 68: SON Standard Deviation + 1% Measurement Error (mm) for the CMIP3 Models, CCSM3 (top left panel) and GISS (top right panel), and CMIP5 Models, CCSM4 (bottom left panel) and GISS-E2 (bottom right panel)

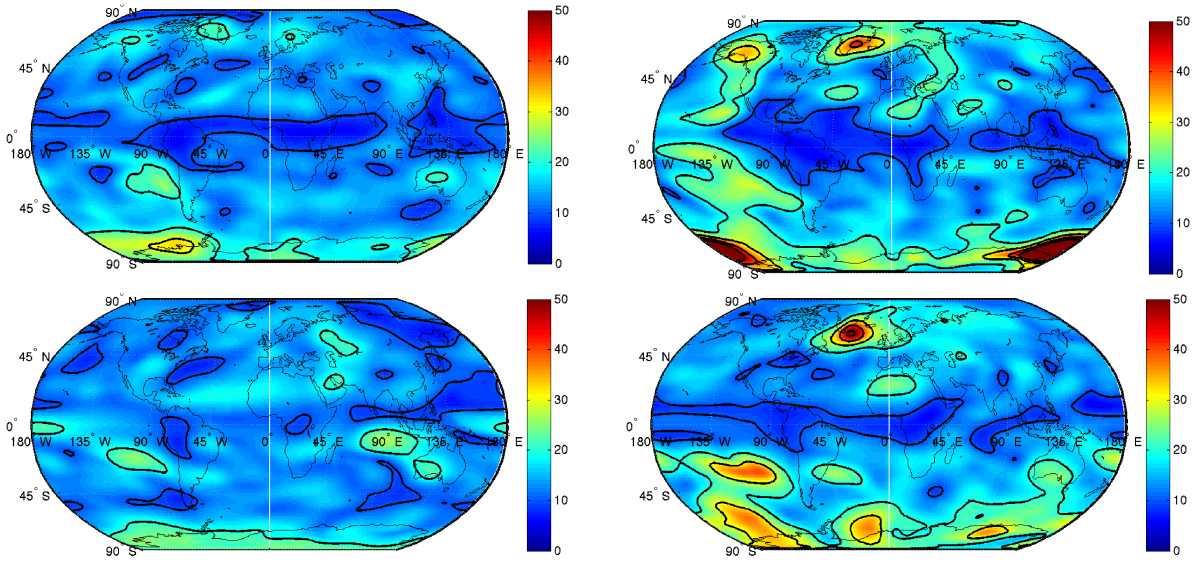

Figure 69: SON TTD (years) with 1% Measurement Error for the CMIP3 Models, CCSM3 (top left panel) and GISS (top right panel), and CMIP5 Models (CCSM4 (bottom left panel) and GISS-E2 (bottom right panel)

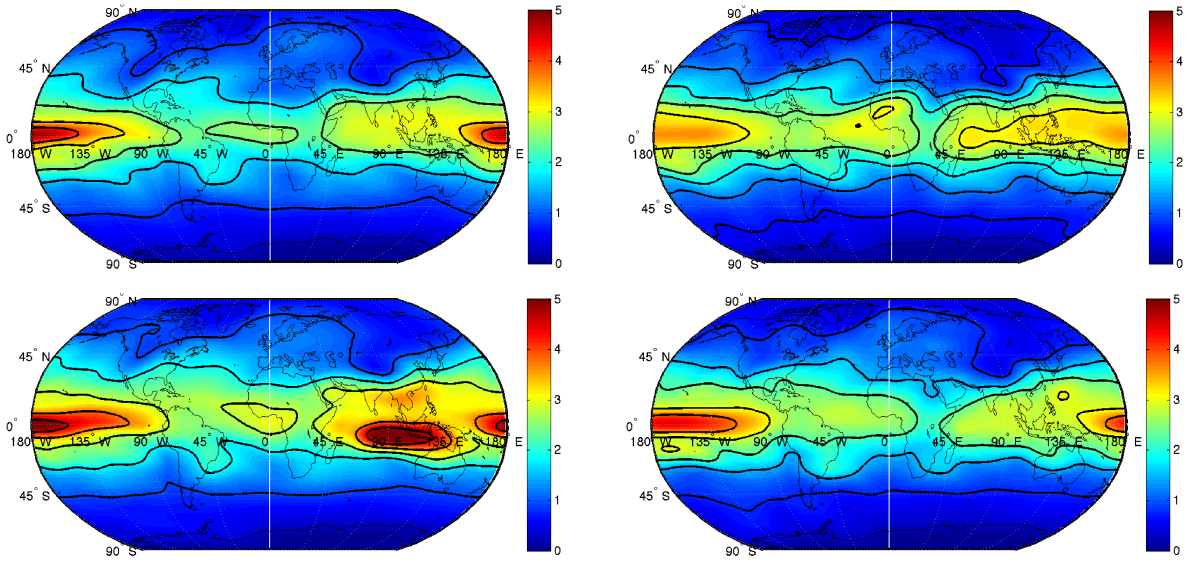

Figure 70: SON Standard Deviation + 5% Measurement Error (mm) for the CMIP3 Models, CCSM3 (top left panel) and GISS (top right panel), and CMIP5 Models, CCSM4 (bottom left panel) and GISS-E2 (bottom right panel)

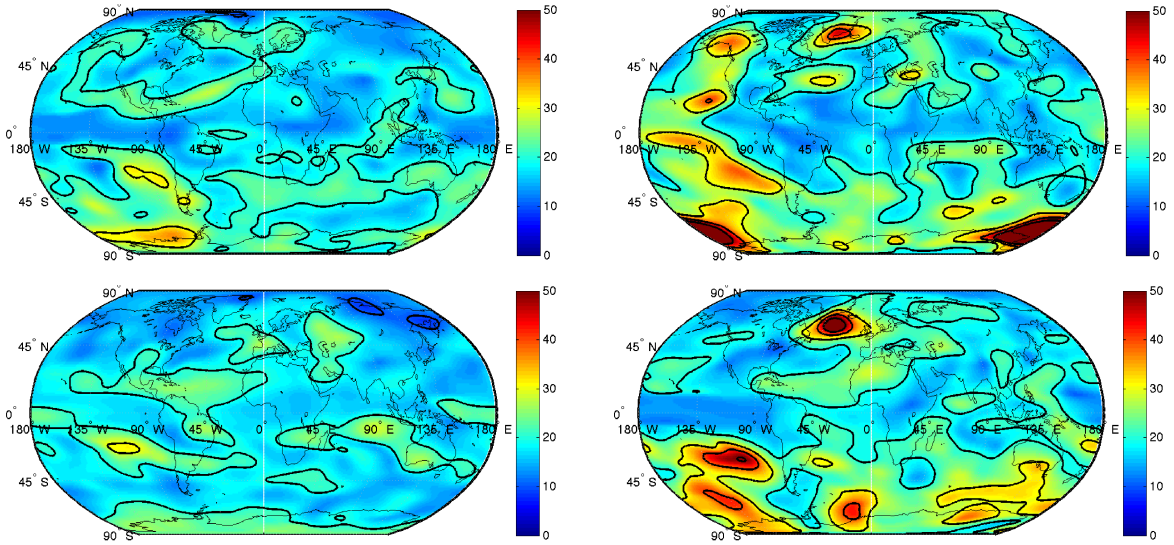

Figure 71: SON TTD (years) with 5% Measurement Error for the CMIP3 Models, CCSM3 (top left panel) and GISS (top right panel), and CMIP5 Models, CCSM4 (bottom left panel) and GISS-E2 (bottom right panel)

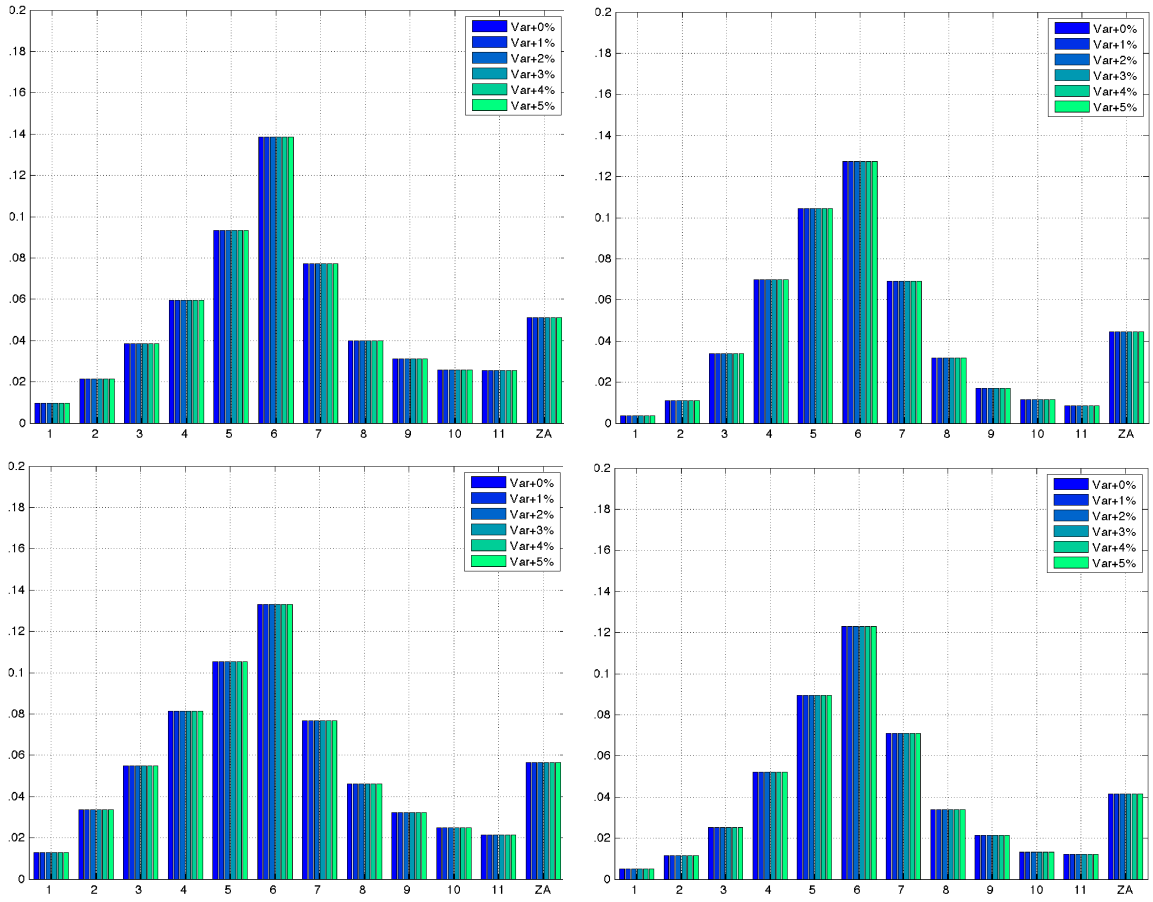

Figure 72: DJF 100 Year Trend (mm/year) for CMIP3 Models, CCSM3 (top left panel) and GISS (top right panel), and CMIP5 Models, CCSM4 (bottom left panel) and GISS-E2 (bottom right panel

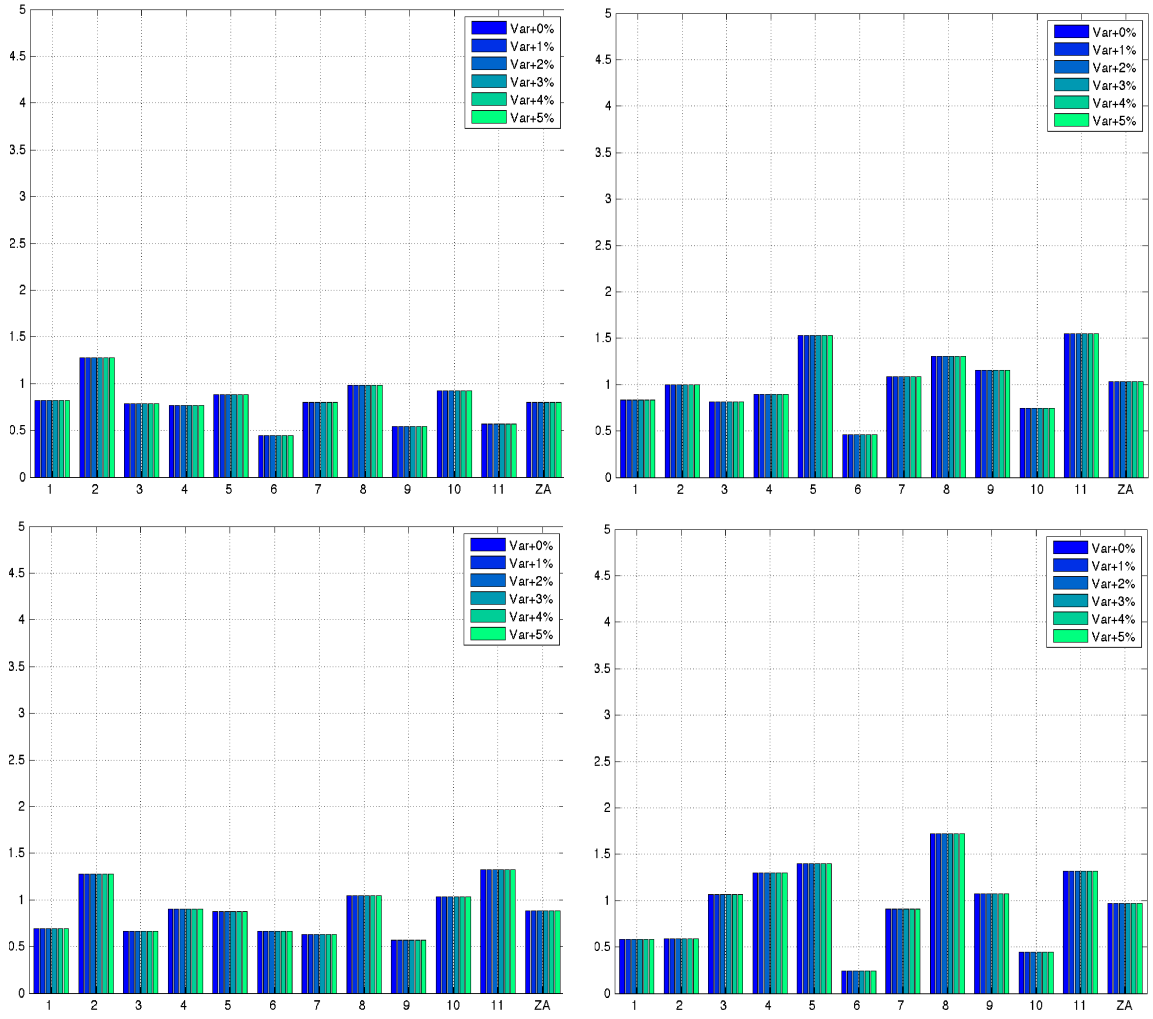

Figure 73: DJF Autocorrelation Factor (1+phi/1-phi) for CMIP3 Models, CCSM3 (top left panel) and GISS (top right panel), and CMIP5 Models, CCSM4 (bottom let panel) and GISS-E2 (bottom right panel)

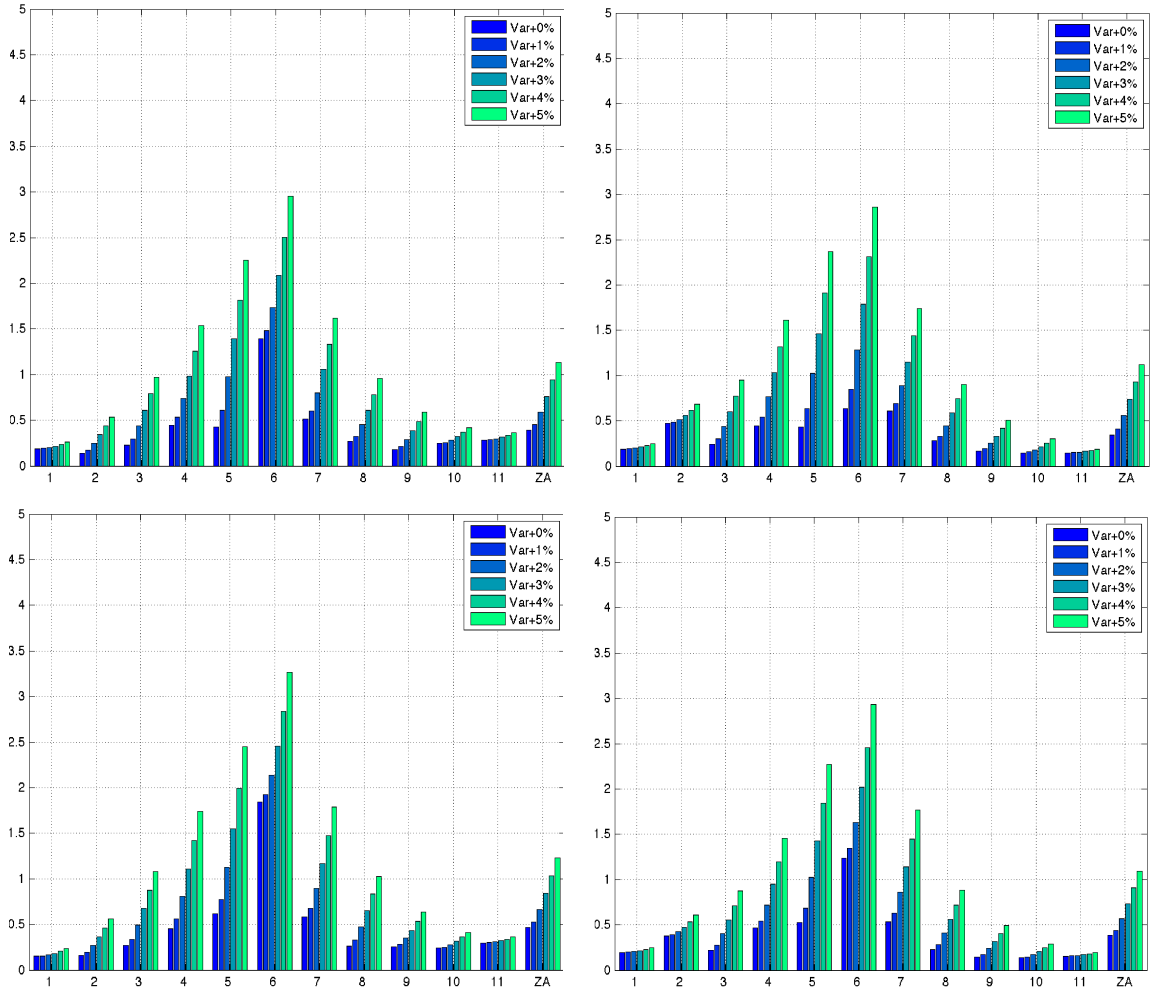

Figure 74: DJF Standard Deviation + Measurement Error (mm) for CMIP3 Models, CCSM3 (top left panel) and GISS (top right panel), and CMIP5 Models, CCSM4 (bottom left panel) and GISS-E2 (bottom right panel)

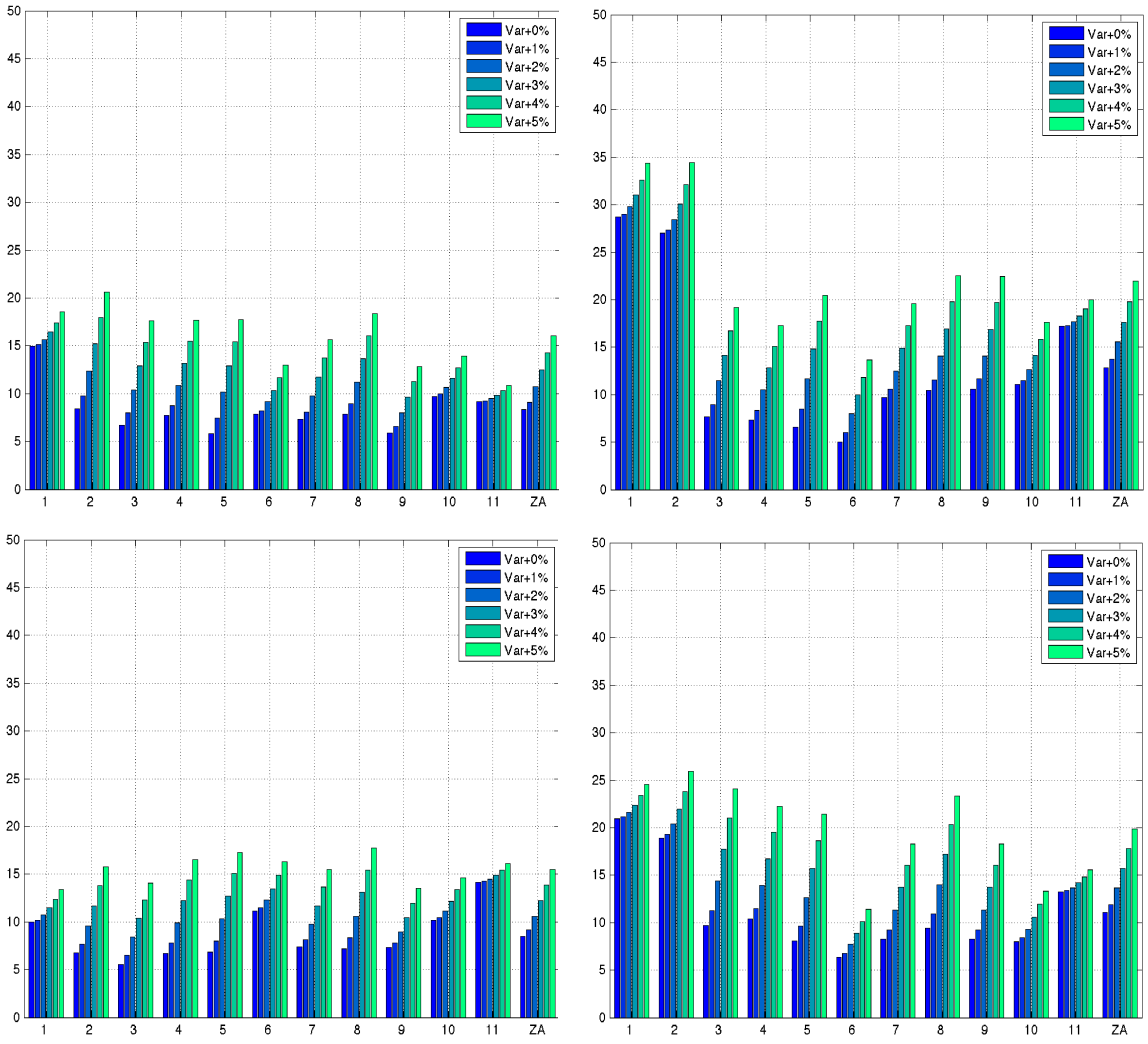

Figure 75: DJF TTD (years) for Measurement Errors for CMIP3 Models, CCSM3 (top left panel) and GISS (top right panel), and CMIP5 Models, CCSM4 (bottom left panel) and GISS-E2 (bottom right panel)

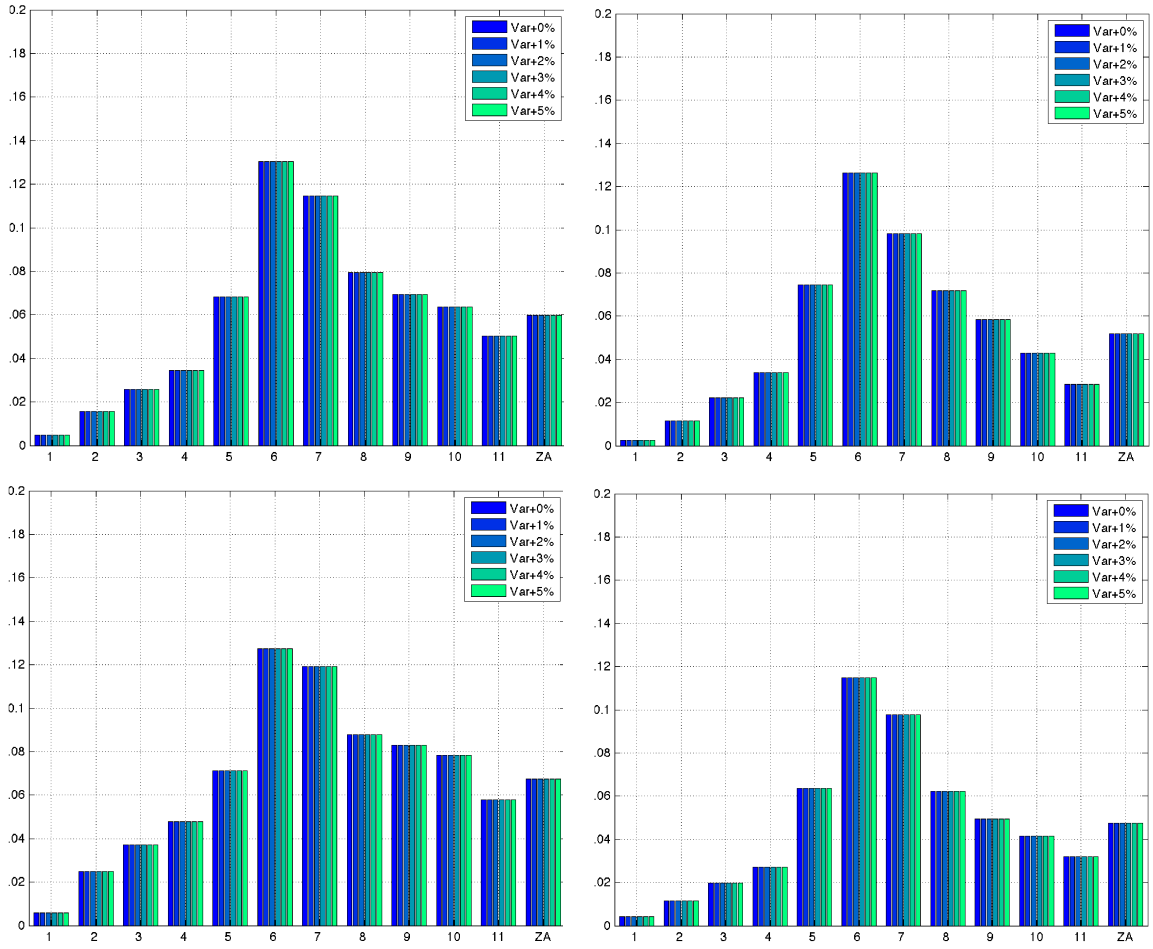

Figure 76: JJA 100 Year Trend (mm/year) for CMIP3 Models, CCSM3 (top left panel) and GISS (top right panel), and CMIP5 Models, CCSM4 (bottom left panel) and GISS-E2 (bottom right panel

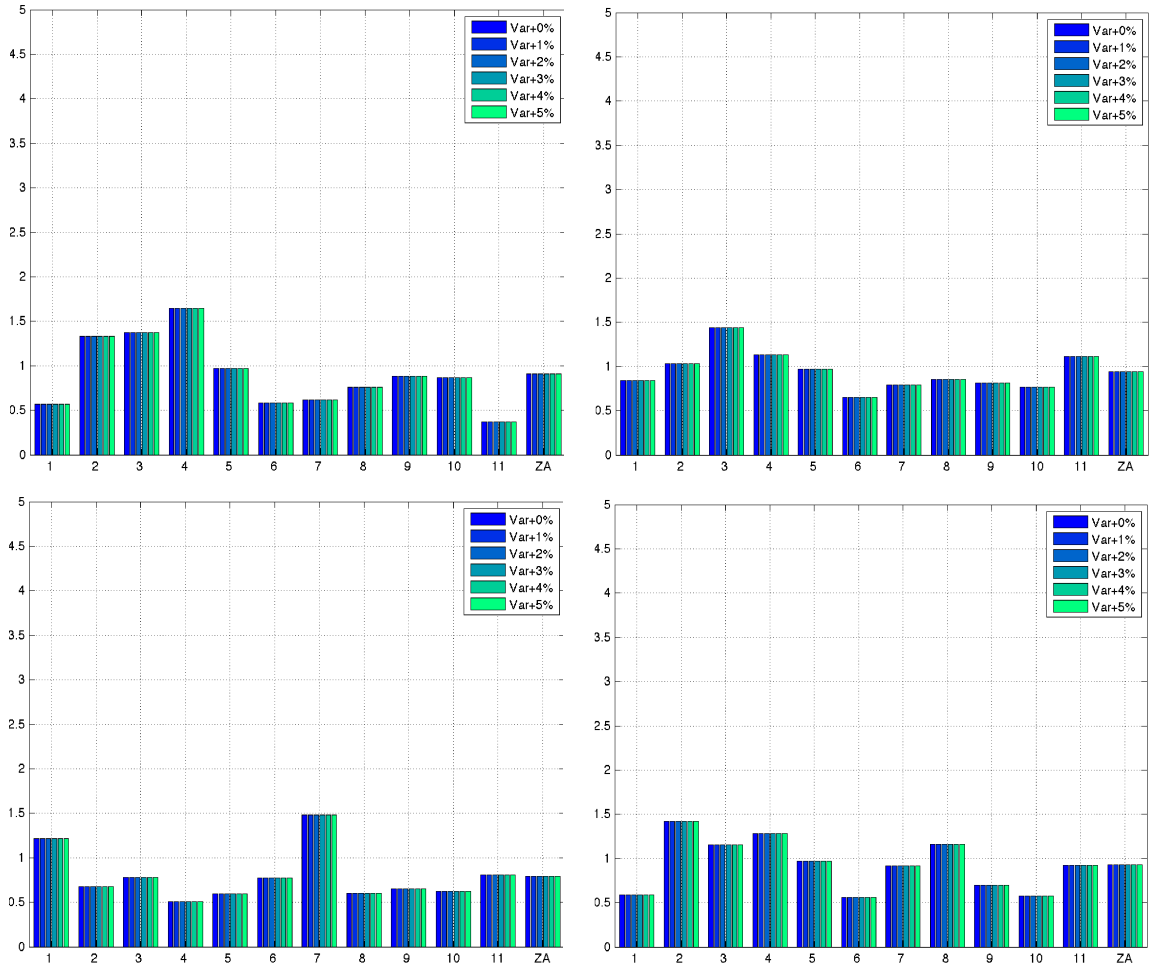

Figure 77: JJA Autocorrelation Factor (1+phi/1-phi) for CMIP3 Models, CCSM3 (top left panel) and GISS (top right panel), and CMIP5 Models, CCSM4 (bottom let panel) and GISS-E2 (bottom right panel)

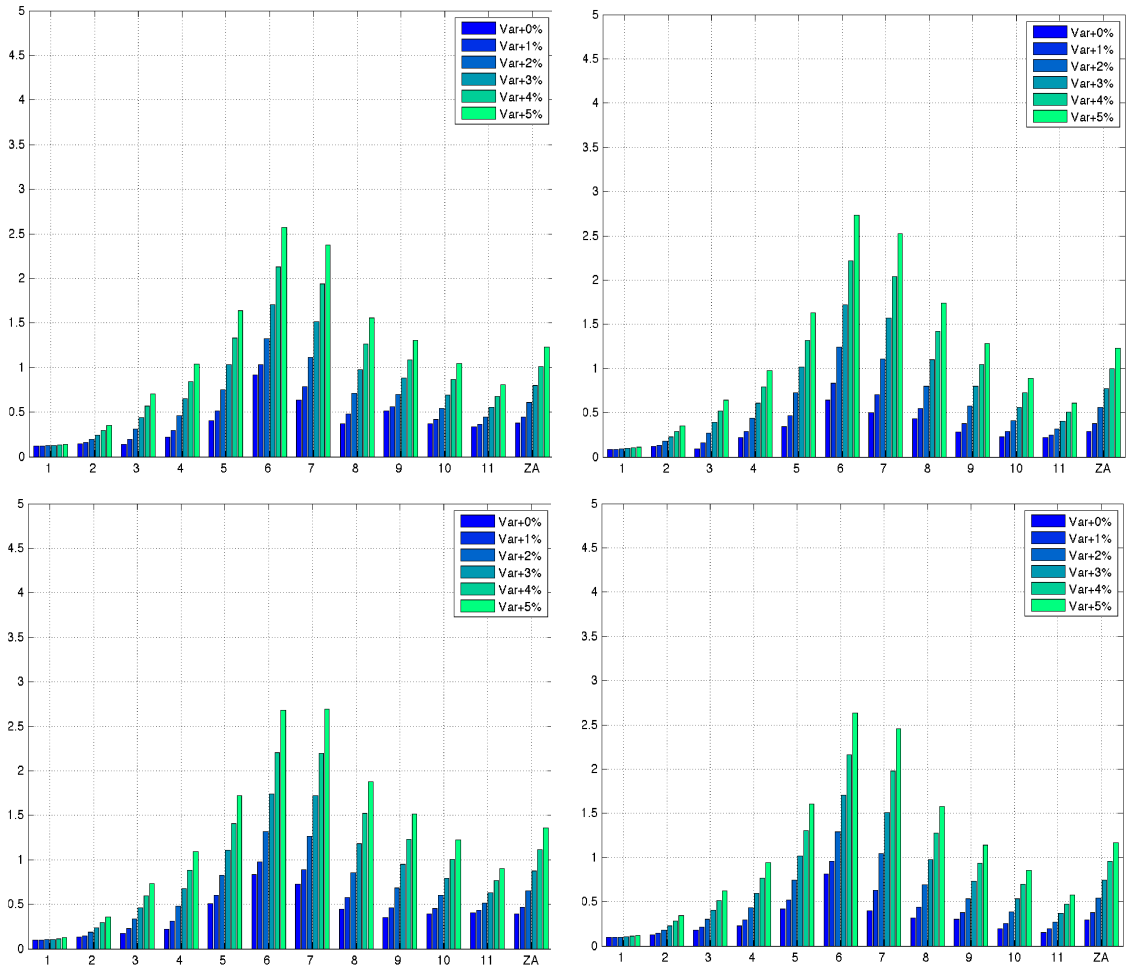

Figure 78: JJA Standard Deviation + Measurement Error (mm) for CMIP3 Models, CCSM3 (top left panel) and GISS (top right panel), and CMIP5 Models, CCSM4 (bottom left panel) and GISS-E2 (bottom right panel)

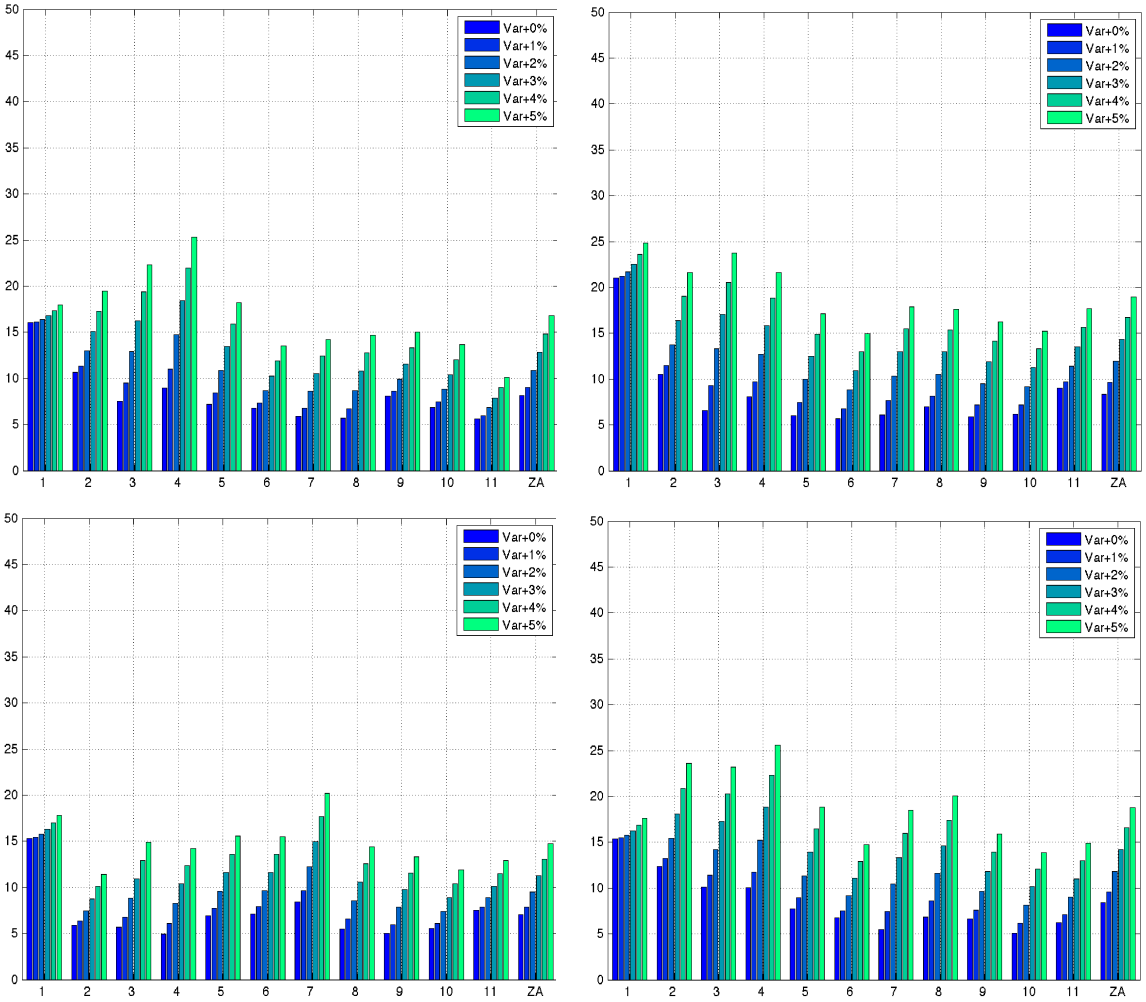

Figure 79: JJA TTD (years) for Measurement Errors for CMIP3 Models, CCSM3 (top left panel) and GISS (top right panel), and CMIP5 Models, CCSM4 (bottom left panel) and GISS-E2 (bottom right panel)

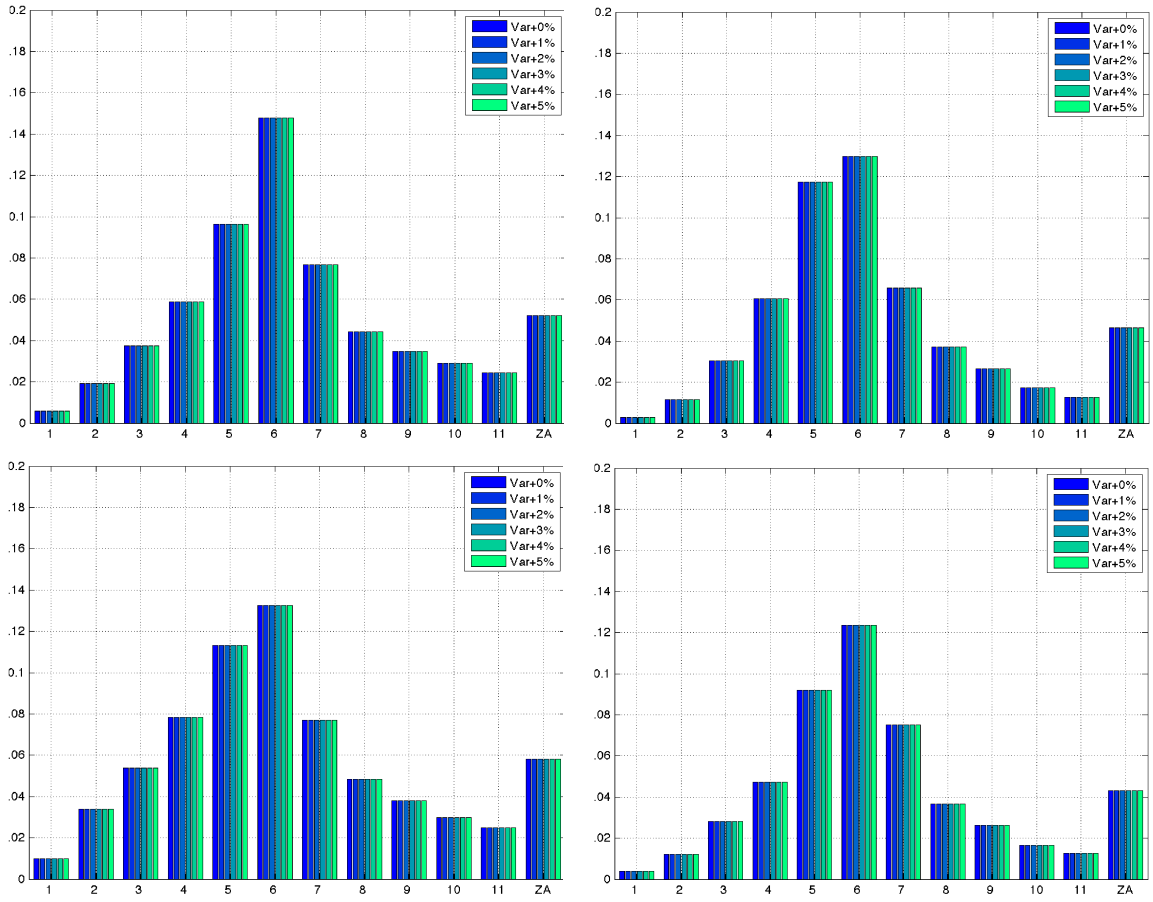

Figure 80: MAM 100 Year Trend (mm/year) for CMIP3 Models, CCSM3 (top left panel) and GISS (top right panel), and CMIP5 Models, CCSM4 (bottom left panel) and GISS-E2 (bottom right panel

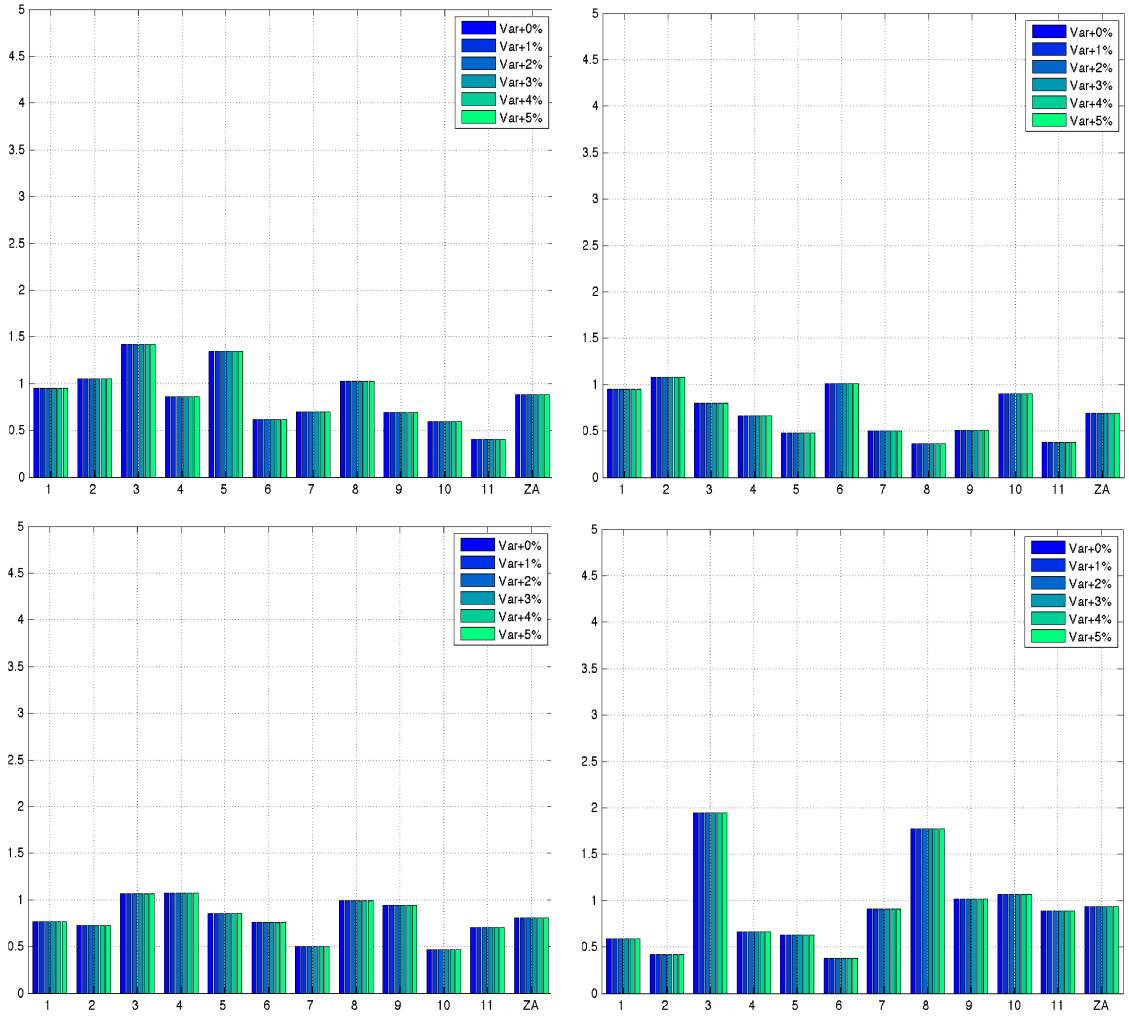

Figure 81: MAM Autocorrelation Factor (1+phi/1-phi) for CMIP3 Models, CCSM3 (top left panel) and GISS (top right panel), and CMIP5 Models, CCSM4 (bottom let panel) and GISS-E2 (bottom right panel)

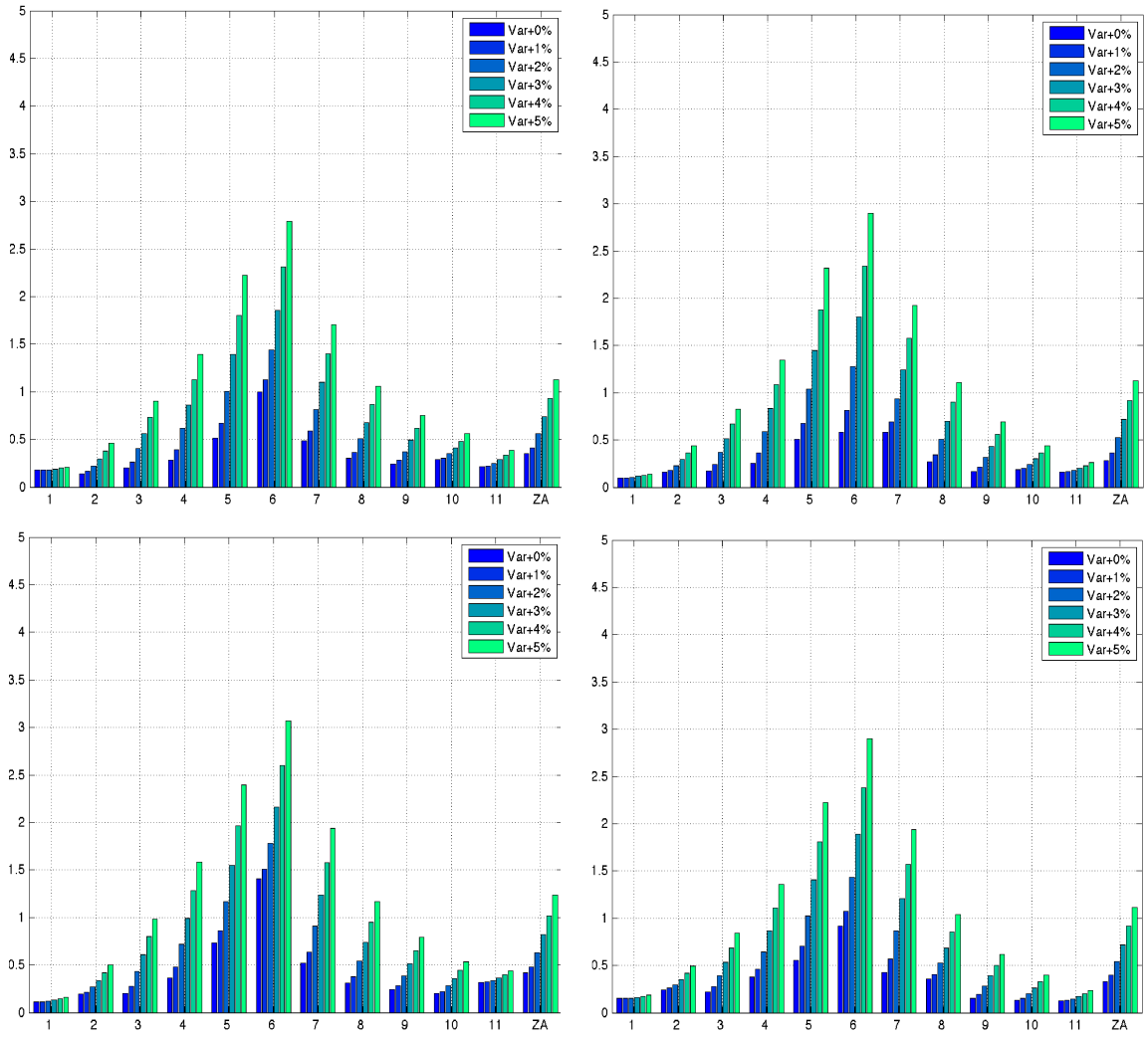

Figure 82: MAM Standard Deviation + Measurement Error (mm) for CMIP3 Models, CCSM3 (top left panel) and GISS (top right panel), and CMIP5 Models, CCSM4 (bottom left panel) and GISS-E2 (bottom right panel)

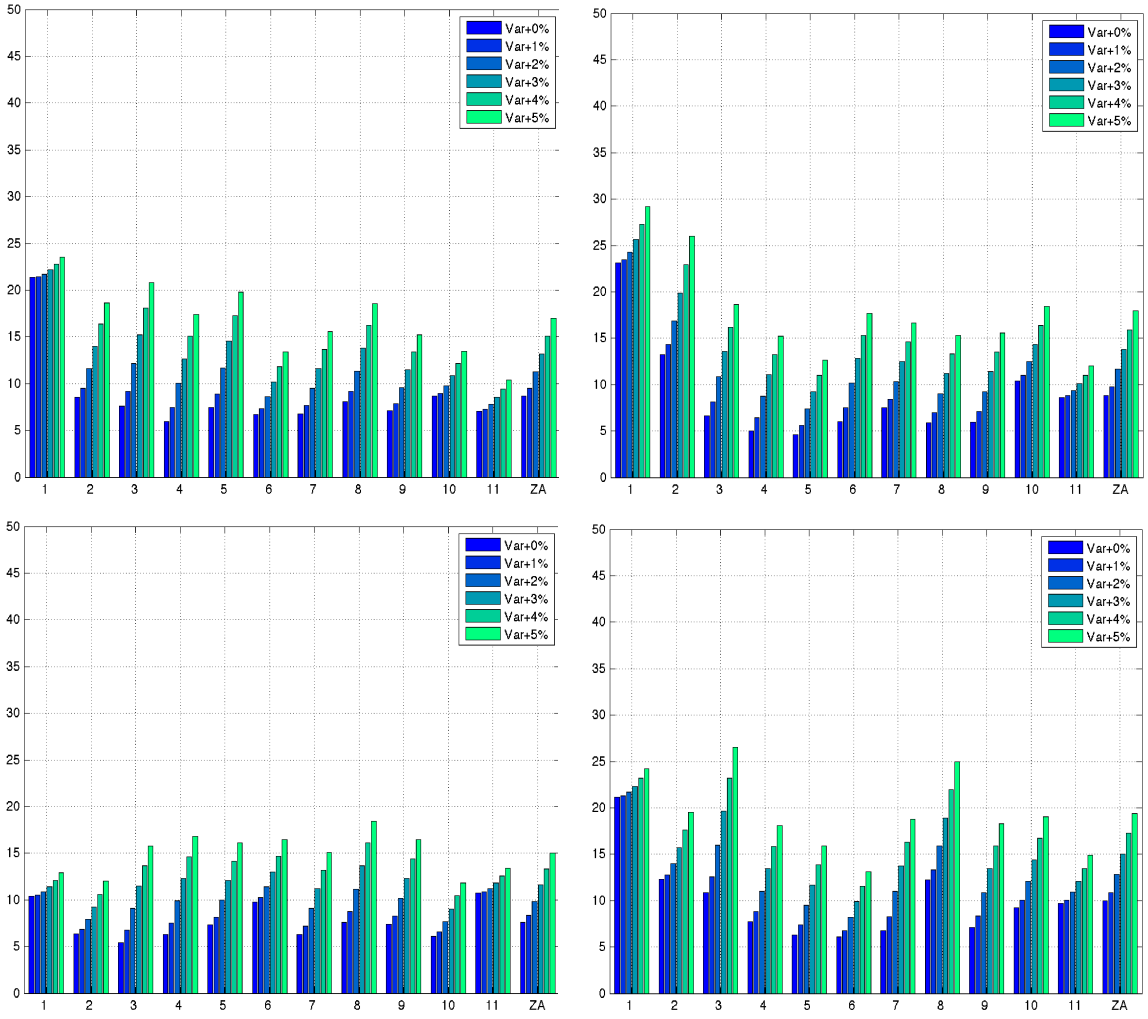

Figure 83: MAM TTD (years) for Measurement Errors for CMIP3 Models, CCSM3 (top left panel) and GISS (top right panel), and CMIP5 Models, CCSM4 (bottom left panel) and GISS-E2 (bottom right panel)

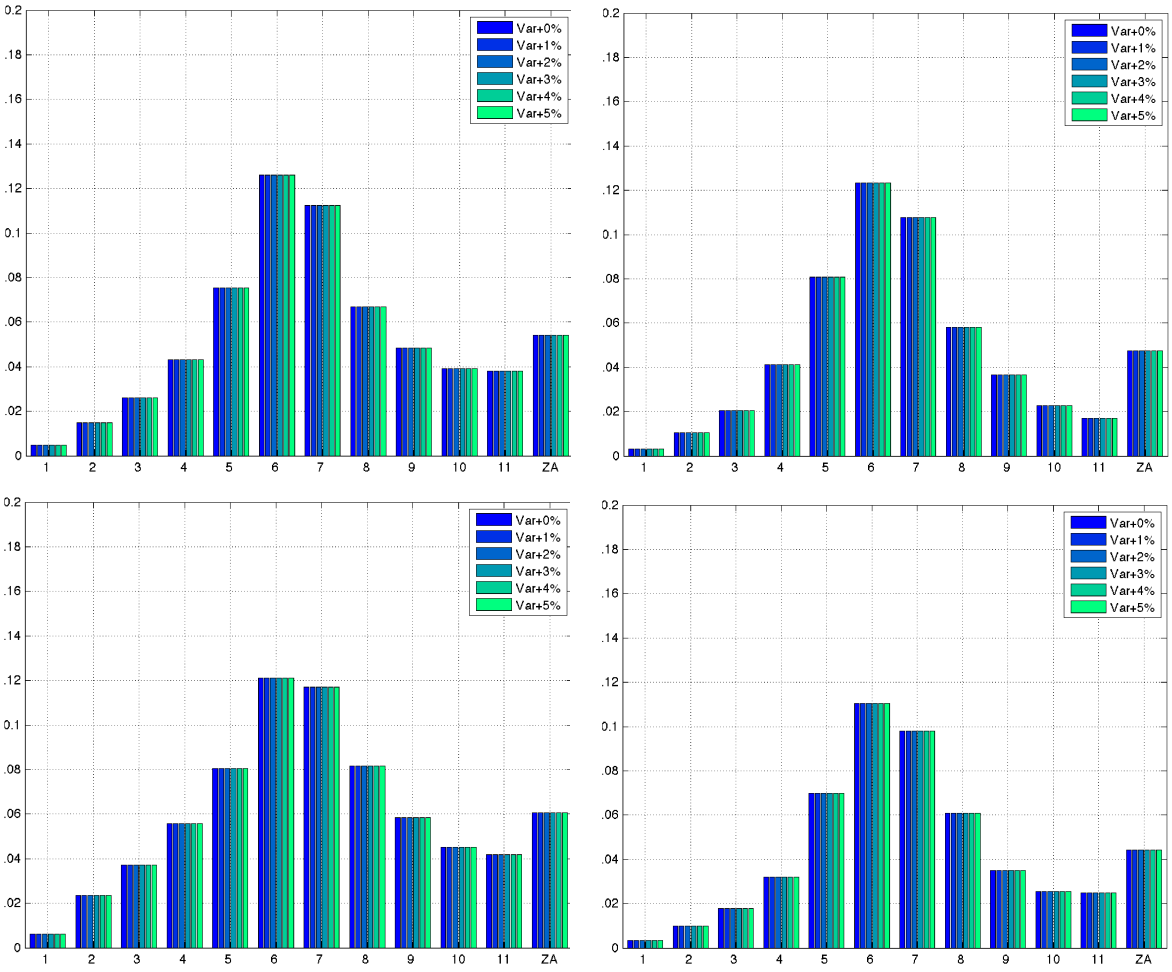

Figure 84: SON 100 Year Trend (mm/year) for CMIP3 Models, CCSM3 (top left panel) and GISS (top right panel), and CMIP5 Models, CCSM4 (bottom left panel) and GISS-E2 (bottom right panel

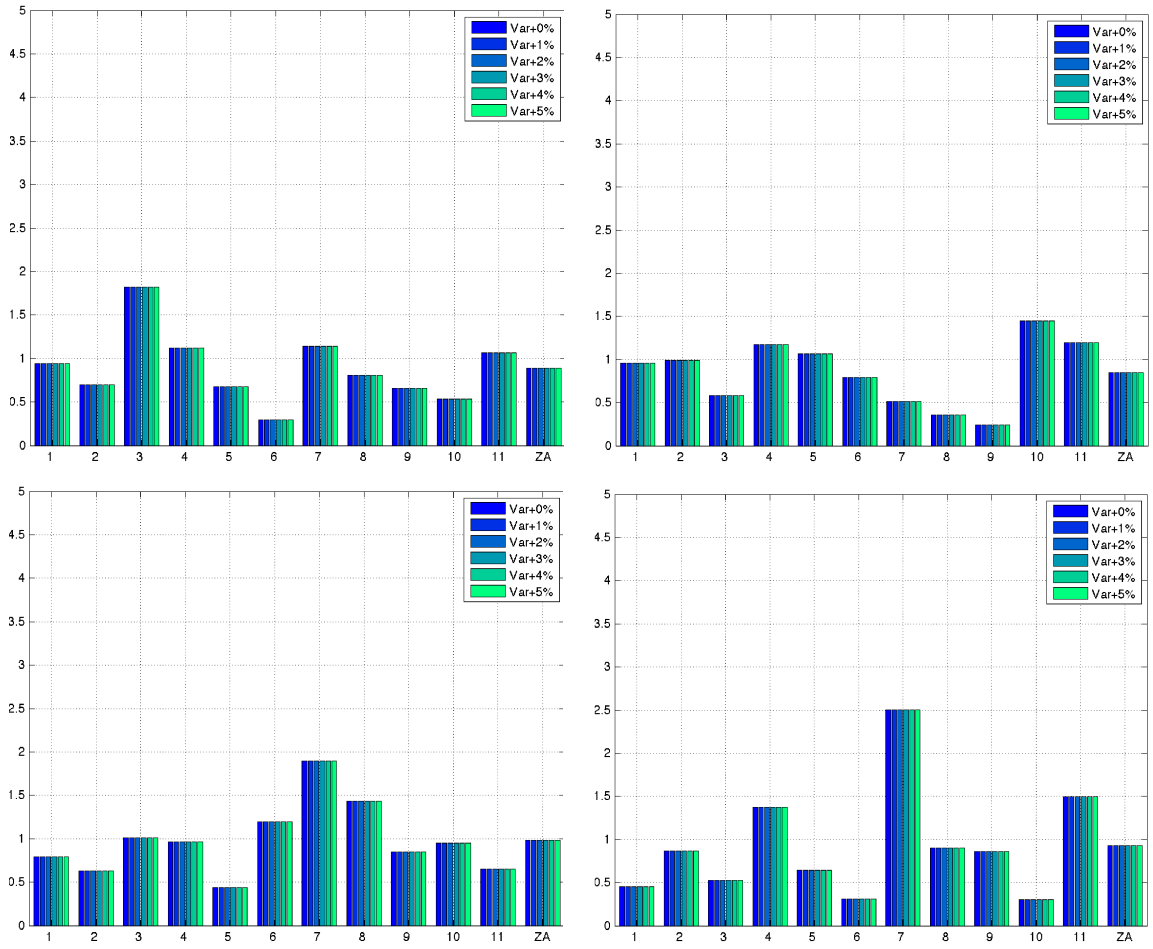

Figure 85: SON Autocorrelation Factor (1+phi/1-phi) for CMIP3 Models, CCSM3 (top left panel) and GISS (top right panel), and CMIP5 Models, CCSM4 (bottom let panel) and GISS-E2 (bottom right panel)

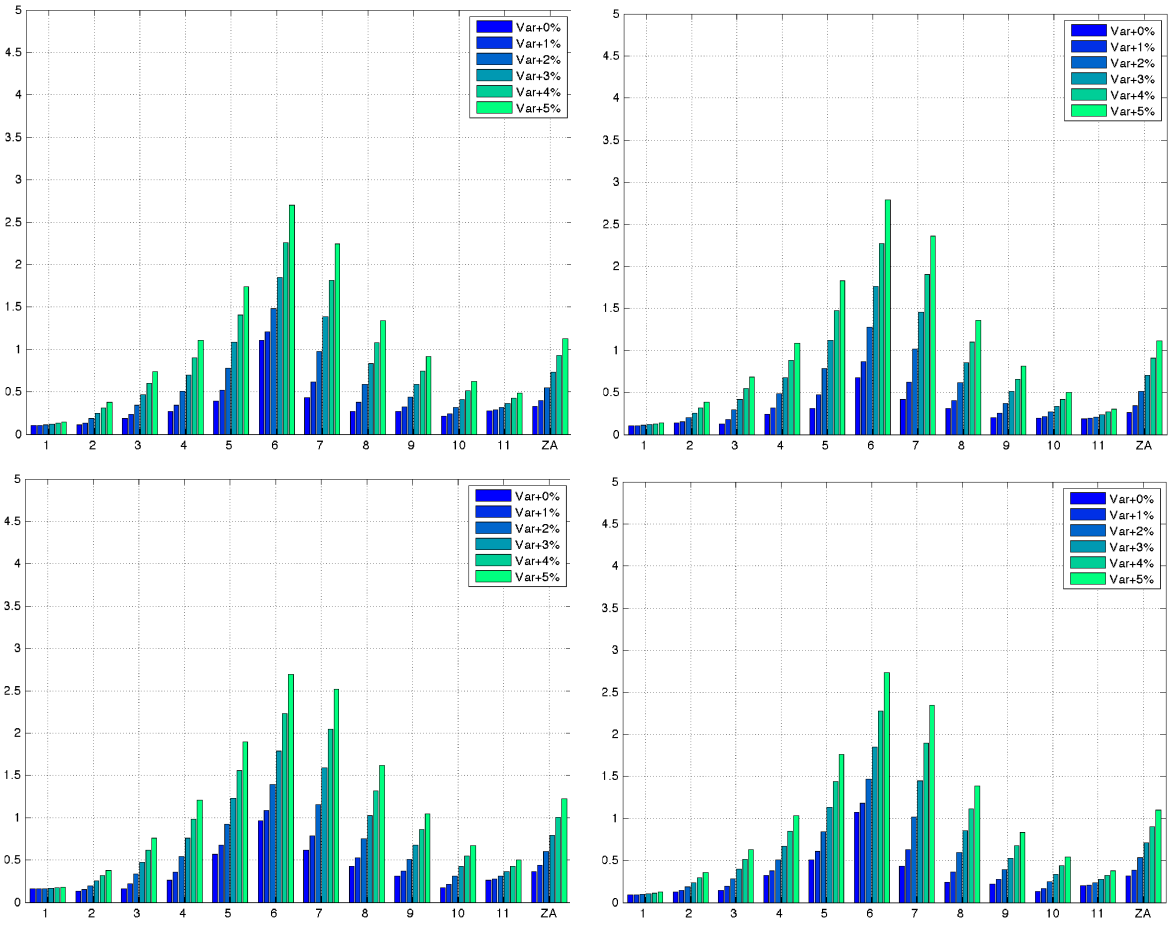

Figure 86: SON Standard Deviation + Measurement Error (mm) for CMIP3 Models, CCSM3 (top left panel) and GISS (top right panel), and CMIP5 Models, CCSM4 (bottom left panel) and GISS-E2 (bottom right panel)

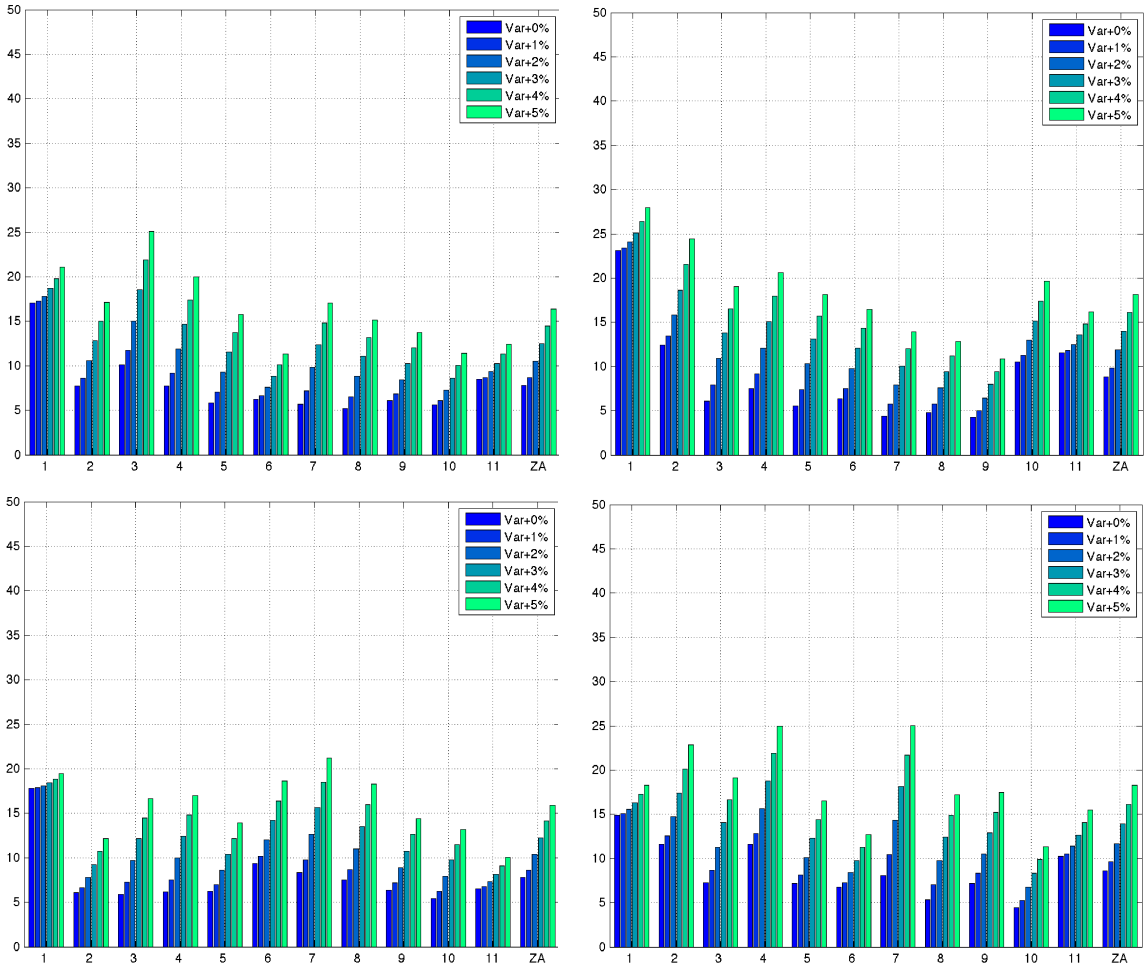

Figure 87: SON TTD (years) for Measurement Errors for CMIP3 Models, CCSM3 (top left panel) and GISS (top right panel), and CMIP5 Models, CCSM4 (bottom left panel) and GISS-E2 (bottom right panel)

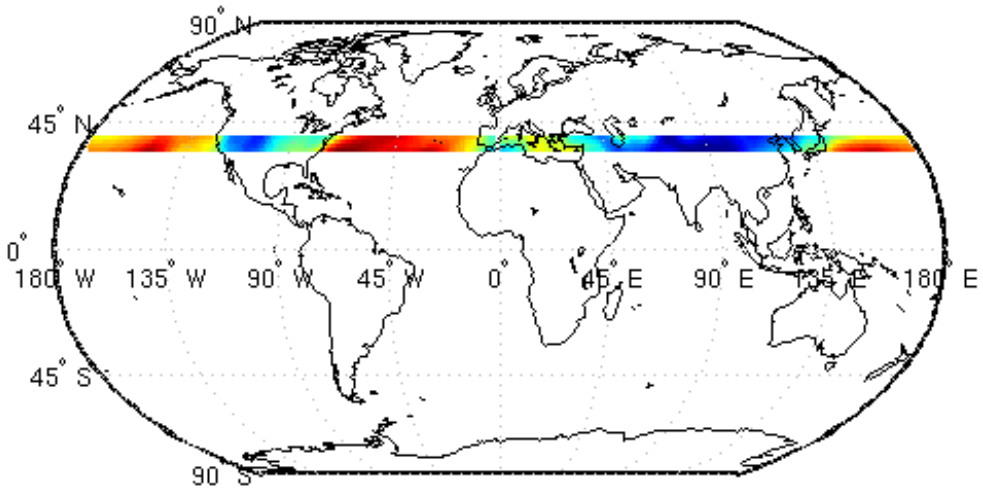

Figure 88: Latitude Averaged Region (34°N to 39°N) Showing the Longitude Dependence

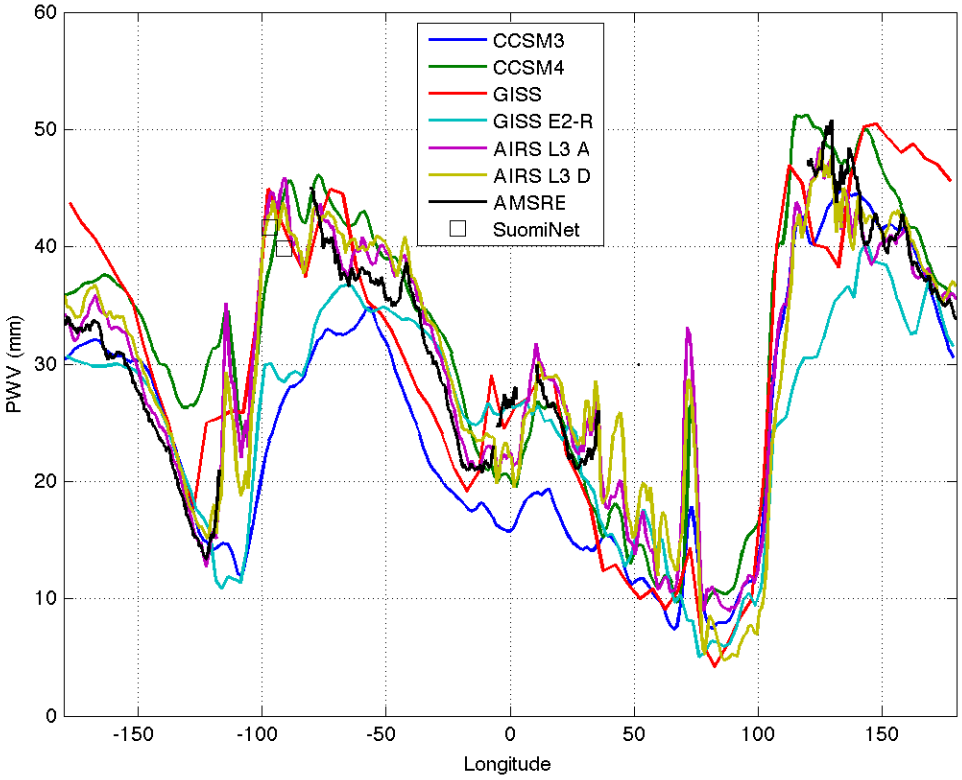

Figure 89: PWV for Models and Observations for August 2006 at 34°N to 39°N

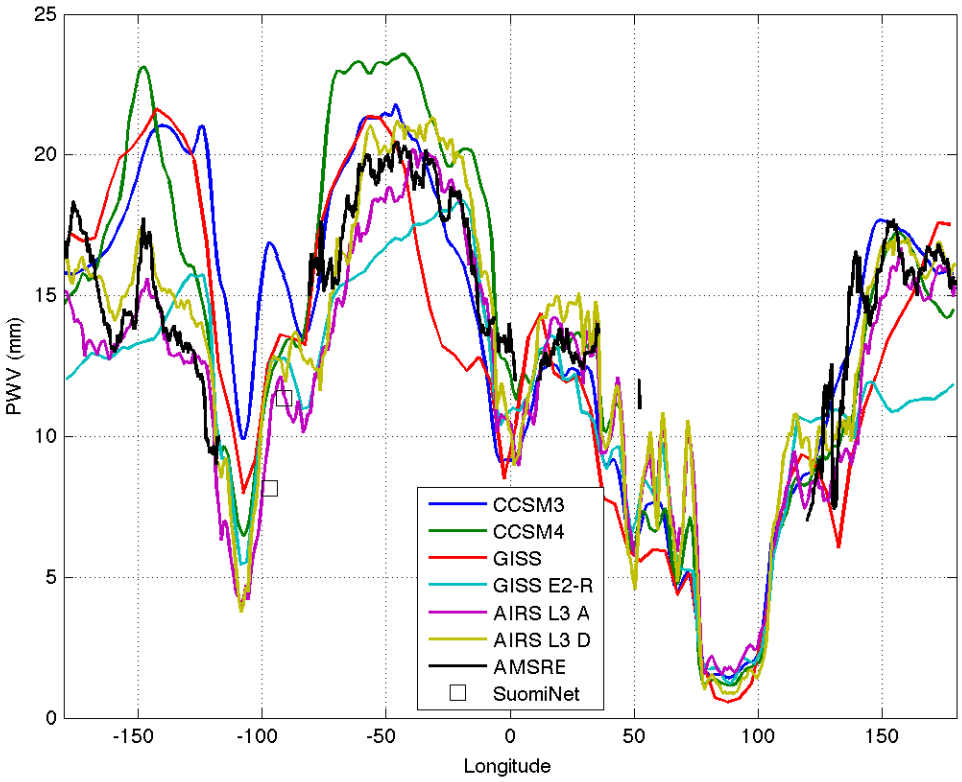

Figure 90: PWV for Models and Observations for February 2006 at 34°N to 39°N

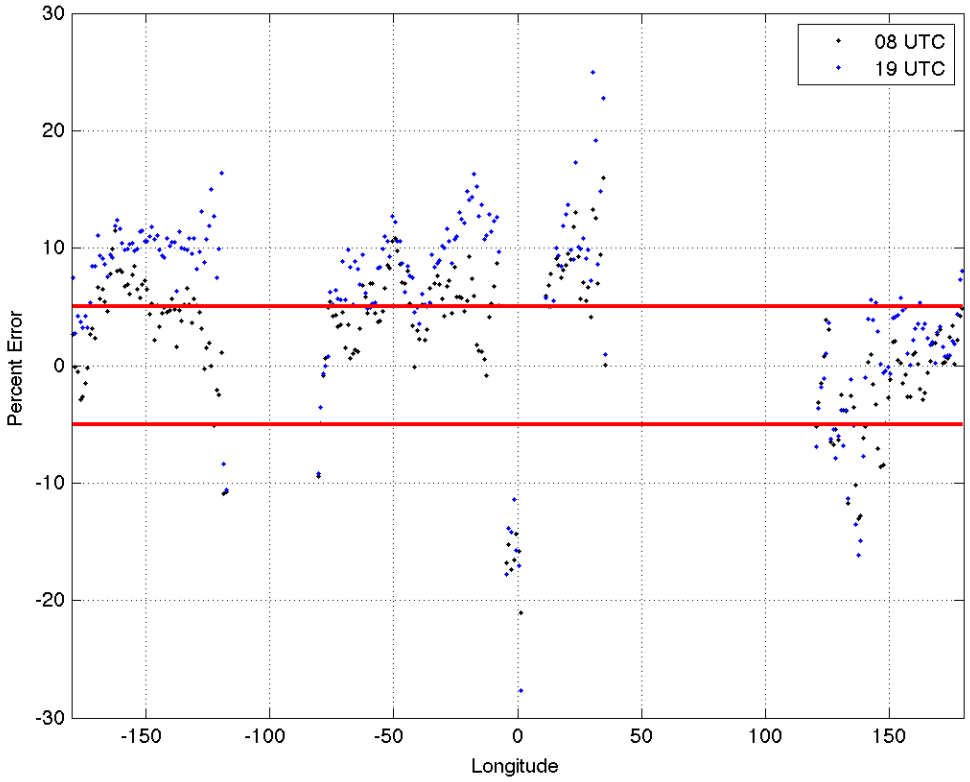

Figure 91: Percent Error (AIRS L3 v5.2 minus AMSRE)/(AMSRE) at the 34°N to 39°N August 2006

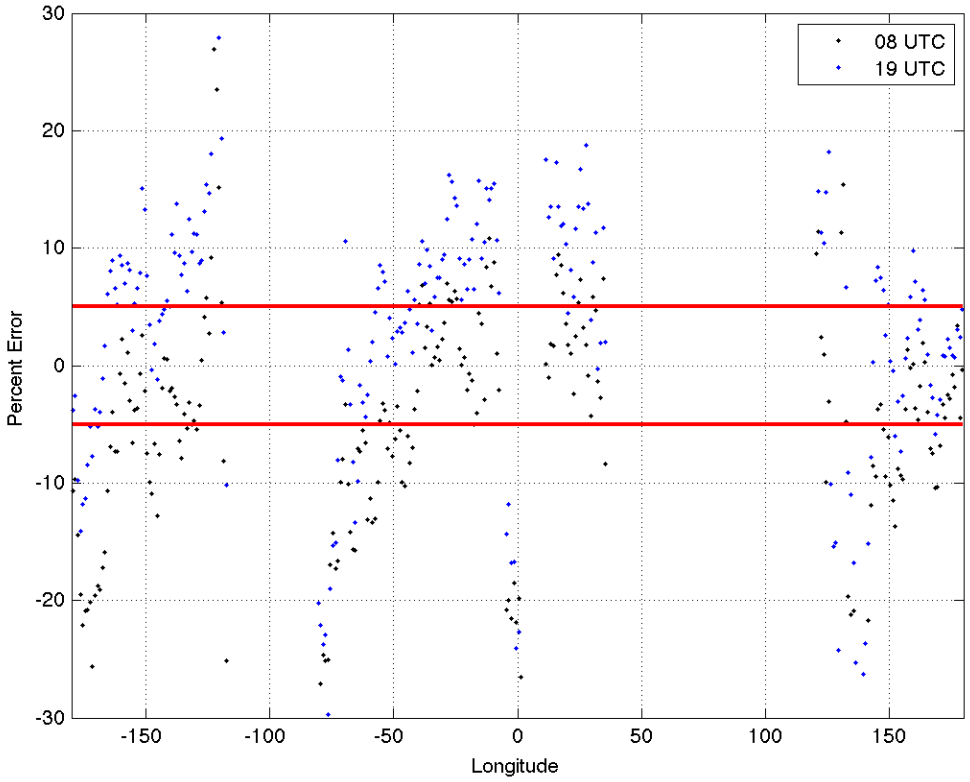

Figure 92: Percent Error (AIRS L3 v5.2 minus AMSRE)/(AMSRE) at the 34°N to 39°N February 2006

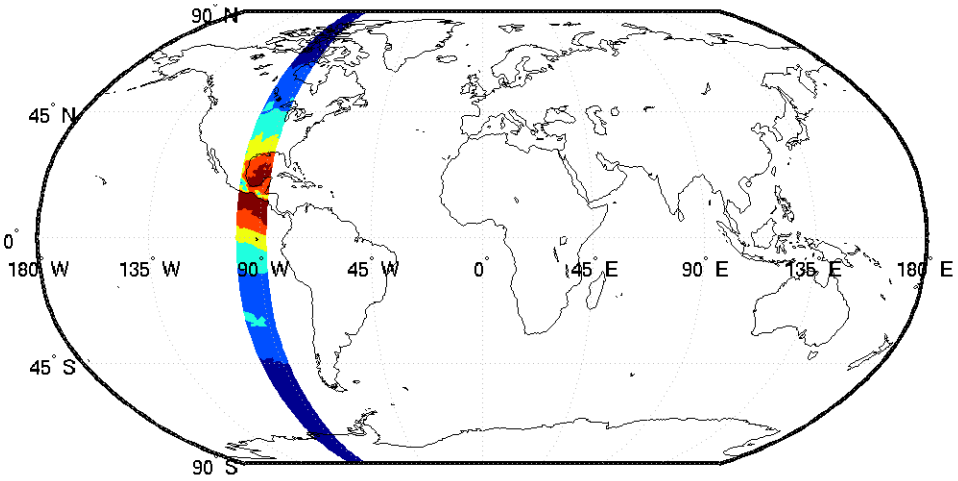

Figure 93: Longitude Averaged Region (87°W to 100°W) Showing the Latitude Dependence

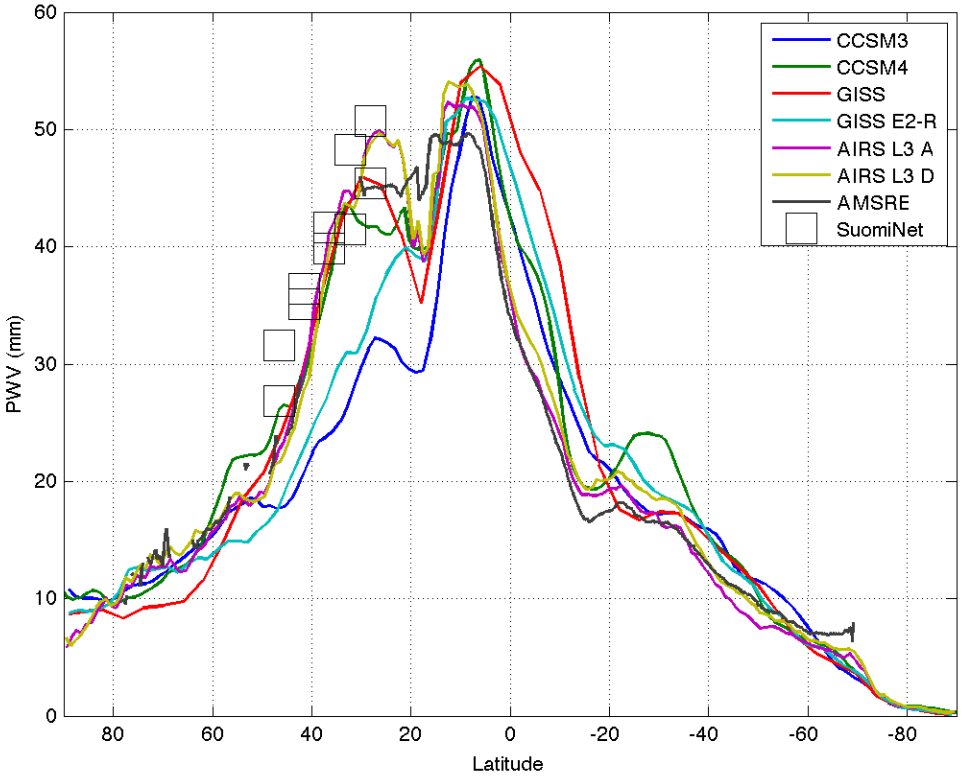

Figure 94: PWV for Models and Observations for August 2006 at 87°W to 100°W

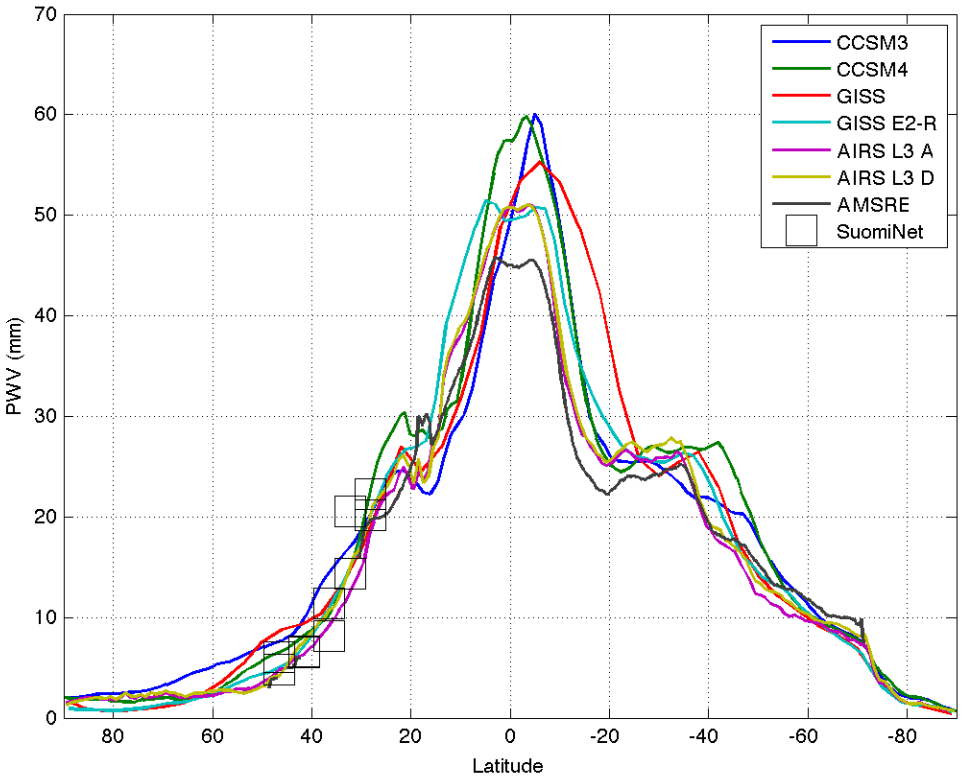

Figure 95: PWV for Models and Observations for February 2006 at 87°W to 100°W

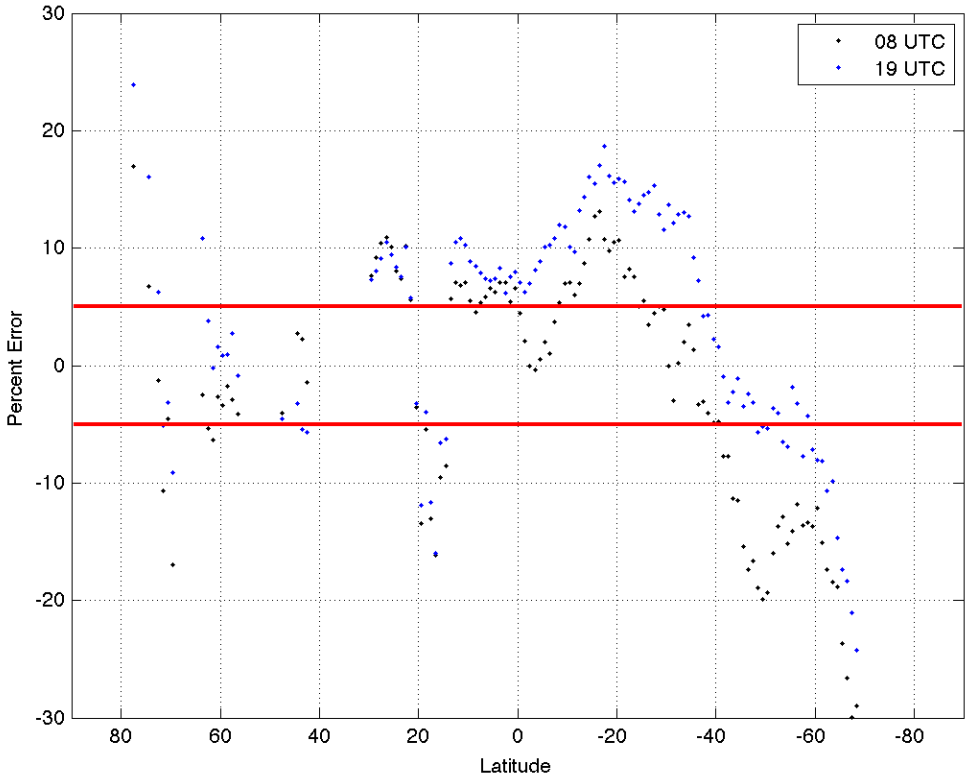

Figure 96: Percent Error (AIRS L3 v5.2 minus AMSRE)/(AMSRE) at the 87°W to 100°W August 2006

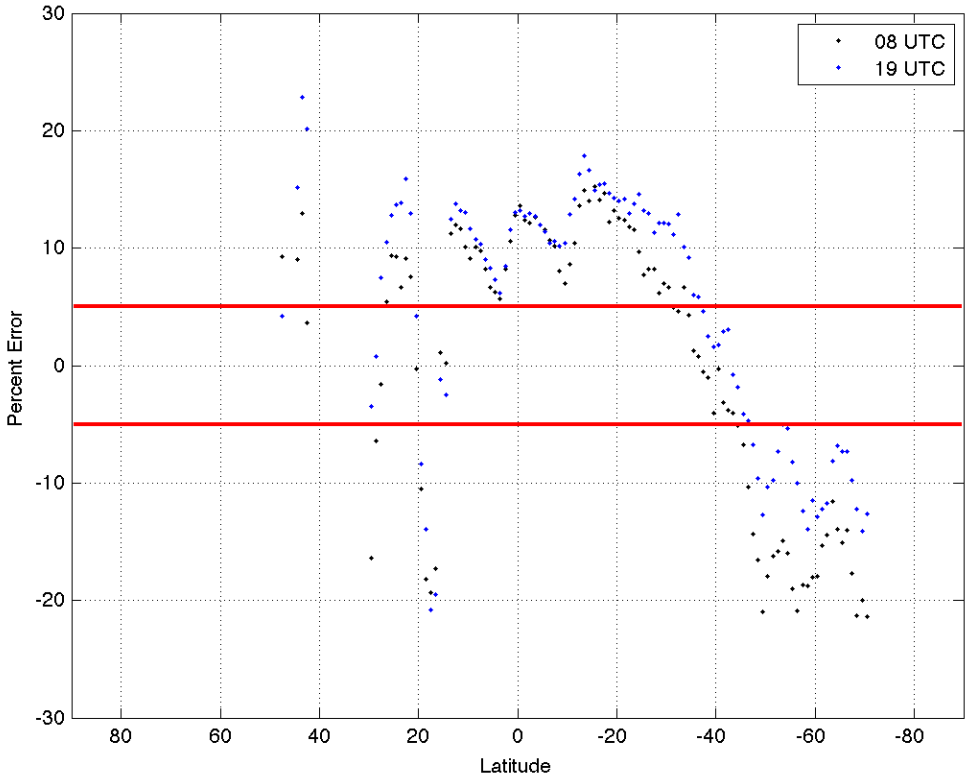

Figure 97: Percent Error (AIRS L3 v5.2 minus AMSRE)/(AMSRE) at the 87°W to 100°W February 2006

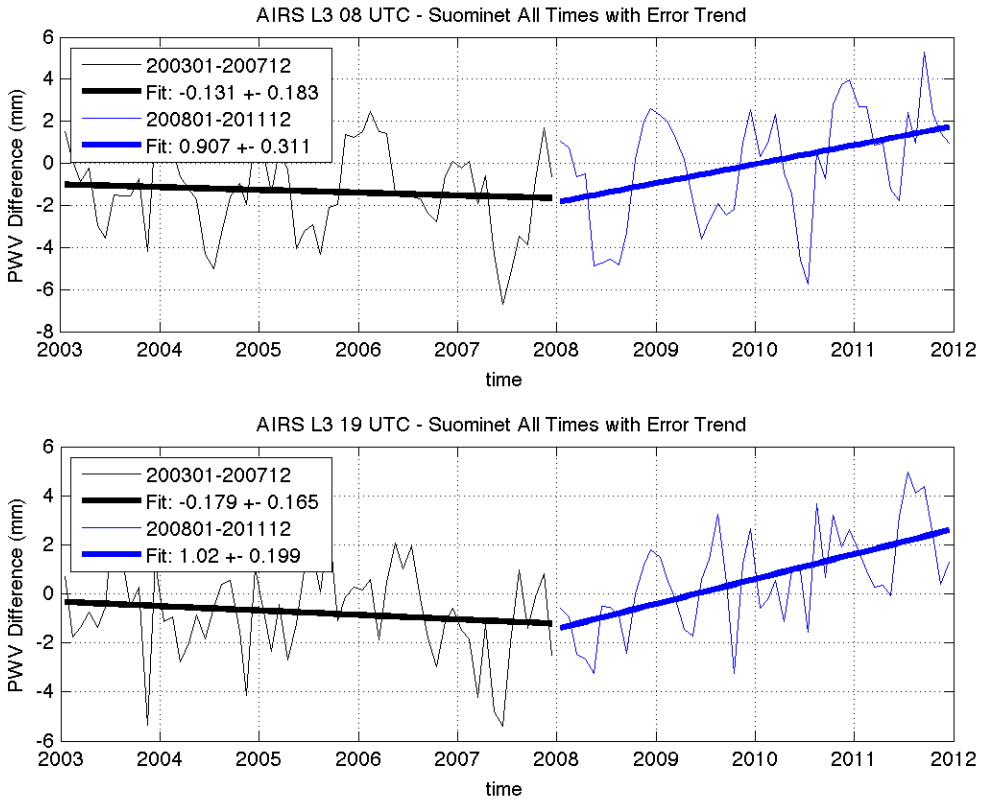

Figure 98: AIRS L3 v5 and v5.2 Compared to ARM SuomiNet GPS (Roman et al. 2013)

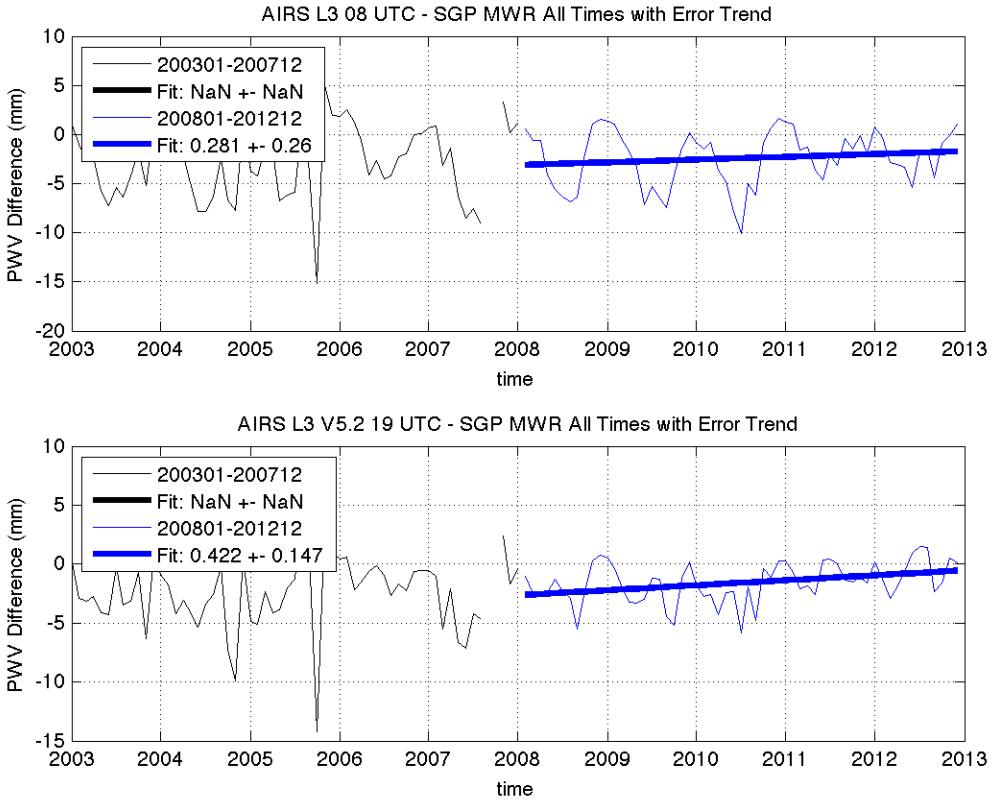

Figure 99: AIRS L3 v5.2 VS MWR All Times Trend Error

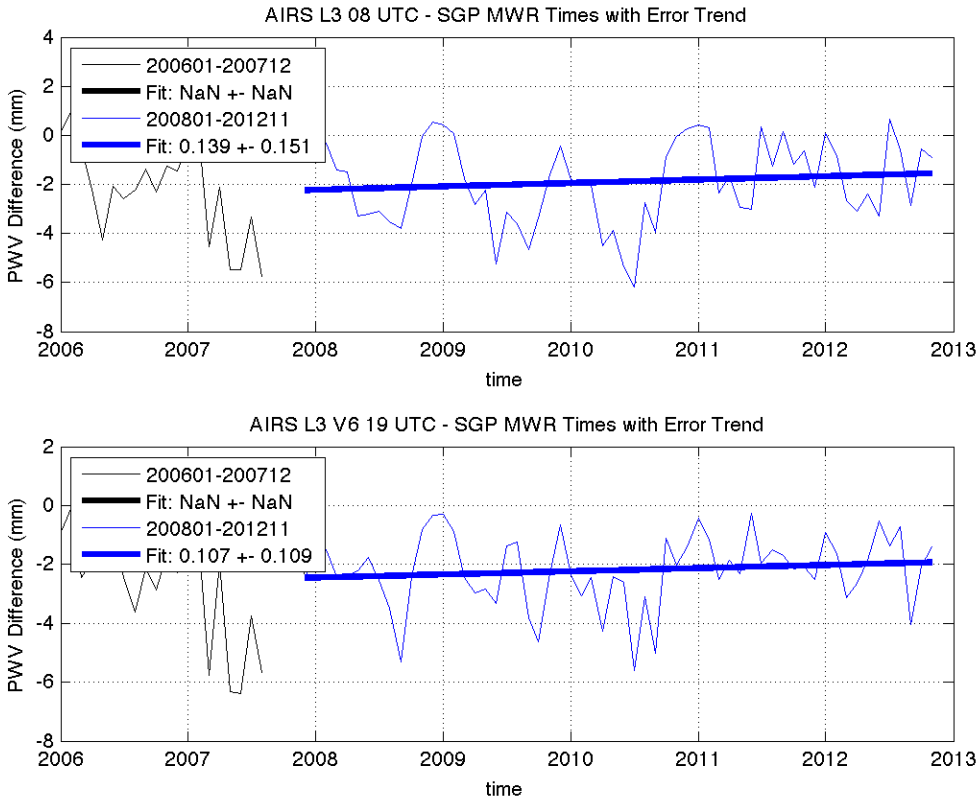

Figure 100: AIRS L3 v6 vs. MWR All Times Trend Error

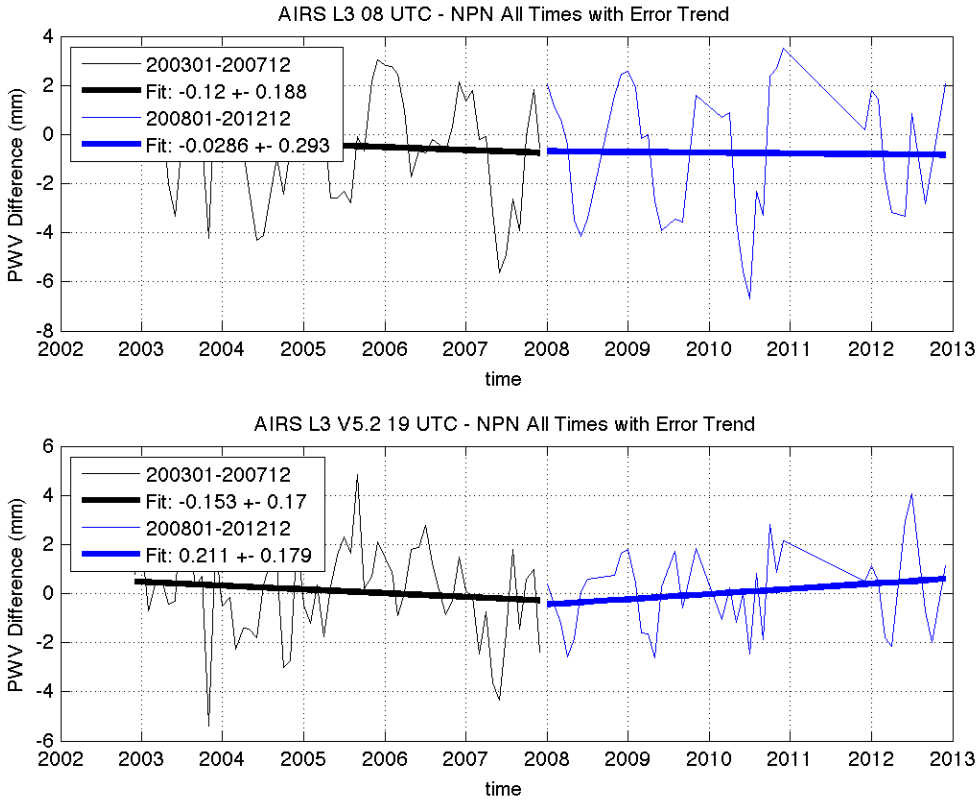

Figure 101: AIRS L3 v5.2 vs. NPN All Times Trend Error

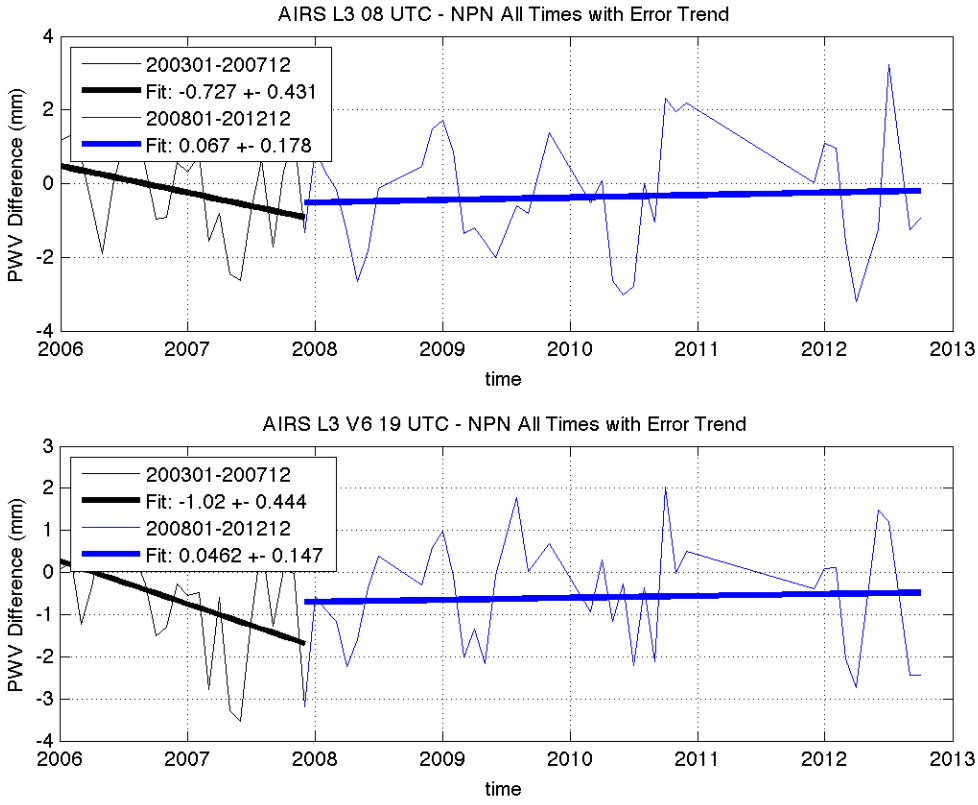

Figure 102: AIRS L3 v6 vs. NPN All Times Trend Error

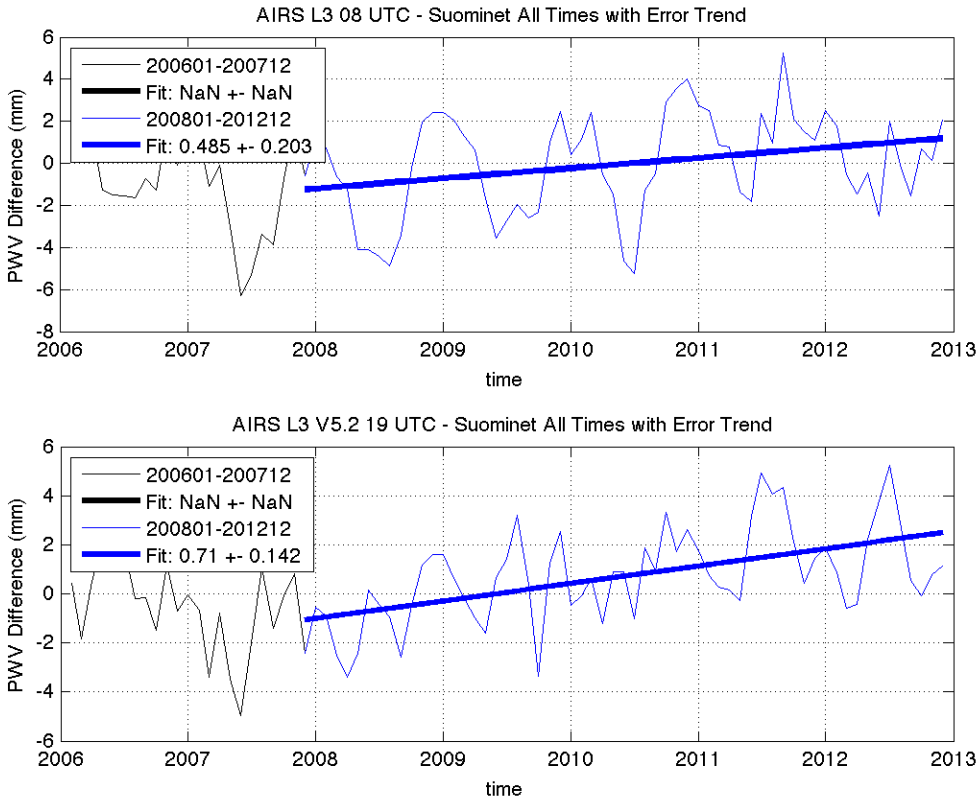

Figure 103: AIRS L3 v5.2 vs. SuomiNet All Times Trend Error

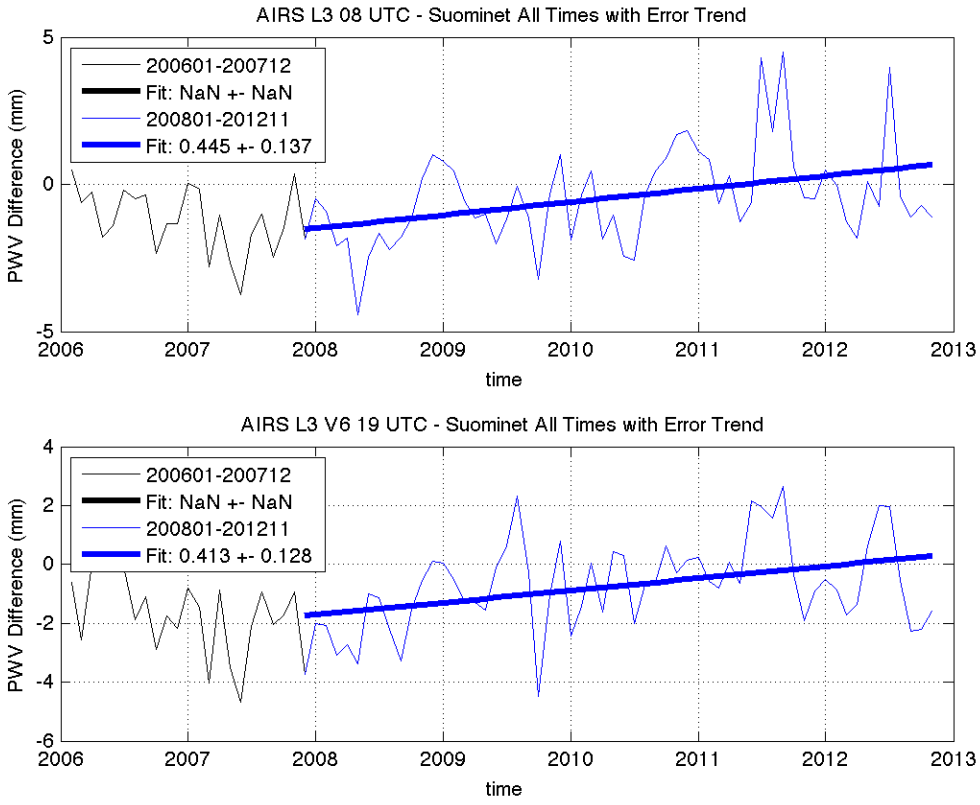

Figure 104: AIRS L3 v6 vs. SuomiNet All Times Trend Error

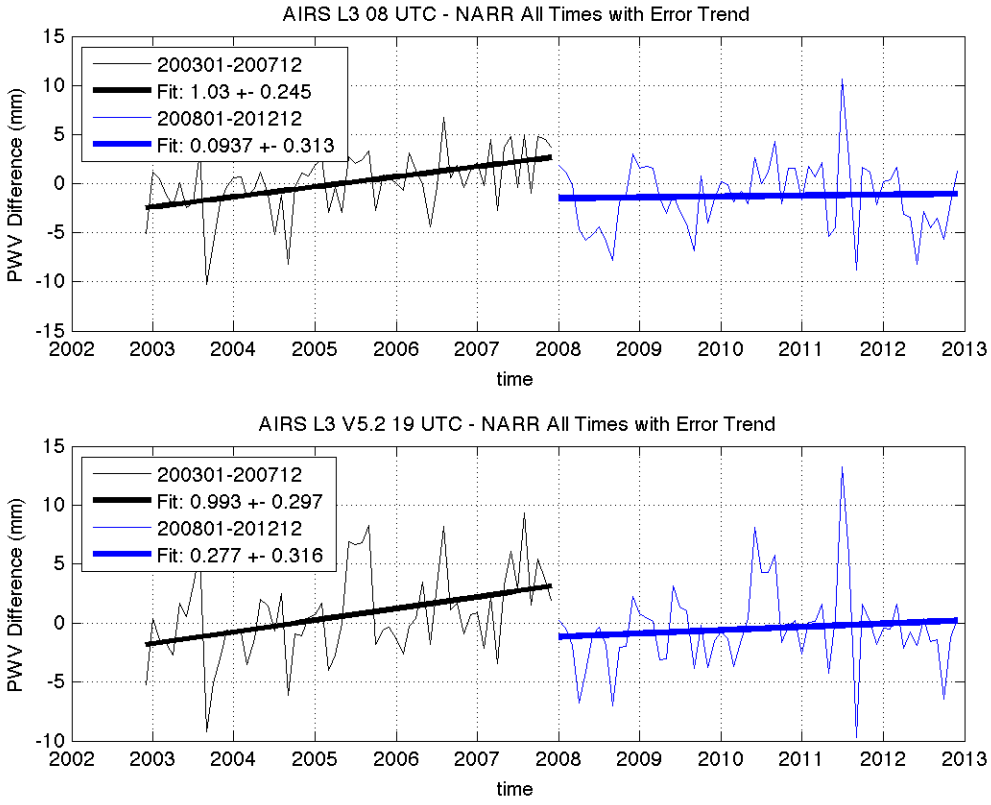

Figure 105: AIRS L3 v5.2 vs. NARR Trend Error

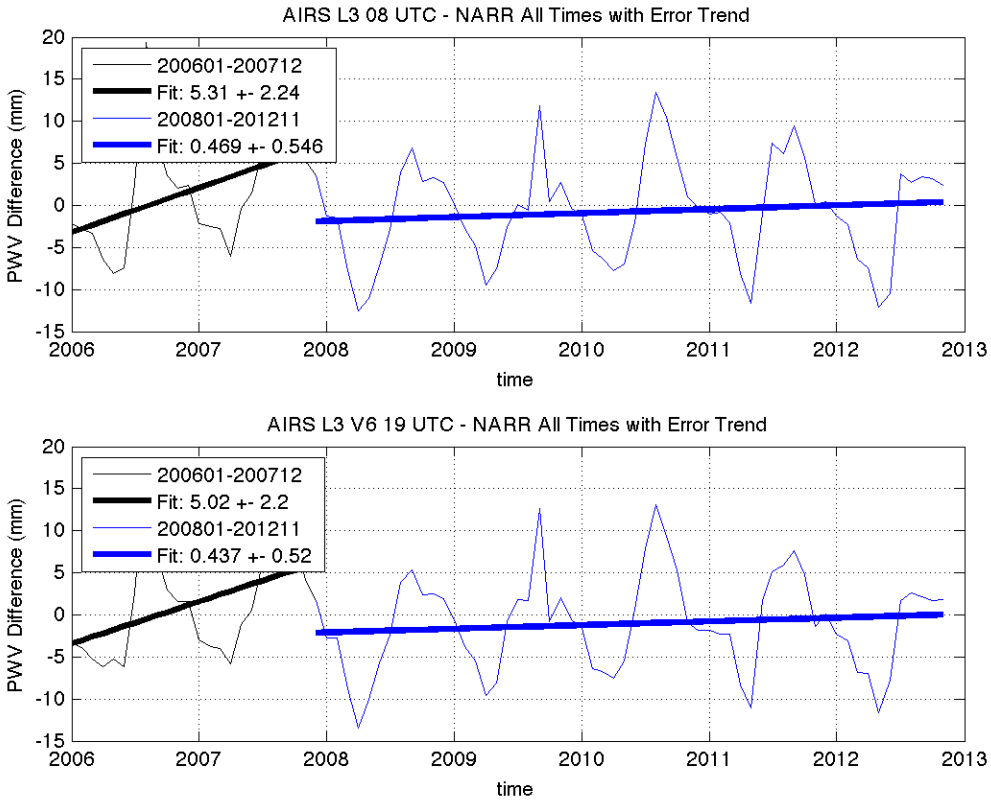

Figure 106: AIRS L3 v6 vs. NARR Trend Error

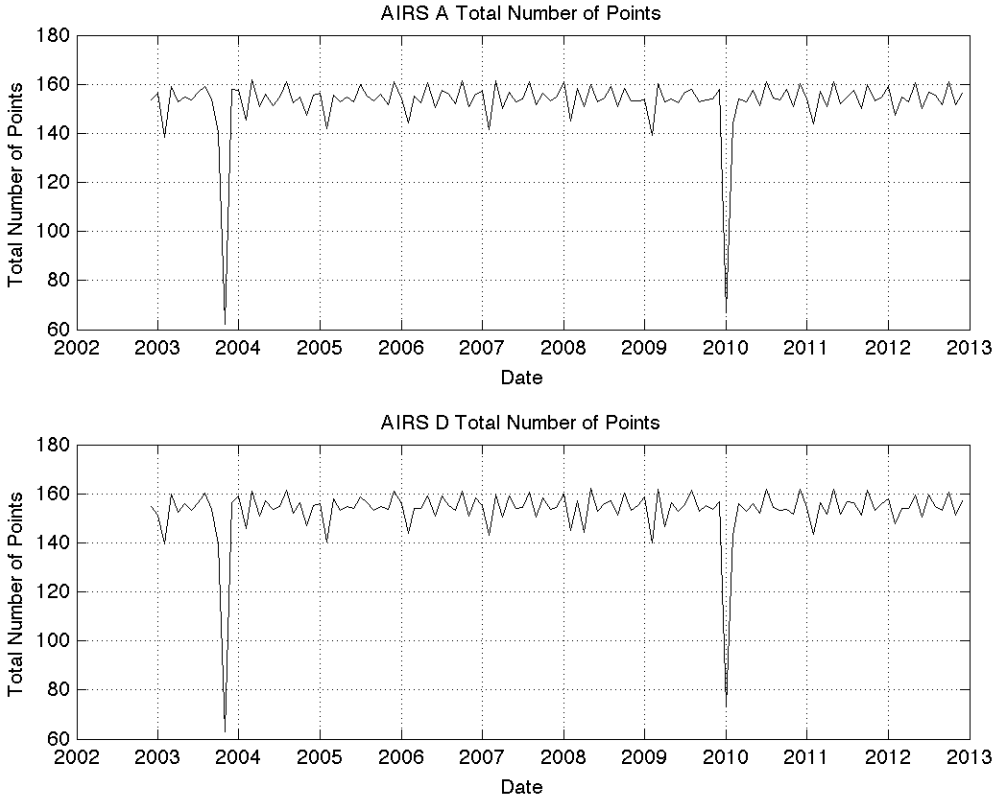

Figure 107: AIRS L3 V5.2 Total Number of Points

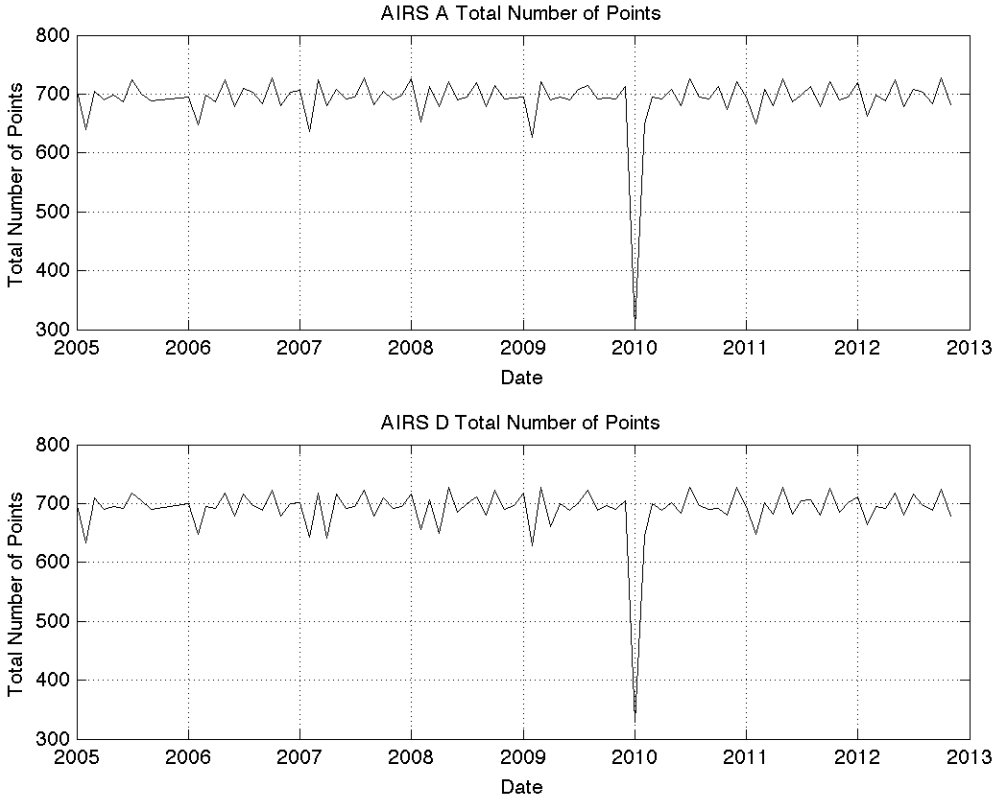

Figure 108: AIRS L3 v6 Total Number of Points

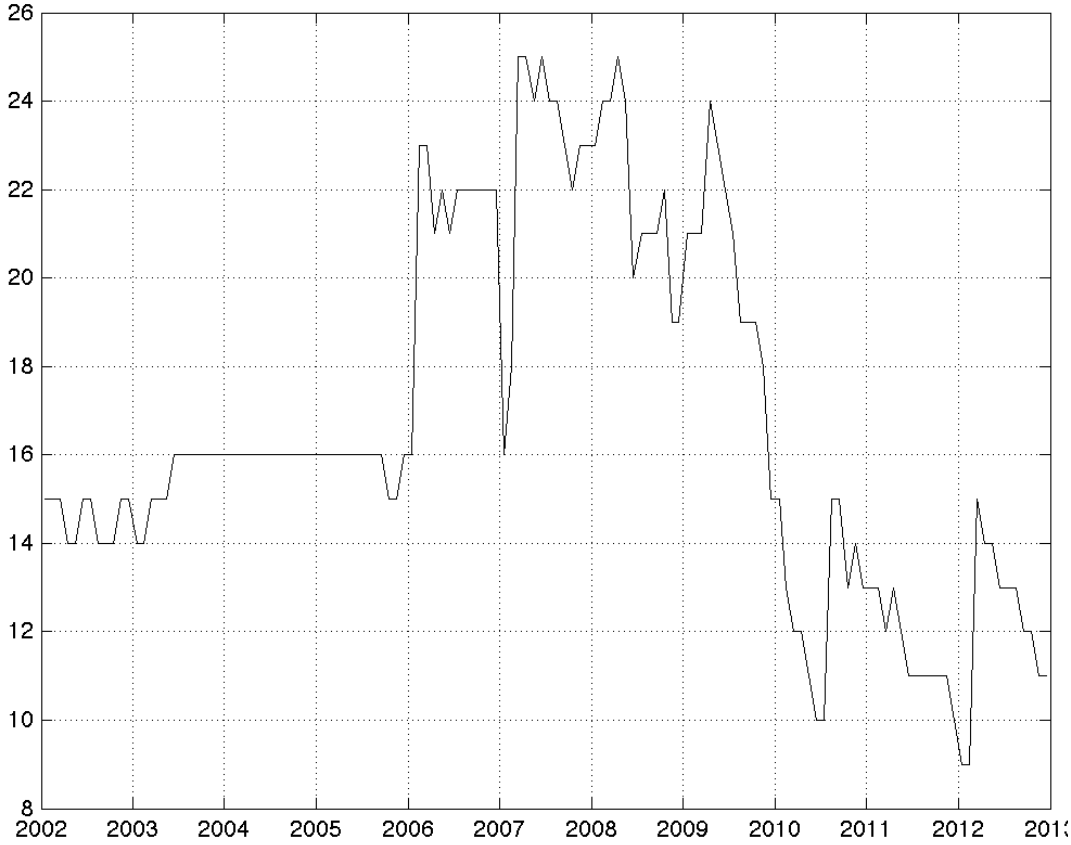

Figure 109: SuomiNet GPS Total Number of Stations

Figure 110: NPN Total Number of Stations

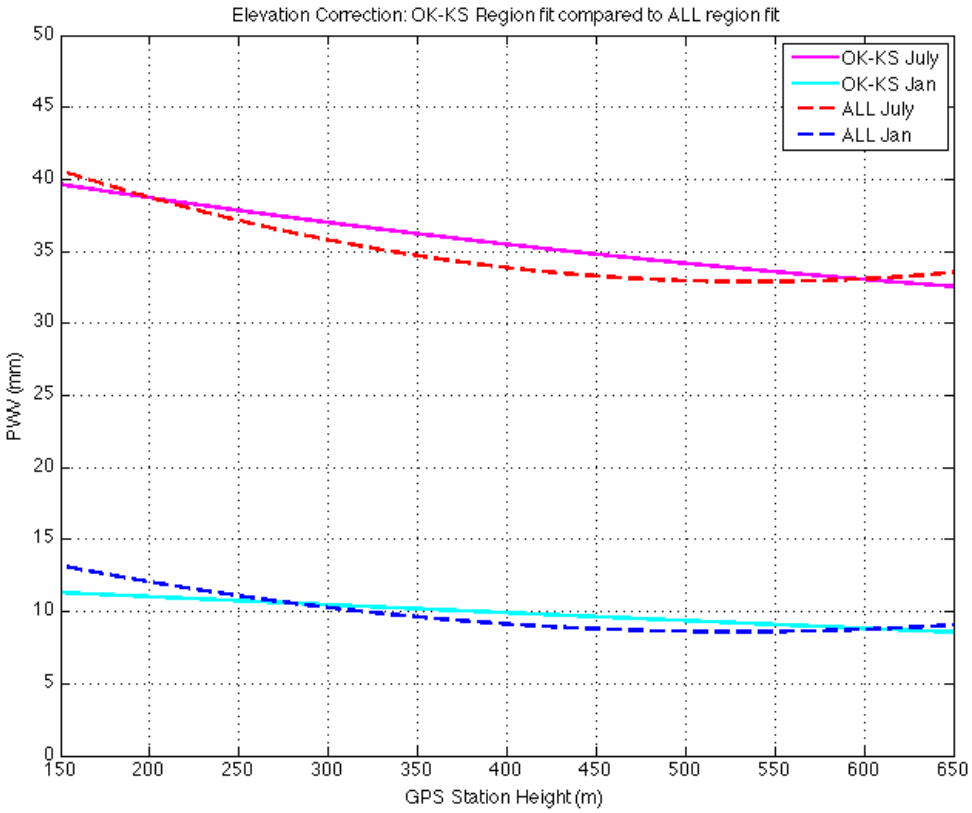

Figure 111: Elevation Correction Comparison

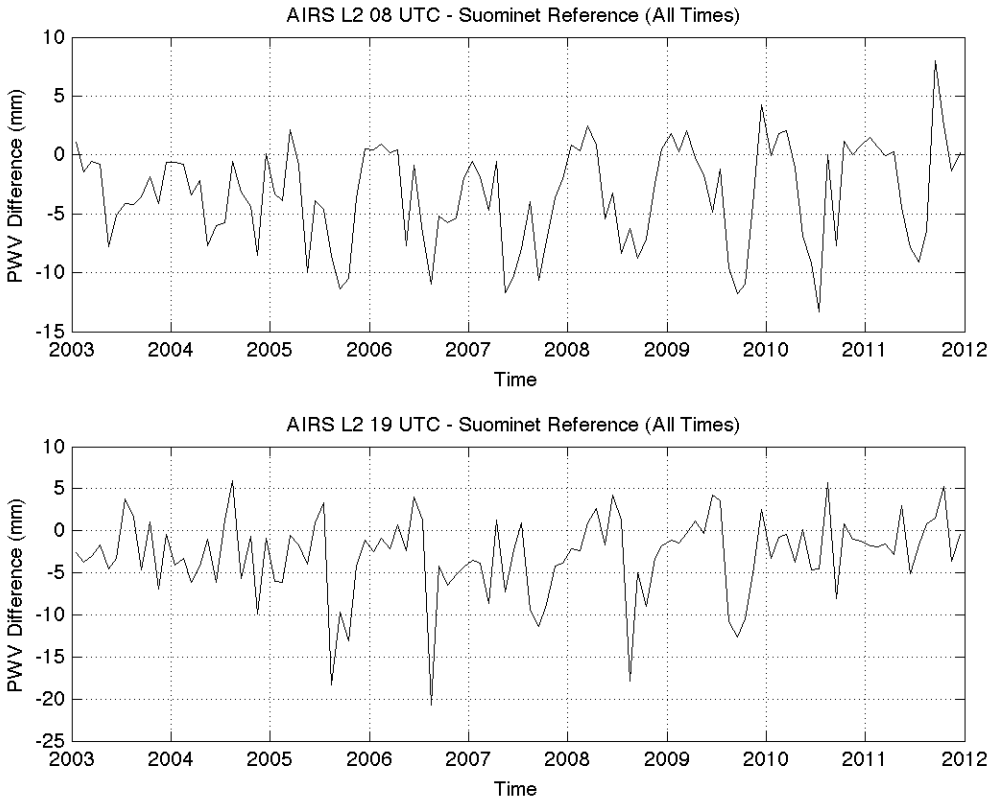

Figure 112: Timeseries of the AIRS L2 Night-Time (08 UTC) and day-time (19 UTC) Relative to the True Diurnal Average (Roman et al. 2013)

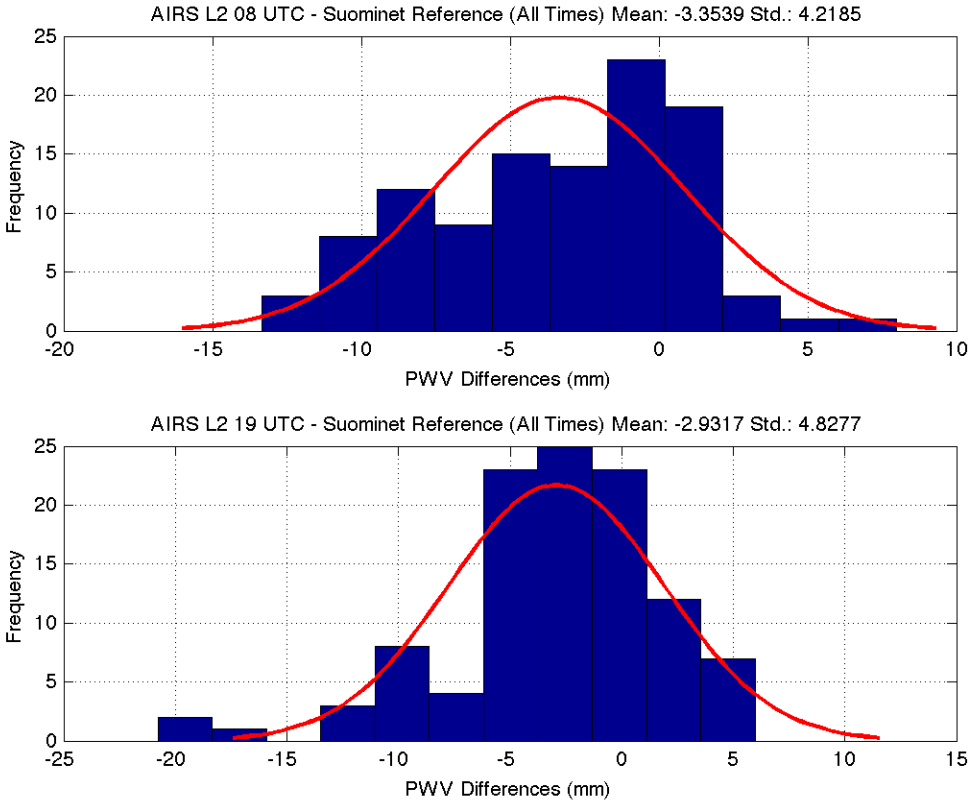

Figure 113: AIRS L2 Histogram of Differences to SuomiNet GPS for Day Time and Night Time (Roman et al. 2013)

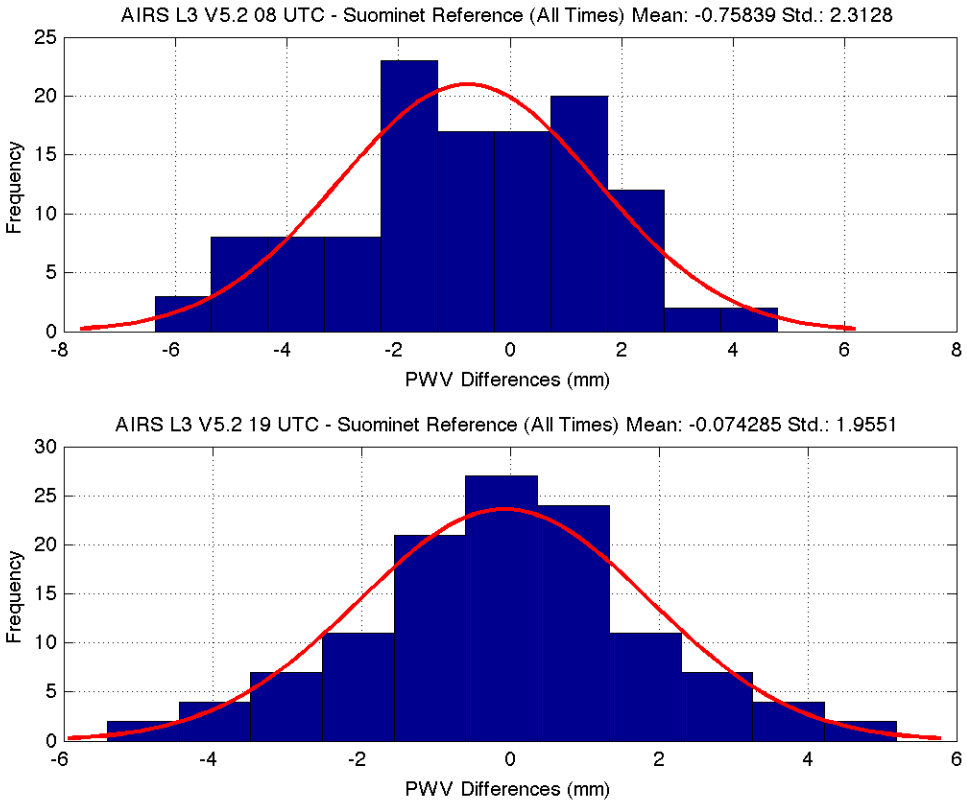

Figure 114: AIRS L3 v5.2 Histogram of Differences to SuomiNet GPS

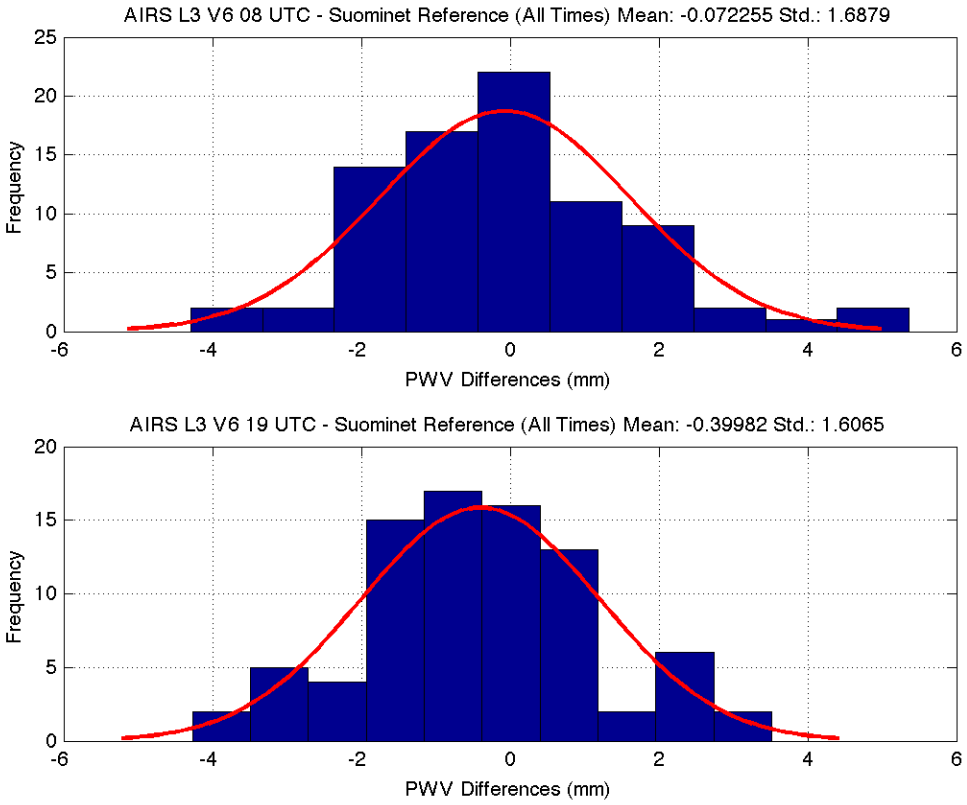

Figure 115: AIRS L3 v6 Histogram of Differences to SuomiNet GPS

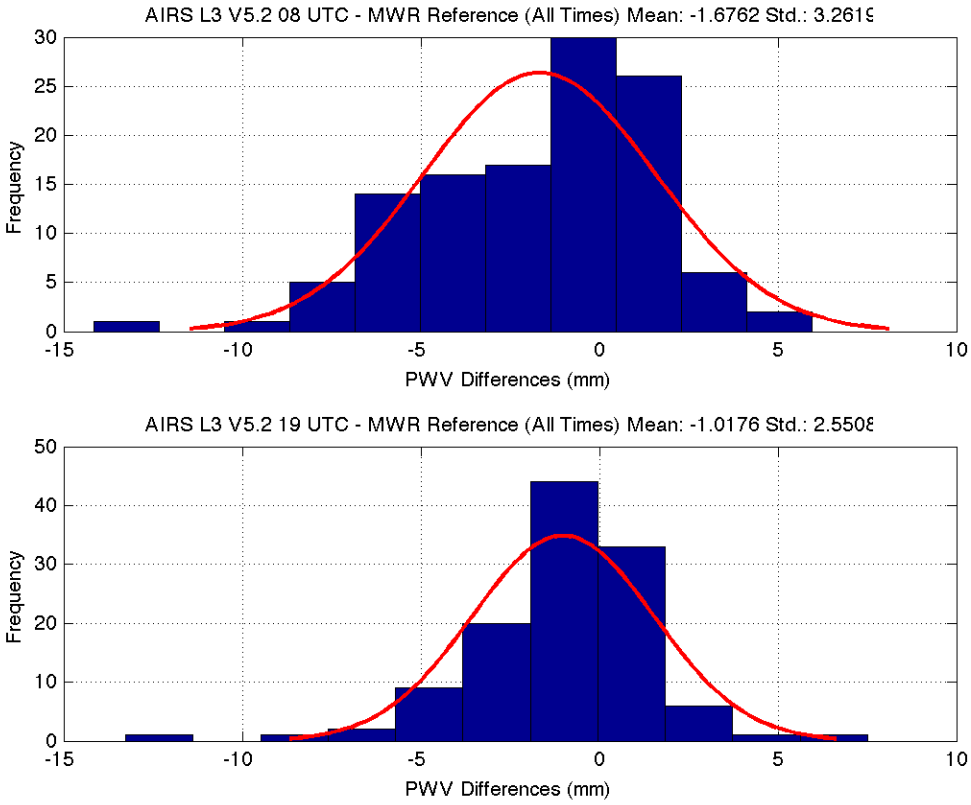

Figure 116: AIRS L3 v5.2 Histogram of Differences to MWR

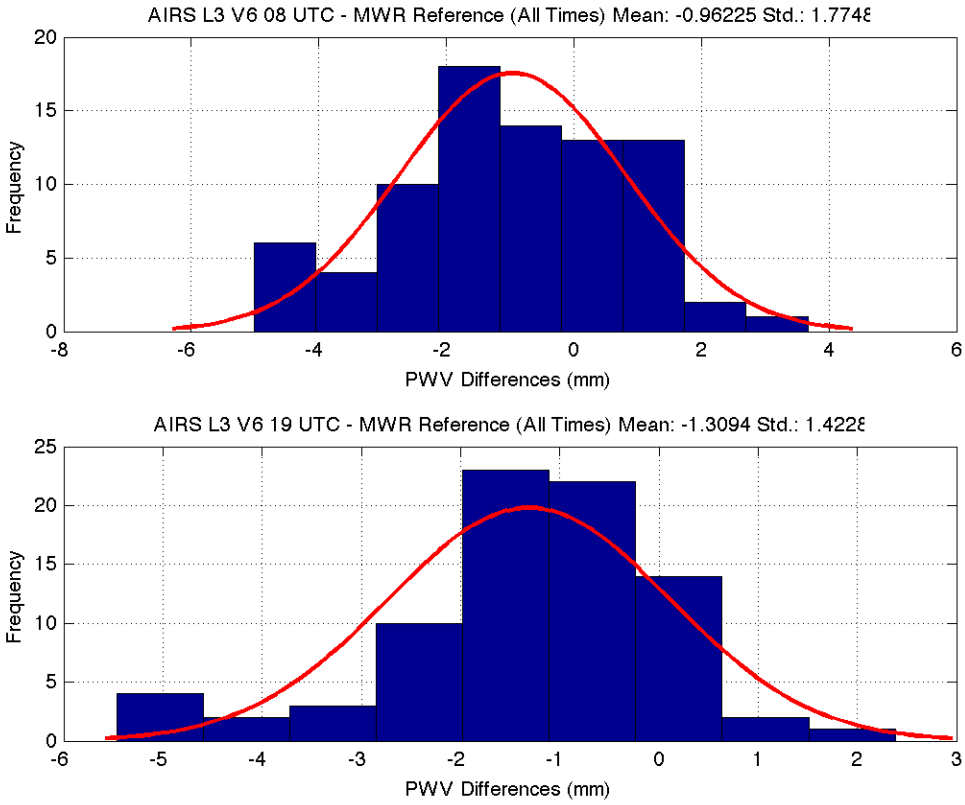

Figure 117: AIRS L3 v6 Histogram of Differences to MWR

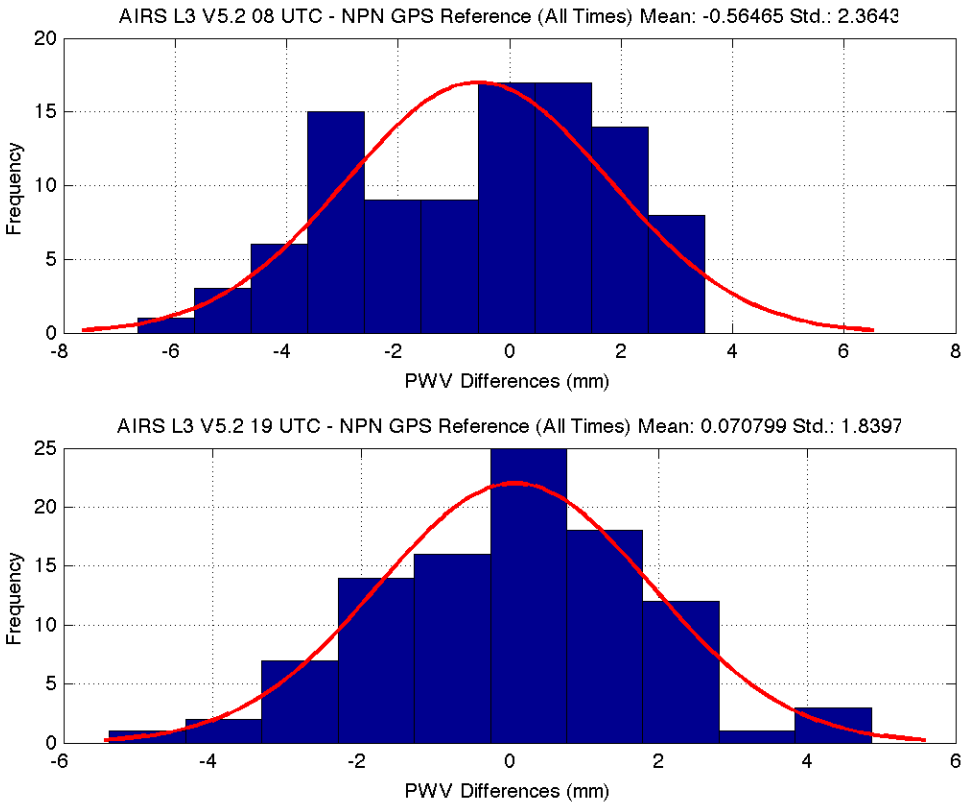

Figure 118: AIRS L3 v5.2 Histogram of Differences to NPN

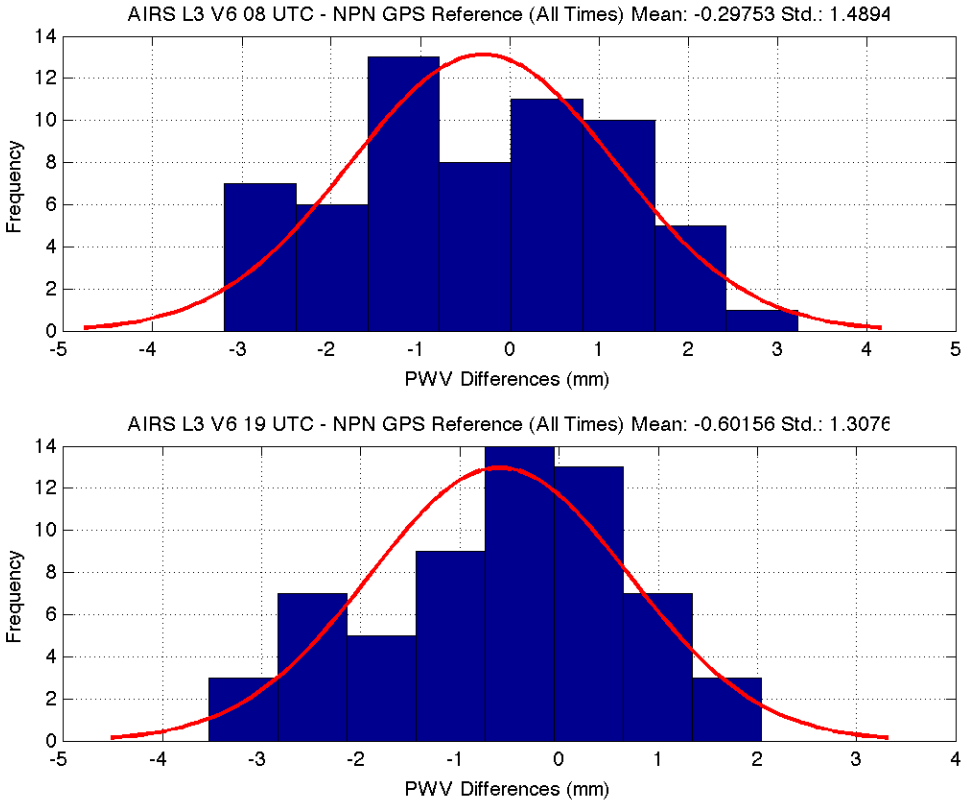

Figure 119: AIRS L3 v6 Histogram of Differences to NPN

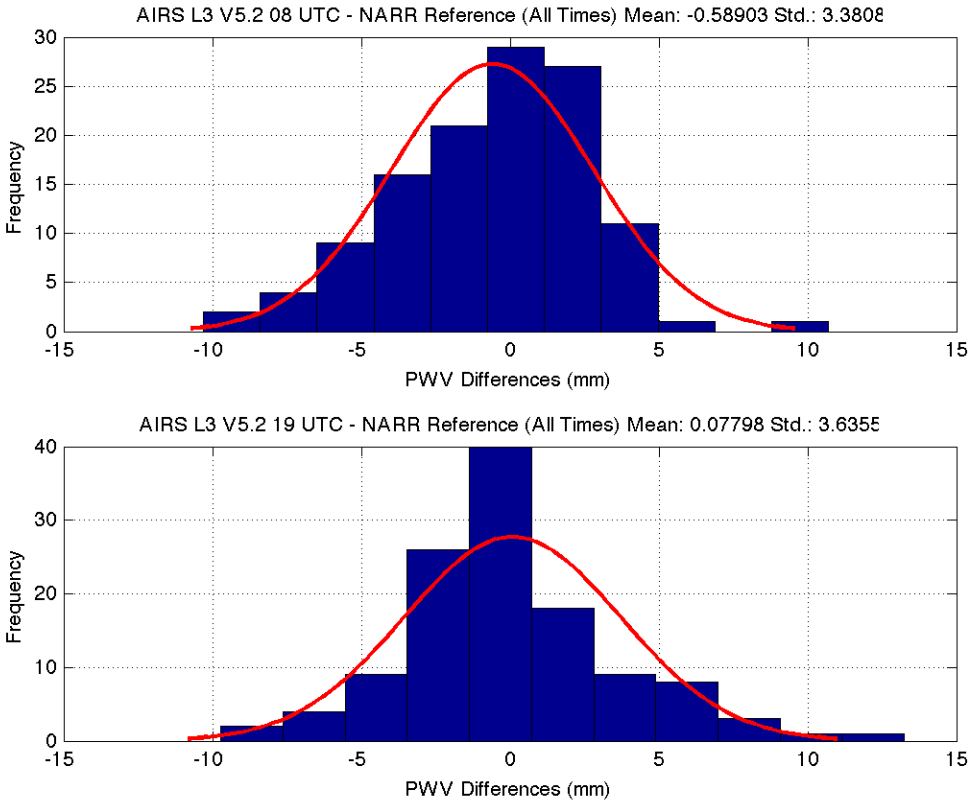

Figure 120: AIRS L3 v5.2 Histogram of Differences to NARR

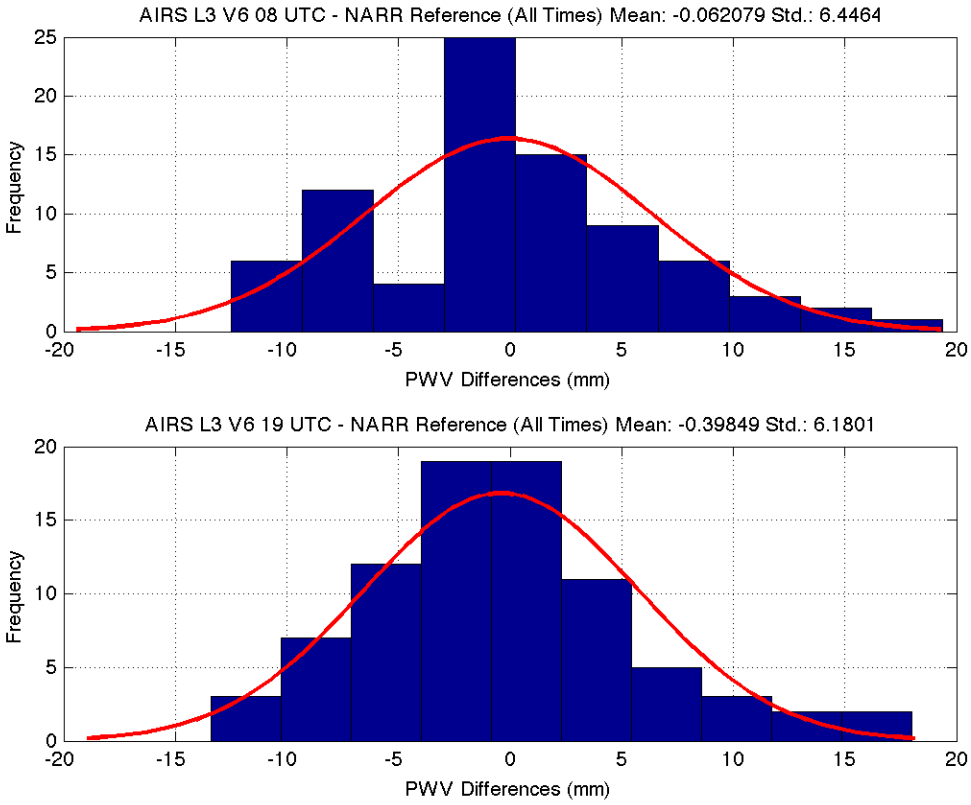

Figure 121: AIRS L3 v6 Histogram of Differences to NARR